Richard Brito Vitor Cardoso Paolo Pani

Superradiance

Energy Extraction, Black-Hole Bombs and Implications for Astrophysics and Particle Physics



Lecture Notes in Physics

Volume 906

Founding Editors

- W. Beiglböck
- J. Ehlers
- К. Нерр
- H. Weidenmüller

Editorial Board

- M. Bartelmann, Heidelberg, Germany
- B.-G. Englert, Singapore, Singapore
- P. Hänggi, Augsburg, Germany
- M. Hjorth-Jensen, Oslo, Norway
- R.A.L. Jones, Sheffield, UK
- M. Lewenstein, Barcelona, Spain
- H. von Löhneysen, Karlsruhe, Germany
- J.-M. Raimond, Paris, France
- A. Rubio, Donostia, San Sebastian, Spain
- S. Theisen, Potsdam, Germany
- D. Vollhardt, Augsburg, Germany
- J.D. Wells, Ann Arbor, USA
- G.P. Zank, Huntsville, USA

The Lecture Notes in Physics

The series Lecture Notes in Physics (LNP), founded in 1969, reports new developments in physics research and teaching-quickly and informally, but with a high quality and the explicit aim to summarize and communicate current knowledge in an accessible way. Books published in this series are conceived as bridging material between advanced graduate textbooks and the forefront of research and to serve three purposes:

- to be a compact and modern up-to-date source of reference on a well-defined topic
- to serve as an accessible introduction to the field to postgraduate students and nonspecialist researchers from related areas
- to be a source of advanced teaching material for specialized seminars, courses and schools

Both monographs and multi-author volumes will be considered for publication. Edited volumes should, however, consist of a very limited number of contributions only. Proceedings will not be considered for LNP.

Volumes published in LNP are disseminated both in print and in electronic formats, the electronic archive being available at springerlink.com. The series content is indexed, abstracted and referenced by many abstracting and information services, bibliographic networks, subscription agencies, library networks, and consortia.

Proposals should be sent to a member of the Editorial Board, or directly to the managing editor at Springer:

Christian Caron Springer Heidelberg Physics Editorial Department I Tiergartenstrasse 17 69121 Heidelberg/Germany christian.caron@springer.com

More information about this series at http://www.springer.com/series/5304

Superradiance

Energy Extraction, Black-Hole Bombs and Implications for Astrophysics and Particle Physics



Richard Brito
CENTRA
Departamento de Física
Instituto Superior Técnico, Universidade
de Lisboa
Lisbon, Portugal

Paolo Pani Dipartimento di Fisica "Sapienza" Universita di Roma & Sezione INFN Roma 1 Rome, Italy Vitor Cardoso
CENTRA
Departamento de Física
Instituto Superior Técnico, Universidade
de Lisboa
Lisbon, Portugal

ISSN 0075-8450 ISSN 1616-6361 (electronic) Lecture Notes in Physics ISBN 978-3-319-18999-4 ISBN 978-3-319-19000-6 (eBook) DOI 10.1007/978-3-319-19000-6

Library of Congress Control Number: 2015943376

Springer Cham Heidelberg New York Dordrecht London © Springer International Publishing Switzerland 2015

This work is subject to copyright. All rights are reserved by the Publisher, whether the whole or part of the material is concerned, specifically the rights of translation, reprinting, reuse of illustrations, recitation, broadcasting, reproduction on microfilms or in any other physical way, and transmission or information storage and retrieval, electronic adaptation, computer software, or by similar or dissimilar methodology now known or hereafter developed.

The use of general descriptive names, registered names, trademarks, service marks, etc. in this publication does not imply, even in the absence of a specific statement, that such names are exempt from the relevant protective laws and regulations and therefore free for general use.

The publisher, the authors and the editors are safe to assume that the advice and information in this book are believed to be true and accurate at the date of publication. Neither the publisher nor the authors or the editors give a warranty, express or implied, with respect to the material contained herein or for any errors or omissions that may have been made.

Printed on acid-free paper

Springer International Publishing AG Switzerland is part of Springer Science+Business Media (www.springer.com)

Preface

Macroscopic objects, as we see them all around us, are governed by a variety of forces, derived from a variety of approximations to a variety of physical theories. In contrast, the only elements in the construction of black holes are our basic concepts of space and time. They are, thus, almost by definition, the most perfect macroscopic objects there are in the universe.

- Subrahmanyan Chandrasekhar

Superradiance is a very generic process involving dissipative systems, whereby energy is transferred from one medium to another, typically stimulated by wave scattering. With a 60-year-old history, superradiance has played a prominent role in optics, quantum mechanics, and especially in relativity and astrophysics. Superradiance in curved spacetime was born by the hand of Yakov Borisovich Zel'dovich, who realized that rotation of any macroscopic body with internal degrees of freedom could amplify incident radiation. Quantization of this process leads rotating objects—including black holes—to spontaneously radiate. Soon after, and inspired by this discovery, Hawking realized that a similar mechanism would trigger black hole evaporation very generically, even in the absence of rotation.

A unified framework for superradiant effects can yield new insights into previously disconnected phenomena, for instance superradiant instabilities can occur in systems as diverse as fluids, stars, and black-hole spacetimes. Furthermore, the very *necessity* of superradiance in a variety of different systems can be understood by simple thermodynamical arguments. Recent developments in theoretical physics—in particular the realization that superradiance leads to new constraints on fundamental bosonic fields and to new hairy black holes—have further highlighted the need for a unified description of superradiant phenomena. Unfortunately, with the exception of the outstanding—but focused—work by Bekenstein and Schiffer [1], a proper overview on superradiance, including various aspects of wave propagation in black-hole spacetimes, does not exist. We hope that the current work will fill this gap.

This book is addressed to researchers embarking on the subject, who wish to find a concise overview of the state-of-the-art and on the relevant methods to attack these problems. This work is also addressed to more experienced researchers wishing to dive quickly into a certain topic, by browsing through the relevant references. In view of the multifaceted nature of this subject, we present a unified treatment

vi Preface

where various aspects of superradiance in flat spacetime are connected to their counterparts in curved spacetime, with particular emphasis on the superradiant amplification by black holes. In addition, we wish to review various applications of black-hole superradiance which have been developed in the last decade. These developments embrace—at least—three different communities, and our scope is to present a concise treatment that can be fruitful for the reader who is not familiar with the specific area. As will become clear throughout this work, some of these topics are far from being fully explored. We hope this study will serve as a guide for the exciting developments lying ahead, including the experimental implementation and observation of rotational superradiance!

This work would not have been possible without the patient and constant encouragement of Ana Sousa (who has also kindly prepared the illustrations for us) and of Giulia Serra. We are indebted to Asimina Arvanitaki, Jacob Bekenstein, Óscar Dias, Sam Dolan, Roberto Emparan, Sean Hartnoll, Shahar Hod, Luis Lehner, Carlos Palenzuela, Robert Penna, Silke Weinfurtner for useful comments on a preliminary draft of this manuscript, and especially to João Rosa for comments and for comparing our superradiant amplification factors with his code. We are also much indebted to Enrico Barausse, Emanuele Berti, Óscar Dias, Roberto Emparan, Leonardo Gualtieri, Carlos Herdeiro, Luis Lehner, Hideo Kodama, Akihiro Ishibashi, José Lemos, Avi Loeb, Hirotada Okawa, Frans Pretorius, Thomas Sotiriou, Ulrich Sperhake, Helvi Witek, Shijun Yoshida, and Hirotaka Yoshino for many and interesting discussions throughout the years.

We benefited from the generous support of a number of institutions. R. B. is supported by FCT foundation through grant SFRH/BD/52047/2012, and from the Fundação Calouste Gulbenkian through the Programa Gulbenkian de Estímulo à Investigação Científica. V.C. acknowledges financial support provided under the European Union's FP7 ERC Starting Grant "The dynamics of black holes: testing the limits of Einstein's theory" grant agreement no. DyBHo–256667. P.P. was supported by the European Community through the Intra-European Marie Curie contracts aStronGR-2011-298297, AstroGRAphy-2013-623439 and by FCT-Portugal through the projects IF/00293/2013 and CERN/FP/123593/2011. This research was supported in part by the Perimeter Institute for Theoretical Physics. Research at Perimeter Institute is supported by the Government of Canada through Industry Canada and by the Province of Ontario through the Ministry of Economic Development and Innovation. This work was supported by the NRHEP 295189 FP7-PEOPLE-2011-IRSES Grant.

Lisbon, Portugal Lisbon, Portugal Rome, Italy Richard Brito Vitor Cardoso Paolo Pani

Reference

Contents

1	Introduction			
	1.1	Milesto	ones	
	Refe	rences		
2	Superradiance in Flat Spacetime			
	2.1	Klein F	Paradox: The First Example of Superradiance	
		2.1.1	Bosonic Scattering	
		2.1.2	Fermionic Scattering	
	2.2	Superra	adiance and Pair Creation	
	2.3	Superra	adiance and Spontaneous Emission by a Moving Object	
		2.3.1	Cherenkov Emission and Superradiance	
		2.3.2	Cherenkov Radiation by Neutral Particles	
		2.3.3	Superradiance in Superfluids and Superconductors	
	2.4	Sound	Amplification by Shock Waves	
		2.4.1	Sonic "Booms"	
		2.4.2	Superradiant Amplification at Discontinuities	
	2.5	Rotatio	tional Superradiance	
		2.5.1	Example 1. Scalar Waves	
		2.5.2	Example 2. Sound and Surface Waves:	
			A Practical Experimental Setup?	
	2.6	Tidal A	Acceleration	
	Refe	rences		
3	Supe	erradian	ce in Black Hole Physics	
	3.1	Action	, Equations of Motion and Black Hole Spacetimes	
		3.1.1	Static, Charged Backgrounds	
		3.1.2	Spinning, Neutral Backgrounds	
		3.1.3	Geodesics and Frame Dragging in the Kerr Geometry	
		3.1.4	The Ergoregion	
		3.1.5	Intermezzo: Stationary and Axisymmetric	
			Black Holes Have an Ergoregion	
	3.2	Area T	heorem Implies Superradiance	

viii Contents

3.3	Energy Extraction <i>from</i> Black Holes: The Penrose Process	43
	3.3.1 The Original Penrose Process	44
	3.3.2 The Newtonian Carousel Analogy	47
	3.3.3 Penrose's Process: Energy Limits	48
	3.3.4 The Penrose Process in Generic Spacetimes	50
	3.3.5 The Collisional Penrose Process:	
	Ultra-High-Energy Debris	52
3.4	The ABC of Black Hole Superradiance	54
3.5	Superradiance from Charged Static Black Holes	56
	3.5.1 Linearized Analysis: Amplification Factors	56
	3.5.2 Backreaction on the Geometry: Mass	
	and Charge Loss	57
3.6	Superradiance from Rotating Black Holes	60
	3.6.1 Bosonic and Fermionic Fields in the Kerr Geometry	60
	3.6.2 Energy Fluxes of Bosonic Fields at Infinity	
	and on the Horizon	62
	3.6.3 Amplification Factors	64
	3.6.4 Dirac Fields on the Kerr Geometry	65
	3.6.5 Linearized Analysis: Analytic Versus Numerics	67
	3.6.6 Scattering of Plane Waves	70
	3.6.7 Nonlinear Superradiant Scattering	73
3.7	Boosted Black Strings: Ergoregions Without Superradiance	74
3.8	Superradiance in Higher Dimensional Spacetimes	77
3.9	Superradiance in Analogue Black Hole Geometries	78
3.10	Superradiance in Nonasymptotically Flat Spacetimes	80
3.11	Superradiance from Stars	81
3.12	Superradiance Beyond General Relativity	83
	3.12.1 Superradiance of Black Holes Surrounded	
	by Matter in Scalar-Tensor Theories	84
3.13	Microscopic Description of Superradiance	
	and the Kerr/CFT Duality	85
3.14	Open Issues	87
	rences	89
	k Holes and Superradiant Instabilities	97
4.1	No Black Hole Fission Processes	97
4.2	Spinning Black Holes in Confining Geometries are Unstable	99
4.3	Superradiant Instabilities: Time-Domain Evolutions	
	Versus an Eigenvalue Search	101
4.4	Black Holes Enclosed in a Mirror	102
	4.4.1 Rotating Black-Hole Bombs	102
	4.4.2 Charged Black-Hole Bombs	105
4.5	Black Holes in AdS Backgrounds	105
	4.5.1 Instability of Small Kerr-AdS Black Holes	
	and New BH Solutions	106

4

Contents ix

		4.5.2	Charged AdS Black Holes: Spontaneous	
			Symmetry Breaking and Holographic Superconductors	110
	4.6	Massiv	e Bosonic Fields	113
		4.6.1	The Zoo of Light Bosonic Fields in Extensions	
			of the Standard Model	114
		4.6.2	Massive Scalar Fields	116
		4.6.3	Massive Vector Fields	119
		4.6.4	Massive Tensor Fields	122
		4.6.5	A Unified Picture of Superradiant Instabilities	
			of Massive Bosonic Fields	124
	4.7	Black H	Holes Immersed in a Magnetic Field	125
	4.8	Superra	adiant Instability of Black Holes Surrounded	
			ducting Rings	127
	4.9		nimal Interactions	128
		4.9.1	Plasma-Triggered Superradiant Instabilities	129
		4.9.2	Spontaneous Superradiant Instabilities	
			in Scalar-Tensor Theories	129
	4.10	Kaluza-	-Klein Mass: Superradiant Instabilities in Higher	
			sions	131
	4.11	Ergoreg	gion Instability	132
		4.11.1	Ergoregion Instability of Rotating Objects:	
			A Consistent Approach	133
		4.11.2	Ergoregion Instability and Long-Lived Modes	138
		4.11.3	Ergoregion Instability in Fluids	140
		4.11.4	Ergoregion Instability and Hawking Radiation	142
	4.12	Black-I	Hole Lasers and Superluminal Corrections	
		to Haw	king Radiation	143
	4.13	- Carlotte		
		Instabil	lities	144
	4.14	Open Is	ssues	144
	Refer	ences		147
_	Dlask	. II.l. C.		157
5	5.1		uperradiance in Astrophysics	157
	5.1	-	adiance and Relativistic Jets	
		5.1.1 5.1.2	Blandford-Znajek Process	158
		5.1.2	Blandford-Znajek Process and the Membrane	1.61
	<i>5</i> 2	C	Paradigm	161 165
	5.2	Superradiance, CFS Instability, and r-Modes of Spinning Stars		103
	5.3	1		160
			tional-Wave Emission and Accretion	168
		5.3.1	Scalar Clouds Around Spinning Black Holes	169
		5.3.2	Gravitational-Wave Emission from the Bosonic	170
		522	Condensate	170
		5.3.3 5.3.4	Gas Accretion	170
		3.3.4	Growth and Decay of Bosonic Condensates	170
			Around Spinning Black Holes	172

x Contents

		5.3.5	Superradiant Instabilities Imply No	
			Highly-Spinning Black Holes	174
		5.3.6	Summary of the Evolution of Superradiant Instabilities	176
	5.4	Astrop	hysical Black Holes as Particle Detectors	177
		5.4.1	Bounds on the Mass of Bosonic Fields from	
			Gaps in the Regge Plane	178
		5.4.2	Gravitational-Wave Signatures and Bosenova	181
		5.4.3	Floating Orbits	185
	5.5	Are Bl	ack Holes in the Universe of the Kerr Family?	187
		5.5.1	Circumventing the No-Hair Theorem with	
			Complex Scalars	188
		5.5.2	Other Hairy Solutions and the Role of Tidal	
			Dissipation	190
		5.5.3	Formation of Hairy Solutions and Bounds on	
			Bosonic Fields	191
	5.6	Plasma	a Interactions	192
	5.7		ic Limits on Magnetic Fields	194
	5.8		menology of the Ergoregion Instability	196
		5.8.1	Ergoregion Instability of Ultracompact Stars	197
		5.8.2	Supporting the Black-Hole Paradigm:	
			Instabilities of Black-Hole Mimickers	198
	5.9	Open I	ssues	202
		-		204
6	Conc	lusions	and Outlook	213
	Lists	e Dubli	cly Available Codes	215
A	List	or Fublic	Ty Available Codes	213
В	Analy	ztic Con	nputation of the Amplification Coefficients	217
	rxiiaij	tic Con	inputation of the Amphileation Coefficients	217
C	Angu	lar Moi	mentum and Energy	221
_	C.1		and Angular Momentum Fluxes at the Horizon	
D	Electi	romagn	etic Fluctuations Around a Rotating Black	
			ed in a Mirror	223
E	Hartl	e-Thori	ne Formalism for Slowly-Rotating Spacetimes	
	and P	erturba	ations	229
	E.1		round	229
	E.2		pations of a Slowly-Rotating Object	230
		E.2.1	Scalar Perturbations of a Slowly-Rotating Star	231
			•	
F	WKB	Analys	sis of Long-Lived and Unstable Modes	
			pact Objects	233
		_		

Notation and Conventions

Azimuthal coordinate

and D-1 spacelike dimensions)

 φ

D

Unless otherwise and explicitly stated, we use geometrized units where G=c=1, so that energy and time have units of length. We also adopt the $(-+++\dots)$ convention for the metric. For reference, the following is a list of symbols that are used often throughout the text.

ı) Angular coordinate Azimuthal number with respect to the axis of rotation, $|m| \le l$ m 1 Integer angular number, related to the eigenvalue $A_{lm} = l(l + 1)$ in four spacetime dimensions Spin of the field S Fourier transform variable. The time dependence of any field is $\sim e^{-i\omega t}$ (ı) For stable spacetimes, $Im(\omega) < 0$ Real and imaginary part of the QNM frequencies ω_R , ω_I Amplitude of reflected and incident waves, which characterize a wave- \mathcal{R}, \mathcal{I} function Φ Amplification factor of fluxes for a wave with spin s and harmonic indices Z_{slm} (l, m). For scalar fields, $Z_{0lm} = |\mathcal{R}|^2/|\mathcal{I}|^2 - 1$ with the asymptotic expansion at spatial infinity, $\Phi \sim \mathcal{R}e^{i\omega t} + \mathcal{I}e^{-i\omega t}$ Occasionally, when clear from the context, we will omit the indices s and l and simply write Z_m Overtone numbers of the eigenfrequencies n

We conventionally start counting from a "fundamental mode" with n = 0

Total number of spacetime dimensions (we always consider one timelike

xii Notation and Conventions

L	Curvature radius of (A)dS spacetime, related to the negative
	cosmological constant Λ in the Einstein equations $(G_{\mu\nu} + \Lambda g_{\mu\nu} = 0)$
L^2	$= \mp (D-2)(D-1)/(2\Lambda)$ is the curvature radius of AdS (- sign) or dS
M	Mass of the BH spacetime
r_+	Radius of the BH event horizon in the chosen coordinates
Ω_{H}	Angular velocity of a zero-angular momentum observer at the BH horizon, as measured by a static observer at infinity
$\mu_{S,V,T}$	Mass parameter of the (scalar, vector or tensor) field
	In geometric units, the field mass is $\mu_{S,V,T}\hbar$, respectively
a	Kerr rotation parameter: $a = J/M \in [0, M]$
$g_{lphaeta}$	Spacetime metric; Greek indices run from 0 to $D-1$
Y_{lm}	Spherical harmonics, orthonormal with respect to the integral over the
	2-sphere
S_{slm}	Spin-weighted spheroidal harmonics

Acronyms

ADM Arnowitt-Deser-Misner
AGN Active Galactic Nucleus

AdS Anti-de Sitter
BH Black hole

CFT Conformal field theory
GR General Relativity
GW Gravitational Wave

LIGO Laser Interferometric Gravitational Wave Observatory

ODE Ordinary differential equation

NS Neutron star

PDE Partial differential equation QCD Quantum Chromodynamics

QNM Quasinormal mode RN Reissner-Nordström

ZAMO Zero Angular Momentum Observer

Chapter 1 Introduction

Radiation-enhancement processes have a long history that can be traced back to the dawn of quantum mechanics, when Klein showed that the Dirac equation allows for electrons to be transmitted even in classically forbidden regions [1]. In 1971 Zel'dovich showed that scattering of radiation off rotating absorbing surfaces results, under certain conditions, in waves with a larger amplitude [2, 3]. This phenomenon is now widely known also as (rotational) superradiance and requires that the incident radiation, assumed monochromatic of frequency ω , satisfies

$$\omega < m\Omega$$
, (1.1)

1

with m the azimuthal number with respect to the rotation axis and Ω the angular velocity of the body. Rotational superradiance belongs to a wider class of classical problems displaying stimulated or spontaneous energy emission, such as the Vavilov-Cherenkov effect, the anomalous Doppler effect and other examples of "superluminal motion". When quantum effects were incorporated, it was argued that rotational superradiance would become a spontaneous process and that rotating bodies—including black holes (BHs)—would slow down by spontaneous emission of photons satisfying (1.1). In parallel, similar conclusions were reached when analyzing BH superradiance from a thermodynamic viewpoint [4, 5]. From a historic perspective, the first studies of BH superradiance played a decisive role in the discovery of BH evaporation [6, 7].

Interest in BH superradiance was recently revived in different areas, including astrophysics and high-energy physics (via the gauge/gravity duality), and fundamental issues in General Relativity (GR). Superradiant instabilities can be used to constrain the mass of ultralight degrees of freedom [8–10], with important applications to dark-matter searches and to physics beyond the Standard Model. BH superradiance is also associated to the existence of new asymptotically flat, hairy BH solutions [11] and to phase transitions between spinning or charged black objects in asymptotically AdS spacetime [12–14] or in higher dimensions [15].

2 1 Introduction

Finally, superradiance is fundamental in deciding the stability of BHs and the fate of the gravitational collapse in confining geometries. In fact, the strong connection between some recent applications and the original phenomenon of superradiance has not always been fully recognized. This is the case, for instance, of holographic models of superfluids [16], which hinge on a spontaneous symmetry breaking of charged BHs in anti-de Sitter (AdS) spacetime [17]. In global AdS, the associated phase transition can be interpreted in terms of *superradiant instability* of a Reissner-Nordstrom AdS BH triggered by a charged scalar field [13, 18].

1.1 Milestones

The term superradiance was coined by Dicke in 1954 [19], but studies on related phenomena date back to at least 1947 with the pioneering work of Ginzburg and Frank [20] on the "anomalous" Doppler effect. It is impossible to summarize all the important work in the field in this book, but we think it is both useful and pedagogical to have a chronogram of some of the most relevant milestones. We will keep this list—necessarily incomplete and necessarily biased—confined mostly to the realm of GR, although we can't help making a reference to some of the breakthrough work in other areas. A more complete set of references can be found in the rest of this book.

- 1915 Einstein develops the General Theory of Relativity [21].
- 1916 Few months later, Schwarzschild derives the first solution of Einstein's equations, describing the gravitational field generated by a mass point [22]. Most of the subtleties and implications of this solution will only be understood many years later.
- 1920s In order to unify electromagnetism with GR, Kaluza and Klein propose a model in which the spacetime has five dimensions, one of which is compactified on a circle [23, 24].
- 1929 In his studies of the Dirac equation, Klein finds that electrons can "cross" a potential barrier without the exponential damping expected from nonrelativistic quantum tunneling [1]. This process was soon dubbed *Klein paradox* by Sauter. The expression was later used to describe an incorrectly obtained phenomenon of fermion superradiance (Klein's original work correctly shows that no superradiance occurs for fermions). An interesting historical account of these events is given by Manogue [25].
- 1931 Chandrasekhar derives an upper limit for white dwarf masses, above which electron degeneracy pressure cannot sustain the star [26]. The Chandrasekhar limit was subsequently extended to NSs by Oppenheimer and Volkoff [27].
- 1934 Vavilov and Cherenkov discover spontaneous emission from a charge moving uniformly and superluminally in a dielectric. The effect was interpreted theoretically by Tamm and Frank in 1937 [28]. In 1958, Tamm, Frank and Cherenkov receive the Nobel prize in physics for these studies.

1.1 Milestones 3

- 1937 Kapitska discovers superfluidity in liquid helium.
- 1945 Ginzburg and Frank discuss transition radiation [29].
- 1947 Ginzburg and Frank discover an "anomalous Doppler effect" [20]: the emission of radiation by a system moving faster than the phase velocity of electromagnetic waves in a medium and followed by the *excitation* (rather than by the standard de-excitation) to a higher energy level.
- 1947 Pierce describes a "travelling wave tube amplifier", where an electron beam *extracts* energy from an electromagnetic wave travelling at a speed less than its vacuum value. The electromagnetic wave is forced to slow down using an helix electrode, a spiral of wire around the electron beam [30, 31].
- 1953 Smith and Purcell experimentally show that motion near finite-size objects induces radiation emission, or "diffraction radiation" [32].
- 1954 Dicke coins the term "superradiance" in the context of coherent emission in quantum optics [19]. The first high-resolution measurement of superradiance using coherent synchrotron radiation was recently achieved [33].
- 1957 Regge and Wheeler [34] analyze a special class of gravitational perturbations of the Schwarzschild geometry. This effectively marks the birth of BH perturbation theory.
- 1958 Finkelstein understands that the r=2M surface of the Schwarzschild geometry is not a singularity but a horizon [35]. The so-called "golden age of GR" begins: in a few years there would be an enormous progress in the understanding of GR and of its solutions.
- 1962 Newman and Penrose [36] develop a formalism to study gravitational radiation using spin coefficients.
- 1963 Kerr [37] discovers the mathematical solution of Einstein's field equations describing rotating BHs. In the same year, Schmidt identifies the first quasar [38]. Quasars are now believed to be supermassive BHs, described by the Kerr solution.
- 1964 The UHURU orbiting X-ray observatory makes the first surveys of the X-ray sky discovering over 300 X-ray "stars". One of these X-ray sources, Cygnus X-1, is soon accepted as the first plausible stellar-mass BH candidate (see e.g. [39]).
- 1967 Wheeler [40, 41] coins the term *black hole* (see the April 2009 issue of *Physics Today*, and [42] for a fascinating, first-person historical account).
- 1969 Hawking's singularity theorems imply that collapse of ordinary matter leads, under generic conditions, to spacetime singularities. In the same year Penrose conjectures that these singularities, where quantum gravitational effects become important, are generically contained within BHs, the so-called *Cosmic Censorship Conjecture* [43, 44].
- 1969 Penrose shows that the existence of an ergoregion allows to extract energy and angular momentum from a Kerr BH and to amplify energy in particle collisions [43].
- 1970 Zerilli [45, 46] extends the Regge-Wheeler analysis to general perturbations of a Schwarzschild BH, reducing the problem to the study of a pair of

4 1 Introduction

- Schrödinger-like equations, and computing the gravitational radiation emitted by infalling test particles.
- 1970 Vishveshwara [47] studies numerically the scattering of gravitational waves by BHs: at late times the waveform consists of damped sinusoids, now called ringdown waves. The latter coincide with the BH quasinormal modes (QNMs) [48–52].
- 1971 Zeldovich shows that dissipative rotating bodies amplify incident waves [2, 3]. In the same study, quantum spontaneous pair creation by rotating bodies is also predicted, which effectively is a precursor to Hawking's result on BH evaporation. Aspects of the quantization procedure of test fields in the Kerr geometry were further independently elaborated by Starobinski [53, 54] and Deruelle and collaborators [55, 56].
- 1972–1974 Teukolsky [57] decouples and separates the equations for perturbations in the Kerr geometry using the Newman-Penrose formalism [36]. In the same year, Teukolsky and Press discuss quantitatively the superradiant scattering from a spinning BH [58]. They predict that, if confined, superradiance can give rise to *BH bombs* and *floating orbits* around spinning BHs [59].
- 1973 Working independently from Teukolsky, Unruh separates the massless spin-1/2 equations on a Kerr background and proves the absence of superradiance for massless fermions [60]. The result was later generalized to massive fermions by Chandrasekhar [61] and by Iyer and Kumar [62].
- 1975 Using quantum field theory in curved space and building on Zeldovich's 1971 result, Hawking finds that BHs have a thermal emission [6]. This result is one of the most important links between general relativity, quantum mechanics and thermodynamics.
- 1977 Blandford and Znajek propose a mechanism to extract energy from rotating BHs immersed in force-free magnetic fields [63]. This is thought to be one of the main mechanisms behind jet formation.
- 1976–1980 Damour, Deruelle and Ruffini discover that superradiance triggers an instability of the Kerr BH solution against massive scalar fields [64]. The study is then formalized by Detweiler [65] and by Zouros and Eardley [66].
- 1978 Friedman [67] shows that horizonless spacetimes with ergoregions are unstable.
- 1983 Chandrasekhar's monograph [68] summarizes the state of the art in BH perturbation theory, elucidating connections between different formalisms.
- 1985 Leaver [69–71] provides the most accurate method to date to compute BH QNMs using continued fraction representations of the relevant wavefunctions. Recently, accurate spectral methods have been developed to handle PDEs [72].
- 1986 McClintock and Remillard [73] show that the X-ray nova A0620-00 contains a compact object of mass almost certainly larger than $3M_{\odot}$, paving the way for the identification of many more stellar-mass BH candidates.
- 1986 Myers and Perry construct higher-dimensional rotating, topologically spherical, BH solutions [74].
- 1992 In a series of papers, Kojima develops the theory of linear perturbations of a slowly-rotating, relativistic star [75–77].

1.1 Milestones 5

1998 Maldacena formulates the AdS/CFT duality conjecture [78]. Shortly afterward, the papers by Gubser et al. [79] and Witten [80] establish a concrete quantitative recipe for the duality. The AdS/CFT era begins. In the same year, the correspondence is generalized to nonconformal theories in a variety of approaches. The terms "gauge/string duality", "gauge/gravity duality" and "holography" appear, referring to these generalized settings (we refer to [81] for a review).

- 1999 Banks and Fischler [82] show that in braneworld scenarios BHs could be produced in particle accelerators. Shortly after, it is proposed to look for BH production in the LHC and in ultra high-energy cosmic rays [83, 84].
- 2001 Emparan and Reall provide the first example of a stationary asymptotically flat vacuum solution with an event horizon of nonspherical topology: the "black ring" [85].
- 2003 In a series of papers [86–88], Kodama and Ishibashi extend the Regge-Wheeler-Zerilli formalism to higher dimensions.
- 2004 Small, rapidly spinning Kerr-AdS BHs are found to be unstable because of the AdS boundary providing a natural confinement mechanism for superradiant radiation [12]. Rigorous growth-rate estimates for generic initial data are provided in [89].
- 2005–2007 The LIGO and Virgo detectors reach design sensitivity [90].
- 2005–2009 The D1-D5 system is used as a toy model to understand the microscopic origin of superradiant scattering [91, 92]. For horizonless geometries, ergoregion instabilities lead precisely to Hawking radiation [93, 94].
- 2008 Gubser proposes a spontaneous symmetry breaking mechanism, giving an effective mass to charged scalars in AdS [17]. Shortly afterwards, Hartnoll, Herzog and Horowitz provide a nonlinear realization of the mechanism, building the holographic analog of a superfluid [16]. Depending on the magnitude of the induced mass, tachyonic or superradiant instabilities may be triggered in BH spacetimes [13, 18, 95, 96].
- 2009 The string-axiverse scenario is proposed, where a number of ultralight degrees of freedom—prone to superradiant instabilities around spinning BHs—are conjectured to exist [97]. Precision measurements of mass and spin of BHs may be used to explore some of the consequences of this scenario [8].
- 2011 Superradiant instabilities are shown to drive AdS BHs to hairy configurations [13, 14].
- 2011 Floating orbits around Kerr BHs are predicted in scalar-tensor theories as a generic outcome of superradiant amplification of scalar waves [98].
- 2012 Rotating Kerr BHs are shown to be linearly unstable against massive vector field perturbations [9, 99, 100] and massive tensor field perturbations [10]. Competitive bounds on the photon and graviton mass are derived from the observations of spinning BHs [101].
- 2013 Superradiance is shown to occur at full nonlinear level [102].
- 2014 The development of superradiant instabilities is studied nonlinearly [103].
- 2014 Asymptotically flat, hairy BH solutions are constructed analytically [104] and numerically [11]. These are thought to be one possible end-state of superra-

6 1 Introduction

diant instabilities for complex scalar fields. The superradiance threshold of the standard Kerr solution marks the onset of a phase transition towards a hairy BH.

2014 Reissner-Nordstrom de Sitter BHs are found to be unstable against charged scalar perturbations [105]. The unstable modes satisfy the superradiant condition [106].

References

- O. Klein, Die reflexion von elektronen an einem potentialsprung nach der relativistischen dynamik von dirac. Z. Phys. 53(3-4), 157-165 (1929). http://dx.doi.org/10.1007/BF01339716
- 2. Y.B. Zel'dovich, Pis'ma Zh. Eksp. Teor. Fiz. 14, 270 (1971) [JETP Lett. 14, 180 (1971)]
- 3. Y.B. Zel'dovich, Zh. Eksp. Teor. Fiz 62, 2076 (1972) [Sov. Phys. JETP 35, 1085 (1972)]
- 4. J. Bekenstein, Extraction of energy and charge from a black hole. Phys. Rev. **D7**, 949–953 (1973)
- 5. J.D. Bekenstein, M. Schiffer, The many faces of superradiance. Phys. Rev. **D58**, 064014 (1998). arXiv:gr-qc/9803033 [gr-qc]
- 6. S. Hawking, Particle creation by black holes. Commun. Math. Phys. 43, 199–220 (1975)
- 7. S. Hawking, A Brief History of Time (Bantam Dell Publishing Group, New York, 1988)
- 8. A. Arvanitaki, S. Dubovsky, Exploring the string axiverse with precision black hole physics. Phys. Rev. **D83**, 044026 (2011). arXiv:1004.3558 [hep-th]
- 9. P. Pani, V. Cardoso, L. Gualtieri, E. Berti, A. Ishibashi, Black hole bombs and photon mass bounds. Phys. Rev. Lett. 109, 131102 (2012). arXiv:1209.0465 [gr-qc]
- R. Brito, V. Cardoso, P. Pani, Massive spin-2 fields on black hole spacetimes: instability of the Schwarzschild and Kerr solutions and bounds on the graviton mass. Phys. Rev. D88, 023514 (2013). arXiv:1304.6725 [gr-qc]
- 11. C.A.R. Herdeiro, E. Radu, Kerr black holes with scalar hair. Phys. Rev. Lett. 112, 221101 (2014). arXiv:1403.2757 [gr-qc]
- 12. V. Cardoso, O.J. Dias, Small Kerr-anti-de Sitter black holes are unstable. Phys. Rev. **D70**, 084011 (2004). arXiv:hep-th/0405006 [hep-th]
- 13. O.J. Dias, P. Figueras, S. Minwalla, P. Mitra, R. Monteiro et al., Hairy black holes and solitons in global AdS_5 . J. High Energy Phys. 1208, 117 (2012). arXiv:1112.4447 [hep-th]
- 14. O.J. Dias, G.T. Horowitz, J.E. Santos, Black holes with only one killing field. J. High Energy Phys. 1107, 115 (2011). arXiv:1105.4167 [hep-th]
- M. Shibata, H. Yoshino, Bar-mode instability of rapidly spinning black hole in higher dimensions: numerical simulation in general relativity. Phys. Rev. D81, 104035 (2010). arXiv:1004.4970 [gr-qc]
- S.A. Hartnoll, C.P. Herzog, G.T. Horowitz, Building a holographic superconductor. Phys. Rev. Lett. 101, 031601 (2008). arXiv:0803.3295 [hep-th]
- S.S. Gubser, Breaking an Abelian gauge symmetry near a black hole horizon. Phys. Rev. D78, 065034 (2008). arXiv:0801.2977 [hep-th]
- 18. S.A. Hartnoll, Horizons, holography and condensed matter (2011). arXiv:1106.4324 [hep-th]
- 19. R. Dicke, Coherence in spontaneous radiation processes. Phys. Rev. 93, 99–110 (1954)
- 20. V.L. Ginzburg, I.M. Frank, Dokl. Akad. Nauk Ser. Fiz. SSSR 56 583 (1947)
- 21. A. Einstein, The foundation of the general theory of relativity. Ann. Phys. 49, 769–822 (1916)
- 22. K. Schwarzschild, On the gravitational field of a mass point according to Einstein's theory. Sitzungsber. Preuss. Akad. Wiss. Berlin (Math. Phys.) 1916, 189–196 (1916). arXiv:physics/9905030 [physics]
- T. Kaluza, On the problem of unity in physics. Sitzungsber. Preuss. Akad. Wiss. Berlin (Math. Phys.) 1921, 966–972 (1921).

References 7

O. Klein, Quantum theory and five-dimensional theory of relativity (In German and English).
 Phys. 37, 895–906 (1926)

- 25. C.A. Manogue, The Klein paradox and superradiance. Ann. Phys. 181, 261–283 (1988)
- 26. S. Chandrasekhar, The maximum mass of ideal white dwarfs. Astrophys. J. 74, 81–82 (1931)
- 27. J. Oppenheimer, G. Volkoff, On massive neutron cores. Phys. Rev. 55, 374–381 (1939)
- 28. I.E. Tamm, I.M. Frank, Dokl. Akad. Nauk SSSR 14, 109 (1937)
- 29. V. Ginzburg, I. Frank, Radiation of a uniformly moving electron due to its transition from one medium into another. J. Phys. (USSR) 9, 353–362 (1945)
- 30. J. Pierce, *Electrons and Waves* (New York, Anchor Books, 1964)
- 31. http://www.r-type.org/articles/art-030.htm
- S. Smith, E. Purcell, Visible light from localized surface charges moving across a grating. Phys. Rev. 92, 1069 (1953)
- 33. B. Billinghurst, J. Bergstrom, L. Dallin, M. de Jong, T. May et al., Observation of superradiant synchrotron radiation in the terahertz region. Phys. Rev. ST Accel. Beams **16**(6), 060702 (2013)
- T. Regge, J.A. Wheeler, Stability of a Schwarzschild singularity. Phys. Rev. 108, 1063–1069 (1957)
- 35. D. Finkelstein, Past-future asymmetry of the gravitational field of a point particle. Phys. Rev. 110, 965–967 (1958)
- 36. E. Newman, R. Penrose, An approach to gravitational radiation by a method of spin coefficients. J. Math. Phys. 3, 566–578 (1962)
- 37. R.P. Kerr, Gravitational field of a spinning mass as an example of algebraically special metrics. Phys. Rev. Lett. 11, 237–238 (1963)
- 38. M. Schmidt, 3C 273: a star-like object with large red-shift. Nature 197, 1040 (1963)
- 39. C.T. Bolton, Cygnus X-1-Dimensions of the system. Nature **240**, 124 (1972)
- 40. R. Ruffini, J.A. Wheeler, Introducing the black hole. Phys. Today 24, 30 (1971)
- 41. J.A. Wheeler, Our universe: the known and the unknown. Phys. Teach. 7, 1 (1969)
- 42. J.A. Wheeler, K. Ford, *Geons, Black Holes, and Quantum Foam: A Life in Physics* (Norton, New York, 1998), p. 380
- 43. R. Penrose, Nuovo Cimento. J. Serie 1, 252 (1969)
- 44. R.M. Wald, Gravitational collapse and cosmic censorship (1997). arXiv:gr-qc/9710068 [gr-qc]
- 45. F.J. Zerilli, Effective potential for even parity Regge-Wheeler gravitational perturbation equations. Phys. Rev. Lett. **24**, 737–738 (1970)
- 46. F. Zerilli, Gravitational field of a particle falling in a schwarzschild geometry analyzed in tensor harmonics. Phys. Rev. **D2**, 2141–2160 (1970)
- 47. C.V. Vishveshwara, Scattering of gravitational radiation by a Schwarzschild black hole. Nature **227**, 936 (1970)
- 48. H.-P. Nollert, TOPICAL REVIEW: quasinormal modes: the characteristic 'sound' of black holes and neutron stars. Classical Quantum Gravity 16, R159–R216 (1999)
- 49. K.D. Kokkotas, B.G. Schmidt, Quasinormal modes of stars and black holes. Living Rev. Relativ. 2, 2 (1999). arXiv:gr-qc/9909058 [gr-qc]
- 50. V. Ferrari, L. Gualtieri, Quasi-normal modes and gravitational wave astronomy. Gen. Relativ. Gravit. 40, 945–970 (2008). arXiv:0709.0657 [gr-qc]
- 51. E. Berti, V. Cardoso, A.O. Starinets, Quasinormal modes of black holes and black branes. Classical Quantum Gravity **26**, 163001 (2009). arXiv:0905.2975 [gr-qc]
- 52. R. Konoplya, A. Zhidenko, Quasinormal modes of black holes: from astrophysics to string theory. Rev. Mod. Phys. 83, 793-836 (2011). arXiv:1102.4014 [gr-qc]
- 53. A. Starobinski, Amplification of waves during reflection from a rotating black hole. Zh. Eksp. Teor. Fiz. **64**, 48. (1973) [Sov. Phys. JETP **37**, 28 (1973)]

8 1 Introduction

 A.A. Starobinski, S.M. Churilov, Amplification of electromagnetic and gravitational waves scattered by a rotating black hole. Zh. Eksp. Teor. Fiz. 65, 3 (1973) [Sov. Phys. JETP 38, 1 (1973)]

- N. Deruelle, R. Ruffini, Quantum and classical relativistic energy states in stationary geometries. Phys. Lett. B52, 437–441 (1974)
- 56. N. Deruelle, R. Ruffini, Klein paradox in a Kerr geometry. Phys. Lett. **B57**, 248 (1975)
- 57. S.A. Teukolsky, Rotating black holes—separable wave equations for gravitational and electromagnetic perturbations. Phys. Rev. Lett. 29, 1114–1118 (1972)
- 58. S. Teukolsky, W. Press, Perturbations of a rotating black hole. III Interaction of the hole with gravitational and electromagnet ic radiation. Astrophys. J. **193**, 443–461 (1974)
- 59. W.H. Press, S.A. Teukolsky, Floating orbits, superradiant scattering and the black-hole bomb. Nature 238, 211–212 (1972)
- W. Unruh, Separability of the Neutrino equations in a Kerr background. Phys. Rev. Lett. 31, 1265–1267 (1973)
- S. Chandrasekhar, The solution of Dirac's equation in Kerr geometry. R. Soc. Lond. Proc. Ser. A 349, 571–575 (1976)
- B.R. Iyer, A. Kumar, Note on the absence of massive fermion superradiance from a Kerr black hole. Phys. Rev. 18, 4799–4801 (1978)
- 63. R. Blandford, R. Znajek, Electromagnetic extractions of energy from Kerr black holes. Mon. Not. R. Astron. Soc. **179**, 433–456 (1977)
- T. Damour, N. Deruelle, R. Ruffini, On quantum resonances in stationary geometries. Lett. Nuovo Cim. 15, 257–262 (1976)
- S.L. Detweiler, Klein-Gordon equation and rotating black holes. Phys. Rev. D22, 2323–2326 (1980)
- T. Zouros, D. Eardley, Instabilities of massive scalar perturbations of a rotating black hole. Ann. Phys. 118, 139–155 (1979)
- 67. J.L. Friedman, Ergosphere instability. Commun. Math. Phys. 63, 243–255 (1978)
- S. Chandrasekhar, The Mathematical Theory of Black Holes (Oxford University Press, Oxford, 1983)
- E. Leaver, An Analytic representation for the quasi normal modes of Kerr black holes. Proc. R. Soc. Lond. A402, 285–298 (1985)
- E.W. Leaver, Solutions to a generalized spheroidal wave equation: Teukolsky's equations in general relativity, and the two-center problem in molecular quantum mechanics. J. Math. Phys. 27, 1238 (1986)
- E.W. Leaver, Spectral decomposition of the perturbation response of the Schwarzschild geometry. Phys. Rev. D34, 384–408 (1986)
- V. Cardoso, S.J. Dias, G.S. Hartnett, L. Lehner, J.E. Santos, Holographic thermalization, quasinormal modes and superradiance in Kerr-AdS. J. High Energy Phys. 1404, 183 (2014). arXiv:1312.5323 [hep-th]
- 73. J.E. McClintock, R.A. Remillard, The black hole binary A0620-00. Astrophys. J. **308**, 110 (1986)
- R.C. Myers, M. Perry, Black holes in higher dimensional space-times. Ann. Phys. 172, 304 (1986)
- 75. Y. Kojima, Equations governing the nonradial oscillations of a slowly rotating relativistic star. Phys. Rev. **D46**, 4289–4303 (1992)
- Y. Kojima, Coupled pulsations between polar and axial modes in a slowly rotating relativistic star. Prog. Theor. Phys. 90, 977–990 (1993)
- Y. Kojima, Normal modes of relativistic stars in slow rotation limit. Astrophys. J. 414, 247– 253 (1993)
- 78. J.M. Maldacena, The large N limit of superconformal field theories and supergravity. Adv. Theor. Math. Phys. 2, 231–252 (1998). arXiv:hep-th/9711200
- S.S. Gubser, I.R. Klebanov, A.M. Polyakov, Gauge theory correlators from non-critical string theory. Phys. Lett. B428, 105–114 (1998). arXiv:hep-th/9802109

References 9

80. E. Witten, Anti-de Sitter space and holography. Adv. Theor. Math. Phys. 2, 253–291 (1998). arXiv:hep-th/9802150

- 81. O. Aharony, S.S. Gubser, J.M. Maldacena, H. Ooguri, Y. Oz, Large N field theories, string theory and gravity. Phys. Rep. 323, 183–386 (2000). arXiv:hep-th/9905111
- 82. T. Banks, W. Fischler, A model for high-energy scattering in quantum gravity (1999). arXiv:hep-th/9906038 [hep-th]
- 83. S. Dimopoulos, G.L. Landsberg, Black holes at the LHC. Phys. Rev. Lett. 87, 161602 (2001). arXiv:hep-ph/0106295 [hep-ph]
- 84. S.B. Giddings, S.D. Thomas, High-energy colliders as black hole factories: the end of short distance physics. Phys. Rev. **D65**, 056010 (2002). arXiv:hep-ph/0106219 [hep-ph]
- 85. R. Emparan, H.S. Reall, A rotating black ring solution in five-dimensions. Phys. Rev. Lett. 88, 101101 (2002). arXiv:hep-th/0110260 [hep-th]
- 86. H. Kodama, A. Ishibashi, A master equation for gravitational perturbations of maximally symmetric black holes in higher dimensions. Prog. Theor. Phys. 110, 701–722 (2003). arXiv:hep-th/0305147
- 87. A. Ishibashi, H. Kodama, Stability of higher-dimensional Schwarzschild black holes. Prog. Theor. Phys. 110, 901–919 (2003). arXiv:hep-th/0305185
- 88. H. Kodama, A. Ishibashi, Master equations for perturbations of generalized static black holes with charge in higher dimensions. Prog. Theor. Phys. 111, 29–73 (2004). arXiv:hep-th/0308128
- 89. Y. Shlapentokh-Rothman, Exponentially growing finite energy solutions for the Klein-Gordon equation on sub-extremal Kerr spacetimes. Commun. Math. Phys. **329**, 859–891 (2014). arXiv:1302.3448 [gr-qc]
- 90. LIGO Scientific Collaboration, LIGO: The Laser Interferometer Gravitational-Wave Observatory (2009). arXiv:0711.3041 [gr-qc]
- 91. V. Cardoso, O.J. Dias, J.L. Hovdebo, R.C. Myers, Instability of non-supersymmetric smooth geometries. Phys. Rev. **D73**, 064031 (2006). arXiv:hep-th/0512277 [hep-th]
- 92. O.J. Dias, R. Emparan, A. Maccarrone, Microscopic theory of black hole superradiance. Phys. Rev. **D77**, 064018 (2008). arXiv:0712.0791 [hep-th]
- 93. B.D. Chowdhury, S.D. Mathur, Radiation from the non-extremal fuzzball. Classical Quantum Gravity 25, 135005 (2008). arXiv:0711.4817 [hep-th]
- 94. B.D. Chowdhury, S.D. Mathur, Pair creation in non-extremal fuzzball geometries. Classical Quantum Gravity 25, 225021 (2008). arXiv:0806.2309 [hep-th]
- O.J. Dias, R. Monteiro, H.S. Reall, J.E. Santos, A scalar field condensation instability of rotating anti-de Sitter black holes. J. High Energy Phys. 1011, 036 (2010). arXiv:1007.3745 [hep-th]
- 96. P. Basu, J. Bhattacharya, S. Bhattacharyya, R. Loganayagam, S. Minwalla et al., Small hairy black holes in global ads spacetime. J. High Energy Phys. **1010**, 045 (2010). arXiv:1003.3232 [hep-th]
- 97. A. Arvanitaki, S. Dimopoulos, S. Dubovsky, N. Kaloper, J. March-Russell, String axiverse. Phys. Rev. **D81**, 123530 (2010). arXiv:0905.4720 [hep-th]
- 98. V. Cardoso, S. Chakrabarti, P. Pani, E. Berti, L. Gualtieri, Floating and sinking: the imprint of massive scalars around rotating black holes. Phys. Rev. Lett. **107**, 241101 (2011). arXiv:1109.6021 [gr-qc]
- 99. P. Pani, V. Cardoso, L. Gualtieri, E. Berti, A. Ishibashi, Perturbations of slowly rotating black holes: massive vector fields in the Kerr metric. Phys. Rev. **D86**, 104017 (2012). arXiv:1209.0773 [gr-qc]
- 100. H. Witek, V. Cardoso, A. Ishibashi, U. Sperhake, Superradiant instabilities in astrophysical systems. Phys. Rev. **D87**, 043513 (2013). arXiv:1212.0551 [gr-qc]
- Particle Data Group Collaboration, K. Olive et al., Review of particle physics. Chin. Phys. C38, 090001 (2014)
- 102. W.E. East, F.M. Ramazanoglu, F. Pretorius, Black hole superradiance in dynamical spacetime. Phys. Rev. **D89**, 061503 (2014). arXiv:1312.4529 [gr-qc]

10 1 Introduction

103. H. Okawa, H. Witek, V. Cardoso, Black holes and fundamental fields in numerical relativity: initial data construction and evolution of bound states. Phys. Rev. **D89**, 104032 (2014). arXiv:1401.1548 [gr-qc]

- 104. S. Hod, Stationary scalar clouds around rotating black holes. Phys. Rev. **D86**, 104026 (2012). arXiv:1211.3202 [gr-gc]
- 105. Z. Zhu, S.-J. Zhang, C. Pellicer, B. Wang, E. Abdalla, Stability of Reissner-Nordström black hole in de Sitter background under charged scalar perturbation. Phys. Rev. D90(4), 044042 (2014). arXiv:1405.4931 [hep-th]
- 106. R. Konoplya, A. Zhidenko, Charged scalar field instability between the event and cosmological horizons. Phys. Rev. **D90**, 064048 (2014). arXiv:1406.0019 [hep-th]

Chapter 2 Superradiance in Flat Spacetime

2.1 Klein Paradox: The First Example of Superradiance

The first treatment of what came to be known as the Klein paradox can be traced back to the original paper by Klein [1], who pioneered studies of Dirac's equation in the presence of a step potential. He showed that an electron beam propagating in a region with a large enough potential barrier V can emerge without the exponential damping expected from nonrelativistic quantum tunneling processes. When trying to understand if such a result was an artifact of the step-potential used by Klein, Sauter found that the essentials of the process were independent on the details of the potential barrier, although the probability of transmission decreases with decreasing slope [2]. *This* phenomenon was originally dubbed "Klein paradox" by Sauter¹ in 1931 [2].

Further studies by Hund in 1941 [5], now dealing with a charged scalar field and the Klein-Gordon equation, showed that the step potential could give rise to the production of pairs of charged particles when the potential is sufficiently strong. Hund tried—but failed—to derive the same result for fermions. It is quite interesting to note that this result can be seen as a precursor of the modern quantum field theory results of Schwinger [6] and Hawking [7] who showed that spontaneous pair production is possible in the presence of strong electromagnetic and gravitational

¹The Klein paradox as we understand it today has an interesting history. Few years after Klein's original study (written in German), the expression *Klein paradox* appeared in some British literature in relation with *fermionic superradiance*: due to some confusion (and probably because Klein's paper didn't have an English translation), some authors wrongly interpreted Klein's results as if the fermionic current reflected by the potential barrier could be greater than the incident current. This result was due to an incorrect evaluation of the reflected and transmitted wave's group velocities, although Klein—following suggestions by Niels Bohr—had the correct calculation in the original work [3]. Although not explicitly mentioned by Klein, this phenomenon can actually happen for bosonic fields [4] and it goes under the name of *superradiant* scattering.

fields for both bosons and fermions. In fact we know today that the resolution of the "old" Klein paradox is due to the creation of particle—antiparticle pairs at the barrier, which explains the undamped transmitted part.

In the remaining of this section we present a simple treatment of bosonic and fermionic scattering, to illustrate these phenomena.

2.1.1 Bosonic Scattering

Consider a massless scalar field Φ minimally coupled to an electromagnetic potential A_{μ} in (1+1)-dimensions, governed by the Klein-Gordon equation

$$\Phi_{:\mu}^{\;\;;\mu} = 0\,, (2.1)$$

where we defined $\Phi_{;\mu} \equiv (\partial_{\mu} - ieA_{\mu})\Phi$ and e is the charge of the scalar field. For simplicity we consider an external potential $A^{\mu} = \{A_0(x), 0\}$, with the asymptotic behavior

$$A_0 \to \begin{cases} 0 & \text{as } x \to -\infty \\ V & \text{as } x \to +\infty \end{cases} . \tag{2.2}$$

With the ansatz $\Phi = e^{-i\omega t} f(x)$, Eq. (2.1) can be separated yielding the ODE

$$\frac{d^2f}{dx^2} + (\omega - eA_0)^2 f = 0. (2.3)$$

Consider a beam of particles coming from $-\infty$ and scattering off the potential with reflection and transmission amplitudes \mathcal{R} and \mathcal{T} respectively. With these boundary conditions, the solution to Eq. (2.1) behaves asymptotically as

$$f_{\rm in}(x) = \mathcal{I}e^{i\omega x} + \mathcal{R}e^{-i\omega x}, \quad \text{as } x \to -\infty,$$

 $f_{\rm in}(x) = \mathcal{T}e^{ikx}, \quad \text{as } x \to +\infty,$ (2.4)

where

$$k = \pm(\omega - eV). \tag{2.5}$$

To define the sign of ω and k we must look at the wave's group velocity. We require the incoming and the transmitted part of the waves to have positive group velocity, $\partial \omega/\partial k > 0$, so that they travel from the left to the right in the x-direction. Hence, we take $\omega > 0$ and the plus sign in (2.5).

The reflection and transmission coefficients depend on the specific shape of the potential A_0 . However one can easily show that the Wronskian

$$W = \tilde{f}_1 \frac{d\tilde{f}_2}{dx} - \tilde{f}_2 \frac{d\tilde{f}_1}{dx}, \qquad (2.6)$$

between two independent solutions, \tilde{f}_1 and \tilde{f}_2 , of (2.3) is conserved. From the Eq. (2.3) on the other hand, if f is a solution then its complex conjugate f^* is another linearly independent solution. Evaluating the Wronskian (2.6), or equivalently, the particle current density, for the solution (2.4) and its complex conjugate we find

$$|\mathcal{R}|^2 = |\mathcal{I}|^2 - \frac{\omega - eV}{\omega} |\mathcal{T}|^2 . \tag{2.7}$$

Thus, for

$$0 < \omega < eV, \tag{2.8}$$

it is possible to have superradiant amplification of the reflected current, i.e, $|\mathcal{R}| > |\mathcal{I}|$.

2.1.2 Fermionic Scattering

Now let us consider the Dirac equation for a spin- $\frac{1}{2}$ massless fermion Ψ , minimally coupled to the same electromagnetic potential A_{μ} as in Eq. (2.2),

$$\gamma^{\mu}\Psi_{;\mu} = 0, \qquad (2.9)$$

where γ^{μ} are the four Dirac matrices satisfying the anticommutation relation $\{\gamma^{\mu}, \gamma^{\nu}\} = 2g^{\mu\nu}$. The solution to (2.9) takes the form $\Psi = e^{-i\omega t}\chi(x)$, where χ is a two-spinor given by

$$\chi = \begin{pmatrix} f_1(x) \\ f_2(x) \end{pmatrix}. \tag{2.10}$$

Using the representation

$$\gamma^0 = \begin{pmatrix} i & 0 \\ 0 & -i \end{pmatrix}, \ \gamma^1 = \begin{pmatrix} 0 & i \\ -i & 0 \end{pmatrix}, \tag{2.11}$$

the functions f_1 and f_2 satisfy the system of equations:

$$df_1/dx - i(\omega - eA_0)f_2 = 0,$$

$$df_2/dx - i(\omega - eA_0)f_1 = 0.$$
(2.12)

One set of solutions can be once more formed by the 'in' modes, representing a flux of particles coming from $x \to -\infty$ being partially reflected (with reflection amplitude $|\mathcal{R}|^2$) and partially transmitted at the barrier

$$(f_1^{\text{in}}, f_2^{\text{in}}) = \begin{cases} (\mathcal{I}e^{i\omega x} - \mathcal{R}e^{-i\omega x}, \mathcal{I}e^{i\omega x} + \mathcal{R}e^{-i\omega x}) & \text{as } x \to -\infty \\ (\mathcal{T}e^{ikx}, \mathcal{T}e^{ikx}) & \text{as } x \to +\infty \end{cases} .$$
 (2.13)

On the other hand, the conserved current associated with the Dirac equation (2.9) is given by $j^{\mu} = -e\Psi^{\dagger}\gamma^{0}\gamma^{\mu}\Psi$ and, by equating the latter at $x \to -\infty$ and $x \to +\infty$, we find some general relations between the reflection and the transmission coefficients, in particular,

$$|\mathcal{R}|^2 = |\mathcal{I}|^2 - |\mathcal{T}|^2 . \tag{2.14}$$

Therefore, $|\mathcal{R}|^2 \leq |\mathcal{I}|^2$ for any frequency, showing that there is no superradiance for fermions. The same kind of relation can be found for massive fields [3].

The difference between fermions and bosons comes from the intrinsic properties of these two kinds of particles. Fermions have positive definite current densities and bounded transmission amplitudes $0 \le |\mathcal{T}|^2 \le |\mathcal{I}|^2$, while for bosons the current density can change its sign as it is partially transmitted and the transmission amplitude can be negative, $-\infty < \frac{\omega - eV}{\omega} |\mathcal{T}|^2 \le |\mathcal{I}|^2$. From the quantum field theory point of view one can understand this process as a spontaneous pair production phenomenon due to the presence of a strong electromagnetic field (see e.g. [3]). The number of fermionic pairs produced spontaneously in a given state is limited by the Pauli exclusion principle, while such limitation does not exist for bosons.

2.2 Superradiance and Pair Creation

To understand how pair creation is related to superradiance consider the potential used in the Klein paradox. Take a superradiant mode obeying Eq. (2.8) and $\mathcal{P} \leq 1$ to be the probability for spontaneous production of a single particle-antiparticle pair. The average number \bar{n} of bosonic and fermionic pairs in a given state follows the Bose-Einstein and the Fermi-Dirac distributions, respectively, [8]

$$\bar{n}_{B,F} = \frac{1}{1/\mathcal{P} \mp 1},$$
(2.15)

where the minus sign refers to bosons, whereas the plus sign in the equation above is dictated by the Pauli exclusion principle, which allows only one fermionic pair to be produced in the same state.

Now, by using a second quantization procedure, the number of pairs produced in a given state for bosons and fermions in the superradiant region (2.8) is [3]

$$\bar{n}_{\rm B} = \left| \frac{\omega - eV}{\omega} \right| |\mathcal{T}|^2 , \qquad \bar{n}_{\rm F} = |\mathcal{T}|^2 .$$
(2.16)

From Eq. (2.15) we see that $0 \le \bar{n}_F \le 1$ while $\bar{n}_B \to \infty$ when $\mathcal{P} \to 1$ and $\bar{n}_B \to 0$ when $\mathcal{P} \to 0$. Equations (2.15), (2.16) and (2.7) show that $|\mathcal{R}|^2 \to |\mathcal{I}|^2$ as $\mathcal{P} \to 0$, so that superradiance is possible only when $\mathcal{P} \neq 0$, i.e. superradiance occurs due to spontaneous pair creation. On the other hand, we also see that the bounded value for the amplification factor in fermions is due to the Pauli exclusion principle.

Although superradiance and spontaneous pair production in strong fields are related phenomena, they are nevertheless distinct. Indeed, pair production can occur without superradiance and it can occur whenever is kinematically allowed. On the other hand, superradiance is enough to ensure that bosonic spontaneous pair emission will occur. This is a well known result in BH physics. For example, in Sect. 3 we shall see that even nonrotating BHs do not allow for superradiance, but nonetheless emit Hawking radiation [7], the latter can be considered as the gravitational analogue of pair production in strong electromagnetic fields.

To examine the question of energy conservation in this process, let us follow the following thought experiment [4]. Consider a battery connected to two boxes, such that a potential V increase occurs between an outer grounded box and an inner box. An absorber is placed at the end of the inner box, which absorbs all particles incident on it. Let us consider an incident superradiant massless bosonic wave with charge e and energy $\omega < eV$. From (2.7) we see that

$$|\mathcal{R}|^2 - \frac{eV - \omega}{\omega} |\mathcal{T}|^2 = |\mathcal{I}|^2, \qquad (2.17)$$

The minus sign in front of $\frac{eV-\omega}{\omega} |\mathcal{T}|^2$ is a consequence of the fact that the current for bosons is not positive definite, and "negatively" charged waves have a negative current density. Since more particles are reflected than incident we can also picture the process in the following way: all particles incident on the potential barrier are reflected, however the incident beam stimulates pair creation at the barrier, which emits particles and antiparticles. Particles join the reflected beam, while the negative transmitted current can be interpreted as a flow of antiparticles with charge -e. All the particles incident with energy ω are reflected back with energy ω and in addition, because of pair creation, more particles with charge e and energy e join the beam. For each additional particle another one with charge e is transmitted to the box and transmits its energy to the absorber, delivering a kinetic energy $eV-\omega$. To keep the potential of the inner box at e0, the battery loses an amount of stored energy equal to e0. The total change of the system, battery plus boxes, is therefore e1 is the particle with energy e2 that is created to join the beam.

Now, imagine exactly the same experiment but $\omega > eV$, when superradiance does not occur, and $|\mathcal{R}|^2 \leq |\mathcal{I}|^2$. In this case the kinetic energy delivered to the absorber

is $\omega - eV$. An amount of energy eV is given to the battery and the system battery plus boxes gains a total energy ω . By energy conservation the reflected beam must have energy $-\omega$, which we can interpret as being due to the fact that the reflected beam is composed by antiparticles and the transmitted beam by particles.

Although the result might seem evident from the energetic point of view, we see that superradiance is connected to dissipation within the system. As we will see in the rest, this fact is a very generic feature of superradiance.

If we repeat the same experiment for fermions we see from (2.14) that $|\mathcal{R}|^2 + |\mathcal{T}|^2 = |\mathcal{I}|^2$. Since the current density for fermions is positive definite the flux across the potential barrier must be positive and, therefore, the flux in the reflected wave must be less than the incident wave. Since fewer particles are reflected than transmitted, then by energy conservation the total energy given to the battery-boxes system must be positive and given by ω . Thus the reflected beam has a negative energy $-\omega$, which can be interpreted as being due the production of antiparticles. In this case the kinetic energy delivered to the absorber will always be $|\omega - eV|$.

2.3 Superradiance and Spontaneous Emission by a Moving Object

As counterintuitive as it can appear at first sight, in fact superradiance can be understood purely kinematically in terms of Lorentz transformations. Consider an object moving with velocity \mathbf{v}_i (with respect to the laboratory frame) and emitting/absorbing a photon. Let the initial 4-momentum of the object be $p_i^{\mu} = (E_i, \mathbf{p}_i)$ and the final one be $p_f^{\mu} = (E_f, \mathbf{p}_f)$ with $E_f = E_i \mp \hbar \omega$ and $\mathbf{p}_f = \mathbf{p}_i \mp \hbar \mathbf{k}$, where $(\hbar \omega, \hbar \mathbf{k})$ is the 4-momentum of the emitted/absorbed photon, respectively. The object's rest mass can be computed by using Lorentz transformations to go to the comoving frame,

$$\mathcal{E}_i = \gamma_i (E_i - \mathbf{v}_i \cdot \mathbf{p}_i) , \qquad (2.18)$$

and similarly for \mathcal{E}_f , where $\gamma_i = 1/\sqrt{1-\mathbf{v}_i^2}$. Assuming $\mathbf{v}_f = \mathbf{v}_i + \delta \mathbf{v}$, to zeroth order in the recoil term $\delta \mathbf{v}$ the increase of the rest mass reads

$$\Delta \mathcal{E} \equiv \mathcal{E}_f - \mathcal{E}_i = \mp \gamma_i \hbar(\omega - \mathbf{v}_i \cdot \mathbf{k}) + \mathcal{O}(\delta \mathbf{v}), \qquad (2.19)$$

where the minus and plus signs refer to emission and absorption of the photon, respectively. Therefore, if the object is in its fundamental state ($\mathcal{E}_i < \mathcal{E}_f$), the emission of a photon can only occur when the Ginzburg-Frank condition is satisfied, namely [9, 10]

$$\omega(k) - \mathbf{v}_i \cdot \mathbf{k} < 0, \tag{2.20}$$

where $k = |\mathbf{k}|$ and $\omega(k)$ is given by the photon's dispersion relation. In vacuum, $\omega(k) = k$ so that the equation above can never be fulfilled. This reflects the obvious fact that Lorentz invariance forbids a particle in its ground state to emit a photon in vacuum. However, spontaneous emission can occur any time the dispersion relation allows for $\omega < k$. For example, suppose that the particle emits a massive wave whose dispersion relation is $\omega = \sqrt{\mu^2 + k^2}$, where μ is the mass of the emitted radiation. For modes with $\mu \ll k$, Eq. (2.20) reads

$$\frac{\mu^2}{2k^2} < v_i \cos \vartheta - 1 \le 0, \tag{2.21}$$

where $\mathbf{v}_i \cdot \mathbf{k} = v_i k \cos \vartheta$. Hence, only unphysical radiation with $\mu^2 < 0$ can be spontaneously radiated, this fact being related to the so-called *tachyonic instability* and it is relevant for those theories that predict radiation with an effective mass μ through nonminimal couplings (e.g. this happens in scalar-tensor theories of gravity [11] and it is associated to so-called spontaneous scalarization [12]).

Another relevant example occurs when the object is travelling through an isotropic dielectric that is transparent to radiation. In this case $\omega = k/n(\omega)$ where $n(\omega) = 1/v_{\rm ph}$ is the medium's refractive index and $v_{\rm ph}$ is the phase velocity of radiation in the medium. In this case Eq. (2.20) reads

$$\cos\vartheta > \frac{v_{\rm ph}}{v_i}.\tag{2.22}$$

Therefore, if the object's speed is smaller than the phase velocity of radiation, no spontaneous emission can occur, whereas in the opposite case spontaneous superradiance occurs when $\vartheta < \vartheta_c = \cos^{-1}(v_{\rm ph}/v_i)$. This phenomenon was dubbed anomalous Doppler effect [9, 10]. The angle ϑ_c defines the angle of coherent scattering, i.e. a photon incident with an angle ϑ_c can be absorbed and re-emitted along the same direction without changing the object motion, even when the latter is structureless, i.e. when $\mathcal{E}_i = \mathcal{E}_f$.

As discussed in [13], spontaneous superradiance is not only a simple consequence of Lorentz invariance, but it also follows from thermodynamical arguments. Indeed, for a finite body that absorbs nearly monochromatic radiation, the second law of thermodynamics implies

$$(\omega - \mathbf{v}_i \cdot \mathbf{k})a(\omega) > 0, \qquad (2.23)$$

where $a(\omega)$ is the characteristic absorptivity of the body. Hence, the superradiance condition is associated with a negative absorptivity, that is, superradiance is intimately connected to *dissipation* within the system.

2.3.1 Cherenkov Emission and Superradiance

The emission of radiation by a charge moving superluminally relative to the phase velocity of radiation in a dielectric—also known as the Vavilov-Cherenkov effect—has a simple interpretation in terms of spontaneous superradiance [14]. A point charge has no internal structure, so $\Delta \mathcal{E} = 0$ in Eq. (2.19). Such condition can only be fulfilled when the charge moves faster than the phase velocity of radiation in the dielectric and it occurs when photons are emitted with an angle

$$\vartheta_c = \cos^{-1}(v_{\rm ph}/v_i). \tag{2.24}$$

In general, $v_{\rm ph}=v_{\rm ph}(\omega)$ and radiation at different frequencies will be emitted in different directions. In case of a dielectric with zero dispersivity, the refraction index is independent from ω and the front of the photons emitted during the charge's motion forms a cone with opening angle $\pi-2\vartheta_c$. Such cone is the electromagnetic counterpart of the Mach cone that characterizes a shock wave produced by supersonic motion as will be discussed in Sect. 2.4.

2.3.2 Cherenkov Radiation by Neutral Particles

In their seminal work, Ginzburg and Frank also studied the anomalous Doppler effect occurring when a charge moves through a pipe drilled into a dielectric [9, 10]. More recently, Bekenstein and Schiffer have generalized this effect to the case of a *neutral* object which sources a large gravitational potential (e.g. a neutral BH) moving through a dielectric [13]. As we now briefly discuss, this effect is similar to Cherenkov emission, although it occurs even in presence of neutral particles.

Consider first a neutral massive object with mass M surrounded by a ionized, two-component plasma of electrons and positively-charged nuclei. It was realized by Milne and Eddington that in hydrostatic and thermodynamic equilibrium, an electric field necessarily develops to keep protons and electrons from separating completely [15–17]. In equilibrium, the partial pressure $P_{\rm e,N}$ of electrons and nuclei is, respectively

$$\frac{\partial \log P_{\rm e,N}}{\partial r} = -\frac{m_{\rm e,N}g}{kT} - \frac{eE}{kT}, \qquad (2.25)$$

where $m_{\rm e,N}$ is the mass of an electron and of the nucleon, k is the Boltzmann constant, T the temperature of the plasma and g the local gravitational acceleration. Equality of the pressure gradient—achieved when electrons and protons are

² Because we want to use thermodynamic equilibrium at the same temperature T, it is physically more transparent to work with a plasma than with a dielectric, as done instead in [13].

separated—happens for an electric field

$$eE = \frac{(m_{\rm N} - m_{\rm e})g}{2} \sim \frac{m_{\rm N}g}{2}$$
 (2.26)

Consider now the same neutral massive object traveling through the ionized plasma. As we saw, the gravitational pull of the object will polarize the plasma because the positively charged nuclei are attracted more than the electrons. The polarization cloud is associated with an electric dipole field **E** that balances the gravitational force **g** and that acts as source of superradiant photons. This follows by thermodynamical arguments, even neglecting the entropy increase due to possible accretion [13]. The superradiant energy in this case comes from the massive object kinetic energy. Thus, the effect predicts that the object slows down because of superradiant emission of photons in the dielectric.

In fact, the effect can be mapped into a Cherenkov process by noting that, in order to balance the gravitational pull, $e\mathbf{E} \sim -m_N \mathbf{g}$. Poisson equation then implies [13]

$$\nabla \cdot \mathbf{E} = 4\pi G \frac{Mm_N}{e} \delta(r - r_0), \qquad (2.27)$$

where r_0 is the massive object position and for clarity we have restored the factor G. This equation is equivalent to that of an electric field sourced by a pointlike charge

$$Q = \frac{Gm_N M}{e} \sim 5 \times 10^4 A \left(\frac{M}{10^{17} \text{g}}\right) e.$$
 (2.28)

where A is the mass number of the atoms. Assuming that the plasma relaxation time is short enough, such effective charge will emit Cherenkov radiation whenever the Ginzburg-Frank condition (2.20) is met. Note that, modulo accretion issues which are not relevant to us here, the above derivation is equally valid for BHs. As already noted in [13] a primordial BH with $M \sim 10^{17} {\rm g}$ moving fast through a dielectric would Cherenkov radiate just like an elementary particle with charge $Q \sim 5 \times 10^4 e$. In particular, the Frank-Tamm formula for the energy dE emitted per unit length dx and per unit of frequency $d\omega$ reads

$$dE = \frac{Q^2}{4\pi}\omega\mu(\omega)\left(1 - \frac{1}{\beta^2 n^2(\omega)}\right)d\omega dx. \tag{2.29}$$

where μ and n are the permeability and the refraction index of the medium, respectively, and $\beta = v/c$. Therefore, the total power reads

$$\dot{E}_{\rm rad} = \frac{cQ^2}{4\pi} \int d\omega \mu(\omega) \omega \left(1 - \frac{1}{\beta^2 n^2(\omega)} \right) \lesssim \frac{Q^2}{8\pi \epsilon_0 c} \omega_c^2$$
 (2.30)

where the integral is taken over the Cherenkov regime. In the last step we assumed $\mu(\omega) \approx \mu_0 = 1/(\epsilon_0 c^2)$ and $\beta \sim 1$. The upper limit is expressed in terms of a cutoff

frequency which depends solely on the plasma's properties $\omega_c \lesssim 2\pi c/a_0$, where a_0 is Bohr's radius. As a result of this energy emission, the BH slows down on a time scale

$$\tau_{\rm C} \sim \frac{M}{\dot{E}_{\rm rad}} \sim \frac{2\epsilon_0}{\pi} \frac{M^2}{Q^2} \frac{a_0^2}{Mc} \sim 10^{12} \left(\frac{10^{17} \text{g}}{M}\right) \text{yr}$$
(2.31)

where we have used Eq. (2.28). Therefore, the effect is negligible for primordial BHs [18] which were originally considered in [13], but it might be relevant for more massive BHs travelling at relativistic velocities in a plasma with short relaxation time.

2.3.3 Superradiance in Superfluids and Superconductors

Another example of linear superradiance in flat spacetime is related to superfluids³ [13]. Superfluids can flow through pipes with no friction when their speed is below a critical value known as Landau critical speed [19]. If the fluid moves faster than the Landau critical speed, quasiparticle production in the fluid becomes energetically convenient at expenses of the fluid kinetic energy.

This process can be understood in terms of linear superradiance similarly to the Cherenkov effect previously discussed. In the fluid rest frame, consider a quasiparticle (e.g. a phonon) with frequency $\omega(\mathbf{k})$ and wavenumber \mathbf{k} . In this frame, the walls of the channel move with velocity \mathbf{v} relative to the fluid. Therefore, the quantity $\omega - \mathbf{v} \cdot \mathbf{k}$ is the analog of the Ginzburg-Frank condition (2.20) and becomes negative when

$$v > v_c \equiv \min \frac{\omega(\mathbf{k})}{|\mathbf{k}|},$$
 (2.32)

where $\omega(\mathbf{k})$ gives the dispersion relation of the quasiparticle. As discussed above, in this configuration it is energetically favorable to create a quasiparticle mode. This quasiparticles formation contributes a component which is not superfluid because its energy can be dissipated in various channels.

The same kind of reasoning can be used to predict the critical current flowing through a superconductor above which superconductivity is disrupted. Supercurrents are carried by Cooper pairs that move through a solid lattice with no resistance. However, whenever the kinetic energy of the current carriers exceeds the binding energy of a Cooper pair, it is energetically more favorable for the electrons in a pair to separate, with these broken pairs behaving as quasiparticles. Consider a

³In the context of the gauge-gravity duality, the holographic dual of a superfluid is also a superradiant state, cf. Sect. 4.5.2.

superconductor, taken to be at zero temperature for simplicity, with supercurrent density $J = nqv_d$, where n is the current carrier density, q is the carrier charge and v_d is the drift velocity of the carriers measured in the frame of the solid lattice. In the rest frame of the superconductor "fluid", a quasiparticle created due to the scattering of a current carrier with the solid lattice has minimum momentum given by $2\hbar k_F$, where k_F is the Fermi momentum of the electrons in the pair, and an energy $2\Delta_0$ which is the minimum energy needed to broke a Cooper pair at zero temperature. Landau arguments then predicts that to break a Cooper pair, i.e., to spontaneously emit a quasiparticle, the drift velocity must be given by

$$v_d > \min \frac{\omega(\mathbf{k})}{|\mathbf{k}|} \equiv \frac{\Delta_0}{\hbar k_F}.$$
 (2.33)

This in turn can be used to estimate the critical magnetic field above which superconductivity is broken. Take, for example, a circular superconductor with radius R, carrying a current density J. The magnetic field at the surface of the superconductor is then given by H = JR/2. The critical current density $J_c = nq\Delta_0/\hbar k_F$, then predicts that the critical magnetic field strength is given by $H_c = J_c R/2$ (see e.g. [20]).

2.4 Sound Amplification by Shock Waves

2.4.1 Sonic "Booms"

Curiously, very familiar phenomena can be understood from the point of view of superradiance. One of the most striking examples is the "sonic boom" originating from the supersonic motion of objects in a fluid.

Imagine a structureless solid object traveling through a quiescent fluid with speed $v_i > c_s$ where c_s is the speed of sound in the medium. Since the object is structureless then $\Delta \mathcal{E} = 0$ in Eq. (2.19), and in analogy with the Vavilov-Cherenkov effect we see that the object will emit *phonons* with dispersion relation $\omega = c_s k$, when their angle with respect to the object's velocity satisfy

$$\vartheta_M = \cos^{-1}(c_s/v_i). \tag{2.34}$$

Due to the supersonic motion of the object the emitted phonons will form a shock wave in the form of a cone, known as the Mach cone, with an opening angle $\pi - 2\vartheta_M$ [21].

If there is any sound wave present in the fluid which satisfy the Ginzburg-Frank condition (2.20), it will be superradiantly amplified as the object overtakes them. In the fluid's rest frame the wave fronts will propagate with an angle

$$\cos\vartheta > c_s/v_i,\tag{2.35}$$

which means that they are emitted inside the Mach cone and the cone surface marks the transition between the superradiant and non-superradiant regions. Thus the "sonic boom" associated with the supersonic motion in a fluid can be understood as a superradiant amplification of sound waves.

Although very different in spirit, the effects we discussed can be all explained in terms of spontaneous superradiance, and they just follow from energy and momentum conservation and by considering the emission in the comoving frame. As we shall discuss in the Sect. 2.5, this guiding principle turns out to be extremely useful also in the case of rotational superradiance.

2.4.2 Superradiant Amplification at Discontinuities

A second instructive example concerning superradiant amplification by shock waves refers to sound waves at a discontinuity. Consider an ideal fluid, locally irrotational (vorticity free), barotropic and inviscid. Focus now on small propagating disturbances—i.e., sound waves—such that $\vec{v} = \vec{v_0} + \delta \vec{v}$, where \vec{v} is the velocity of the perturbed fluid. Then, by linearizing the Navier-Stokes equations around the background flow, it can be shown that small irrotational perturbations $\delta \vec{v} = -\nabla \Phi$ are described by the Klein-Gordon equation [22, 23],⁴

$$\Box \Phi = 0, \qquad (2.36)$$

where the box operator is defined in the effective spacetime

$$g^{\mu\nu} \equiv \frac{1}{\rho c_s} \begin{bmatrix} -1 & \vdots & -v_0^j \\ \dots & \dots & \dots \\ -v_0^i & \vdots (c_s^2 \delta_{ij} - v_0^i v_0^j) \end{bmatrix} . \tag{2.37}$$

and where $\rho(r)$ and $c_s(r)$ are the density of the fluid and the local speed of sound, respectively. The effective geometry on which sound waves propagate is dictated solely by the background velocity v_0 and local speed of sound c. The (perturbed) fluid velocity and pressure can be expressed in terms of the master field Φ as

$$\delta \vec{v} = -\vec{\nabla} \Phi \,, \tag{2.38}$$

$$\delta P = \rho_0 \left(\frac{\partial \Phi}{\partial t} + \vec{v_0} \cdot \vec{\nabla} \Phi \right). \tag{2.39}$$

⁴This formal equivalence will prove useful later on when discussing analogue BHs.

We consider now a very simple example worked out by in [24] (and reproduced also in Landau and Lifshitz monograph [21]), where the normal to the discontinuity lies on the z=0 plane. Suppose that the surface of discontinuity separates a medium "2" at rest (z<0) from a medium "1" moving with velocity $\vec{v}_0=v_x\equiv v$ along the x-axis. The scattering of a sound wave in medium 2 gives rise in medium 1 to a transmitted wave with the form⁵

$$\Phi_1 = \frac{\omega}{\omega - k_x v_0} \mathcal{T} e^{ik_x x + ik_y y + ik z - i\omega t}.$$
 (2.40)

The equation of motion (2.36) forces the dispersion relation

$$(\omega - v_0 k_x)^2 = c_s^2 (k_x^2 + k_y^2 + k^2).$$
 (2.41)

In medium 2, the incident wave gets reflected, and has the general form

$$\Phi_2 = \mathcal{I}e^{ik_x x + ik_y y + ik_z z - i\omega t} + \mathcal{R}e^{ik_x x + ik_y y - ik_z z - i\omega t}. \tag{2.42}$$

There are two boundary conditions relevant for this problem. The pressure must be continuous at the interface, yielding the condition

$$\mathcal{R} + \mathcal{I} = \mathcal{T}. \tag{2.43}$$

Finally, the vertical displacement $\zeta(x,t)$ of the fluid particles at the interface must also be continuous. The derivative $\partial \zeta/\partial t$ is the rate of change of the surface coordinate ζ for a given x. Since the fluid velocity component normal to the surface of discontinuity is equal to the rate of displacement of the surface itself, we have

$$\partial \zeta / \partial t = \delta v_z - v_0 \partial \zeta / \partial x. \tag{2.44}$$

Assuming for the displacement ζ the same harmonic dependence as we took for Φ , we then have the second condition

$$\frac{k}{(\omega - v_0 k_x)^2} \mathcal{T} = \frac{k_z}{\omega^2} (\mathcal{I} - \mathcal{R}) . \tag{2.45}$$

The sign of k is as yet undetermined, and it is fixed by the requirement that the velocity of the refracted wave is away from the discontinuity, i.e., $\partial \omega/\partial k = c_s^2 k/(\omega - v_0 k_x) > 0$. It can be verified that for $v_0 > 2c_s$ superradiant amplification of the reflected waves $(\mathcal{R} > \mathcal{I})$ is possible, provided that k < 0 and consequently that $\omega - v_0 k_x < 0$ [21, 24]. The energy carried away is supposedly being drawn from the whole of the medium "1" in motion, although a verification of this would

⁵The slightly unorthodox normalization of the transmitted wave was chosen so that the final result for the amplification factor exactly matches Landau and Lifshitz's result, in their formalism.

require nonlinearities to be taken into account. Such nonlinear results have not been presented in the original work [21, 24]; in the context of BH superradiance, we show in Sect. 3.5.2 that superradiance does result in mass (and charge) loss from the (BH) medium, at nonlinear order in the fluctuation.

This example considers compressible fluids and sound waves, but it can be shown that similar energy extraction mechanisms are at play for waves in *incompressible* stratified fluids with shear flow [25–27]. An intuitive explanation in terms of negative-energy states is given in [27].

2.5 Rotational Superradiance

One important aspect of the previous examples is that the linear velocity of the medium from which the energy is drawn exceeds the phase velocity of the corresponding oscillations [28]. It is clearly impossible to extend such process to waves in vacuum and in plane geometry, because it would require superluminal velocities, as already pointed out. However, in a cylindrical or spherical geometry the angular phase velocity of an m-pole wave (m is an azimuthal number, specified in more detail below), is ω/m . If the body is assumed to rotate with angular velocity Ω , then amplification is in principle possible for waves satisfying condition (1.1), $\omega < m\Omega$, if the previous example is faithful.

It should be also clear from all the previous examples that rotating bodies with internal degrees of freedom (where energy can be dumped into) display superradiance. Two different arguments can be made in order to show this rigorously [13, 28].

The first is of a thermodynamic origin. Consider an axi-symmetric macroscopic body rotating rigidly with constant angular velocity about its symmetry axis. Assume also the body has reached equilibrium, with well defined entropy S, rest mass M and temperature T. Suppose now that a wavepacket with frequency $(\omega, \omega + d\omega)$ and azimuthal number m is incident upon this body, with a power $P_m(\omega)d\omega$. Radiation with a specific frequency and azimuthal number carries angular momentum at a rate $(m/\omega)P_m(\omega)d\omega$ (c.f. Appendix C). Neglecting any spontaneous emission by the body (of thermal or any other origin), the latter will absorb a fraction Z_m of the incident energy and angular momentum,

$$\frac{dE}{dt} = Z_m P_m d\omega , \quad \frac{dJ}{dt} = Z_m \frac{m}{\omega} P_m d\omega . \tag{2.46}$$

Notice that the assumption of axi-symmetry is crucial. No precession occurs during the interaction, and no Doppler shifts are involved. This implies that both the frequency and multipolarity of the incident and scattered wave are the same, as assumed in the equations above. Now, in the frame co-rotating with the body, the change in energy is simply [19]

$$dE_0 = dE - \Omega dJ = dE \left(1 - \frac{m\Omega}{\omega} \right), \qquad (2.47)$$

and thus the absorption process is followed by an increase in entropy, $dS = dE_0/T$, of

$$\frac{dS}{dt} = \frac{\omega - m\Omega}{\omega T} Z_m P_m(\omega) d\omega. \qquad (2.48)$$

Finally, the second law of thermodynamics demands that

$$(\omega - m\Omega)Z_m > 0, (2.49)$$

and superradiance $(Z_m < 0)$ follows in the superradiant regime $\omega - m\Omega < 0$.

Consider next Zel'dovich's original "dynamical" argument, and take for definiteness a scalar field Φ , governed in vacuum by the Lorentz-invariant Klein-Gordon equation, $\Box \Phi = 0$. An absorbing medium breaks Lorentz invariance. Assume that, in a coordinate system in which the medium is at rest, the absorption is characterized by a parameter α as

$$\Box \Phi + \alpha \frac{\partial \Phi}{\partial t} = 0. \tag{2.50}$$

The \square term is Lorentz-invariant, but if the frequency in the accelerated frame is ω and the field behaves as $e^{-i\omega t + im\varphi}$ in the inertial frame the azimuthal coordinate is $\varphi = \varphi' - \Omega t$, and hence the frequency is $\omega' = \omega - m\Omega$. In other words, the effective damping parameter $\alpha\omega'$ becomes negative in the superradiant regime and the medium amplifies—rather than absorbing—radiation.

A very appealing classical example of rotational (electromagnetic) superradiance is worked out in some detail for the original model by Zel'dovich [13, 28]. We now present two further examples, one of which can also potentially be implemented in the laboratory.

2.5.1 Example 1. Scalar Waves

Let us work out explicitly the case of a rotating cylinder in (r, z, φ) spatial coordinates with a dissipative surface at r = R. For simplicity the scalar is assumed to be independent of z, $\Phi = \phi(r)e^{-i\omega t + im\varphi}$. From what we said, by using Eq. (2.50), the problem can be modelled by

$$\frac{1}{r} \left(r \phi' \right)' + \left(\omega^2 - i \alpha (\omega - m \Omega) \delta(r - R) - \frac{m^2}{r^2} \right) \phi = 0, \qquad (2.51)$$

which can be solved analytically in terms of Bessel functions,

$$\phi = \begin{cases} C_0 J_m(\omega r) & r < R \\ C_1 J_m(\omega r) + C_2 Y_m(\omega r) & r > R \end{cases}$$
 (2.52)

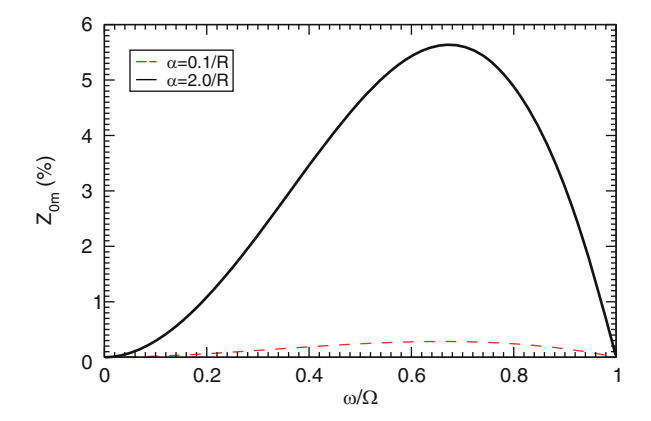


Fig. 2.1 Amplification values $Z_{0m} = |\mathcal{R}|^2/|\mathcal{I}|^2 - 1$ of the scalar toy model for m = 1, $\Omega R = 0.5$ and $\alpha R = 0.1$, 2

The constants C_1 , C_2 can be determined by continuity at r=R along with the jump implied by the delta function. At infinity the solution is a superposition of ingoing and outgoing waves, $\phi \to \mathcal{I}e^{-i\omega r}/(r\omega)^{3/2} + \mathcal{R}e^{i\omega r}/(r\omega)^{3/2}$, where the constants \mathcal{I} and \mathcal{R} can be expressed in terms of C_1 and C_2 . Figure 2.1 shows a typical amplification factor $Z_{0m} \equiv |\mathcal{R}|^2/|\mathcal{I}|^2 - 1$ (in percentage) for m=1, $\Omega R=0.5$ and $\alpha R=0.1,2$.

2.5.2 Example 2. Sound and Surface Waves: A Practical Experimental Setup?

A second example concerns amplification of *sound waves* at the surface of a rotating cylinder of radius *R*, but can also be directly used with *surface gravity waves*. As we discussed in Sect. 2.4.2, sound waves propagate in moving fluids as a massless scalar field in curved spacetime, with an effective geometry dictated by the background fluid flow (2.37).

We focus here on fluids at rest, so that the effective metric is Minkowskian, $ds^2 = \frac{\rho}{c_s} \left(-c_s^2 dt^2 + dr^2 + r^2 d\vartheta^2 + dz^2 \right)$ in cylindrical coordinates. Coincidentally, exactly the same equation of motion governs small gravity waves in a shallow basin [29], thus the results below apply equally well to sound and gravity waves.⁶

Solutions to Eq. (2.36) are better studied using the cylindrical symmetry of the effective background metric. In particular, we may decompose the field Φ in terms

⁶Notice that [29] always implicitly assumes a nontrivial background flow and the presence of a horizon in the effective geometry. In contrast, in our setup this is not required. All that it needs is a rotating boundary.

of azimuthal modes,

$$\Phi(t, r, \vartheta, z) = \frac{\phi(r)}{\sqrt{r\rho(r)}} e^{-i\omega t + im\vartheta + ikz}, \qquad (2.53)$$

and we get

$$\frac{d^2\phi}{dr^2} + \left[\frac{\omega^2}{c_s^2} - k^2 - \frac{m^2 - 1/4}{r^2} - \frac{\rho'}{2r\rho} + \frac{\rho'^2}{4\rho^2} - \frac{\rho''}{2\rho}\right]\phi(r) = 0.$$
 (2.54)

For simplicity, let us focus on k=0 modes and assume that the density and the speed of sound are constant, so that the last three terms in the potential above vanishes and the background metric can be cast in Minkowski form. In this case, Eq. (2.54) admits the general solution $\phi = C_1 \sqrt{r} J_m(\omega r/c_s) + C_2 \sqrt{r} Y_m(\omega r/c_s)$. The constants C_1 and C_2 are related to the amplitude of the ingoing and outgoing wave at infinity, i.e., asymptotically one has

$$\phi \sim \mathcal{I}e^{-i\omega r} + \mathcal{R}e^{i\omega r}$$

$$= \sqrt{\frac{c_s}{2\pi\omega}} \left((C_1 - iC_2)e^{i(\omega r/c_s - m\pi/2 - \pi/4)} + (C_1 + iC_2)e^{-i(\omega r/c_s - m\pi/2 - \pi/4)} \right). \tag{2.55}$$

The ratio \mathcal{R}/\mathcal{I} can be computed by imposing appropriate boundary conditions. For nonrotating cylinders the latter read [30]

$$\left(\frac{r\Phi'}{\Phi}\right)_{r=R} = -\frac{i\rho\omega R}{\Upsilon}\,,\tag{2.56}$$

in terms of the original perturbation function, where Υ is the impedance of the cylinder material. As explained before, when the cylinder rotates uniformly with angular velocity Ω , it is sufficient to transform to a new angular coordinate $\vartheta' = \vartheta + \Omega t$ which effectively amounts to the replacement of ω with $\omega - m\Omega$ in the boundary condition (2.56). An empirical impedance model for fibrous porous materials was developed in [31], yielding a universal function of the flow resistance σ and frequency of the waves,

$$\Upsilon = \rho c_s \left[1 + 0.0511 \left(2\pi\sigma/\omega \text{ kg}^{-1} \text{m}^3 \right)^{0.75} - i0.0768 \left(2\pi\sigma/\omega \text{ kg}^{-1} \text{m}^3 \right)^{0.73} \right].$$
(2.57)

Typical values at frequencies $\omega \sim 1000 {\rm s}^{-1}$ are $\Upsilon \sim \rho c_s (1 - 0.2i)$ [31].

We will define the amplification factor Z_m to be

$$Z_m = |\mathcal{R}|^2 / |\mathcal{I}|^2 - 1$$
. (2.58)

Notice that, from (2.39), the amplification factor measures the gain in pressure. Using Eq. (2.56) and the exact solution of Eq. (2.54), the final result for the

amplification factor reads

$$Z_{m} = \left| \frac{i\tilde{\omega}\tilde{\Upsilon}J_{m-1} - 2(\tilde{\omega} - 1)J_{m} - i\tilde{\omega}\tilde{\Upsilon}J_{m+1} + \tilde{\omega}\tilde{\Upsilon}Y_{m-1} + 2i(\tilde{\omega} - 1)Y_{m} - \tilde{\omega}\tilde{\Upsilon}Y_{m+1}}{\tilde{\omega}\tilde{\Upsilon}J_{m-1} + 2i(\tilde{\omega} - 1)J_{m} - \tilde{\omega}\tilde{\Upsilon}J_{m+1} + i\tilde{\omega}\tilde{\Upsilon}Y_{m-1} - 2(\tilde{\omega} - 1)Y_{m} - i\tilde{\omega}\tilde{\Upsilon}Y_{m+1}} \right|^{2} - 1,$$
(2.59)

where we have defined the dimensionless quantities $\tilde{\Upsilon} = \Upsilon/(\rho c_s)$, $\tilde{\omega} = \omega/(m\Omega)$ and we indicate $J_i = J_i(\omega R/c_s)$ and $Y_i = Y_i(\omega R/c_s)$ for short. Note that the argument of the Bessel functions reads $m\tilde{\omega}v/c_s$, where v is the linear velocity at the cylinder's surface. Therefore, the amplification factor does not depend on the fluid density and it only depends on the dimensionless quantities v/c_s and $\tilde{\omega}$. Although not evident from Eq. (2.59), $Z_m = 0$ when $\tilde{\omega} = 1$ and it is positive (i.e. there is superradiant amplification) for $\tilde{\omega} < 1$, for any v/c_s .

As a point of principle, let us use a typical value for the impedance, $\tilde{\Upsilon} \approx (1-0.2i)$, to compute the amplification of sound waves in air within this setup. We take $\Omega = 1000, \, 2000 \, \mathrm{s}^{-1}$ and a cylinder with radius $R = 10 \, \mathrm{cm}$, corresponding to linear velocities at the cylinder surface of the order of $v = 100, \, 200 \, \mathrm{ms}^{-1}$, but below the sound speed. The (percentage) results are shown in Fig. 2.2, and can be close to $100 \, \%$ amplification for large enough cylinder angular velocity. Note the result only depends on the combination $\Omega R/c_s$, which can be tweaked to obtain the optimal experimental configuration.

Another interesting application is to build an "acoustic bomb", similar in spirit with the "BH bombs" that we discuss in Sect. 4. In other words, by confining the superradiant modes near the rotating cylinder we can amplify the superradiant extraction of energy and trigger an instability. In this simple setup, confinement can be achieved by placing a cylindrical reflecting surface at some distance R_2 (note that this configuration is akin to the "perfect mirror" used by Press and Teukolsky to create what they called a BH bomb [32]). The details of the instability depend quantitatively on the outer boundary, specifically on its acoustic impedance. We will

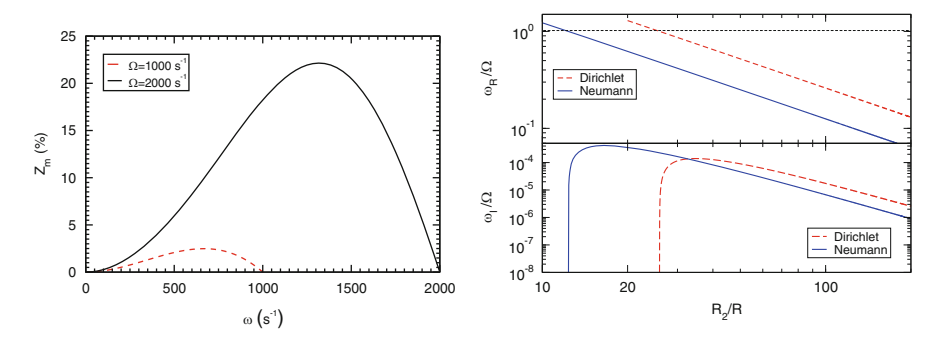


Fig. 2.2 Left panel: Amplification values Z_m of acoustic waves for m=1, $R=10\,\mathrm{cm}$ and $\Omega=1000,\,2000\,\mathrm{s}^{-1}$. Right panel: fundamental unstable mode for the "acoustic bomb", a rotating cylinder with radius R enclosed in a cylindrical cavity at distance R_2 . In this example we set m=1 and $v/c_s\approx 0.147$. Note that the mode becomes unstable $(\omega_I>0)$ precisely when the superradiance condition $\omega_R<\Omega$ is fulfilled

2.6 Tidal Acceleration 29

not perform a thorough parameter search, but focus on two extreme cases: Dirichlet and Neumann conditions. Imposing the boundary conditions at $r = R_2$, we obtain the equation that defines the (complex) eigenfrequencies of the problem analytically,

$$\tilde{\omega}\tilde{\Upsilon}\left[\hat{J}_{m}(Y_{m-1}-Y_{m+1})+\hat{Y}_{m}(J_{m+1}-J_{m-1})\right]+2i(\tilde{\omega}-1)\left[\hat{J}_{m}Y_{m}-J_{m}\hat{Y}_{m}\right]=0, \quad (2.60)$$

$$\tilde{\omega}\tilde{\Upsilon}\left[(J_{m-1}-J_{m+1})\left(\hat{Y}_{m+1}-\hat{Y}_{m-1}\right)+\hat{J}_{m-1}\left(Y_{m-1}-Y_{m+1}\right)+\hat{J}_{m+1}\left(Y_{m+1}-Y_{m-1}\right)\right]$$

$$+2i(\tilde{\omega}-1)\left[J_{m}\left(\hat{Y}_{m+1}-\hat{Y}_{m-1}\right)+\hat{J}_{m-1}Y_{m}-\hat{J}_{m+1}Y_{m}\right]=0, \quad (2.61)$$

for Dirichlet ($\Phi(r=R_2)=0$) and Neumann ($\Phi'(r=R_2)=0$) conditions, respectively. In the equations above, we have further defined $\hat{J}_i=J_i(\omega R_2/c_s)$ and $\hat{Y}_i=Y_i(\omega R_2/c_s)$ for short. In both cases the eigenmode equation only depends on the ratio R_2/R , $\tilde{\omega}$ and v/c_s . Neumann conditions, $\Phi'(r=R_2)=0$, mimic rigid outer boundaries. The fundamental eigenfrequencies $\omega=\omega_R+i\omega_I$ for these two cases are shown in the right panel of Fig. 2.2 as functions of the mirror position R_2/R . Within our conventions, the modes are unstable when the imaginary part is positive (because of the time dependence $e^{-i\omega t}$). As expected, the modes become unstable when $\omega_R < m\Omega$, i.e. when the superradiance condition is satisfied. In the example shown in Fig. 2.2, the maximum instability occurs for $R_2 \sim 30R$ and corresponds to a very short instability time scale,

$$\tau \equiv \frac{1}{\omega_I} \sim 10 \left(\frac{1000 \,\text{Hz}}{\Omega} \right) \,\text{s} \,. \tag{2.62}$$

Although our model is extremely simple, these results suggest the interesting prospect of detecting sound-wave superradiance amplification and "acoustic bomb" instabilities in the laboratory.

Finally, note that an alternative to make the system unstable is to have the fluid confined within a *single*, *rotating* absorbing cylinder. We find however, that in this particular setup the instability only sets in for supersonic cylinder surface velocities, presumably harder to achieve experimentally.

2.6 Tidal Acceleration

Although the processes we have discussed so far all involve radiation, it is possible to extract energy away from rotating bodies even in the absence of waves. A prime example concerns "tidal acceleration", which is most commonly known to occur in the Earth-Moon system.

⁷This statement can be disputed however, since the phenomenon we discuss in the following does involve time retardation effects and is therefore intimately associated with wave phenomena.

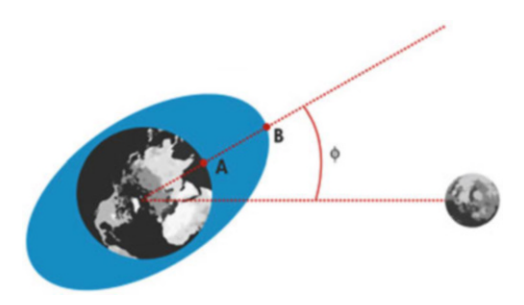


Fig. 2.3 Tides on the Earth caused by our moon (as seen by a frame anchored on the Moon). The tidal forces create a bulge on Earth's ocean surface, which leads Moon's orbital position by a constant angle ϕ . Earth rotates faster than the Moon in its orbit, thus a point A on the surface of the Earth will differentially rotate with respect to the oceans, causing dissipation of energy and decrease of Earth's rotation period

As explained by George Darwin back in 1880 [33] (see also [34, 35] which are excellent overviews of the topic), tides are caused by differential forces on the oceans, which raise tidal bulges on them, as depicted in Fig. 2.3. Because Earth rotates with angular velocity $\Omega_{\rm Earth}$, these bulges are not exactly aligned with the Earth-Moon direction. In fact, because Earth rotates faster than the Moon's orbital motion ($\Omega_{\rm Earth} > \Omega$), the bulges *lead* the Earth-Moon direction by a constant angle. This angle would be zero if friction were absent, and the magnitude of the angle depends on the amount of friction. Friction between the ocean and the Earth's crust slows down Earth's rotation by roughly $\dot{\Omega}_{\rm Earth} \sim -5.6 \times 10^{-22}/s^2$, about 0.002 s per century. Conservation of angular momentum of the entire system lifts the Moon into a higher orbit with a longer period and larger semi-major axis. Lunar ranging experiments have measured the magnitude of this tidal acceleration to be about $\dot{a}=3.82$ cm/yr [36].

Tidal Acceleration and Superradiance in the "Newtonian" Approximation Let us consider a generic power-law interaction between a central body of gravitational mass M and radius R and its moon with mass m_p at a distance r_0 . The magnitude is (in this section we re-insert factors of G and C for clarity)

$$F = \frac{GMm_p}{r_0^n} \,, \tag{2.63}$$

and Newton's law is recovered for n = 2. The tidal acceleration in M is given by

$$a_{\text{tidal}} = \frac{nGm_p}{R^n} \left(\frac{R}{r_0}\right)^{n+1} = ng_M \left(\frac{R}{r_0}\right)^{n+1} \frac{m_p}{M},$$
 (2.64)

where g_M is the surface gravity on M. This acceleration causes tidal bulges of height h and mass μ to be raised on M. These can be estimated by equating the specific energy of the tidal field, $E_{\text{tidal}} \sim a_{\text{tidal}} R$, with the specific gravitational energy,

2.6 Tidal Acceleration 31

 $E_G \sim g_M h$, needed to lift a unit mass from the surface of M to a distance h. We get

$$\frac{h}{R} = n \left(\frac{R}{r_0}\right)^{n+1} \frac{m_p}{M},\tag{2.65}$$

which corresponds to a bulge mass of approximately $\mu = \frac{\kappa}{4} n m_p (R/r_0)^{n+1}$, where κ is a constant of order 1, which encodes the details of Earth's internal structure. Without dissipation, the position angle ϕ in Fig. 2.3 is $\phi = 0$, while the tidal bulge is aligned with moon's motion. Dissipation contributes a constant, small, time lag τ such that the lag angle is $\phi = (\Omega_{\text{Earth}} - \Omega)\tau$.

With these preliminaries, a trivial extension of the results of [34] yields a tangential tidal force on M, assuming a circular orbit for the moon,

$$F_{\vartheta} \sim \frac{n(n+1)G\kappa}{2} m_p^2 \frac{R^{n+3}}{r_0^{2n+3}} (\Omega_{\text{Earth}} - \Omega) \tau$$
 (2.66)

The change in orbital energy over one orbit is related to the torque r_0F_{ϑ} and reads $\int_0^{2\pi} r_0F_{\vartheta} \Omega/2\pi d\vartheta = \Omega r_0F_{\vartheta}$. Thus, we get

$$\dot{E}_{\text{orbital}} = \frac{n(n+1)G\kappa m_p^2}{2} \frac{R^{n+3}}{r_0^{2n+2}} \Omega(\Omega_{\text{Earth}} - \Omega)\tau, \qquad (2.67)$$

and, for gravitational forces obeying Gauss's law (n = 2), the latter reduces to

$$\dot{E}_{\text{orbital}} = 3G\kappa m_p^2 \frac{R^5}{r_0^6} \Omega(\Omega_{\text{Earth}} - \Omega)\tau.$$
 (2.68)

Summarizing, tidal acceleration extracts energy and angular momentum from the Earth. Conservation of both these quantities then requires the moon to slowly spiral outwards. It can be shown that tidal acceleration works in any number of spacetime dimensions and with other fields (scalar or electromagnetic) [37, 38].

This and the previous examples make it clear that any rotating object should be prone to energy extraction and superradiance, provided some dissipation mechanism of any sort is at work. When the tidally distorted object is a BH, the dissipation mechanism is naturally provided by the presence of an event horizon which—as we discuss in the next section—behaves in many respects as a viscous one-way membrane [39]. Interestingly, by substituting $\Omega_{\text{Earth}} \to \Omega_{\text{H}}$ in Eq. (2.68), setting $\kappa \sim 1/3 \approx \mathcal{O}(1)$, and with the simple argument that the only relevant dissipation time scale in the BH case is the light-crossing time $\tau \sim M$, Eq. (2.68) was found to agree [37] with the exact result for BH tidal heating obtained through BH perturbation theory [40–44].

References

- O. Klein, Die reflexion von elektronen an einem potentialsprung nach der relativistischen dynamik von dirac. Z. Phys. 53(3-4), 157-165 (1929). http://dx.doi.org/10.1007/BF01339716
- F. Sauter, Uber das Verhalten eines Elektrons im homogenen elektrischen Feld nach der relativistischen Theorie Diracs. Z. Phys. 69, 742–764 (1931)
- 3. C.A. Manogue, The Klein paradox and superradiance. Ann. Phys. 181, 261-283 (1988)
- R.G. Winter, Klein paradox for the klein-gordon equation. Am. J. Phys. 27(5), 355–358 (1959). http://scitation.aip.org/content/aapt/journal/ajp/27/5/10.1119/1.1934851
- 5. F. Hund, Z. Phys. 117, 1 (1941)
- 6. J.S. Schwinger, On gauge invariance and vacuum polarization. Phys. Rev. 82, 664–679 (1951)
- 7. S. Hawking, Particle creation by black holes. Commun. Math. Phys. 43, 199–220 (1975)
- 8. A. Hansen, F. Ravndal, Klein's paradox and its resolution. Phys. Scripta 23, 1036 (1981)
- 9. V. Ginzburg, I. Frank, Radiation of a uniformly moving electron due to its transition from one medium into another. J. Phys. (USSR) 9, 353–362 (1945)
- 10. V.L. Ginzburg, I.M. Frank, Dokl. Akad. Nauk Ser. Fiz. SSSR 56 583 (1947)
- 11. C.M. Will, The Confrontation between general relativity and experiment. Living Rev. Relativ 9, 3 (2006). arXiv:gr-qc/0510072 [gr-qc]
- T. Damour, G. Esposito-Farese, Nonperturbative strong field effects in tensor—scalar theories of gravitation. Phys. Rev. Lett. 70, 2220–2223 (1993)
- 13. J.D. Bekenstein, M. Schiffer, The many faces of superradiance. Phys. Rev. **D58**, 064014 (1998). arXiv:gr-qc/9803033 [gr-qc]
- V. Ginzburg, Radiation from uniformly moving sources (vavilov-cherenkov effect, transition radiation, and some other phenomena). Acoust. Phys. 51(1), 11–23 (2005). http://dx.doi.org/ 10.1134/1.1851624
- 15. E.A. Milne, Trans. Camb. Philos. Soc. 26, 63 (1923)
- A.S. Eddington, The Internal Constitution of the Stars (Cambridge University Press, Cambridge, 1988)
- G. Michaud, G. Fontaine, Electric fields, accretion, and stellar winds in helium rich atmospheres. Astrophys. J. 229, 694–699 (1979)
- 18. B. Carr, K. Kohri, Y. Sendouda, J. Yokoyama, New cosmological constraints on primordial black holes. Phys. Rev. **D81**, 104019 (2010). arXiv:0912.5297 [astro-ph.CO]
- 19. L. Landau, E.M. Lifshitz, L.P. Pitaevskii, Statistical Physics (Pergamon, Oxford, 1980)
- D. Dew-Hughes, The critical current of superconductors: an historical review. Low Temp. Phys. 27(9), 713–722 (2001). http://scitation.aip.org/content/aip/journal/ltp/27/9/10.1063/1.1401180
- 21. L. Landau, E.M. Lifshitz, Fluid Mechanics (Pergamon, Oxford, 1976)
- 22. W. Unruh, Experimental black hole evaporation. Phys. Rev. Lett. 46, 1351–1353 (1981)
- 23. M. Visser, Acoustic black holes: horizons, ergospheres, and hawking radiation. Classical Quantum Gravity 15, 1767–1791 (1998). arXiv:gr-qc/9712010 [gr-qc]
- H.S. Ribner, Reflection, transmission and amplification of sound by a moving medium. J. Acoust. Soc. Am. 29, 435–441 (1957)
- 25. J.R. Booker, F.P. Bretherton, The critical layer for internal gravity waves in a shear flow. J. Fluid Mech. 27, 513–539 (1967)
- 26. W.L. Jones, Reflection and stability of waves in stably stratified fluids with shear flow: a numerical study. J. Fluid Mech. 34, 609–624 (1968)
- J.F. McKenzie, Reflection and amplification of acoustic-gravity waves at a density and velocity discontinuity. J. Geophys. Res. 77, 2915 (1972)
- 28. Y.B. Zel'dovich, Zh. Eksp. Teor. Fiz **62**, 2076 (1972) [Sov. Phys. JETP **35**, 1085 (1972)]
- 29. R. Schutzhold, W.G. Unruh, Gravity wave analogs of black holes. Phys. Rev. **D66**, 044019 (2002). arXiv:gr-qc/0205099 [gr-qc]
- M. Lax, H. Feshbach, Absorption and scattering for impedance f on spheres and circular cylinders. J. Acoust. Soc. Am. 20, 108 (1948)

References 33

31. M.E. Delany, E.N. Bazley, Acoustical properties of fibrous absorbent materials. Appl. Acoust. **3**, 105 (1969)

- 32. W.H. Press, S.A. Teukolsky, Floating orbits, superradiant scattering and the black-hole bomb. Nature 238, 211–212 (1972)
- 33. G.H. Darwin, On the secular changes in the elements of the orbit of a satellite revolving about a tidally distorted planet. Philos. Trans. R. Soc. Lond. 171, 713 (1880)
- 34. P. Hut, Tidal evolution in close binary systems. Astron. Astrophys. 99, 126–140 (1981)
- 35. The earth and moon: from halley to lunar ranging and shells. http://www.astro.ru.nl/~fverbunt/binaries/earth.pdf
- 36. J.O. Dickey, P.L. Bender, J.E. Faller, X.X. Newhall, R.L. Ricklefs, J.G. Ries, P.J. Shelus, C. Veillet, A.L. Whipple, J.R. Wiant, J.G. Williams, C.F. Yoder, Lunar laser ranging: a continuing legacy of the apollo program. Science 265(5171), 482–490 (1994). http://www.sciencemag.org/content/265/5171/482.abstract
- 37. V. Cardoso, P. Pani, Tidal acceleration of black holes and superradiance. Classical Quantum Gravity 30, 045011 (2013). arXiv:1205.3184 [gr-qc]
- 38. R. Brito, V. Cardoso, P. Pani, Tidal effects around higher-dimensional black holes. Phys. Rev. **D86**, 024032 (2012). arXiv:1207.0504 [gr-qc]
- K.S. Thorne, R. Price, D. Macdonald, *Black Holes: The Membrane Paradigm* (Yale University Press, New Haven, 1986)
- 40. J.B. Hartle, Tidal friction in slowly rotating black holes. Phys. Rev. D8, 1010–1024 (1973)
- 41. J.B. Hartle, Tidal shapes and shifts on rotating black holes. Phys. Rev. D9, 2749–2759 (1974)
- 42. E. Poisson, Tidal interaction of black holes and Newtonian viscous bodies. Phys. Rev. **D80**, 064029 (2009). arXiv:0907.0874 [gr-qc]
- T. Binnington, E. Poisson, Relativistic theory of tidal Love numbers. Phys. Rev. D80, 084018 (2009). arXiv:0906.1366 [gr-qc]
- 44. K. Glampedakis, S.J. Kapadia, D. Kennefick, Superradiance-tidal friction correspondence. Phys. Rev. **D89**(2), 024007 (2014). arXiv:1312.1912 [gr-qc]

Chapter 3 Superradiance in Black Hole Physics

As discussed in the previous section, superradiance requires *dissipation*. The latter can emerge in various forms, e.g. viscosity, friction, turbulence, radiative cooling, etc. All these forms of dissipation are associated with some medium or some matter field that provides the *arena* for superradiance. It is thus truly remarkable that—when spacetime is *curved*—superradiance can also occur in vacuum, even at the classical level. In this section we discuss in detail *BH superradiance*, which is the main topic of this book.

BHs are classical vacuum solutions of essentially any relativistic (metric) theory of gravity, including Einstein General Theory of Relativity (GR). Despite their simplicity, BHs are probably the most fascinating predictions of GR and enjoy some extremely nontrivial properties. The most important property (which also defines the very concept of BH) is the existence of an event horizon, a boundary in spacetime which separates two causally disconnected regions. Among the various properties of BH event horizons, the one that is most relevant for the present discussion is that BHs behave in many respects as a viscous one-way membrane in flat spacetime. This is the so-called BH membrane paradigm [1]. Thus, the existence of an event horizon provides vacuum with an intrinsic dissipative mechanism, which is naturally prone to superradiance. As we shall see, the very existence of event horizons allows to extract energy from the vacuum, basically in any relativistic theory of gravity.

While most of our discussion is largely model- and theory-independent, for calculation purposes we will be dealing with the Kerr-Newman family of BHs [2], which describes the most general stationary electrovacuum solution of the Einstein-Maxwell theory [3]. We will be specially interested in two different spacetimes which display superradiance of different nature, the uncharged Kerr and the nonrotating charged BH geometry.

3.1 Action, Equations of Motion and Black Hole Spacetimes

We consider a generic action involving one complex, charged massive scalar Ψ and a massive vector field A_{μ} with mass $m_S = \mu_S \hbar$ and $m_V = \mu_V \hbar$, respectively,

$$S = \int d^4x \sqrt{-g} \left(\frac{R - 2\Lambda}{\kappa} - \frac{1}{4} F^{\mu\nu} F_{\mu\nu} - \frac{\mu_V^2}{2} A_{\nu} A^{\nu} - \frac{1}{2} g^{\mu\nu} \Psi_{,\mu}^* \Psi_{,\nu} - \frac{\mu_S^2}{2} \Psi^* \Psi \right)$$
$$+ \int d^4x \sqrt{-g} \left(i \frac{q}{2} A_{\mu} \left(\Psi \nabla^{\mu} \Psi^* - \Psi^* \nabla^{\mu} \Psi \right) - \frac{q^2}{2} A_{\mu} A^{\mu} \Psi \Psi^* \right) + S_M . \quad (3.1)$$

where $\kappa=16\pi$, Λ is the cosmological constant, $F_{\mu\nu}\equiv\nabla_{\mu}A_{\nu}-\nabla_{\nu}A_{\mu}$ is the Maxwell tensor, and S_M is the standard matter action that we neglect henceforth. More generic actions could include a coupling between the scalar and vector sector, and also higher-order self-interaction terms. However, most of the work on BH superradiance is framed in the above theory and we therefore restrict our discussion to this scenario. The resulting equations of motion are

$$(\nabla_{\mu} - iqA_{\mu})(\nabla^{\mu} - iqA^{\mu})\Psi = \mu_{S}^{2}\Psi, \qquad (3.2a)$$

$$\nabla_{\mu} F^{\mu\nu} = \mu_V^2 A^{\nu} + q^2 \Psi \Psi^* A^{\nu} - i \frac{q}{2} \left(\Psi \nabla^{\nu} \Psi^* - \Psi^* \nabla^{\nu} \Psi \right) , \qquad (3.2b)$$

$$\begin{split} &\frac{1}{\kappa} \left(R^{\mu\nu} - \frac{1}{2} g^{\mu\nu} R + \Lambda g^{\mu\nu} \right) = -\frac{1}{8} F^{\alpha\beta} F_{\alpha\beta} g^{\mu\nu} + \frac{1}{2} F^{\mu}_{\alpha} F^{\nu\alpha} - \frac{1}{4} \mu_V^2 A_{\alpha} A^{\alpha} g^{\mu\nu} + \frac{\mu_V^2}{2} A^{\mu} A^{\nu} \\ &- \frac{1}{4} g^{\mu\nu} \left(\Psi^*_{,\alpha} \Psi^{,\alpha} + \mu_S^2 \Psi^* \Psi \right) + \frac{1}{4} \left(\Psi^{*,\mu} \Psi^{,\nu} + \Psi^{,\mu} \Psi^{*,\nu} \right) - i \frac{q}{2} A^{\mu} \left(\Psi \nabla^{\nu} \Psi^* - \Psi^* \nabla^{\nu} \Psi \right) \end{split}$$

$$-\frac{q^{2}}{4}g^{\mu\nu}\Psi\Psi^{*}A_{\alpha}A^{\alpha} + \frac{q^{2}}{2}\Psi\Psi^{*}A^{\mu}A^{\nu} + i\frac{q}{4}g^{\mu\nu}A_{\alpha}\left(\Psi\nabla^{\alpha}\Psi^{*} - \Psi^{*}\nabla^{\alpha}\Psi\right). \tag{3.2c}$$

These equations describe the fully nonlinear evolution of the system. For the most part of our work, we will specialize to perturbation theory, i.e. we consider A^{μ} and Ψ to be small—say of order $\mathcal{O}(\epsilon)$ —and include their backreaction on the metric only perturbatively. Because the stress-energy tensor is quadratic in the fields, to order $\mathcal{O}(\epsilon)$ the gravitational sector is described by the standard Einstein equations in vacuum, $R_{\mu\nu}=0$, so that the scalar and Maxwell field propagate on a Kerr-Newman geometry. Backreaction on the metric appears at order $\mathcal{O}(\epsilon^2)$ in the fields. We consider two particular cases and focus on the following background geometries:

3.1.1 Static, Charged Backgrounds

For static backgrounds, the uniqueness theorem [3] guarantees that the only regular, asymptotically flat solution necessarily has $\psi=0$ and belongs to the Reissner-Nordström (RN) family of charged BHs. In the presence of a cosmological constant, $\Lambda \neq 0$, other solutions exist, some of them are in fact allowed by

superradiant mechanisms, as we shall discuss. For definiteness, we focus for the most part of our work on the fundamental family of RN-(A)dS solution, described by the metric

$$ds^{2} = -fdt^{2} + fdr^{2} + r^{2}d\vartheta^{2} + r^{2}\sin^{2}\vartheta d\varphi^{2},$$
(3.3)

where

$$f(r) = 1 - \frac{2M}{r} + \frac{Q^2}{r^2} - \frac{\Lambda}{3}r^2, \qquad (3.4)$$

and the background vector potential $A_{\mu}=(Q/r,0,0,0)$, where M and Q are the mass and the charge of the BH, respectively. When $\Lambda=0$ the spacetime is asymptotically flat and the roots of f(r) determine the event horizon, located at $r_{+}=M+\sqrt{M^{2}-Q^{2}}$, and a Cauchy horizon at $r_{-}=M-\sqrt{M^{2}-Q^{2}}$. In this case the electrostatic potential at the horizon is $\Phi_{H}=Q/r_{+}$. When $\Lambda>0$, the spacetime is asymptotically de Sitter (dS) and the function f(r) has a further positive root which defines the cosmological horizon r_{c} , whereas when $\Lambda<0$ the spacetime is asymptotically anti-de Sitter (AdS) and the function f(r) has only two positive roots.

Fluctuations of order $\mathcal{O}(\epsilon)$ in the scalar field in this background induce changes in the spacetime geometry and in the vector potential which are of order $\mathcal{O}(\epsilon^2)$, and therefore to leading order can be studied on a fixed RN-(A)dS geometry. This is done in Sect. 3.5 below.

3.1.2 Spinning, Neutral Backgrounds

For neutral backgrounds $A_{\mu}=0$ to zeroth order, and the uniqueness theorems guarantee that the scalar field is trivial and the only regular, asymptotically flat solution to the background equations is given by the Kerr family of spinning BHs. Because we also wish to consider the effect of a cosmological constant, we will enlarge it to the Kerr-(A)dS family of spinning BHs, which in standard Boyer-Lindquist coordinates reads (for details on the Kerr spacetime, we refer the reader to the monograph [4])

$$ds^{2} = -\frac{\Delta_{r}}{\rho^{2}} \left(dt - \frac{a}{\Sigma} \sin^{2} \vartheta \, d\varphi \right)^{2} + \frac{\rho^{2}}{\Delta_{r}} \, dr^{2} + \frac{\rho^{2}}{\Delta_{\vartheta}} \, d\vartheta^{2}$$
$$+ \frac{\Delta_{\vartheta}}{\rho^{2}} \sin^{2} \vartheta \left(a \, dt - \frac{r^{2} + a^{2}}{\Sigma} \, d\varphi \right)^{2} , \tag{3.5}$$

with

$$\Delta_r = (r^2 + a^2) \left(1 - \frac{\Lambda}{3} r^2 \right) - 2Mr, \qquad \Sigma = 1 + \frac{\Lambda}{3} a^2,$$

$$\Delta_{\vartheta} = 1 + \frac{\Lambda}{3} a^2 \cos^2 \vartheta, \qquad \rho^2 = r^2 + a^2 \cos^2 \vartheta. \tag{3.6}$$

This metric describes the gravitational field of a spinning BH with mass M/Σ^2 and angular momentum $J = aM/\Sigma^2$. When $\Lambda = 0$, the roots of Δ determine the event horizon, located at $r_+ = M + \sqrt{M^2 - a^2}$, and a Cauchy horizon at $r_- = M - \sqrt{M^2 - a^2}$. The static surface $g_{tt} = 0$ defines the ergosphere given by $r_{\rm ergo} = M + \sqrt{M^2 - a^2 \cos^2 \vartheta}$. As in the static case, when $\Lambda > 0$ the spacetime possesses also a cosmological horizon.

A fundamental parameter of a spinning BH is the angular velocity of its event horizon, which for the Kerr-(A)dS solution is given by

$$\Omega_{\rm H} = \frac{a}{r_+^2 + a^2} \left(1 + \frac{\Lambda}{3} a^2 \right) \,. \tag{3.7}$$

The area and the temperature of the BH event horizon respectively read

$$A_{H} = \frac{4\pi(r_{+}^{2} + a^{2})}{\Sigma}, \qquad T_{H} = \frac{r_{+} \left(1 - \frac{\Lambda}{3}a^{2} - \Lambda r_{+}^{2} - a^{2}r_{+}^{-2}\right)}{4\pi(r_{+}^{2} + a^{2})}.$$
(3.8)

3.1.3 Geodesics and Frame Dragging in the Kerr Geometry

The motion of free pointlike particles in the equatorial plane of this geometry is described by the following geodesic equations [5, 6],

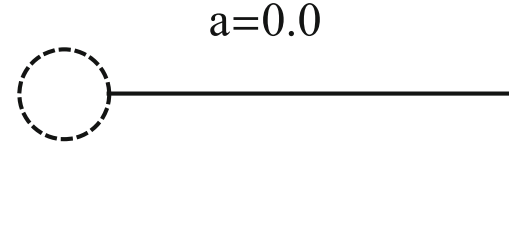
$$\dot{t} = \frac{1}{\Delta} \left[\left(r^2 + a^2 + \frac{2a^2M}{r} \right) E - \frac{2aM}{r} L \right],$$
 (3.9)

$$\dot{\varphi} = \frac{1}{\Delta} \left[\frac{2aM}{r} E + \left(1 - \frac{2M}{r} \right) L \right], \tag{3.10}$$

$$r^{2}\dot{r}^{2} = r^{2}E^{2} + \frac{2M}{r}(aE - L)^{2} + (a^{2}E^{2} - L^{2}) - \delta_{1}\Delta, \qquad (3.11)$$

where $\delta_1 = 1,0$ for timelike and null geodesics, respectively, and the dot denotes differentiation with respect to the geodesic's affine parameter. The first two equations follow from the symmetry of the Kerr background under time translations and rotations, while the last equation is simply the defining relation for timelike and null geodesics. A more thorough analysis of the geodesics of the Kerr geometry can

Fig. 3.1 Frame dragging effects: sketch of the trajectory of a zero-angular-momentum observer as it falls into a BH. The BH is either static (*upper panel*) or rotating clockwise (*lower panel*). The infall into a rotating BH is drag along the BH's sense of rotation



a=0.9, clockwise

be found in the classic work by Bardeen et al. [5] or in Chandrasekhar's book [6]. The conserved quantities E, L are, respectively, the energy and angular momentum per unit rest mass of the object undergoing geodesic motion (or the energy and angular momentum for massless particles).

Consider an observer with timelike four-velocity which falls into the BH with zero angular momentum. This observer is known as the ZAMO (Zero Angular Momentum Observer). From Eqs. (3.9) and (3.10) with L=0, we get the following angular velocity, as measured at infinity,

$$\Omega \equiv \frac{\dot{\varphi}}{\dot{t}} = -\frac{g_{t\varphi}}{g_{\varphi\varphi}} = \frac{2Mar}{r^4 + r^2a^2 + 2a^2Mr}.$$
 (3.12)

At infinity $\Omega=0$ consistent with the fact that these are zero angular momentum observers. However, $\Omega \neq 0$ at any finite distance and at the horizon one finds

$$\Omega_{\rm H}^{\rm ZAMO} = \frac{a}{2Mr_{+}} \,. \tag{3.13}$$

Thus, observers are frame-dragged and forced to co-rotate with the geometry. This phenomenon is depicted in Fig. 3.1, where we sketch the trajectory of a ZAMO in a nonrotating and rotating BH background.

3.1.4 The Ergoregion

The Kerr geometry is also endowed with an infinite-redshift surface outside the horizon. These points define the ergosurface and are the roots of $g_{tt} = 0$. The ergosurface exterior to the event horizon is located at

$$r_{\rm ergo} = M + \sqrt{M^2 - a^2 \cos^2 \vartheta}$$
 (3.14)

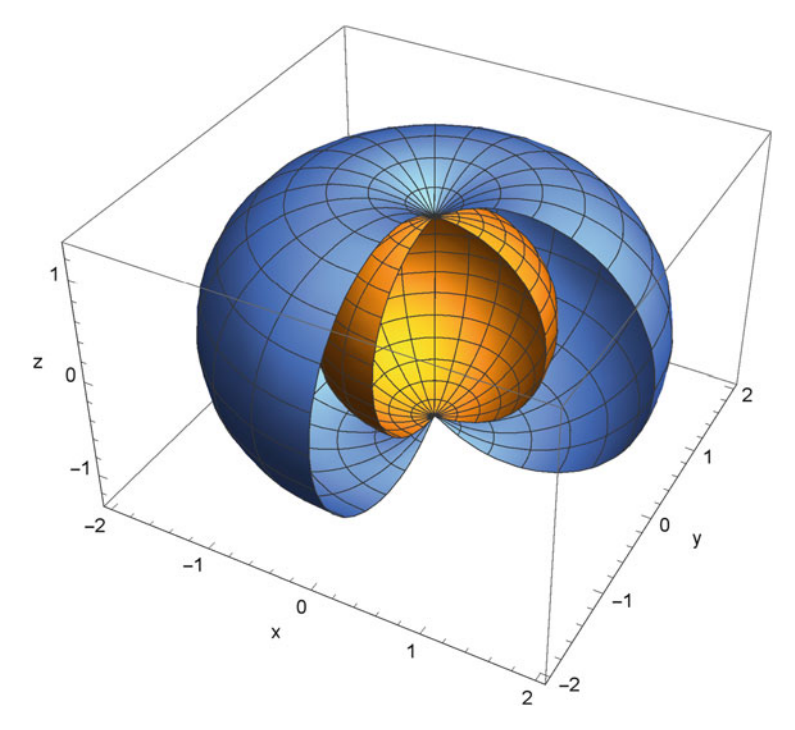


Fig. 3.2 The ergosphere of a Kerr BH is shown together with the horizon for a nearly-extremal BH with $a \sim 0.999$ M. The coordinates (x, y, z) are similar to standard Cartesian-coordinate but obtained from the Boyer-Lindquist coordinates

In particular, it is defined by r=2M at the equator and $r=r_+$ at the poles. The region between the event horizon and the ergosurface is the ergoregion. The ergosurface is an infinite-redshift surface, in the sense that any light ray emitted from the ergosurface will be infinitely redshifted when observed at infinity. The ergosphere of a Kerr BH is shown in Fig. 3.2.

The ergosurface is also the static limit, as no static observer is allowed inside the ergoregion. Indeed, the Killing vector $\xi^{\mu}=(1,0,0,0)$ becomes spacelike in the ergoregion $\xi^{\mu}\xi^{\mu}g_{\mu\nu}=g_{tt}>0$. We define a static observer as an observer (i.e., a timelike curve) with tangent vector proportional to ξ^{μ} . The coordinates (r,ϑ,ϕ) are constant along this wordline. Such an observer cannot exist inside the ergoregion, because ξ^{μ} is spacelike there. In other words, an observer cannot stay still, but is forced to rotate with the BH.

Let's consider this in more detail, taking a stationary observer at constant (r, ϑ) , with four-velocity

$$v^{\mu} = (\dot{t}, 0, 0, \dot{\varphi}) = \dot{t}(1, 0, 0, \Omega), \tag{3.15}$$

This observer can exist provided its orbit is time-like, which implies $v^2 < 0$. This translates in a necessary condition for an existence of a stationary observer, which reads

$$g_{tt} + 2\Omega g_{t\varphi} + \Omega^2 g_{\varphi\varphi} < 0. \tag{3.16}$$

Let's consider the zeroes of the above. We have

$$\Omega_{\pm} = \frac{-g_{t\varphi} \pm \sqrt{g_{t\varphi}^2 - g_{tt}g_{\varphi\varphi}}}{g_{\varphi\varphi}} = \frac{-g_{t\varphi} \pm \sqrt{\Delta}\sin\vartheta}{g_{\varphi\varphi}}.$$
 (3.17)

Thus, a stationary observer cannot exist when $r_- < r < r_+$. In general, the allowed range of Ω is $\Omega_- \le \Omega \le \Omega_+$. On the outer horizon, we have $\Omega_- = \Omega_+$ and the only possible stationary observer on the horizon has

$$\Omega = -\frac{g_{t\varphi}}{g_{\varphi\varphi}} = \Omega_{\rm H} \,, \tag{3.18}$$

which coincides with the angular velocity of a ZAMO at the event horizon. Note also that a static observer is a stationary observer with $\Omega=0$. Indeed, it is easy to check that Ω_- changes sign at the static limit, i.e. $\Omega=0$ is not allowed within the ergoregion.

3.1.5 Intermezzo: Stationary and Axisymmetric Black Holes Have an Ergoregion

At this point it is instructive to take one step back and try to understand what are the minimal ingredients for the existence of an ergoregion in a BH spacetime. Indeed, in many applications it would be useful to disentangle the role of the ergoregion from that of the horizon. Unfortunately, this cannot be done because, as we now prove, the existence of an event horizon in a stationary and axisymmetric spacetime automatically implies the existence of an ergoregion [7].

Let us consider the most general stationary and axisymmetric metric¹:

$$ds^2 = g_{tt}dt^2 + g_{rr}dr^2 + 2g_{t\varphi}dtd\varphi + g_{\varphi\varphi}d\varphi^2 + g_{\vartheta\vartheta}d\vartheta^2, \qquad (3.19)$$

¹We also require the spacetime to be invariant under the "circularity condition", $t \to -t$ and $\varphi \to -\varphi$, which implies $g_{t\vartheta} = g_{t\varphi} = g_{r\vartheta} = g_{r\varphi} = 0$ [6]. While the circularity condition follows from Einstein and Maxwell equations in electrovacuum, it might not hold true in modified gravities or for exotic matter fields.

where g_{ij} are functions of r and ϑ only. The event horizon is the locus $r_+ = r_+(\vartheta)$ defined as the largest root of the lapse function:

$$N_{r=r_{+}} \equiv \left(g_{t\varphi}^{2} - g_{\varphi\varphi}g_{tt}\right)_{r=r_{+}} = 0.$$
 (3.20)

In a region outside the horizon N > 0, whereas N < 0 inside the horizon. As we discussed, the boundary of the ergoregion, $r_{\text{ergo}} = r_{\text{ergo}}(\vartheta)$, is defined by $g_{tt}|_{r=r_{\text{ergo}}} = 0$, and $g_{tt} < 0$ in a region outside the ergoregion, whereas $g_{tt} > 0$ inside the ergoregion. From Eq. (3.20) we get, at the horizon,

$$g_{tt}|_{r=r_{+}} = \frac{g_{t\varphi}^{2}}{g_{\varphi\varphi}}\Big|_{r=r_{+}} \ge 0,$$
 (3.21)

where, in the last inequality, we assumed no closed timelike curves outside the horizon, i.e. $g_{\varphi\varphi} > 0$. The inequality is saturated only when the gyromagnetic term vanishes, $g_{t\varphi}\big|_{r=r_+} = 0$. On the other hand, at asymptotic infinity $g_{tt} \to -1$. Therefore, by continuity, there must exist a region $r_{\rm ergo}(\vartheta)$ such that $r_+ \le r_{\rm ergo} < \infty$ and where the function g_{tt} vanishes. This proves that an ergoregion necessarily exists in the spacetime of a stationary and axisymmetric BH. As a by-product, we showed that the boundaries of the ergoregion (i.e. the ergosphere) must lay outside the horizon or coincide with it, $r_{\rm ergo} \ge r_+$. In the case of a static and spherically symmetric spacetime, $g_{t\varphi} \equiv 0$ and the ergosphere coincides with the horizon.

3.2 Area Theorem Implies Superradiance

It was realized by Bekenstein that BH superradiance can be naturally understood using the classical laws of BH mechanics [8]. In fact, given these laws, the argument in Sect. 2.5 can be applied *ipsis verbis*. The first law relates the changes in mass M, angular momentum J, horizon area A_H and charge Q, of a stationary BH when it is perturbed. To first order, the variations of these quantities in the vacuum case satisfy

$$\delta M = \frac{k}{8\pi} \delta A_H + \Omega_H \delta J + \Phi_H \delta Q, \qquad (3.22)$$

with $k \equiv 2\pi T_H$ the BH surface gravity, Ω_H the angular velocity of the horizon (3.7) and Φ_H is the electrostatic potential at the horizon [9]. The first law can be shown to be quite generic, holding for a class of field equations derived from a diffeomorphism covariant Lagrangian with the form $\mathcal{L}(g_{ab}; R_{abcd}; \nabla_a R_{bcde}, \ldots; \psi, \nabla_a \psi, \ldots)$. The second law of BH mechanics states that, if matter obeys the weak energy condition [6, 8, 10] (see also the discussion in Sect. 3.6.4 for a counterexample with fermions), then $\delta A_H \geq 0$.

Whether or not the second law can be generalized to arbitrary theories is an open question, but it seems to hinge on energy conditions [11, 12].

For the sake of the argument, let us consider a neutral BH, $\Phi=0$. The ratio of angular momentum flux L to energy E of a wave with frequency ω and azimuthal number m is $L/E=m/\omega$ (see Appendix C). Thus, interaction with the BH causes it to change its angular momentum as

$$\delta J/\delta M = m/\omega \,. \tag{3.23}$$

Substitution in the first law of BH mechanics (3.22) yields

$$\delta M = \frac{\omega k}{8\pi} \frac{\delta A_H}{\omega - m\Omega_H} \,. \tag{3.24}$$

Finally, the second law of BH thermodynamics, $\delta A_H \ge 0$, implies that waves with $\omega < m\Omega_{\rm H}$ extract energy from the horizon, $\delta M < 0$.

Likewise, the interaction between a static charged BH and a wave with charge q causes a change in the BH charge as

$$\delta Q/\delta M = q/\omega \,, \tag{3.25}$$

and therefore in this case Eq. (3.24) reads

$$\delta M = \frac{\omega k}{8\pi} \frac{\delta A_H}{\omega - q\Phi_H} \,. \tag{3.26}$$

This argument holds in GR in various circumstances, but note that it assumes that the wave is initially ingoing at infinity and that the matter fields obey the weak energy condition. The latter condition is violated for fermions in asymptotically flat spacetimes (cf. Sect. 3.6.4 below), while the former needs to be carefully analyzed in asymptotically de Sitter spacetimes where a subtlety arises at the cosmological horizon [13].

3.3 Energy Extraction *from* Black Holes: The Penrose Process

Despite being classically perfect absorbers, BHs can be used as a "catalyst" to extract the rest energy of a particle or even as an energy reservoir themselves, if they are spinning or charged.

Classical energy extraction with BHs works in exactly the same way as in Newtonian mechanics, by converting into useful work the binding energy of an object orbiting around another. Let's take for simplicity a point particle of mass μ around a much more massive body of mass M. In Newtonian mechanics, the

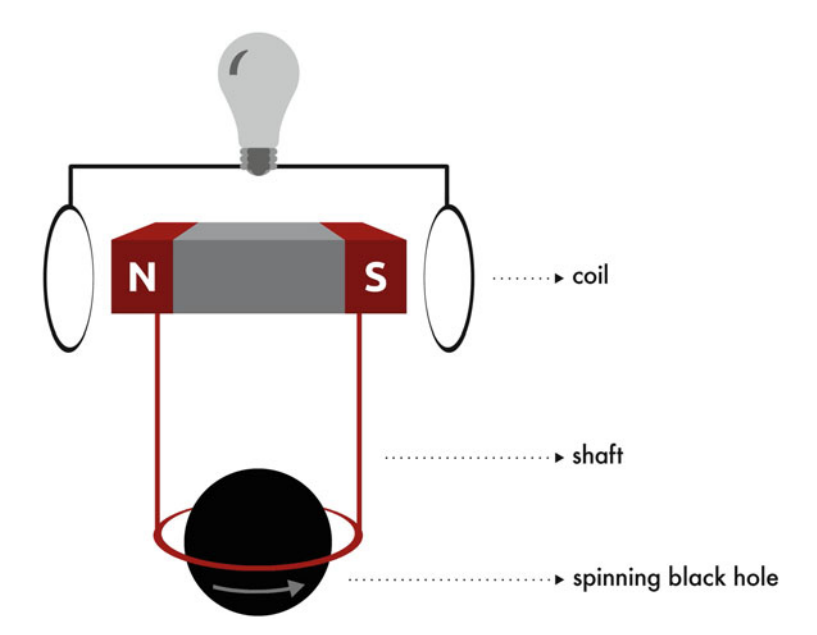


Fig. 3.3 Cartoon of a BH-powered circuit. Two shafts are rigidly attached to a ring, which is inside the ergoregion. The ring and therefore the shafts, are forced to rotate with the BH, turning the magnet at the other end of the shafts end over end, thereby producing a current in any closed circuit. Adapted from a diagram by Dan Watson [14]

maximum energy that can be converted in this way is given by the potential difference between infinity and the surface of the planet, $\operatorname{Work}/(\mu c^2) = GM/(c^2R)$, where R is the planet's radius. A similar result holds true when the planet is replaced by a BH; for a nonrotating BH, all the object's mass energy can be extracted as useful work as the particle is lowered towards the BH, as the Newtonian calculation suggests! Notice that in the previous example, what one accomplished was to trade binding energy with useful work, no energy was extracted from the BH itself.

Ways to extract energy from BHs make use of the existence of the ergoregion whose boundary is also a static limit: all observers are dragged along with the spacetime and cannot remain at rest with respect to distant observers. A cartoonish application of this property to extract energy is depicted in Fig. 3.3. Quantitative estimates of energy extraction from BHs were first made in a simpler context, which we now discuss.

3.3.1 The Original Penrose Process

The possibility to extract energy *from* a spinning BH was first quantified by Roger Penrose [15] some years before the discovery of BH superradiance, and

it is related to the fact that the energy of a particle within the ergoregion, as perceived by an observer at infinity, can be negative. Penrose conceived the following *gedankenexperiment*. Consider the Kerr geometry (3.5) with vanishing cosmological constant. Penrose's thought experiment consists on a particle of rest mass μ_0 , at rest at infinity, decaying into two identical particles each with rest mass $\mu_{\rm fin}$ (Penrose considered these two to be photons, we will keep it generic) at a turning point in its (geodesic) trajectory. Because the particle is initially at rest, the conserved dimensionless energy parameter is $E^{(0)} = \mathcal{E}^{(0)}/\mu_0 = 1$, and we denote the conserved energy and angular momentum parameters of the two decay-products by $(E^{(1)}, L^{(1)}) = (\mathcal{E}^{(1)}/\mu_{\rm fin}, \mathcal{L}^{(1)}/\mu_{\rm fin})$ and $(E^{(2)}, L^{(2)}) = (\mathcal{E}^{(2)}/\mu_{\rm fin}, \mathcal{L}^{(2)}/\mu_{\rm fin})$. Here \mathcal{E} , \mathcal{L} are the physical dimensionful energy and angular momentum of the particles. From (3.11), the turning point condition, $\dot{r}(r=r_0)=0$, immediately gives

$$L^{(0)} = \frac{1}{r_0 - 2M} \left(-2aM + \sqrt{2Mr_0\Delta} \right), \tag{3.27}$$

$$L^{(1),(2)} = \frac{\pm 2aM E^{(1),(2)} + \sqrt{r_0 \Delta \left(2M + r(\left(E^{(1),(2)}\right)^2 - 1)\right)}}{r_0 - 2M}.$$
 (3.28)

Imposing conservation of energy and angular momentum,

$$\mathcal{E}^{(1)} + \mathcal{E}^{(2)} = \mathcal{E}^{(0)} = \mu_0, \qquad \mathcal{L}^{(1)} + \mathcal{L}^{(2)} = \mathcal{L}^{(0)},$$
 (3.29)

one gets finally,

$$\mathcal{E}^{(1)} = \frac{\mu_0}{2} \left(1 \pm \sqrt{\frac{2M(1 - 4\mu_{\text{fin}}^2/\mu_0^2)}{r_0}} \right),$$

$$\mathcal{E}^{(2)} = \frac{\mu_0}{2} \left(1 \mp \sqrt{\frac{2M(1 - 4\mu_{\text{fin}}^2/\mu_0^2)}{r_0}} \right). \tag{3.30}$$

It is thus clear that one of the decay products will have an energy larger than the incoming particle. This is schematically shown in Fig. 3.4. How much larger, depends on the details of the break-up process and is encoded in the quantity $0 < 1 - 4\mu_{\rm fin}^2/\mu_0^2 < 1$. That is, there will be a gain in energy at infinity provided that the turning point satisfies $r_0 < 2M(1 - 4\mu_{\rm fin}^2/\mu_0^2) < 2M$ or, in other words, provided that the decay takes place between the ergosurface and the event horizon.

The maximum gain of energy is obtained when the decay takes place at the horizon and reads

$$\eta_{\text{max}} = \frac{\mathcal{E}^{(1)}}{\mathcal{E}^{(0)}} = \frac{1}{2} \left(\sqrt{\frac{2M(1 - 4\mu_{\text{fin}}^2/\mu_0^2)}{r_+}} + 1 \right).$$
(3.31)

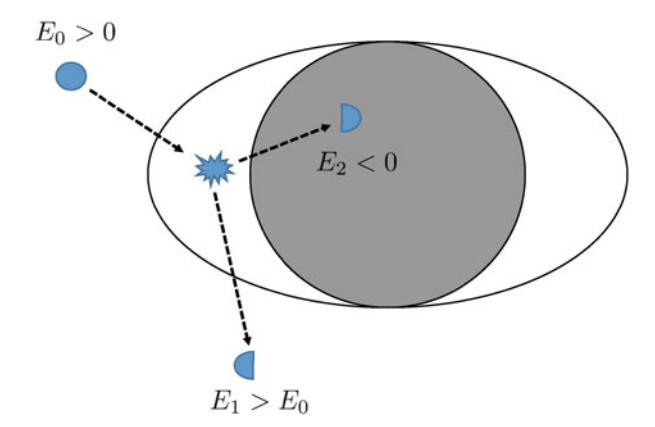


Fig. 3.4 Pictorial view of the original Penrose processes. A particle with energy E_0 decays inside the ergosphere into two particles, one with negative energy $E_2 < 0$ which falls into the BH, while the second particle escapes to infinity with an energy higher than the original particle, $E_1 > E_0$

As we noted, the efficiency depends on the details of the process. The maximum efficiency occurs for conversion into photons, such that $\mu_{\rm fin}^2/\mu_0^2=0$, and for which we recover Penrose's result $2\mathcal{E}^{(1)}/\mathcal{E}^{(0)}=\left(\sqrt{2M/r_+}+1\right)$.

In this latter case, it is possible to show that the negative-energy photon is doomed to fall into the horizon [16], decreasing the BH mass and angular momentum by δE and δL but in such a way that the irreducible mass, $M_{\rm irr} = \sqrt{Mr_+/2}$, actually increases [6]. Furthermore, a generic condition on the energy and angular momentum of the infalling particle can be computed as follows. In the ZAMO frame the energy flux across the horizon is given by

$$\delta E_H = -\int_{r_+} d\Sigma_\mu T_\nu^\mu n^\nu \propto \delta E - \Omega_{\rm H} \delta L, \qquad (3.32)$$

where $T_{\mu\nu}$ is a generic stress-energy tensor of the matter/radiation crossing the horizon, $n^{\mu}=\xi^{\mu}_{(t)}+\Omega_{\rm H}\xi^{\mu}_{(\varphi)}, \, \xi^{\mu}_{(t)}\equiv \partial^{\mu}t$ is the time Killing vector, $\xi^{\mu}_{(\varphi)}\equiv \partial^{\mu}\varphi$ is the axial Killing vector (see Appendix C), while E and L are the (conserved) specific energy and angular momentum of the particle crossing the horizon. Since the locally measured energy must be positive, assuming δE and δL are small, it follows that

$$E_H \propto E - \Omega_H L > 0 \implies \Omega_H L < E$$
. (3.33)

The result above applies to any form of energy and angular momentum crossing the horizon and is related to the area theorem. In addition, if the infalling particle has a negative energy, the bound above implies that J < 0, i.e. the negative-energy particle must be counter-rotating.

3.3.2 The Newtonian Carousel Analogy

A simple Newtonian, non-relativistic analog of the Penrose process is the "carousel process" depicted in Fig. 3.5. The process consists of two steps. In the first step a point particle collides with a rotating thin cylinder with a "sticky" surface and angular velocity Ω_i . The calculations will be done in the inertial frame centered at the cylinder's original axis. For simplicity, we assume the collision to be completely inelastic and we take the particle's mass m to be much smaller than the mass m of the cylinder so that, to first approximation, after the collision the particle is absorbed by the cylinder without changing its shape. Furthermore, consider the particle to have a velocity v_{in} perpendicular to the axis of rotation of the cylinder and with a zero impact parameter. Because of the sticky surface, after the collision the particle is forced to co-rotate with the cylinder. In the second step a fraction ϵ of the initial mass is ejected from the surface of the cylinder. We want to understand under which conditions the ejected particle has an energy larger than the initial one.

Conservation of angular and linear momenta implies that, after the collision with the cylinder, the linear and angular velocities of the cylinder respectively are

$$v_f = \frac{m}{M+m}v_{\rm in}, \qquad \Omega_f = \frac{M}{M+m}\Omega_i.$$
 (3.34)

Because in this example the impact parameter vanishes, the particle has zero angular momentum and the angular velocity of the cylinder decreases. After the collision, the particle is stuck to the surface. Let a fraction ϵ of the initial mass be ejected at the radial direction forming an angle ϑ with the initial direction of the particle (and in the same direction of the angular velocity of the disk). Then, the components of



Fig. 3.5 The carousel analogy of the Penrose process. A body falls nearly from rest into a rotating cylinder, whose surface is sprayed with glue. At the surface the body is forced to co-rotate with the cylinder (analog therefore of the BH ergosphere, the surface beyond which no observer can remain stationary with respect to infinity). The negative energy states of the ergoregion are played by the potential energy associated with the sticky surface. If now half the object (*in reddish*) is detached from the first half (*yellowish*), it will reach infinity with more (kinetic) energy than it had initially, extracting rotational energy out of the system

the particle's velocity in the collision plane, $v_{\text{out}} = (v_x, v_y)$, read

$$v_x = -\Omega_f R \cos \vartheta$$
, $v_y = v_f + \Omega_f R \sin \vartheta$, (3.35)

where *R* is the radius of the cylinder. Finally, we can compare the final energy of the ejected particle, $K_{\text{out}} = \epsilon m v_{\text{out}}^2/2$, with the initial energy $K_{\text{in}} = m v_{\text{in}}^2/2$. To first order in the mass ratio m/M, the efficiency reads

$$\eta \equiv \frac{K_{\text{out}}}{K_{\text{in}}} = 1 + \left(\epsilon \frac{R^2 \Omega_i^2}{v_{\text{in}}^2} - 1\right) + 2\epsilon \frac{R \Omega_i}{v_{\text{in}}} \left(\sin \vartheta - \frac{R \Omega_i}{v_{\text{in}}}\right) \frac{m}{M} + \mathcal{O}\left[\left(\frac{m}{M}\right)^2\right]. \tag{3.36}$$

Interestingly, the efficiency does not depend on the angle ϑ to lowest order in the mass ratio. When $m \ll M$ the energy of the ejected particle is larger than the initial kinetic energy provided

$$\Omega_i > \frac{v_{\rm in}}{\sqrt{\epsilon}R} \,. \tag{3.37}$$

Thus, the rotating "sticky" surface plays the same role as the BH ergosphere. The perfectly inelastic collision is the analog of the frame-dragging effect according to which no observer within the ergoregion can remain stationary with respect to infinity. The negative energy states of the ergoregion are played by the potential energy associated with the sticky surface.

3.3.3 Penrose's Process: Energy Limits

We have seen already that the energy gain provided by the Penrose mechanism is modest, at least for equal-rest-mass fragments. Still open however, is the possibility that the efficiency, or that the Lorentz factor of one of the fragments, is large for some situations.² Strong limits on the energy that can be extracted from the Penrose process can be obtained [5, 17]: consider a particle with four-velocity U^{μ} and conserved energy parameter E that breaks up and emits a fragment with energy E' and four-velocity u^{μ} . We want to impose limits on E', given the three-velocity of the fragment \vec{v} as measured in the rest frame of the incident body. Suppose that the breakup occurs in a spacetime with a Killing vector $\xi^{\mu} = \partial^{\mu} t$ which is timelike at infinity. In the laboratory frame we define an orthonormal tetrad, $e_{(\alpha)}^{\mu}$, where

²This possibility was at some stage considered of potential interest for the physics of jets emitted by quasars.

 $e_{(0)}^{\mu} = U^{\mu}$. The four-velocity of the fragment in the locally flat space is given by

$$u^{(\alpha)} = \frac{dx^{(\alpha)}}{d\tau} = \gamma \frac{dx^{(\alpha)}}{dx^{(0)}},$$
 (3.38)

where $\gamma = dx^{(0)}/d\tau = \left(1 - v^2\right)^{-1/2}$ and $v^2 = v^{(i)}v_{(i)}$. In the frame defined by $e^{\mu}_{(\alpha)}$ we can write $u^{\mu} = e^{\mu}_{(\alpha)}u^{(\alpha)} = \gamma(U^{\mu} + v^{(i)}e^{\mu}_{(i)})$ and $\xi^{\mu} = \xi^{(0)}U^{\mu} + \xi^{(i)}e^{\mu}_{(i)}$ (with i = 1, 2, 3). We then have

$$E = -\xi_{\mu}U^{\mu} = -\xi_{(0)} = -\xi^{\mu}U_{\mu} = -\xi^{(0)}, \quad g_{tt} = \xi^{\mu}\xi_{\mu} = -E^2 + \xi^2,$$
 (3.39)

where $\xi^2 = \xi^{(i)}\xi_{(i)}$. The energy of the ejected particle reads

$$E' = -\xi_{\mu} u^{\mu} = \gamma \left(E + v^{(i)} \xi_{(i)} \right) = \gamma \left(E + v \xi \cos \vartheta \right) , \tag{3.40}$$

where ϑ is the angle between the fragment velocity $v^{(i)}$ and $\xi_{(i)}$. Using (3.39) we can write

$$E' = \gamma E + \gamma v \left(E^2 + g_{tt}\right)^{1/2} \cos \vartheta, \tag{3.41}$$

which implies the inequality

$$\gamma E - \gamma v \left(E^2 + g_{tt} \right)^{1/2} \le E' \le \gamma E + \gamma v \left(E^2 + g_{tt} \right)^{1/2}.$$
 (3.42)

In the Kerr metric (3.5), g_{tt} is always less than 1 outside the horizon; furthermore, realistic configurations of matter outside BHs are likely to be well approximated with circular geodesics, for which the maximum possible energy is $E = 1/\sqrt{3}$ [5]. Thus, for E' to be negative, or equivalently, for the Penrose process to be *possible*, it is necessary that

$$v > \frac{E}{\sqrt{E^2 + 1}} = \frac{1}{2} \,. \tag{3.43}$$

This means that the disintegration process must convert most of the rest mass energy of the initial body into kinetic energy for any extraction of energy to become possible. In other words, the breakup process itself is relativistic. Such conclusion might be avoided if one is willing to accept the existence of naked singularities or wormholes, where g_{tt} can in principle become very large.

It is interesting to note that the inequality (3.42) applies also in flat space, where $g_{tt} = -1$. In this case the bound reads

$$\gamma E - \gamma v \left(E^2 - 1\right)^{1/2} \le E' \le \gamma E + \gamma v \left(E^2 - 1\right)^{1/2}.$$
 (3.44)

We conclude that (i) there is no great gain compared to what could be achieved from a breakup process in flat space and (ii) the left-hand-side can never become negative, as expected.

Bardeen et al. also showed that similar limits can be derived by following two particles which collide at some point inside the ergoregion [5]. Following similar steps to the ones we discussed above, they computed a lower bound on the magnitude of the relative three-velocity w between them, obtaining $w \ge 1/2$, in agreement with [17]. This leads to the conclusion that for the Penrose process to be possible, the particles must first acquire relativistic energies through some other mechanism.

In its simplest incarnation, energy extraction from spinning BHs in vacuum is not efficient enough to explain highly-energetic phenomena such as the emission of relativistic jets from quasars. However, in the presence of magnetic fields the limits discussed above can be lowered significantly for charged particles [18, 19], or as we discuss in Sect. 3.3.5, the situation can change completely by considering a variant of the Penrose process known as the *collisional Penrose process*.

3.3.4 The Penrose Process in Generic Spacetimes

The overall picture discussed above for the Penrose's extraction of energy from a Kerr BH can be actually generalized to any stationary and axisymmetric spacetime with an ergoregion. Consider a massive particle with specific energy $E^{(0)}$ at infinity, falling along the equatorial plane and finally decaying into two photons within the ergoregion. In such circumstances, one photon can have negative energy, $E^{(1)} < 0$, so that by energy conservation the second photon must have $E^{(2)} > E^{(0)}$. In the case of a Kerr BH the negative-energy photon is forced to fall into the horizon [16], whereas the other can escape to infinity with an energy excess compensated by the BH angular momentum. In fact, as shown by Chandrasekhar [6], the process can be also understood in terms of the BH area theorem, i.e. energy extraction is related to the property that the surface area of a BH never decreases in a continuous process.

Probably because of this analogy with the area theorem, there is some confusion in the literature about the connection between the Penrose process and superradiance. It is customary to claim that superradiance is the "wave analog" of the Penrose process. In fact, we now discuss that these processes are distinct from each other. Indeed, in the absence of other forms of dissipation, superradiance requires the presence of an event horizon [7, 20], whereas the Penrose process only hinges on the existence of an ergoregion. The latter can exist in rotating spacetimes other than BHs (e.g. in very compact, fastly rotating stars).

Let us start by repeating the essentials of the Penrose process in a generic stationary, axisymmetric spacetime. Focusing on equatorial motion, the line element (E.1) can be simplified as

$$ds^{2} = g_{tt}(r)dt^{2} + g_{rr}(r)dr^{2} + g_{\varphi\varphi}(r)d\varphi^{2} + 2g_{t\varphi}(r)dtd\varphi, \qquad (3.45)$$

where all metric coefficients are evaluated at $\vartheta = \pi/2$. Generalizing the geodesics analysis presented in Sect. 3.3.1, it is easy to show that a massive particle in this spacetime has a negative energy if and only if it is counter-rotating (i.e. its angular momentum along the rotation axis is negative, L < 0) and

$$g_{tt}\left(1 + \frac{g_{\varphi\varphi}}{L^2}\right) < \frac{g_{t\varphi}^2}{L^2}.\tag{3.46}$$

Because the right-hand side of the equation above is positive and regularity of the spacetime requires $g_{\varphi\varphi} > 0$, the condition above implies $g_{tt} > 0$, i.e. that the negative-energy particle is confined within the ergoregion. Likewise, for a particle with specific energy $E^{(0)} = 1$ decaying into two particles with specific energies $E^{(1)}$ and $E^{(2)}$ at its turning point and rest masses μ_{fin} each, we obtain

$$\mathcal{E}^{(1)} = \frac{\mu_0}{2} \left(1 \pm \sqrt{(1 + g_{tt})(1 - 4\mu_{\text{fin}}^2/\mu_0^2)} \right),$$

$$\mathcal{E}^{(2)} = \frac{\mu_0}{2} \left(1 \mp \sqrt{(1 + g_{tt})(1 - 4\mu_{\text{fin}}^2/\mu_0^2)} \right).$$
(3.47)

The efficiency reads

$$\eta = \frac{\mathcal{E}^{(1)}}{\mathcal{E}^{(0)}} = \frac{1}{2} \left[\sqrt{(1 + g_{tt})(1 - 4\mu_{\text{fin}}^2/\mu_0^2)} + 1 \right], \tag{3.48}$$

and is limited by the maximum value of $|g_{tt}|$. The latter must be finite to ensure regularity of the geometry³ and this limits the efficiency of Penrose's process, in addition to the bounds discussed above for the case of a Kerr BH.

Crucially, this derivation does *not* assume the existence of an event horizon and is valid for any stationary and axisymmetric spacetime. At variance with superradiance [7, 20], energy extraction from Penrose's process only requires the presence of an ergoregion.

While in the case of a Kerr BH the negative-energy particle is doomed to fall into the BH [16], if the spacetime does not possess an event horizon Eq. (3.46) requires that the negative-energy particle be confined within the ergoregion. In this case there are two possibilities: (i) the particle does not interact with the rotating object and it remains in orbital motion in the region $g_{tt} > 0$, or (ii) the particle is absorbed by the object and transfers its negative energy and angular momentum through other

³Interestingly, in the case of a naked singularity large-curvature regions become accessible to outside observers and g_{tt} can be arbitrarily large. This suggests that the Penrose effects around spinning naked singularities can be very efficient. It is also possible that rotating wormholes are prone to efficient Penrose-like processes, although to the best of our knowledge a detailed investigation has not been performed.

(nongravitational) mechanisms. As we will see in Sect. 4.11 the former possibility is related to the so-called ergoregion instability.

As we discussed in Sect. 3.1.5 (see also [7]), any stationary and axisymmetric spacetime with a horizon also possesses an ergoregion. Therefore, if the spacetime is described by a spinning BH geometry, both superradiance and Penrose's process can occur. However, the converse is not necessarily true, e.g. a perfect-fluid star may allow for Penrose's process but not for superradiant scattering.

We showed that the Penrose mechanism extends trivially to generic axisymmetric stationary spacetimes. Specifically, it has been studied for rotating wormholes [21], BHs in other theories of gravity such as the "Horava-Lifshitz" gravity BH [22], Kerr-NUT BHs [23], BHs with a global monopole [24], charged rotating BHs in Einstein-Maxwell axion-dilaton coupled gravity [25], and to arbitrarily "deformed" Kerr BHs [26], where it was shown that the maximum energy gain can be several times larger than for a Kerr BH.

The efficiency of the Penrose mechanism was also studied in the context of higher-dimensional physics, for higher dimensional BHs and black rings [27], to the five-dimensional supergravity rotating BH [28], and even to arbitrarily deformed BHs [29].

Finally, the astrophysically more relevant Penrose process for a Kerr BH immersed in a magnetic field, was studied in [18, 19, 30, 31] where it was shown that the maximum efficiency could be up to ten times larger than in a vacuum Kerr BH.

3.3.5 The Collisional Penrose Process: Ultra-High-Energy Debris

A variant of the Penrose process which might be astrophysically more promising is the *collisional Penrose process*, first proposed in 1975 [38] and studied in detail in [32]. The process consists of two particles 1 and 2 colliding with four-momenta p_1^{μ} and p_2^{μ} at some Boyer-Lindquist coordinate position r, and resulting in the emission of two bodies 3 and 4 with four-momenta p_3^{μ} and p_4^{μ} . This process was mostly studied in the equatorial plane where the geodesic equations are given by Eqs. (3.9)–(3.11). In the local 'lab' reference frame, the four-momentum is $p^{\mu} = \dot{x}^{\mu}$ for massless particles, while for massive particles we can choose the geodesic's affine parameter to be τ/μ (τ being the proper time and μ the particle rest mass), so that $p_{\mu}p^{\mu} = -\mu^2$. Using (3.9)–(3.11) and imposing the local conservation of four-momentum

$$p_1^{\mu} + p_2^{\mu} = p_3^{\mu} + p_4^{\mu} \,, \tag{3.49}$$

it is possible to numerically compute the ratio η between the energy of the postcollision escaping particle 3 and the energy of the colliding particles, $\eta \equiv \mathcal{E}_3/(\mathcal{E}_1 +$

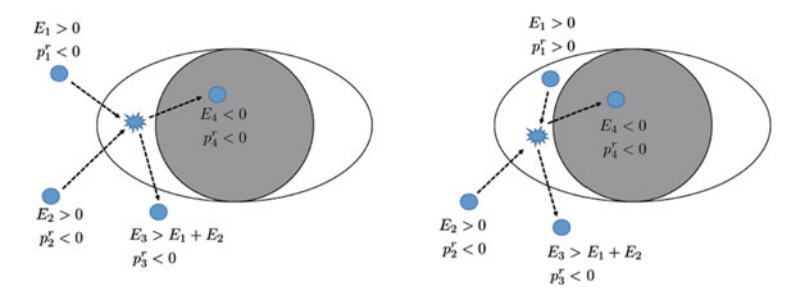


Fig. 3.6 Pictorial view of the different collisional Penrose processes. *Left*: initial particles with ingoing radial momentum ($p_1^r < 0$ and $p_2^r < 0$). Particle 3 has initial ingoing radial momentum, but eventually finds a turning point and escapes to infinity. The maximum efficiency for this was shown to be quite modest $\eta \sim 1.5$ [32–35]. *Right*: initial particles with $p_1^r > 0$ and $p_2^r < 0$. In this case particle 1 must have $p_1^r > 0$ inside the ergosphere. For this process the efficiency can be unbound for extremal BHs [35, 36]

 \mathcal{E}_2). Imposing that the initial particles have *ingoing* radial momentum $(p_1^r < 0)$ and $p_2^r < 0$) and that particle 3 can escape and reach an observer at infinity, it was shown that the process would result in modest maximum efficiencies ($\eta \lesssim 1.5$) for the escaping particle, where the precise upper bound depends on the nature of the colliding particles [32-35]. However, recently, Schnittman [36] found the surprising result that one could achieve much higher energy gains ($\eta \lesssim 15$) by allowing one of the colliding particles (say, particle 1) to rebound at a turning point, so it has *outgoing* radial momentum $(p_1^r > 0)$ when it collides with the incoming particle 2. This outgoing momentum favors ejection of a high-energy particle after the collision. A schematic view of the two processes is shown in Fig. 3.6. This was further extended in [37], with the striking conclusion that particle collisions in the vicinity of rapidly rotating BHs could, in principle, reach arbitrarily high efficiencies. They allowed for one of the particles to have outgoing radial momentum but with angular momentum $L_1 < 2E_1M$, such that this particle cannot come from infinity but is still kinematically allowed to be created inside the ergosphere by previous scattering events (however see [39] for a particular case where there is no energy amplification taking into account multiple scattering). These results are summarized in Fig. 3.7.

In principle multiple scattering events can also be used to increase the efficiency of any possible collisional Penrose process. The energy of particles that cannot escape to infinity may be substantially larger than the energy of those that can, and even if these particles are unable to escape themselves, they may collide with other particles and give rise to high-energy collision products that may escape and be detected at infinity. This may lead to very large efficiencies, even away from a = M [36, 37]. However, whether these processes play a role in the production of observable gamma rays or ultra-high-energy cosmic rays is still an open problem.

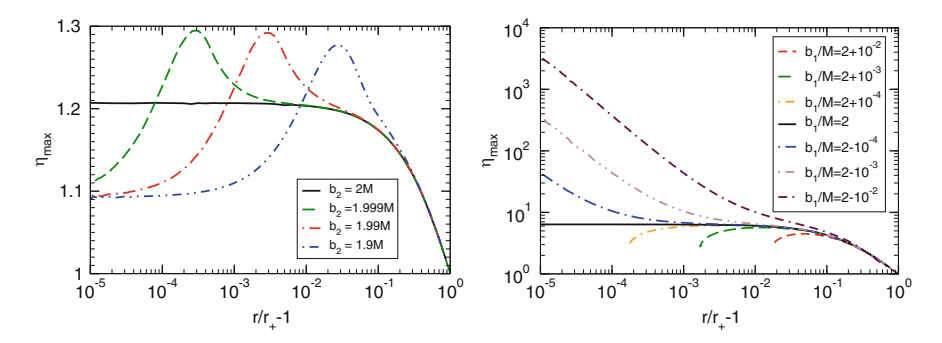


Fig. 3.7 Left: Maximum efficiency η_{max} for the collision of equal-energy particles as a function of the radius at which the reaction occurs, for $p_1^r < 0$, $p_2^r < 0$, $L_1/E_1 \equiv b_1 = 2M$, and an extremal black hole (a = M). The case $b_1 = b_2 = 2M$ corresponds to the decay of a single particle into two photons discussed in Sect. 3.3.1. The maximum efficiency for this case is $\eta_{\text{max}} \sim 1.3$, as shown in [34]. Right: Same, but for $p_1^r > 0$, $p_2^r < 0$ and $b_2 = -2(1 + \sqrt{2})M$. The curves for $b_1 > 2M$ terminate at the turning point of particle 1. The process considered in [36] corresponds to the case $b_1 \ge 2M$, while [37] extended these results to the case $b_1 < 2M$. From [37]

3.4 The ABC of Black Hole Superradiance

In this section we introduce the theory of superradiant scattering of test fields on a BH background. Fluctuations of order $\mathcal{O}(\epsilon)$ in the scalar or vector field in a given background induce changes in the spacetime geometry of order $\mathcal{O}(\epsilon^2)$, and therefore to leading order can be studied on a fixed BH geometry. Before entering in the details of the problem, it is instructive to consider a model that captures the basic ingredients of superradiant scattering in curved spacetime. For simplicity, we assume asymptotic flatness.

Let us assume that the spacetime is stationary and axisymmetric. As we shall see, in this case various types of perturbations propagating on fixed BH metrics can be expressed in terms of a single master variable Ψ which obeys a Schroedinger-type equation of the form

$$\frac{d^2\Psi}{dr_*^2} + V_{\text{eff}}\Psi = 0\,, (3.50)$$

where the potential $V_{\rm eff}(r)$ is model dependent and encodes the curvature of the background and the properties of the test fields. The coordinate r_* maps the region $r \in [r_+, \infty[$ to the entire real axis. Given the symmetries of the background, we consider a scattering experiment of a monochromatic wave with frequency ω and azimuthal and time dependence $e^{-i\omega t + im\varphi}$. Assuming $V_{\rm eff}$ is constant at the boundaries, Eq. (3.50) has the following asymptotic behavior

$$\Psi \sim \begin{cases} \mathcal{T}e^{-ik_H r_*} + \mathcal{O}e^{ik_H r_*} & \text{as } r \to r_+, \\ \mathcal{R}e^{ik_\infty r_*} + \mathcal{I}e^{-ik_\infty r_*} & \text{as } r \to \infty. \end{cases}$$
(3.51)

where r_+ is the horizon radius in some chosen coordinates, $k_H^2 = V_{\rm eff}(r \to r_+)$ and $k_\infty^2 = V_{\rm eff}(r \to \infty)$. These boundary conditions correspond to an incident wave of amplitude $\mathcal I$ from spatial infinity giving rise to a reflected wave of amplitude $\mathcal R$ and a transmitted wave of amplitude $\mathcal I$ at the horizon. The $\mathcal O$ term describes a putative outgoing flux across the surface at $r=r_+$. Although the presence of a horizon and a well-posed Cauchy problem would imply $\mathcal O\equiv 0$, here we shall generically keep this term, in order to allow for a nonvanishing outgoing flux in absence of an event horizon.

Let us assume that the potential is real.⁴ Then, since the background is stationary, the field equations are invariant under the transformations $t \to -t$ and $\omega \to -\omega$. Thus, there exists another solution $\bar{\Psi}$ to Eq. (3.50) which satisfies the complex conjugate boundary conditions. The solutions Ψ and $\bar{\Psi}$ are linearly independent and standard theory of ODEs tells us that their Wronskian is independent of r_* . Thus, the Wronskian evaluated near the horizon, $W = -2ik_H (|\mathcal{T}|^2 - |\mathcal{O}|^2)$, must equal the one evaluated at infinity, $W = 2ik_{\infty}(|\mathcal{R}|^2 - |\mathcal{I}|^2)$, so that

$$|\mathcal{R}|^2 = |\mathcal{I}|^2 - \frac{k_H}{k_\infty} (|\mathcal{T}|^2 - |\mathcal{O}|^2),$$
 (3.52)

independently from the details of the potential in the wave equation.

In the case of a one-way membrane boundary conditions at the horizon, i.e. $\mathcal{O}=0$, one gets $|\mathcal{R}|^2<|\mathcal{I}|^2$ when $k_H/k_\infty>0$, as is to be expected for scattering off perfect absorbers. However, for $k_H/k_\infty<0$, the wave is superradiantly amplified, $|\mathcal{R}|^2>|\mathcal{I}|^2$ [40].

Again, we stress how *dissipation* is a crucial ingredient for superradiance: without ingoing boundary conditions at the horizon, no superradiant scattering can occur [7, 8, 20, 41, 42]. In absence of a horizon (for example in the case of rotating perfect-fluid stars), regularity boundary conditions must be imposed at the center of the object. By applying the same argument as above, the Wronskian at the center vanishes, which implies $|\mathcal{R}|^2 = |\mathcal{I}|^2$, i.e. no superradiance. If the rotating object does not possess a horizon, superradiance can only come from some other dissipation mechanism, like friction due the atmosphere or viscosity, which anyway require a precise knowledge of the microphysics governing the interior of the object. Equivalently, we can argue that $|\mathcal{O}|^2$ and $|\mathcal{T}|^2$ are respectively proportional to the outgoing and transmitted energy flux across the surface at r_+ . In absence of dissipation, energy conservation implies that the outgoing flux will equal the transmitted one, i.e. $|\mathcal{O}|^2 = |\mathcal{T}|^2$ and Eq. (3.52) would again prevent superradiance, $|\mathcal{R}|^2 = |\mathcal{I}|^2$.

⁴As we shall discuss, this condition does not hold in various cases, for example for electromagnetic and gravitational perturbations of a Kerr BH, whereas it holds for scalar perturbations of spinning and charged BHs. When such condition does not hold, a more sophisticated analysis is needed, as discussed below.

3.5 Superradiance from Charged Static Black Holes

From the discussion of the previous section, it is clear that BH superradiance also occurs for electrically charged waves scattered by a static, charged BHs whenever (cf. Eq. (3.26))

$$\omega - q\Phi_H < 0. \tag{3.53}$$

Because the background is spherically symmetric, this type of superradiance is simpler to treat and in this section we start our analysis with this simpler case.

3.5.1 Linearized Analysis: Amplification Factors

The problem can be investigated at linearized level by considering a charged scalar field Ψ propagating on a RN background, which is defined by Eq. (3.4) with $\Lambda=0$. The Klein-Gordon equation for a minimally coupled charged scalar field in this curved spacetime was given in Eq. (3.2a). Using the ansatz $\Psi(t,r,\vartheta,\varphi)=\int d\omega \sum_{lm} e^{-i\omega t} Y_{lm}(\vartheta,\varphi) \psi(r)/r$, the equation above can be written in the Schroedinger-like form (3.50) with the potential

$$V_{\text{eff}}(r) = \omega^2 - f\left(\frac{l(l+1)}{r^2} + \frac{f'(r)}{r} + \mu_S^2\right) - \frac{2qQ\omega}{r} + \frac{q^2Q^2}{r^2},$$
 (3.54)

where r is defined in terms of r_* through $dr/dr_*=f=(r-r_+)(r-r_-)/r^2$. We can compute the reflectivity of a scattering experiment as done at the beginning of Sect. 3.4. In this specific case $k_H=\omega-q\Phi_H=\omega-qQ/r_+$ and $k_\infty=\sqrt{\omega^2-\mu_S^2}$. Equation (3.52) then reduces to

$$|\mathcal{R}|^2 = |\mathcal{I}|^2 - \frac{\omega - qQ/r_+}{\sqrt{\omega^2 - \mu_S^2}} |\mathcal{T}|^2.$$
 (3.55)

This equation shows that only waves with $\omega > \mu_S$ propagate to infinity and that superradiant scattering occurs, $|\mathcal{R}|^2 > |\mathcal{I}|^2$, whenever $\omega < qQ/r_+$, which coincides with the condition (3.53) derived from thermodynamical arguments.

The amplification factor for each frequency can be computed by integrating numerically the wave equation (cf. available MATHEMATICA® notebook in Appendix A). Figure 3.8 shows the amplification factor as a function of the frequency for monopole, l=0, waves and different BH Q and field q charge parameters. The amplification factor can be as high as 40% for nearly extreme BHs, substantially larger than the amplification factors of scalar fields in Kerr backgrounds, as we will see. Note also that the critical threshold for superradiance

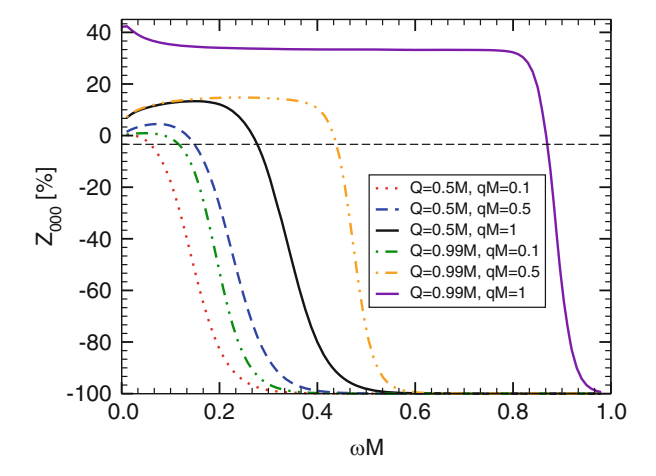


Fig. 3.8 Amplification factor $Z_{000} = |\mathcal{R}|^2/|\mathcal{I}|^2 - 1$ as a function of the frequency for a massless bosonic wave with l=0 and charge q scattered off a RN BH with charge Q and mass M. The threshold of superradiance, $Z_{000} > 0$, occurs when $\omega = qQ/r_+$

to occur, $Z_{000} > 0$, is to numerical accuracy described by condition (3.53). The amplification factor is proportional to Qq at intermediate values, but tends to 100 % at large values of q. We find that at large qM, the amplification factor satisfies

$$Z_{000} \sim 100 - \frac{80}{Qq} \quad (\%) \,.$$
 (3.56)

A detailed analysis in the time-domain has also recently been performed in [43]. Their results agree with the frequency-domain computation here presented and show indications that the maximum energy gain is always finite, independently of the initial conditions, in accord with the linear stability of the (sub-extremal) RN geometry. These results, in particular (3.56), are fully consistent with an analytical, small-frequency expansion for the amplification factors [44].

As we shall see in the next sections, the existence of superradiance for static charged BHs is a crucial ingredient for interesting applications in the context of the gauge/gravity duality. For example the spontaneous symmetry breaking mechanism near a RN-AdS BH [45], and applications therein related to holographic models of superconductors [46], all hinge on this superradiant phenomenon.

3.5.2 Backreaction on the Geometry: Mass and Charge Loss

Superradiant scattering seems to imply that energy is being extracted from the background which—at linearized order where superradiance is observed—is kept fixed. This is not a particularity of superradiant scattering from BHs, but rather

a very generic property. We will now show that when backreaction effects are included, both the mass and charge of the BH decrease.

Take a spherically symmetric, linearized charged scalar field

$$\Psi = \epsilon \frac{\psi(t, r)}{r} \,, \tag{3.57}$$

where now we explicitly introduced a bookkeeping parameter ϵ to help keep track of the expansion order. When allowed to propagate in a RN background, such field introduces backreactions in both the geometry and vector potential which are both of order ϵ^2 ,

$$A_{\mu} = \left(\frac{Q}{r} + \epsilon^2 \frac{Q_t(t, r)}{r}, \epsilon^2 \frac{\int dt Q_r(t, r)}{r^2}, 0, 0\right), \tag{3.58}$$

where the form of the perturbation quantities $Q_t(t, r)$, $Q_r(t, r)$ at order $\mathcal{O}(\epsilon^2)$ was chosen so that the radial electric field \mathcal{E}_r at large distances is

$$r^{2}\mathcal{E}_{r} = Q + \epsilon^{2} \left(Q_{r}(t, r) - rQ'_{t}(t, r) + Q_{t}(t, r) \right), \tag{3.59}$$

and therefore the charge flux can be obtained via Gauss's law to be

$$\dot{Q}_{\text{tot}} = \epsilon^2 \left(\dot{Q}_r - r \dot{Q}_t' + \dot{Q}_t \right) \,. \tag{3.60}$$

Likewise, the metric gets $\mathcal{O}(\epsilon^2)$ corrections of the form

$$ds^{2} = -\left(f - \epsilon^{2} \frac{2\mu(t, r)}{r}\right) dt^{2} + \left(f - \epsilon^{2} \frac{2\mu(t, r)}{r} - \epsilon^{2} \frac{X(t, r)}{r}\right)^{-1} dr^{2} + r^{2} d\Omega^{2},$$
(3.61)

with μ the mass loss (or gain) induced by the scalar field. At large distances, we know from the previous analysis of the scalar field equation at order $\mathcal{O}(\epsilon)$ that the solutions are oscillatory. Let the solutions at large distances be

$$\psi \sim f(t-r) + g(t+r), \qquad (3.62)$$

where the first term represents an outgoing wave and the second an ingoing wave. The field equations yield a vanishing $\dot{X}(t,r)$ at large distances, whereas the (t,r) component of Einstein's equations yields

$$2\frac{r}{f}\dot{\mu} = r\left[\left(\psi^{*}\right)'\dot{\psi} + \psi'\dot{\psi}^{*}\right] - \psi\dot{\psi}^{*} - \psi^{*}\dot{\psi} - iqQ\left[\psi\left(\psi^{*}\right)' - \psi^{*}\psi'\right], \quad (3.63)$$

where the first term on the r.h.s dominates at large distance. Because $(\psi^*)'\dot{\psi} + \psi'\dot{\psi}^* = 2g'(g^*)' - 2f'(f^*)'$, we obtain

$$\dot{\mu} \sim g'(g^*)' - f'(f^*)',$$
 (3.64)

where now primes stand for derivative with respect to the argument ((t-r)) and (t+r) for f and g respectively). In other words, for f' > g'—which can be seen to be the condition for superradiance at order $\mathcal{O}(\epsilon)$ —the mass of the BH does decrease at order $\mathcal{O}(\epsilon^2)$. From the scalar field stress-tensor, which can be read off from (3.2c), the energy flux at infinity can be computed using only the linearized result and reads

$$\dot{E}_{\infty} = -\left(g'(g^*)' - f'(f^*)'\right). \tag{3.65}$$

In other words, Eq. (3.64) tells us that the BH looses or gains mass at a rate which matches *exactly* the energy dissipated or ingoing at infinity, respectively and which is evaluated using only the linearized quantities. This is an important consistency result and shows that the energy for superradiant amplification does come—at the nonlinear level—from the medium, in this case the BH. For monochromatic scalar waves, $\psi \sim \mathcal{I}e^{-i\omega(t+r)} + \mathcal{R}e^{-i\omega(t-r)}$ at large distances, one gets

$$\dot{\mu} = -\omega^2 \left(|\mathcal{R}|^2 - |\mathcal{I}|^2 \right) \,, \tag{3.66}$$

indicating that superradiance extracts mass.

Finally, the r component of Maxwell's equations (3.2b) yields

$$qf \left[\psi^* \psi' - \psi(\psi^*)' \right] + 2i \left[\dot{Q}_r - r \dot{Q}_t' + \dot{Q}_t \right] = 0.$$
 (3.67)

From (3.60) this can be re-written as

$$2\dot{Q}_{\text{tot}} = iqf \left[\psi^* \psi' - \psi(\psi^*)' \right], \qquad (3.68)$$

which leads to loss of charge at order $\mathcal{O}(\epsilon^2)$ whenever the superradiance condition for the scalar field is satisfied at order $\mathcal{O}(\epsilon^2)$. For monochromatic scalar waves, $\psi \sim \mathcal{I}e^{-i\omega(t+r)} + \mathcal{R}e^{-i\omega(t-r)}$ at large distances, one finds

$$\dot{Q}_{\text{tot}} = -\omega q \left(|\mathcal{R}|^2 - |\mathcal{I}|^2 \right). \tag{3.69}$$

One can now use the first law of BH mechanics (3.22) to find

$$\dot{A}_H = \frac{8\pi}{k} \left(\dot{M} - \Phi_H \dot{Q} \right) = -\frac{8\pi}{k} \omega \left(\omega - q \Phi_H \right) \left(|\mathcal{R}|^2 - |\mathcal{I}|^2 \right). \tag{3.70}$$

In the superradiant regime, $|\mathcal{R}|^2 - |\mathcal{I}|^2 > 0$ but a necessary condition is that $\omega - q\Phi_H < 0$ thus yielding a positive area increase. Outside the superradiant regime

 $\omega - q\Phi_H > 0$ but there is no amplification and $|\mathcal{R}|^2 - |\mathcal{I}|^2 < 0$. In conclusion, the area always increases in agreement with the second law of BH mechanics.

3.6 Superradiance from Rotating Black Holes

Here we introduce the superradiant scattering of rotating BHs. We focus on the asymptotically-flat case and consider the geometry (3.5) with $\Lambda = 0$.

3.6.1 Bosonic and Fermionic Fields in the Kerr Geometry

The wave equation for linearized fluctuations around the Kerr geometry was studied by Teukolsky, Press and collaborators in great detail [40, 48–50]. Following Carter's unexpected result on the separability of the Hamilton-Jacobi equation for the geodesics in a Kerr geometry [51], he also noted that the analogue scalar field equation was separable [52], as was explicitly shown in [53]. In a breakthrough work (see [54] for a first-person historical account), it was shown that linearized perturbations of the Kerr geometry could be described with a single master equation, describing "probe" scalar (s = 0), massless Dirac ($s = \pm 1/2$), electromagnetic ($s = \pm 1$) and gravitational ($s = \pm 2$) fields in a Kerr background [48]. The master equation reads

$$\left[\frac{(r^2 + a^2)^2}{\Delta} - a^2 \sin^2 \vartheta \right] \frac{\partial \psi^2}{\partial t^2} + \frac{4Mar}{\Delta} \frac{\partial \psi^2}{\partial t \partial \varphi} + \left[\frac{a^2}{\Delta} - \frac{1}{\sin^2 \vartheta} \right] \frac{\partial \psi^2}{\partial \varphi^2}
- \Delta^{-s} \frac{\partial}{\partial r} \left(\Delta^{s+1} \frac{\partial \psi}{\partial r} \right) - \frac{1}{\sin \vartheta} \frac{\partial}{\partial \vartheta} \left(\sin \vartheta \frac{\partial \psi}{\partial \vartheta} \right) - 2s \left[\frac{a(r-M)}{\Delta} + \frac{i \cos \vartheta}{\sin^2 \vartheta} \right] \frac{\partial \psi}{\partial \varphi}
- 2s \left[\frac{M(r^2 - a^2)}{\Delta} - r - ia \cos \vartheta \right] \frac{\partial \psi}{\partial t} + \left(s^2 \cot^2 \vartheta - s \right) \psi = 0,$$
(3.71)

where s is the field's spin weight, and the field quantity ψ is directly related to Newman-Penrose quantities as shown in Table 3.1. By Fourier transforming

Table 3.1 Wavefunction ψ for each value of the spin weight-s

S	0	(1/2, -1/2)	(1, -1)	(2, -2)
ψ	Φ	$(\chi_0, \rho^{-1}\chi_1)$	$(\phi_0, \rho^{-2}\phi_2)$	$(\Psi_0, \rho^{-4}\Psi_4)$

The spin coefficient is given by $\rho \equiv -1/(r-ia\cos\vartheta)$. The quantities ϕ_0 , ϕ_2 , Ψ_0 and Ψ_4 are Newman-Penrose scalars [47] describing electromagnetic and gravitational perturbations, respectively. The quantities χ_0 and χ_1 denote components of the Dirac spinor along dyad legs

 $\psi(t, r, \vartheta, \varphi)$ and using the ansatz

$$\psi = \frac{1}{2\pi} \int d\omega e^{-i\omega t} e^{im\varphi} S(\vartheta) R(r) , \qquad (3.72)$$

Teukolsky found separated ODE's for the radial and angular part, which read, respectively

$$\Delta^{-s} \frac{d}{dr} \left(\Delta^{s+1} \frac{dR}{dr} \right) + \left(\frac{K^2 - 2is(r - M)K}{\Delta} + 4is\omega r - \lambda \right) R = 0, \qquad (3.73)$$

and

$$\frac{1}{\sin\vartheta} \frac{d}{d\vartheta} \left(\sin\vartheta \frac{dS}{d\vartheta} \right) + \left(a^2 \omega^2 \cos^2\vartheta - \frac{m^2}{\sin^2\vartheta} - 2a\omega s \cos\vartheta - \frac{2ms\cos\vartheta}{\sin^2\vartheta} - s^2\cot^2\vartheta + s + A_{slm} \right) S = 0,$$
(3.74)

where $K \equiv (r^2 + a^2)\omega - am$ and $\lambda \equiv A_{slm} + a^2\omega^2 - 2am\omega$. Together with the orthonormality condition

$$\int_0^{\pi} |S|^2 \sin \vartheta d\vartheta = 1, \qquad (3.75)$$

the solutions to the angular equation (3.74) are known as spin-weighted spheroidal harmonics $e^{im\varphi}S \equiv S_{slm}(a\omega, \vartheta, \varphi)$. When $a\omega = 0$ they reduce to the spin-weighted spherical harmonics $Y_{slm}(\vartheta, \varphi)$ [55]. For small $a\omega$ the angular eigenvalues are (cf. [56] for higher-order terms)

$$A_{slm} = l(l+1) - s(s+1) + \mathcal{O}(a^2\omega^2). \tag{3.76}$$

The computation of the eigenvalues for generic spin can only be done numerically [56].

Besides these equations, to have complete information about the gravitational and electromagnetic fluctuations, we need to find the relative normalization between ϕ_0 and ϕ_2 for electromagnetic fields and between Ψ_0 and Ψ_4 for gravitational perturbations. This was done in [40, 57, 58] assuming the normalization condition (3.75) and using what is now known as the Teukolsky-Starobinsky identities (see also [6] for details).

Defining the tortoise coordinate r_* as $dr/dr_* = \Delta/(r^2 + a^2)$, Eq. (3.73) has the following asymptotic solutions

$$R_{slm} \sim \mathcal{T}\Delta^{-s}e^{-ik_H r_*} + \mathcal{O}e^{ik_H r_*}$$
, as $r \to r_+$,
 $R_{slm} \sim \mathcal{I}\frac{e^{-i\omega r}}{r} + \mathcal{R}\frac{e^{i\omega r}}{r^{2s+1}}$, as $r \to \infty$, (3.77)

where $k_H = \omega - m\Omega_{\rm H}$ and $\Omega_{\rm H} = a/(2Mr_+)$ is the angular velocity of the BH horizon. Regularity at the horizon requires purely ingoing boundary conditions, i.e., $\mathcal{O} = 0$ (see Sect. 3 in [59] for a careful discussion of boundary conditions).

3.6.2 Energy Fluxes of Bosonic Fields at Infinity and on the Horizon

The perturbation equations (3.73) and (3.74) and their asymptotic behavior (3.77) can be used to define the energy fluxes that the fields carry through the horizon and to infinity. The expressions for the energy fluxes were computed in [40], to which we refer the reader for further details. The total energy fluxes at infinity per unit solid angle for scalar s = 0 and electromagnetic $s = \pm 1$ are given by (see Appendix C):

$$\frac{d^2E}{dtd\Omega} = \lim_{r \to +\infty} r^2 T_t^r, \tag{3.78}$$

where $T_{\mu\nu}$ is the stress-energy tensor of the test field. For the scalar case s=0, one has

$$\frac{dE_{\text{out}}}{dt} = \frac{\omega^2}{2} |\mathcal{R}|^2 , \quad \frac{dE_{\text{in}}}{dt} = \frac{\omega^2}{2} |\mathcal{I}|^2 , \qquad (3.79)$$

whereas, for the electromagnetic case $s \pm 1$,

$$\frac{d^2 E_{\text{out}}}{dt d\Omega} = \lim_{r \to +\infty} \frac{r^2}{2\pi} |\phi_2|^2 , \quad \frac{d^2 E_{\text{in}}}{dt d\Omega} = \lim_{r \to +\infty} \frac{r^2}{8\pi} |\phi_0|^2 . \tag{3.80}$$

From these definitions it can be shown that the fluxes, valid for s = 1, are given by

$$\frac{dE_{\text{out}}}{dt} = \frac{4\omega^4}{R^2} |\mathcal{R}|^2 , \quad \frac{dE_{\text{in}}}{dt} = \frac{1}{4} |\mathcal{I}|^2 , \qquad (3.81)$$

where $B^2 = Q^2 + 4ma\omega - 4a^2\omega^2$ and $Q = \lambda + s(s+1)$. The corresponding fluxes for s = -1 can be found using the Teukolsky-Starobinsky identities and can be obtained from the above relations by doing the transformation: $\mathcal{I} \to -(8\omega^2/B)\mathcal{I}$ and $\mathcal{R} \to -B/(2\omega^2)\mathcal{R}$. Finally, for gravitational perturbations $s \pm 2$ the fluxes

can be computed using the effective stress-energy tensor for linearized gravitational waves [60]. In terms of the Weyl scalars they are given by

$$\frac{d^2 E_{\text{out}}}{dt d\Omega} = \lim_{r \to +\infty} \frac{r^2}{4\pi\omega^2} |\Psi_4|^2 , \quad \frac{d^2 E_{\text{in}}}{dt d\Omega} = \lim_{r \to +\infty} \frac{r^2}{64\pi\omega^2} |\Psi_0|^2 , \qquad (3.82)$$

which can be shown to give for s = 2,

$$\frac{dE_{\text{out}}}{dt} = \frac{8\omega^6}{|C|^2} |\mathcal{R}|^2 , \quad \frac{dE_{\text{in}}}{dt} = \frac{1}{32\omega^2} |\mathcal{I}|^2 , \qquad (3.83)$$

where $|C|^2 = B^2 \left[(Q-2)^2 + 36a\omega m - 36a^2\omega^2 \right] + (2Q-1)(96a^2\omega^2 - 48a\omega m) + 144\omega^2(M^2 - a^2)$. For s = -2 the fluxes can be found once again using the Teukolsky-Starobinsky identities and can be obtained from the above relations by doing the transformation: $\mathcal{I} \to (64\omega^4/C)\mathcal{I}$ and $\mathcal{R} \to C^*/(4\omega^4)\mathcal{R}$.

The flux at the horizon for $s=0,\pm 1$ can be computed evaluating the change in energy of the hole. As showed in Appendix C it is given by

$$\frac{d^2 E_{\text{hole}}}{dt d\Omega} = \frac{\omega}{k_H} 2M r_+ T^{\mu\nu} n_\mu n_\nu , \qquad (3.84)$$

where n_{μ} is an inward unit vector, normal to the horizon surface.

Using (3.77), one finds for the scalar case

$$\frac{d^2 E_{\text{hole}}}{dt d\Omega} = M r_{+} \omega k_H \frac{S_{0lm}^2(\vartheta)}{2\pi} |\mathcal{T}|^2 , \qquad (3.85)$$

whereas, the electromagnetic case for s = 1 gives

$$\frac{d^2 E_{\text{hole}}}{dt d\Omega} = \frac{\omega}{8Mr_+ k_H} \frac{S_{1lm}^2(\vartheta)}{2\pi} |\mathcal{T}|^2.$$
 (3.86)

The case s=-1 can be obtained doing the transformation $B\mathcal{T} \rightarrow -32ik_HM^2r_+^2(-ik_H+2\epsilon)\mathcal{T}$, where $\epsilon=\sqrt{M^2-a^2}/(4Mr_+)$.

For gravitational perturbations one can use the first law of BH mechanics (3.22) to find the flux at the horizon [61]. The rate of change of the area can be found from Eq. (3.24). Since $\delta M = \delta E_{\text{hole}}$ we find

$$\frac{d^2A}{dtd\Omega} = \frac{16\pi r_+ k_H}{(M^2 - a^2)^{1/2} \omega} \frac{d^2E_{\text{hole}}}{dtd\Omega}.$$
 (3.87)

We can also show that [61]

$$\frac{d^2A}{dtd\Omega} = \frac{2Mr_{+}\Delta^4}{16(r^2 + a^2)^4 \epsilon (k_H^2 + 4\epsilon^2)} |\Psi_0|^2 , \qquad (3.88)$$

Equating (3.87) with (3.88) at the horizon, we find for s = 2

$$\frac{d^{2}E_{\text{hole}}}{dtd\Omega} = \frac{S_{2lm}^{2}(\vartheta)}{2\pi} \frac{\omega}{32k_{H}(k_{H}^{2} + 4\epsilon^{2})(2Mr_{+})^{3}} |\mathcal{T}|^{2}.$$
 (3.89)

whereas the corresponding for s=-2 can be found doing the transformation $CT \rightarrow 64(2Mr_+)^4 i k_H (k_H^2 + 4\epsilon^2) (-i k_H + 4\epsilon) T$.

From Eqs. (3.85), (3.86) and (3.89) one can see that if the superradiance condition is met, $k_H < 0$, the energy flux at the horizon is negative, i.e. energy (and angular momentum) are extracted from the BH.

3.6.3 Amplification Factors

For any scattering process experiment, energy conservation implies that

$$\frac{dE_{\rm in}}{dt} - \frac{dE_{\rm out}}{dt} = \frac{dE_{\rm hole}}{dt} \,. \tag{3.90}$$

This equation relates the asymptotic coefficients \mathcal{R} , \mathcal{I} and \mathcal{T} , which can be used to check the consistency of numerical computations *a posteriori*. Using Eqs. (3.85), (3.86) and (3.89), it is also clear that when energy is extracted from the BH, $k_H < 0 \implies \frac{dE_{\text{hole}}}{dt} < 0$, there is superradiance, $\frac{dE_{\text{in}}}{dt} < \frac{dE_{\text{out}}}{dt}$, as it should by energy conservation. Finally, from the energy fluxes at infinity one can define the quantity

$$Z_{slm} = \frac{dE_{\text{out}}}{dE_{\text{in}}} - 1, \qquad (3.91)$$

which, depending on whether the superradiance condition is met or not, provides the amplification or the absorption factor for a bosonic wave of generic spin s and quantum numbers (l, m) scattered off a Kerr BH. Using Eqs. (3.79), (3.80) and (3.81) we find

$$Z_{slm} = \begin{cases} \frac{|\mathcal{R}|^2}{|\mathcal{I}|^2} - 1, & \text{if } s = 0, \\ \frac{|\mathcal{R}|^2}{|\mathcal{I}|^2} \left(\frac{16\omega^4}{B^2}\right)^{\pm 1} - 1, & \text{if } s = \pm 1, \\ \frac{|\mathcal{R}|^2}{|\mathcal{I}|^2} \left(\frac{256\omega^8}{|C|^2}\right)^{\pm 1} - 1, & \text{if } s = \pm 2. \end{cases}$$
(3.92)

From the symmetries of the differential equations (3.73) and (3.74), one can prove the following relation

$$Z_{slm}(\omega) = Z_{sl-m}(-\omega). \tag{3.93}$$

This symmetry relation can be used to fix the sign of ω . In other words, if the full dependence on m is known for a given (s, l) and $\omega > 0$, the corresponding amplification factor for $-\omega$ follows immediately from Eq. (3.93). Thus, the amplification factor Z_{slm} in the entire real ω -axis can be obtained by only looking at $\omega > 0$. In the following we will exploit these symmetries when computing superradiant amplification factors numerically.

3.6.4 Dirac Fields on the Kerr Geometry

The absence of superradiance for massless Dirac fields was proved in 1973, through the separation of the massless spin-1/2 equations on a Kerr background [10]. In 1976, the separation of variables was extended to massive Dirac particles [62], a result soon generalized to the Kerr-Newman geometry [63, 64]. In 1978, these results were used to show that generic massive Dirac fields do not exhibit superradiant scattering in the Kerr BH background geometry [65] (thereby correcting a previous analysis [66]). The Dirac equation in curved spacetime is

$$\gamma^{\mu}\nabla_{\mu}\psi + i\mu_{e}\psi = 0, \qquad (3.94)$$

where $[\gamma^{\mu}, \gamma^{\nu}] = 2g^{\mu\nu}$, $\nabla_{\mu}\psi = \partial_{\mu}\psi - \Gamma_{\mu}\psi$, $\nabla_{\mu}\bar{\psi} = \partial_{\mu}\bar{\psi} + \bar{\psi}\Gamma_{\mu}$, $\bar{\psi} = \psi^{\dagger}\gamma^{0}$ is the Dirac adjoint, Γ_{μ} is the spinor affine connection [6] and μ_{e} is the fermion mass. The Dirac equation can be separated on a Kerr background using the ansatz

$$\psi = \left(\frac{R - S_{-}}{\sqrt{2}\rho^{*}}, \frac{R + S_{+}}{\sqrt{\Delta}}, -\frac{R + S_{-}}{\sqrt{\Delta}}, -\frac{R - S_{+}}{\sqrt{2}\rho}\right)^{T} e^{-i\omega t} e^{im\varphi},$$
(3.95)

where $\rho = r + ia\cos\vartheta$. The functions $R_{\pm}(r)$ and $S_{\pm}(\vartheta)$ satisfy a system of first-order differential equations, which can be reduced to the following second-order form [63]

$$\sqrt{\Delta} \frac{d}{dr} \left(\sqrt{\Delta} \frac{dR_{-}}{dr} \right) - \frac{i\mu_{e}\Delta}{\sqrt{\lambda} + i\mu_{e}r} \frac{dR_{-}}{dr}
+ \left[\frac{K^{2} + i(r - M)K}{\Delta} - 2i\omega r - \frac{\mu_{e}K}{\sqrt{\lambda} + i\mu_{e}r} - \mu_{e}^{2}r^{2} - \lambda \right] R_{-} = 0,$$

$$\frac{1}{\sin \vartheta} \frac{d}{d\vartheta} \left(\sin \vartheta \frac{dS_{-}}{d\vartheta} \right) + \frac{a\mu_{e}\sin \vartheta}{\sqrt{\lambda} + a\mu_{e}\cos \vartheta} \frac{dS_{-}}{d\vartheta}
+ \left[a^{2}\omega^{2}\cos^{2}\vartheta - \frac{m^{2}}{\sin^{2}\vartheta} + a\omega\cos\vartheta + \frac{m\cos\vartheta}{\sin^{2}\vartheta} - \frac{\cot^{2}\vartheta}{4} - \frac{1}{2} + \lambda - 2am\omega - a^{2}\omega^{2} \right]
+ \frac{a\mu_{e}(1/2\cos\vartheta + a\omega\sin^{2}\vartheta - m)}{\sqrt{\lambda} + a\mu_{e}\cos\vartheta} - a^{2}\mu_{e}^{2}\cos^{2}\vartheta \right] S_{-} = 0,$$
(3.97)

and R_+ and S_+ can be obtained once R_- and S_- are known [62]. The equations above were extended by Page to the case of Kerr-Newman metric and they reduce to Teukolsky's equations (3.73) and (3.74) when $\mu_e = 0$ and setting s = -1/2. Near the horizon, the radial functions behave as

$$R_{\pm}(r) \to A_{\pm} \Delta^{\frac{1\mp 1}{4}} e^{-ik_H r_*}$$
, (3.98)

so that R_- is vanishing at the horizon. Although the asymptotic solution exhibits the usual k_H term that appears due to the BH rotation relative to the reference frame (cf. Eq. (3.77)), in this case superradiance is forbidden to occur, as we now discuss.

Absence of superradiance is a direct consequence of the properties of the stressenergy tensor for fermions. Dirac's equation (3.94) is associated with a conserved current

$$J^{\mu} = \bar{\psi}\gamma^{\mu}\psi\,,\tag{3.99}$$

whose conservation, $\nabla_{\mu}J^{\mu}=0$, implies that the net number current flowing down the horizon is always positive

$$\frac{dN}{dt} = -\int d\vartheta d\varphi \sqrt{-g} J^r = \pi \sum_{lm} |A_+|^2 \int d\vartheta \sin\vartheta (|S_+|^2 + |S_-|^2), \qquad (3.100)$$

where the last step follows from the representation (3.95) and the orthonormality of the eigenfunctions, Eq. (3.75) [65]. From the equation above, it is clear that dN/dt > 0, i.e. there is no net flux coming *from* the horizon, for any frequency. Indeed, using the stress-energy tensor for a Dirac field, it is easy to show that the net energy flow across the horizon per unit time and solid angle is $\sim \omega dN/dt$, signaling the absence of energy and angular momentum extraction for fermions.

The same conclusion can be obtained by studying the reflection and transmission coefficients in the scattering of a fermionic wave off a Kerr BH. Chandrasekhar showed that Eq. (3.96) can be written as a Schroedinger-like equation in modified tortoise coordinates [6]. Using the homogeneity of the Wronskian, the same analysis performed at the beginning of Sect. 3.4, allows to relate the reflection coefficient \mathcal{R} and the transmission coefficient \mathcal{T} as

$$|\mathcal{R}|^2 = |\mathcal{I}|^2 - \frac{\omega}{\sqrt{\omega^2 - \mu_e^2/2}} |\mathcal{T}|^2.$$
 (3.101)

The reflection coefficient is always less than unity, showing that superradiance cannot occur.

As discussed in Sect. 3.2, at the classical level superradiant amplification is a consequence of Hawking's area theorem [8, 67]. It might appear that the absence of superradiance for fermions is at odds with this fact. However, as already pointed out in the original analysis [10], the stress-energy tensor for fermions does not satisfy

the weak energy condition, $T_{\mu\nu}t^{\mu}t^{\nu} > 0$ for any timelike vector t^{μ} , which is one of the assumptions behind Hawking's theorem.

3.6.5 Linearized Analysis: Analytic Versus Numerics

The amplification factors Z_{slm} for a bosonic wave of generic spin s and quantum numbers (l, m) (cf. Eq. (3.92)) scattered off a Kerr BH can be computed by integrating numerically the Teukolsky equations presented in Sect. 3.6.1. When the superradiance condition is not fulfilled, the same computation provides the absorption cross section of a spinning BH. Remarkably, the problem was also solved analytically in the low-frequency regime [68, 69]. Using matching-asymptotic techniques (see Appendix B), the authors showed that in the low-frequency regime

$$Z_{slm} = Z_{0lm} \left[\frac{(l-s)!(l+s)!}{(l!)^2} \right]^2, \qquad (3.102)$$

$$Z_{0lm} = -8Mr_{+}(\omega - m\Omega_{\rm H})\omega^{2l+1} (r_{+} - r_{-})^{2l} \left[\frac{(l!)^{2}}{(2l)!(2l+1)!!} \right]^{2}$$

$$\prod_{k=1}^{l} \left[1 + \frac{M^{2}}{k^{2}} \left(\frac{\omega - m\Omega_{\rm H}}{\pi r_{+} T_{H}} \right)^{2} \right], \qquad (3.103)$$

where $T_H = (r_+ - r_-)/(4\pi r_+^2)$ is the BH temperature and Z_{0lm} is the amplification factor for scalar waves. The formulas above are valid for any spin $a \le M$ provided $\omega M \ll 1$. The superradiant condition is independent of the spin of the field and $Z_{slm} > 0$ whenever $\omega < m\Omega_H$ for any l and s. In addition, Eq. (3.102) shows that: (i) the amplification factor is independent of the spin of the field when $l \gg 2s^2$, and (ii) in the low-frequency limit the amplification of electromagnetic waves is only a factor 4 larger than that of scalar waves (this maximum is obtained when l = m = 1), whereas the amplification of gravitational waves is a factor 36 larger than that of scalar waves for l = m = 2.

Defining $\alpha=1-\omega/(m\Omega_{\rm H})$, the equations above predict $Z_{slm} \propto \alpha$ when $|\alpha| \ll (r_+-r_-)/(am)$, and the exact coefficient can be extracted from Eqs. (3.102) and (3.103). Thus, in this regime Z_{slm} is linear and continuous in $\omega-m\Omega_{\rm H}$ near the threshold. Furthermore, the amplification is largest at $\omega_{\rm max} \sim (2l+1)/(2l+2)m\Omega_{\rm H}$, independently of s.

With the further assumption $\omega \ll m\Omega_{\rm H}$, Eq. (3.102) reduces to

$$Z_{slm} = 8r_{+}^{2} T_{H} \omega^{2l+1} (r_{+} - r_{-})^{2l} \left[\frac{\Gamma(1 + l - s)\Gamma(1 + l + s)}{(2l + 1)!!\Gamma(l + 1)\Gamma(2l + 1)} \right]^{2} \times \sinh\left(\frac{m\Omega_{H}}{r_{+}T_{H}}\right) \Gamma\left(l - \frac{im\Omega_{H}}{\pi r_{+}T_{H}} + 1\right) \Gamma\left(l + \frac{im\Omega_{H}}{\pi r_{+}T_{H}} + 1\right). \quad (3.104)$$

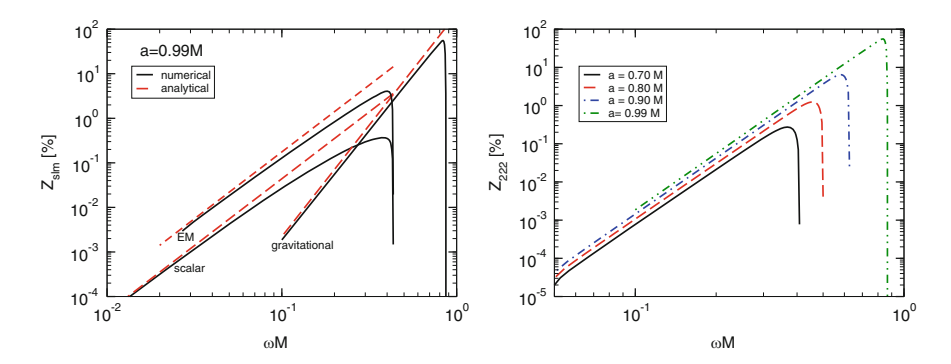


Fig. 3.9 Left: Amplification factor Z_{slm} as a function of the frequency ω of a wave scattered off a Kerr BH with spin parameter $a=0.99\,\mathrm{M}$ obtained by solving numerically the Teukolsky equations and compared to the analytical result in the low-frequency limit. We consider scalar and electromagnetic waves with l=m=1 and gravitational waves with l=m=2. Superradiance, $Z_{slm}>0$, occurs when $0<\omega< m\Omega_\mathrm{H}$ in all cases. Right: The amplification factor for gravitational waves and for different values of the BH spin

which, although not reproducing the threshold behavior $Z_{slm} \rightarrow 0$ as $\omega \rightarrow m\Omega_{\rm H}$, reproduces well the exact numerical results even at moderately large frequencies, whereas the full equation (3.102) breaks down before. A comparison between the low-frequency analytical result (3.104) and the exact result obtained by solving the Teukolsky equation numerically (the MATHEMATICA® notebook to compute this factor and data tables are publicly available at [70], cf. Appendix A) is presented in the left panel of Fig. 3.9 for scalar, electromagnetic and gravitational waves scattered off a nearly-extremal BH with a=0.99M. In this figure we only focus on the superradiant regime, $0<\omega< m\Omega_{\rm H}$. Data files of the amplification factors in the entire parameter spaces are provided in a supplementary file (cf. Appendix A).

Equations (3.102) and (3.104) break down when $\omega M \sim 1$, a condition which is generically fulfilled near the superradiant threshold $\omega \sim m\Omega_{\rm H}$ (equivalently $\alpha \sim 0$) and in the quasi-extremal limit, even at low m. In fact, it is clear from Fig. 3.9 that the low-frequency limit (3.104) generically overestimates the amplification factors. The behavior near the threshold has been also studied analytically using a different matching asymptotic technique [68]. In the extremal case, a = M, defining $\delta^2 = 2m^2 - A_{slm} - (s+1/2)^2$ [we recall that A_{slm} are the eigenvalues of the spin-s spheroidal harmonics which satisfy Eq. (3.74)], when $\delta^2 < 0$ one finds [69]

$$Z_{slm} = 4 S_{\alpha} |\delta|^{2} \left(2m^{2} |\alpha| \right)^{2|\delta|} \frac{|\Gamma(1/2 + s + |\delta| + im)|^{2} |\Gamma(1/2 - s + |\delta| + im)|^{2}}{\Gamma(1 + 2|\delta|)^{4}} e^{\pi n[1 - S_{\alpha}]},$$
(3.105)

where $S_{\alpha} = \operatorname{sgn}(\alpha)$, and

$$Z_{slm}^{-1} = \frac{S_{\alpha}e^{\pi m[S_{\alpha}-1]}}{\sinh(2\pi\delta)^{2}} \left\{ \cosh[\pi(m-\delta)]^{2}e^{\pi\delta[S_{\alpha}-1]} + \cosh[\pi(m+\delta)]^{2}e^{-\pi\delta[S_{\alpha}-1]} - 2\cosh[\pi(m-\delta)]\cosh[\pi(m+\delta)]\cos[\gamma_{0} - 2\delta\log(2m^{2}|\alpha|)] \right\}, \quad (3.106)$$

for $\delta^2 > 0$ and $|\alpha| \ll m^{-4} \max(1, |\alpha|^2)$. In the equation above

$$\gamma_0 = 4 \arg[\Gamma(1+2i\delta)] + 2 \arg[\Gamma(1/2+s+im-i\delta)] + 2 \arg[\Gamma(1/2+s-im-i\delta)].$$
(3.107)

Note that the condition $\delta^2 > 0$ is satisfied by almost all modes [71], for example it is satisfied for s=1 for any $l=m \geq 1$ and for s=2 for any $l=m \geq 2$, i.e. for the cases that correspond to the largest amplification. The behaviors described by Eqs. (3.105) and (3.106) are quite different. When $\delta^2 < 0$, Z_{slm} is continuous and monotonic near $\alpha \sim 0$, whereas when $\delta^2 > 0$ it displays an infinite number of oscillations as $\alpha \to 0$ in the region $|\alpha| \ll 1/m^2$ (provided $\delta \ll 1$). Remarkably, as understood already in [68], these oscillations are related to the existence of quasistationary bound states near the event horizon of a nearly-extremal Kerr BH. These quasi-bound states have been computed in [72–74].

When $\delta^2>0$, the oscillations have a small amplitude and—except for the exceptional case m=1 and $\pi\delta\lesssim 1$ —can be ignored. In such case, for $\alpha>0$ one finds

$$Z_{slm} \sim e^{2\pi(\delta - m)}, \qquad (3.108)$$

and the amplification factor is discontinuous near the superradiant threshold. Finally, when $\alpha < 0$ we have $\min(Z_{slm}) = -1$, i.e. there are regions of the parameter space in which the reflectivity is zero and the BH is totally transparent [68, 69].

Equations (3.105) and (3.106) are also valid in the quasi-extremal limit, $a \sim M$, provided $m < \sqrt{M/(M-a)}$ and $(r_+ - r_-)/(am) \ll |\alpha| \ll 1/m^2$. Since when $|\alpha| \ll (r_+ - r_-)/(am)$ the amplification factor is described by Eq. (3.102), near the threshold $Z_{slm} \propto \alpha$ and it is continuous for any a < M. Note however that there exists a regime which is not captured by the formulas above, namely when $a \sim M$ and $\omega \sim m\Omega_H$ such that $\alpha \ll (r_+ - r_-)/(am)$. Describing this regime analytically requires more sophisticated matching techniques. Various analytical treatments of the Teukolsky's equation can be found in [75–79] and they are in agreement with the exact results. A representative example of the dependence of Z_{slm} with the BH spin is presented in the right panel of Fig. 3.9.

The maximum amplification factors are about 0.4, 4.4 and 138 % for scattering of massless scalar, electromagnetic and gravitational waves, respectively, and for the minimum value of l=m allowed (namely l=m=1 for scalar and electromagnetic waves and l=m=2 for gravitational waves). As evident from Fig. 3.9, the maximum amplification occurs for BHs with $a\approx M$ and very close to the superradiant threshold, $\omega\sim m\Omega_{\rm H}$. Indeed, near the threshold the curve

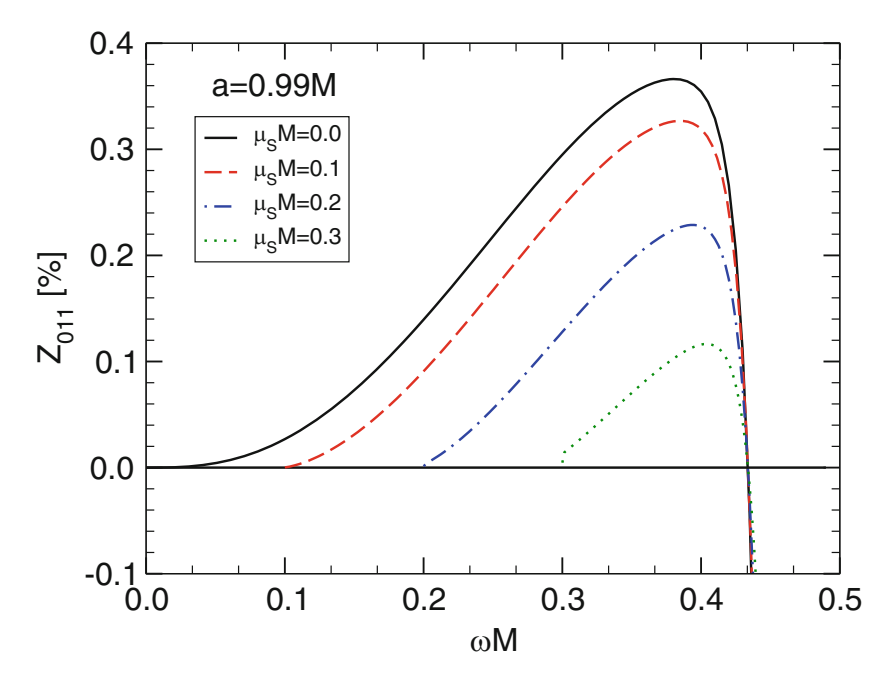


Fig. 3.10 Amplification factor $Z_{0lm} = |\mathcal{R}|^2/|\mathcal{I}|^2 - 1$ as a function of the frequency for a massive scalar field with l = m = 1 and mass μ_S scattered off a Kerr BH with angular momentum parameter a = 0.99 M. Superradiance, $Z_{0lm} > 0$, occurs when $\mu_S < \omega < m\Omega_{\rm H}$

becomes very steep (with a steepness that increases with the BH spin) and it attains a maximum right before reaching $\omega = m\Omega_{\rm H}$ where superradiance stops. Detailed tables of the amplification factors for scalar, EM and gravitational waves for various parameters are provided in accompanying data files (cf. Appendix A).

The previous analysis concerns massless fields, but the extension to massive fields is, in principle, straightforward. As an example, we show in Fig. 3.10 the amplification factors of a massive scalar field—with mass $\mu_S \bar{h}$ —in the background of a Kerr BH. It is clear from Eq. (3.2a) that no propagation is possible for energies $\omega < \mu_S$. Thus, superradiance can also occur for massive waves as long as the condition $\mu_S < \omega < m\Omega_H$ is satisfied. Waves with $\omega < \mu_S$ are trapped near the horizon and are exponentially suppressed at infinity. Figure 3.10 shows that superradiance is *less* pronounced for massive fields; the larger the field mass μ_S , the smaller the amplification factors are.

3.6.6 Scattering of Plane Waves

Generically, the field scattering off a BH is a superposition of multipoles. Of particular interest for a variety of applications is a field which is a plane wave

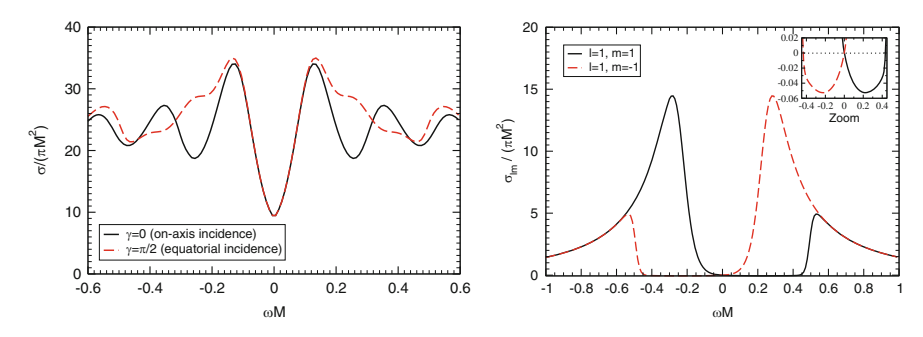


Fig. 3.11 Absorption cross-section of a scalar plane wave incident on a rotating Kerr BH (a/M = 0.99) along the axis and equator. The *left panel* shows that the absorption cross-section is always positive, i.e., plane waves are never superradiantly amplified. However, as expected some partial waves are indeed subjected to superradiance, as the *right panel* shows

at infinity. The multipolar expansion of a plane wave is straightforward to perform [80].

Scalar Waves Let us focus on a massless scalar field, and assume without loss of generality that there is an incoming monochromatic plane wave propagating along the $(\sin \gamma, 0, \cos \gamma)$ -direction. The absorption cross section σ of a spinning BH can then be computed as [80, 81]

$$\sigma = \frac{4\pi^2}{\omega^2} \sum_{lm} \sigma_{lm} \equiv \sum_{lm} |S_{0lm}(\gamma)|^2 \left(1 - \frac{|\mathcal{R}|^2}{|\mathcal{I}|^2} \right) = -\frac{4\pi^2}{\omega^2} \sum_{lm} |S_{0lm}(\gamma)|^2 Z_{0lm},$$
(3.109)

where we used the asymptotic behavior as defined in (3.77). In other words, once the amplification factors have been computed for any l and m, the cross-section is trivial to obtain.

The results for two extreme cases—incidence along the equatorial ($\gamma = \pi/2$) and axial ($\gamma = 0$) directions—are summarized in Fig. 3.11 for a rapidly spinning BH with a/M = 0.99. Because $S_{0lm}(0) = 0$ unless m = 0, the cross-section for waves incident along the axial direction simplifies as

$$\sigma(\gamma = 0) = -\frac{4\pi^2}{\omega^2} \sum_{l=0}^{\infty} |S_{0l0}(0)|^2 Z_{0l0}.$$
 (3.110)

For generic incidence angles, the total cross-section is symmetric along the $\omega=0$ axis, as could be anticipated from the general symmetry properties of the wave equation, cf. Eq. (3.93). The first important conclusion is that plane scalar waves are never superradiantly amplified, or in other words, the absorption cross-section is positive for all values of frequency ω . As might be expected from the general

equation (3.109), because the amplification factor can become positive, some of the partial cross-sections σ_{lm} can become negative, as shown in the right panel of Fig. 3.11 for the l = |m| = 1 modes [81].

Gravitational Waves The scattering of plane GWs off rotating BHs is an important, decades-old problem [82–86]. One of the important differences with respect to scalar waves, is that the symmetry along the $\omega=0$ axis is lost. In fact, for scattering along the symmetry axis of a Kerr BH, the low-frequency differential scattering cross reads

$$M^{-2}\frac{d\sigma}{d\Omega} \approx \frac{\cos^8(\vartheta/2)}{\sin^4(\vartheta/2)} \left(1 - 4a\omega \sin^2(\vartheta/2)\right) + \frac{\sin^8(\vartheta/2)}{\sin^4(\vartheta/2)} \left(1 + 4a\omega \sin^2(\vartheta/2)\right). \tag{3.111}$$

Thus, waves of different sign of ω are scattered differently from a rotating BH, generically inducing nontrivial polarization on the scattered field.

The absorption cross-section of GWs off rotating BHs can be obtained in a similar fashion to those of scalar waves. One finds, for incidence along the axis of symmetry of a Kerr BH [82–86],

$$\sigma(\gamma = 0) = \frac{4\pi^2}{\omega^2} \sum_{l=2}^{\infty} |S_{2l2}(\vartheta = 0)|^2 Z_{2l2}, \qquad (3.112)$$

where again $Z_{2/2}$ are the amplification factors studied previously⁵ (see Fig. 3.9). Because the amplification of GWs can be two orders of magnitude larger than that of scalars, the cross-section for scattering of plane waves can now become *negative*. Thus, plane GWs *can* be superradiantly amplified. This is shown in Fig. 3.12, from which two features stand out: negative-frequency waves—or waves counter-rotating with respect to the BH—are always absorbed. On the other hand, positive-frequency waves (which co-rotate with the BH) are amplified in the superradiant regime.

Generically, a plane wave is a superposition of positive and negative-frequencies. For linearly polarized waves, for example, one can easily show that the net effect always results in absorption [86].

Recently, the scattering of plane waves off a Kerr BH has been analyzed in the context of superradiant amplification of the radiation from a BH-pulsar system [87]. In this case, the pulsar's GW and EM luminosities show a characteristic modulation, which is due to superradiant scattering and depends on the pulsar position relative to the BH.

⁵Note that a planar tensor wave along $\gamma=0$ in Cartesian coordinates will have a $\sin 2\varphi$ modulation when transformed to spherical coordinates, in which the multipolar decomposition is performed. This explains why Eq. (3.112) depends only on |m|=2 and on a sum over all multipolar indices $l\leq 2$. Likewise, an EM wave along $\gamma=0$ would be modulated by $\sin\varphi$ and its cross-section would only depend on |m|=1, whereas the cross-section (3.110) for a scalar wave along $\gamma=0$ only depends on m=0.

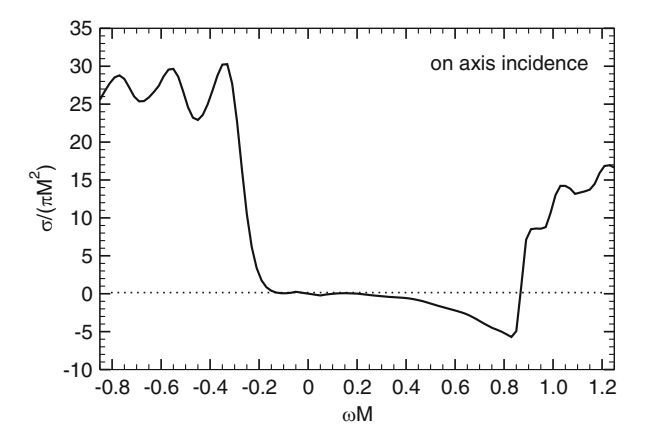


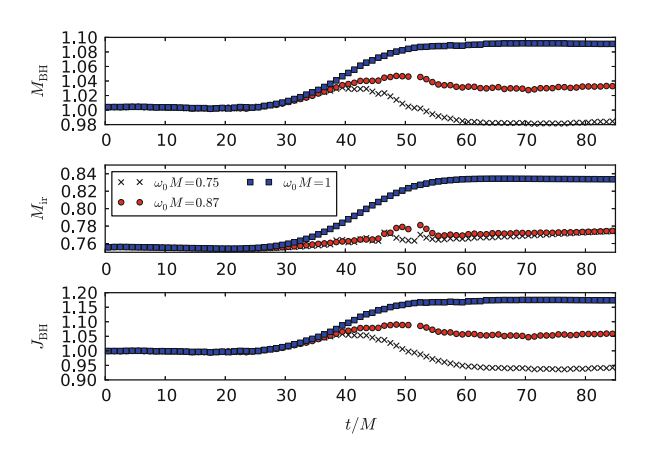
Fig. 3.12 Absorption cross-section of a gravitational plane wave incident on a rotating Kerr BH (a/M=0.99) along the rotation axis. The figure shows that counter-rotating $(\omega<0)$ plane waves are more absorbed than co-rotating waves $(\omega>0)$, and that in the superradiant regime plane waves are amplified

Acoustic Geometries The scattering of sounds waves off acoustic BH geometries, in particular the one discussed in Sect. 3.9 was studied recently [88]. Clear hints of superradiance were found, manifested as negative partial absorption "lengths" (as this is a (2 + 1)-dimensional geometry) for co-rotating modes at low frequencies.

3.6.7 Nonlinear Superradiant Scattering

In Sect. 3.5.2 we showed that when backreaction effects are taken into account then superradiance of charged fields does indeed extract mass and charge away from the BH. Fully nonlinear studies of superradiance—either for charged or rotating BHs—are extremely scarse, with one notable exception. The authors of [89] performed nonlinear scattering experiments, constructing initial data representing a BH with dimensionless spin a/M=0.99, and an incoming quadrupolar GW packet. Their results are summarized in Fig. 3.13, for three different wavepacket frequencies, $M\omega=0.75$, 0.87, 1 (note that only the first is in the superradiant regime (1.1)). The wavepackets carry roughly 10% of the spacetime's total mass. These results confirm that low frequency radiation does extract mass and spin from the BH (both the mass $M_{\rm BH}$ and spin $J_{\rm BH}$ of the BH decrease for the superradiant wavepacket with $M\omega=0.75$), and that nonlinear results agree quantitatively with linear predictions for small wavepacket amplitudes [40]. To summarize, although further studies would certainly be interesting, superradiance is confirmed at full nonlinear level for rotating BHs.

Fig. 3.13 Evolution of a highly spinning BH (a/M = 0.99) during interaction with different frequency GW packets, each with initial mass $\approx 0.1M$. Shown (in units where M = 1) are the mass, irreducible mass, and angular momentum of the BH as inferred from AH properties. From [89]



3.7 Boosted Black Strings: Ergoregions Without Superradiance

In the previous sections, we saw that superradiance is generically caused by a medium moving faster than the speed of the interaction in the medium (for example the Cherenkov effect of Sect. 2.3.1 or sound amplification at discontinuities explained in Sect. 2.4.2), or when the "angular velocity of the medium" is larger than the angular phase velocity of the interaction (an example was discussed in Sect. 2.5, another is provided by the topic of this work, rotating BHs). These considerations seem to forbid gravitational superradiance for linear motion. However, there are simple gravitational systems with ergoregions whose only motion is linear: consider a black string in five-dimensional spacetime, ⁶

$$ds^{2} = -f(r)dt^{2} + \frac{dr^{2}}{f(r)} + r^{2}d\Omega_{2}^{2} + dz^{2},$$
(3.113)

where f(r) = 1 - 2M/r. Now boost the spacetime along the z-direction with boost $v = \tanh \beta$ and get [90]

$$ds^{2} = -dt^{2} + \frac{dr^{2}}{f(r)} + r^{2}d\Omega_{2}^{2} + dz^{2} + (1 - f(r))\cosh^{2}\beta (dt + \tanh\beta dz)^{2}, \quad (3.114)$$

It is easy to check that this solution has an event horizon at r=2M and a "momentum" ergosurface at $r=2M\cosh^2\beta$. Since this solution is just a non-

⁶This example was suggested to us by Luis Lehner and Frans Pretorius.

⁷We follow the terminology of Dias, Emparan and Maccarrone who, in a completely different context, arrived at conclusions very similar to ours, see Sect. 2.4 in [91].

boosted black string as seen by a boosted observer, it is clear that no superradiant amplification nor Penrose processes are possible. Let us show how this comes about.

Superradiance Consider perturbations of the metric (3.114) due to a scalar field Ψ . Using the ansatz

$$\Psi = \frac{\psi(r)}{r} Y(\vartheta, \varphi) e^{-i(\omega t + kz)}, \qquad (3.115)$$

where $Y(\vartheta, \varphi)$ are the spherical harmonics, the radial function ψ follows a Schroedinger-type equation of the form (3.50). The solution ψ has the asymptotic behavior given by (3.51) with $k_H = \omega \cosh \beta - k \sinh \beta$ and $k_\infty = \sqrt{\omega^2 - k^2}$, from which condition (3.52) follows. Now, at first sight one could be led to think that superradiance is possible whenever the following condition is met:

$$k_H < 0 \implies \omega < kv$$
. (3.116)

However the boundary condition at infinity also implies $|\omega| > |k|$. Since -1 < v < 1 we can see that the condition (3.116) is never met and, as expected, superradiance does not occur in this geometry. In other words, the potentially dangerous modes are redshifted away.

Penrose Process To understand why the Penrose process is not possible consider the negative energy particle that falls into the BH with energy and total linear momentum given by $\mathcal{E} < 0$ and p, respectively. Denoting the particle's linear momentum along the z-direction by p_z , from arguments similar to those leading to Eq. (3.33) it follows that (note that $v_{\rm H} = -v$ is the velocity of a zero linear momentum observer at the horizon)

$$\mathcal{E} + p_z v \ge 0 \implies |\mathcal{E}| \le |p_z v|. \tag{3.117}$$

The first condition also implies that, for negative energy particles and 0 < v < 1, $p_z > 0$. Moreover, since 0 < v < 1, we have

$$|\mathcal{E}| < p_z. \tag{3.118}$$

On the other hand, any particle must satisfy the relation

$$\mathcal{E}^2 = p^2 + m^2 \ge p_z^2 \implies |\mathcal{E}| \ge |p_z|.$$
 (3.119)

Therefore, energy extraction is impossible because the inequality (3.118) is never satisfied for a negative energy particle.⁸

⁸This simple proof was suggested to us by Roberto Emparan.

The absence of the Penrose process can also be understood through an analysis of geodesic motion. Let us focus on zero angular momentum trajectories for simplicity. Geodesics in the spacetime (3.114) are then described by the equations of motion,

$$\dot{t} - (1 - f(r))\cosh^2\beta(\dot{t} + \tanh\beta\dot{z}) = E,$$
 (3.120)

$$\dot{z} + (1 - f(r))\cosh^2\beta(\dot{t} + \tanh\beta\dot{z})\tanh\beta = P,$$
(3.121)

$$\dot{r}^2 = (E^2 - P^2) \left(1 - \frac{M}{r} \right) - f(r)\delta_1 + \frac{M \left[\left(E^2 + P^2 \right) \cosh 2\beta + 2EP \sinh 2\beta \right]}{r},$$
(3.122)

where E, P are the (conserved) energy and linear momentum per unit rest mass. In the Penrose process, the breakup occurs at a turning point inside the ergoregion and with negative energy, E < 0. From (3.122), the turning point condition, $\dot{r}(r = r_0) = 0$, gives

$$E = \frac{-PM \sinh 2\beta + \sqrt{f(r_0)r_0 \left[\delta_1(r_0 + 2M(\cosh^2 \beta - 1)) + P^2 r_0\right]}}{r_0 + 2M(\cosh^2 \beta - 1)}, (3.123)$$

$$P = \frac{EM \sinh 2\beta \pm \sqrt{f(r_0)r_0 \left[\delta_1(2M \cosh^2 \beta - r_0) + E^2 r_0\right]}}{r_0 - 2M \cosh^2 \beta},$$
 (3.124)

where E has been chosen such that when $r_0 \to \infty$ we have E > 0. It is clear from (3.123) that for E < 0 we need $P \tanh \beta > 0$ and

$$PM \sinh 2\beta > \sqrt{f(r_0)r_0 \left[\delta_1(r_0 + 2M(\cosh^2 \beta - 1)) + P^2 r_0\right]}$$

$$\implies P^2 M^2 \sinh^2 2\beta > f(r_0)r_0 \left[\delta_1(r_0 + 2M(\cosh^2 \beta - 1)) + P^2 r_0\right]$$

$$\implies P^2 (r - 2M\cosh^2 \beta) < (2M - r)\delta_1 < 0 \implies r - 2M\cosh^2 \beta < 0.$$
(3.125)

Thus the particle needs to be inside the ergosphere to have a negative energy. For the Penrose process to occur we also need the positive energy fragment to be able to travel back to infinity. When $r \to \infty$ we have

$$\dot{r}^2 = E^2 - P^2 - \delta_1, \quad r \to \infty.$$
 (3.126)

This means that only when $E^2 - P^2 - \delta_1 > 0$ is motion from r_0 to infinity allowed. Equation (3.122) however, says that there is only one turning point satisfying $\dot{r}(r = r_0) = 0$, given by

$$r_0 = \frac{2M \left[(P \cosh \beta + E \sinh \beta)^2 + \delta_1 \right]}{P^2 + \delta_1 - E^2} \,. \tag{3.127}$$

The condition that $r_0 > 0$ implies that the particles are not allowed to escape to infinity since $E^2 - P^2 - \delta_1 < 0$. In fact since there is only one turning point and at the horizon we have

$$\dot{r}^2 = (E \cosh \beta + P \sinh \beta)^2, \quad r \to 2M, \tag{3.128}$$

which is always positive, both particles are forced to fall into the horizon and there is no extraction of energy from the BH.

3.8 Superradiance in Higher Dimensional Spacetimes

With the exception of the boosted black string just discussed, we have so far only considered BH superradiance in four-dimensional spacetimes. Generalization to higher dimensions can be done along the same lines. The multitude of black objects in higher dimensions makes this an interesting and relatively unexplored subject (for a review on BHs in higher dimensions see [94]).

From the rigidity theorem, a stationary D-dimensional BH must be axisymmetric [95, 96], meaning that it must have D-3 rotational Killing vectors in addition to the time translation Killing vector. Thus, to study superradiance in higher-dimensions, one must take into account that there exist at most D-3 rotation axis. The condition for superradiance in the background of a five-dimensional, topologically spherical BH was computed in [97]; using the area theorem this condition was generalized to arbitrary dimensions for Myers-Perry BHs with a single angular momentum parameter [98] and finally with multiple angular momentum parameters in [99]. More recently the condition was computed for asymptotically flat rotating BHs with generic spacetime dimension and horizon topology using a Wronskian approach [100]. The generalized superradiance condition (1.1) is given by

$$\omega < \sum_{i=1}^{i \le D-3} m_i \Omega_{\mathrm{H}}^i, \qquad (3.129)$$

where m_i is a set of integers, corresponding to the azimuthal numbers with respect to the different rotation axis, and Ω_H^i represents the multi-component angular velocity of the horizon.

Amplification factors for a scalar field where computed for Myers-Perry BH with a single angular momentum parameter in [101–103]. They showed that the superradiant amplification is less efficient in higher dimensions and the maximum

⁹There are no gravitational degrees of freedom in less than four dimensions, and a BH solution only exists for a negative cosmological constant, the so-called BTZ solution [92]. This solution has some similarities with the Kerr-AdS metric and, as we shall discuss in Sect. 3.10, superradiance does not occur when reflective boundary conditions at infinity are imposed [93].

amplification factor decreases with the dimension of the spacetime; for a doubly spinning Myer-Perry BH in 5D, the amplification factors were computed in [104]. Motivated by extra dimensional models which predicted the possibility of creating micro BHs in particle accelerators such as the LHC, amplification factors for a singly-spinning higher-dimensional Myers-Perry BH induced on an asymptotically flat four-dimensional brane were also computed. This was done for spin-0 particles [105–107] and spin-1 fields [108]. Superradiant amplification on the brane was shown to be much larger than in the *D*-dimensional bulk and to be greatly enhanced compared to the four-dimensional Kerr BH case.

Interesting tidal effects related to the superradiant energy extraction in higher-dimensions were shown to occur in [7, 109]. As first suggested in [7] and later confirmed [109], the energy extracted by superradiant scalar waves generated by the circular motion of a point particle around a singly-spinning Myers-Perry BH could be higher than the energy lost to infinity through the emission of scalar waves, in contrast to the four-dimensional case, where the BH energy absorption (or extraction) is negligible compared to the energy emitted to infinity [110].

3.9 Superradiance in Analogue Black Hole Geometries

The construction outlined in Sect. 2.4 established a formal equivalence between the propagation of sound waves and the Klein Gordon equation in an effective, curved spacetime. Under certain conditions, a horizon in the effective metric is present, when the local fluid velocity surpasses the local sound speed. This object is usually called an acoustic BH or "dumb hole" (cf. [112] for a review). Superradiance in acoustic BH geometries was studied in some detail for the two-dimensional draining geometry ("draining bathtub vortex"), described by a two dimensional fluid flow

$$\vec{v} = \frac{-A\vec{r} + C\vec{\phi}}{r} \,, \tag{3.130}$$

in polar coordinates, where \vec{r} and $\vec{\phi}$ are orthogonal unit basis vectors. The flow above is that of an ideal fluid, which is locally irrotational (vorticity free), barotropic and inviscid. The quantity A thus measures the flow radial speed and the circulation C measures its angular speed. In these setups the notion of horizon and ergospheres is very intuitive: the effective spacetime has an acoustic horizon at the point where the radial speed is equal to the local sound speed, $r_+ = Ac^{-1}$ and an ergosurface at the location where the total speed equal the speed of sound, $r_{\rm ergo}^2 = c^{-2}(A^2 + C^2)$.

With the following coordinate transformation [111],

$$dt \to d\tilde{t} = dt - \frac{Ar}{r^2c^2 - A^2}dr \tag{3.131}$$

$$d\phi \to d\tilde{\phi} = d\phi - \frac{CA}{r(r^2c^2 - A^2)}dr, \qquad (3.132)$$

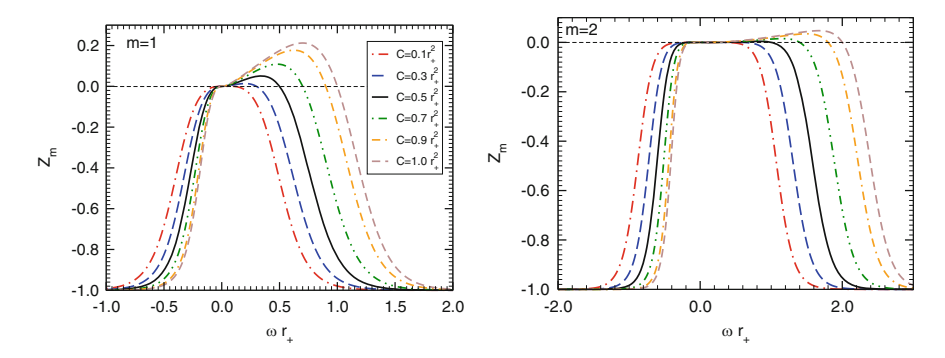


Fig. 3.14 Amplification factor Z_m for the draining vortex as a function of ω for m=1 (left panel) and m=2 (right panel), for a unit-amplitude incident wave. Results are normalized by the effective horizon r_+ . Each curve corresponds to a different value of rotation C, as indicated. Adapted from [111]

the effective metric (2.37) takes the form

$$ds^{2} = -\left(1 - \frac{A^{2} + C^{2}}{c^{2}r^{2}}\right)c^{2}d\tilde{t}^{2} + \left(1 - \frac{A^{2}}{c^{2}r^{2}}\right)^{-1}dr^{2} - 2Cd\tilde{\phi}d\tilde{t} + r^{2}d\tilde{\phi}^{2}.$$
 (3.133)

Superradiance was studied in this effective acoustic spacetime in the frequency domain, by studying the amplification factors [111]. For an incident wave of amplitude \mathcal{I} , the reflection coefficients are shown in Fig. 3.14, the amplification factors for fluxes are $Z_m = |\mathcal{R}|^2 - |\mathcal{I}|^2$; the reflection coefficient depends only on the dimensionless parameter C/A [111] and therefore without loss of generality one can set A = c = 1. the amplification factor grows with rotation parameter C, albeit slowly (the numerics indicate a logarithmic growth at large C). At a moderately large value of C = 1, the peak amplification factor for m = 1 modes is 21.2%. Amplification factors higher that 100% are extremely hard to achieve, which might be connected to entropy bounds, see Sect. 3.14 for a further discussions on this. Superradiant wave scattering for the same geometry was analyzed in the time domain in [113]. These studies were complemented by a low-frequency analysis [114] and by an energy flux analysis [115].

Recently, [116] considered a similar, but slightly more realistic draining geometry taking into account the varying depth of water. Superradiance in this analog system depends now on two parameters, and can be as large as 60 % or higher.

Analogue geometries can be realized outside acoustic setups, and include Bose-Einstein condensates for instance [112]. Superradiant scattering of sound wave fluctuations from vortex excitations of Bose-Einstein condensates was considered in [117, 118]. Bose-Einstein condensates are also interesting models for dark-matter halos and boson stars; in this context, a gravitational analogue description also displays superradiant scattering [119].

3.10 Superradiance in Nonasymptotically Flat Spacetimes

The literature on superradiance amplification from BHs in Einstein's theory with a cosmological constant is limited. The dS and the AdS cases behave in a completely different way: when the cosmological constant $\Lambda>0$ new effects related to the presence of a dS cosmological horizon can occur, whereas when $\Lambda<0$ the AdS boundary can effectively confine superradiantly-amplified waves thus providing the arena for BH bomb instabilities. The latter effect is discussed at length in Sect. 4 so in this section we focus only on the superradiant amplification, neglecting possible instabilities that it might trigger.

Extracting Energy from dS BHs Superradiance of Kerr-dS BHs has also been studied [13]. Extending the analysis of Sect. 3.4, the radial Teukolsky equation can be solved in the asymptotic regions and the solution reads as in Eq. (3.51) with

$$k_H = \omega - m\Omega_H$$
, $k_{\infty} = \omega - m\Omega_C$, (3.134)

where Ω_c is the angular velocity of the cosmological horizon at $r = r_c$. Imposing $\mathcal{O} = 0$ at the event horizon, Eq. (3.52) takes the form

$$|\mathcal{R}|^2 = |\mathcal{I}|^2 - \frac{\omega - m\Omega_{\rm H}}{\omega - m\Omega_{\rm c}} |\mathcal{T}|^2, \qquad (3.135)$$

and therefore superradiance occurs only when

$$m\Omega_c < \omega < m\Omega_H$$
. (3.136)

Although the range of superradiant frequencies is smaller than in the asymptotically flat case, the maximum superradiance amplification is slightly larger for positive values of Λ [13].

On a more formal account, [120] has proved asymptotic completeness for a class of Klein-Gordon equations which allow for superradiance, including the scalar equation on a Kerr-dS BH (see also references in [120] for recent formal development on the local energy for the wave equation on the Kerr-dS metric).

Finally, an interesting effect related to dS superradiance was recently discovered in [121]. There, it was shown that RN-dS BHs are linearly unstable to spherical, charged scalar perturbations. The unstable modes were subsequently found to satisfy a superradiance condition analog to Eq. (3.136) for static charged dS BHs [122].

Extracting Energy from Black Holes in AdS Backgrounds AdS spacetime is not globally hyperbolic, so fields which satisfy a hyperbolic wave equation on AdS might not have a well-defined dynamics. Nonetheless scalar, vector and gravitational waves propagating on AdS can be shown to possess some conserved energy, and their dynamics correspond to that defined by choosing some positive, self-adjoint wave operator [123]. Such formal analysis also determines all possible boundary conditions that can be imposed at AdS infinity.

These boundary conditions are indeed crucial for superradiance. It was shown that, using "reflective" boundary conditions (i.e. either Dirichlet or Neumann) at timelike infinity, all modes of a scalar field on a Kerr-Newman-AdS BH are *not* superradiant whereas, for "transparent" boundary conditions, the presence of superradiance depends on the definition of positive frequencies, which is subtle in AdS [124]. For those BHs having a globally timelike Killing vector, a natural definition of positive frequency implies absence of superradiance. This is to be contrasted with the situation in asymptotically flat space previously discussed, where superradiance occurs regardless of the definition of positive frequency. This result has important implications for constructing a quantum field theory on a BH background in AdS.

Nonetheless, even at the classical level, the issue of boundary conditions in rotating AdS spacetimes is subtle. Imposing that the perturbations conserve the symmetries of asymptotically global AdS, a set of Robin boundary conditions for the Teukolsky equation of a Kerr-AdS BH was found [125] (cf. also [126] for some applications). Furthermore, in a scattering experiment the boundary conditions at infinity should allow for a nonvanishing flux, thus corresponding to the "transparent" case discussed above. A thorough analysis of this problem was recently performed in [127], where it was shown that superradiance occurs for AdS BHs in any spacetime dimension whenever transmittive boundary conditions are allowed at the AdS boundaries.

3.11 Superradiance from Stars

As is clear from the entire discussion and from the classical examples of Sect. 2, rotation and a dissipation channel are enough to trigger superradiance. As such, ordinary stars are also prone to superradiant amplification. A formal proof of this was recently produced for stars in GR [128]. Explicit calculations require a modeling of dissipation, which can be performed within a toy model similar to that adopted by Zeldovich in his original study [129] (see also [130] who studied the correspondence between superradiance and tidal friction on viscous Newtonian anisotropic stars).

The toy model assumes the modified Klein-Gordon equation (2.50) *inside* the star and in a co-rotating frame [131]. The term proportional to α in Eq. (2.50) is added to break Lorentz invariance, and describes absorption on a timescale $\tau \sim 1/\alpha$. The constant α can be related to more physical parameters describing the microscopic details of the absorption process [129]. Following Zeldovich, if the frequency in the accelerated frame is ω and the field behaves as $e^{-i\omega t + im\varphi}$, then in the inertial frame the azimuthal coordinate is $\varphi = \varphi' - \Omega t$, and hence the frequency is $\omega' = \omega - m\Omega$ (see also Sect. 2.5). In other words, the effective damping parameter $\alpha\omega'$ becomes negative in the superradiant regime and the medium amplifies—rather than absorbing—radiation [41, 42].

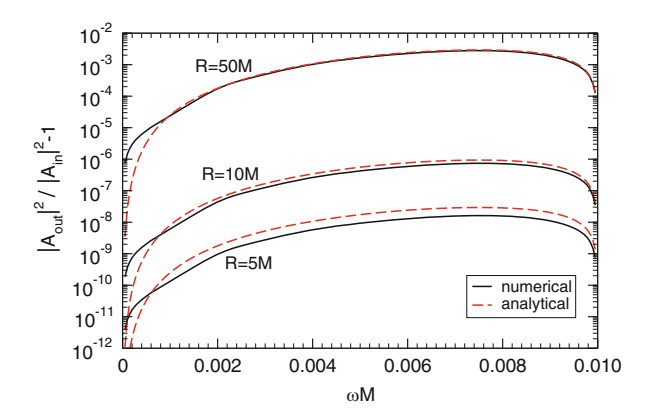


Fig. 3.15 Superradiant amplification of a scalar field by a rotating star, where dissipation is modeled through Eq. (2.50). Here, $M\alpha = 0.1$, $M\Omega = 0.01$. The amplification factor scales with the dissipation parameter α for small $M\alpha$. For non-compact, slowly-rotating stars, the amplification factor (*solid lines*) is well described by the analytic result (3.138), shown as a *dashed curve* in the plot

The modified wave equation (2.50) can be solved in any generic background describing a Newtonian or GR star. Figure 3.15 shows the amplification factor for a constant-density star in GR, with mass M, radius R, angular rotation frequency $M\Omega=0.01$ and dissipation parameters $M\alpha=0.1$. Superradiant amplification does exist, as shown generically in [128], and the amplification can be significant. We find that the superradiant amplification factor scales linearly with $M\alpha$ for small $M\alpha$ and it increases significantly as the star's surface velocity increases. The amplification factors can be of order of those around rotating Kerr BHs or higher.

For non-relativistic, Newtonian configurations $(M/R, \Omega R \ll 1)$ the wave equation can be solved analytically inside and outside the star in terms of Bessel functions. In this regime there is a simple analytic expression for the amplification factor [129],

$$\frac{|A_{\text{out}}|^2}{|A_{\text{in}}|^2} - 1 = \frac{4\alpha R^2 (\Omega - \omega) (\omega R)^{2l+1}}{(2l+1)!!(2l+3)!!}.$$
 (3.137)

As can be seen from Fig. 3.15, this relation gives a very good approximation to the numerical results for a good fraction of the parameter space, including relatively compact stars. This relation is also interesting, as it allows one to predict the amplification factor for rotating BHs. In the latter case, $R \sim 2M$ and $1/\alpha = M$ is the only possible timescale in the problem. With this identification, the above relation predicts that the amplification factor for l=1 scalar waves scattered off a slowly rotating BHs in GR reads

$$\frac{|A_{\text{out}}|^2}{|A_{\text{in}}|^2} - 1 = \frac{16}{45} M \left(\Omega - \omega\right) \left(2M\omega\right)^3. \tag{3.138}$$

On the other hand, a matched-asymptotic expansion calculation in full GR yields approximately the same result (the coefficient turns out to be 2/9 instead of 16/45, see Sect. 3.6.5).

3.12 Superradiance Beyond General Relativity

From our previous discussion, it is clear that superradiance is not a prerogative of BHs in GR but it would occur in any gravitational theory that admits BH solutions. Indeed, the analysis of Sect. 3.4 only requires the presence of an event horizon and an asymptotically-flat spacetime. Clearly, the details of the superradiance amplification would depend on the specific BH geometry and on the wave dynamics in the modified theory and an interesting problem is to understand whether superradiance can be stronger in modified theories of gravity.

Extended theories of gravity usually predict novel BH solutions which reduce to the Kerr metric in the GR limit (see e.g. [132–134] for reviews). On the other hand, constructing rotating metrics in closed form is usually very challenging and most solutions are known analytically only in the slow-rotation limit [135] or fully numerically [136]. To the best of our knowledge, no studies of superradiance amplification in these spacetimes is available to date. However, at least for the slowly-rotating BH solutions predicted in quadratic gravity [135], the deformations from the Kerr geometry tend to *decrease* the proper volume of the ergoregion. This suggests that at least the background geometry would contribute to decrease the amplification factor. A simpler analysis would be to focus on theories which admit the same BH solutions as GR [134, 137] but for which wave propagation is different. In some of these theories the superradiance amplification has been shown to lead to "BH-bomb instabilities" [138, 139] analog to those discussed in Sect. 4 below.

Another strategy consists in considering phenomenological nonKerr geometries which are not necessarily solutions of any specific theory [140, 141]. However, the lack of an underlying theory prevents to study the dynamics of gravitational waves and only test fields propagating in a fixed background can be analyzed. Even in this case, the separability properties of the Kerr metric are generically lost and even the Klein-Gordon equation might not be separable. Probably because of these technicalities, superradiance in such geometries has not been studied to date. On the other hand, the Penrose process in a restricted class of such metrics was studied in [26], showing that the maximum energy gain can be several times larger than for a Kerr BH.

Finally, superradiance amplification of test fields propagating on some exact solutions of Einstein's equations which represent spinning geometries other than Kerr were analyzed recently [142, 143]. Although strictly speaking these geometries are GR solutions, they possess peculiar matter fields and they might be considered as modified BH solutions.

3.12.1 Superradiance of Black Holes Surrounded by Matter in Scalar-Tensor Theories

In the context of scalar-tensor theories, superradiance amplification from spinning BHs has been investigated in [144, 145], which showed that the presence of matter may drastically affect the amplification of scalar waves. In these theories the Klein-Gordon equation on a Kerr BH surrounded by matter takes the form $[\Box -\mu_{\text{eff}}^2]\Psi = 0$, where the effective mass term μ_{eff} depends on the specific scalar-tensor theory and it is proportional to the trace of the stress-energy tensor.

Figure 3.16 shows a representative example of superradiance amplification for a specific matter profile, namely

$$\mu_{\text{eff}}^{2}(r,\vartheta) = \frac{2\mathcal{G}(r)}{a^{2} + 2r^{2} + a^{2}\cos 2\vartheta}.$$
 (3.139)

This choice simplifies the treatment significantly because the corresponding Teukolsky equation is separable and the problem can be solved with standard methods. For small coupling, the standard GR results are recovered, with a maximum amplification of about 0.4%. On the other hand, as the scalar-tensor coupling to matter increases, the amplification factor can exceed the standard value by orders of magnitude. This is due to the appearance of resonances at specific frequencies $\omega =$

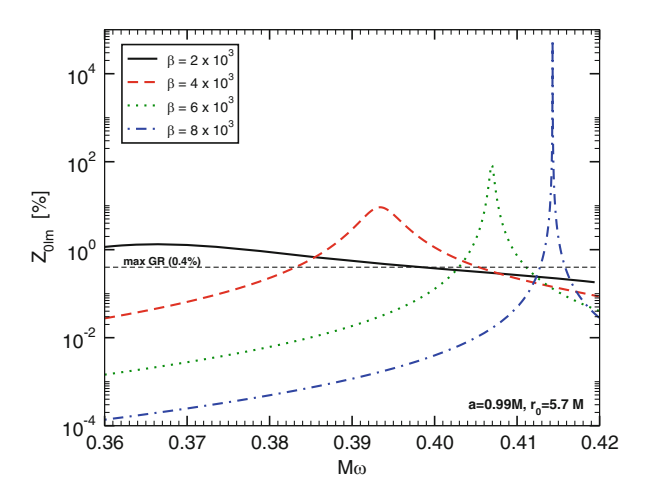


Fig. 3.16 Percentage superradiant amplification factor, $Z_{0lm} = 10^2 \left(|\mathcal{R}|^2 - |\mathcal{I}|^2 \right)$, for a scalar wave scattered off a Kerr BH with $a = 0.99\,\mathrm{M}$ in a matter profile (3.139) with $\mathcal{G} = \beta\,\Thetar - r_0/r^3$ as a function of the wave frequency ω in a generic scalar tensor theory (where β parametrizes the scalar-tensor coupling [145]). As a reference, the *horizontal line* corresponds to the maximum amplification for scalar waves in vacuum, $Z_{0lm}^{\mathrm{max}} \approx 0.4\,\%$. This example refer to $r_0 = 5.7\,\mathrm{M}$, but similar results hold for other choices of r_0 and for different matter profiles. The resonances correspond to the excitation of a new class of *stable* QNMs

 $\omega_{\rm res}$ that depend on the parameters of the model. In some cases, the amplification factor can increase by six orders of magnitude or more, even in regions of the parameter space which are phenomenologically allowed [145]. Understanding the astrophysical implications of such huge amplification may be used to constrain the parameter space of scalar-tensor theories.

The presence of Breit-Wigner resonances [146] in the amplification factor has been interpreted in terms of very long-lived QNMs with $\omega_R \sim \omega_{\rm res}$ and $\omega_I \ll \omega_R$ [144, 145]. Such long-lived modes are associated to trapping by potential barriers (see also Sect. 4.11.2 for a related problem) and they also exist in the case of *massive* scalar perturbations of Kerr BHs [147], but in that case the potential well extends to infinity, so that waves whose frequency is larger than the mass are exponentially suppressed and no superradiant amplification can occur, as previously discussed. Nonminimal scalar-matter interactions in scalar-tensor gravity produce an *effective* scalar mass which is localized near the BH and vanishes at large distances. This effective mass can trap long-lived modes and, nonetheless, allows for propagation of scalar waves to infinity. This allows for a new class of long-lived QNMs of Kerr BHs surrounded by matter. Correspondingly to the excitation of these modes, the superradiant gain factor is resonantly amplified. ¹⁰

3.13 Microscopic Description of Superradiance and the Kerr/CFT Duality

It was shown by Hawking that when quantum effects are taken into account BHs emit thermal radiation with the expected number of emitted particles given by [148]

$$\langle N \rangle = -\frac{Z_{slm}}{e^{(\omega - m\Omega_{\rm H})/T_{\rm H}} \pm 1}, \qquad (3.140)$$

where the minus sign is for bosons and the plus sign for fermions and Z_{slm} is the absorption/amplification factor given by Eq. (3.102), whereas the same factor for fermions can be found in [149] (in this case, as discussed in Sect. 3.6.4, we always have $Z_{slm} < 0$). In the extremal limit $T_{\rm H} \rightarrow 0$ there is only emission in the superradiant regime $\omega < m\Omega_{\rm H}$ with a rate $\mp Z_{slm}$, where here the minus and the plus signs are for fermions and bosons, respectively. This clearly shows that when the BH temperature is different from zero, thermal Hawking radiation and spontaneous superradiant emission are strongly mixed. In fact, as discussed in detail in [150], the power spectrum of Hawking radiation comprises two terms: a black body term and a greybody term. The former is associated to the probability that a certain

¹⁰It would be interesting to understand the large amplification of the superradiance energy in terms of violation of some energy condition due to the effective coupling that appears in scalar-tensor theories.

particle is thermally produced near the horizon, whereas the latter term modifies the thermal radiation due to the existence of the potential barrier created by the BH. While the probability of Hawking emission (for both bosons and fermions) can be greatly amplified by spin-spin interactions [150], one can show that superradiance affects only the greybody term. Therefore, Hawking fermion emission can also be amplified by the BH rotation even if fermions do not experience superradiance amplification.

In the extremal limit, the only modes that are spontaneously emitted are superradiant. This was used in [91, 151] to investigate the microscopic description of superradiance within a string theory and gauge/gravity duality context. These studies—which are closely related to the program aiming to account for the microscopic degrees of freedom of BHs—have been met with a moderate degree of success.

In [91] the authors were able to account for superradiant effects in a certain extremal BH background (more specifically the D1-D5-P BH solutions of type IIB supergravity), where the AdS₃/CFT₂ duality applies. In their picture the superradiant spontaneous emission was modeled as being due to the weak interaction between left and right-moving modes in the CFT. From this picture they argued that the superradiant bound (1.1) follows directly from the Fermi-Dirac statistics of the spin-carrying degrees of freedom in the dual CFT. More importantly, they showed that the superradiant emission rates agree in both sides of the duality. In the future it would be interesting to extend this study to other systems, and recover completely the superradiant amplification factors from the microscopic description.

Another important step was done within the so-called Kerr/CFT duality [152] (see also [153] for a recent review). The Kerr/CFT duality conjectures that the near-horizon extremal Kerr BH is holographically dual to a chiral left-moving (half of a) two-dimensional CFT with central charge $c=12J/\hbar$, where J is the angular momentum of the extremal Kerr BH. In this picture the asymptotically flat region is removed from the spacetime and the CFT lives in the timelike boundary of the resulting spacetime. In [151] the authors attempted to reproduce the superradiant scattering of a scalar field in a near-extremal Kerr geometry in terms of a dual two-dimensional CFT in which the BH corresponds to a thermal state while the scalar field is dual to a specific operator. They successfully showed that the amplification factor (3.102) could be reproduced by the two point function of the operator dual to the scalar field. The analysis and results should however be taken with caution, as the boundary conditions—fundamental for the analysis—were shown to be inconsistent with the field equations [155, 156].

¹¹The geometry used in the original Kerr/CFT duality is the so-called near-horizon extreme Kerr "NHEK" geometry found by Bardeen and Horowitz [154] which is not asymptotically flat but resembles AdS₃. That this geometry could have a dual CFT description was first pointed out in [154].

3.14 Open Issues 87

3.14 Open Issues

The following is an incomplete list of the issues that are, in our opinion, not completely understood and which would merit further study.

- The Penrose process and BH superradiance has so far been explored only for single spinning BHs. It is possible that they can occur also in BH binaries even when the individual BHs are non-spinning. These are naturally much more complex systems, but given that binaries are also relatively common in our universe, they are worthwhile to explore. Furthermore, it would be interesting to study the effect of spinning particles to the amplification factor in the Penrose process.
- Superradiance in a BH-pulsar system has been recently discussed in [87], showing that superradiance of GWs from the pulsar can produce a peculiar modulation of the pulsar's GW luminosity at the percent level. Whether or not such effect is observationally important clearly deserves further study.
- Is there a fundamental bound on superradiant amplification? All the examples we have dealt with so far share a common denominator: the amplification factors $Z_{slm} \lesssim 100 \,\%$. There are in fact suggestions that such bound also holds in some acoustic BH geometries [115]. Such relatively small amplification factors may be a consequence of a more fundamental principle at play. Hints of such principle can be found with the following reasoning. Recall that the area law for rotating BHs can be written as (3.22) or, in terms of Bekenstein-Hawking entropy S_H , as $\delta M = \frac{\omega k}{2\pi} \frac{\delta S_H}{\omega m\Omega_H}$. We can write this explicitly in terms of the amplification factor, by considering that a wavepacket of energy δE was thrown into the BH,

$$Z_m \equiv \frac{-\delta M}{\delta E} = \frac{\omega k}{2\pi} \frac{\delta S_H/\delta E}{m\Omega_H - \omega}.$$
 (3.141)

It is clear that the BH mass decreases in the superradiant regime simply because the BH entropy must increase. This version of the first law doesn't immediately impose upper limits on the amplification factors, but that one should exist follows from Bekenstein's entropy bound for any infalling matter [157],

$$\delta S \le 2\pi R \,\delta E \,, \tag{3.142}$$

where R is the size of the object and E its energy. This implies that

$$Z_m \le kr_+ \frac{\omega}{m\Omega_{\rm H} - \omega} \,, \tag{3.143}$$

¹²The only exception to this rule concerns BHs surrounded by matter coupled to scalar fields, where the amplification factors can become unbounded (see Sect. 3.12.1). Because the laws of BH mechanics will be different, these fall outside the scope of this discussion.

leading to a competitive bound on the amplification factor for small frequencies. Such bound becomes weaker close to the superradiant threshold. It is possible that a more refined argument can strengthen the bound in this regime as well.

This analysis is over-simplified¹³ In particular, the Bekenstein entropy bound (3.142) is valid only for systems with a fixed radius; in general, there will be charge-dependent corrections. These may be important, as the bound (3.143) predicts that $Z_m \to 0$ when $\omega \to 0$, in conflict with Fig. 3.8 (see, in particular, the purple curve).

- The scattering of massive Dirac waves off a Kerr BH has some connection with the original Klein paradox. Indeed, Chandrasekhar suggested that the effective potential for the Schroedinger-like problem can display some singularities outside the horizon in a certain region of the parameter space and in the case of rotation [6]. If the potential is discontinuous, the transmission coefficient would be prone to the Klein paradox, as discussed in Sect. 2.1. To the best of our knowledge a quantitative analysis of this phenomenon has not been performed yet.
- Clearly, an outstanding open issue is the systematic calculation of the absorption cross-section of rotating BHs for generic angles of incidence. In particular, a generalization of the low-frequency formulas available for GWs [86] to lower spin-fields would certainly be of interest, as well as thorough numerical studies.
- Nonlinear effects and induced superradiance. The effect of nonlinear couplings
 have practically been ignored in all existing literature on BH superradiance.
 Interesting effects could include induced superradiant-like effects in fermions
 when coupled to bosonic fields, or mass-like effects when higher-order selfinteraction terms are taken into account for boson fields. The backreaction of
 superradiant waves on the metric has been investigated only very recently, see
 Sect. 3.6.7.
- Sound waves in matter outside *gravitational BHs* can itself feel an effective geometry with sonic horizons (differing from the true gravitational event horizon) and be subjected to superradiant effects. Although this is one more example of superradiance in analogue models, it is one with potentially important applications in astrophysical environments and may even lead to superradiant instabilities, c.f. Sect. 4 and [158, 159]) (see also [160] for a recent related realization in the case of nonspinning BHs).
- Superradiance from BHs in modified theories of gravity has not been studied yet. At linearized level this requires having a stationary, axisymmetric BH solution and solving the modified wave dynamics in this background. Catalogs of interesting gravity theories and corresponding BH solutions can be found in a recent review [134].
- Superradiance and non-axisymmetric spacetimes. All vacuum stationary solutions of Einstein's equations are also axisymmetric. This simplifies the treatment of superradiance considerably, because mode-mixing between different

¹³We thank Shahar Hod for drawing our attention to this point.

azimuthal numbers are avoided. However, this property can be broken in other theories or in non-stationary configurations. Whether or not mode mixing would quench or favor superradiance is an interesting open problem.

References

- 1. K.S. Thorne, R. Price, D. Macdonald, *Black Holes: The Membrane Paradigm* (Yale University Press, New Haven, 1986)
- E.T. Newman, R. Couch, K. Chinnapared, A. Exton, A. Prakash et al., Metric of a rotating, charged mass. J. Math. Phys. 6, 918–919 (1965)
- 3. D. Robinson, *The Kerr Spacetime: Rotating Black Holes in General Relativity* (Cambridge University Press, Cambridge, 2009)
- 4. D.L. Wiltshire, M. Visser, S.M. Scott, *The Kerr Spacetime: Rotating Black Holes in General Relativity* (Cambridge University Press, Cambridge, 2009)
- J.M. Bardeen, W.H. Press, S.A. Teukolsky, Rotating black holes: locally nonrotating frames, energy extraction, and scalar synchrotron radiation. Astrophys. J. 178, 347 (1972)
- S. Chandrasekhar, The Mathematical Theory of Black Holes (Oxford University Press, New York, 1983)
- 7. V. Cardoso, P. Pani, Tidal acceleration of black holes and superradiance. Classical Quantum Gravity 30, 045011 (2013). arXiv:1205.3184 [gr-qc]
- 8. J. Bekenstein, Extraction of energy and charge from a black hole. Phys. Rev. **D7**, 949–953 (1973)
- 9. R.M. Wald, The thermodynamics of black holes. Living Rev. Relativ. 4, 6 (2001). arXiv:gr-qc/9912119 [gr-qc]
- W. Unruh, Separability of the Neutrino equations in a Kerr background. Phys. Rev. Lett. 31, 1265–1267 (1973)
- 11. R.M. Wald, Black hole entropy is the Noether charge. Phys. Rev. **D48**, 3427–3431 (1993). arXiv:gr-qc/9307038 [gr-qc]
- 12. V. Iyer, R.M. Wald, Some properties of Noether charge and a proposal for dynamical black hole entropy. Phys. Rev. **D50**, 846–864 (1994). arXiv:gr-qc/9403028 [gr-qc]
- T. Tachizawa, K.-I. Maeda, Superradiance in the Kerr-de Sitter space-time. Phys. Lett. A 172, 325–330 (1993)
- 14. http://www.pas.rochester.edu/~dmw/ast102/
- 15. R. Penrose, Nuovo Cimento. J. Serie 1, 252 (1969)
- 16. G. Contopoulos, Orbits through the ergosphere of a kerr black hole. Gen. Relativ. Gravit. **16**(1), 43–70 (1984). http://dx.doi.org/10.1007/BF00764017
- 17. R.M. Wald, Energy limits on the Penrose process. Astrophys. J. 191, 231 (1974)
- S. Wagh, S. Dhurandhar, N. Dadhich, Revival of penrose process for astrophysical applications. Astrophys. J. 290(12), 1018 (1985)
- 19. S.M. Wagh, S.V. Dhurandhar, N. Dadhich, Revival of the Penrose process for astrophysical applications: Erratum. Astrophys. J. **301**, 1018 (1986)
- M. Richartz, S. Weinfurtner, A. Penner, W. Unruh, General universal superradiant scattering. Phys. Rev. D80, 124016 (2009). arXiv:0909.2317 [gr-qc]
- 21. E. Teo, Rotating traversable wormholes. Phys. Rev. **D58**, 024014 (1998). arXiv:gr-qc/9803098 [gr-qc]
- A. Abdujabbarov, B. Ahmedov, B. Ahmedov, Energy extraction and particle acceleration around rotating black hole in Horava-Lifshitz gravity. Phys. Rev. D84, 044044 (2011). arXiv:1107.5389 [astro-ph.SR]
- A. Abdujabbarov, B. Ahmedov, S. Shaymatov, A. Rakhmatov, Penrose process in Kerr-Taub-NUT spacetime. Astrophys. Space Sci. 334, 237–241 (2011). arXiv:1105.1910 [astro-ph.SR]

- 24. S. Chen, J. Jing, Gravitational field of a slowly rotating black hole with a phantom global monopole. Classical Quantum Gravity 30, 175012 (2013). arXiv:1301.1440 [gr-gc]
- C. Ganguly, S. SenGupta, Penrose process in charged axion-dilaton coupled black hole. arXiv:1401.6826 [hep-th]
- 26. C. Liu, S. Chen, J. Jing, Rotating non-Kerr black hole and energy extraction. Astrophys. J. **751**, 148 (2012). arXiv:1207.0993 [gr-qc]
- M. Nozawa, K.-I. Maeda, Energy extraction from higher dimensional black holes and black rings. Phys. Rev. D71, 084028 (2005). arXiv:hep-th/0502166 [hep-th]
- 28. K. Prabhu, N. Dadhich, Energetics of a rotating charged black hole in 5-dimensional gauged supergravity. Phys. Rev. **D81**, 024011 (2010). arXiv:0902.3079 [hep-th]
- 29. S.G. Ghosh, P. Sheoran, Higher dimensional non-Kerr black hole and energy extraction. Phys. Rev. **D89**, 024023 (2014). arXiv:1309.5519 [gr-gc]
- S. Parthasarathy, S.M. Wagh, S.V. Dhurandhar, N. Dadhich, High efficiency of the Penrose process of energy extraction from rotating black holes immersed in electromagnetic fields. Astrophys. J. 307, 38–46 (1986)
- 31. S.M. Wagh, N. Dadhich, The energetics of black holes in electromagnetic fields by the Penrose process. Phys. Rep. 183(4), 137–192 (1989)
- 32. T. Piran, J. Shaham, Upper bounds on collisional Penrose processes near rotating black hole horizons. Phys. Rev. **D16**, 1615–1635 (1977)
- T. Harada, H. Nemoto, U. Miyamoto, Upper limits of particle emission from high-energy collision and reaction near a maximally rotating Kerr black hole. Phys. Rev. D86, 024027 (2012). arXiv:1205.7088 [gr-qc]
- 34. M. Bejger, T. Piran, M. Abramowicz, F. Hakanson, Collisional Penrose process near the horizon of extreme Kerr black holes. Phys. Rev. Lett. 109, 121101 (2012). arXiv:1205.4350 [astro-ph.HE]
- 35. O.B. Zaslavskii, On energetics of particle collisions near black holes: BSW effect versus Penrose process. Phys. Rev. **D86**, 084030 (2012). doi:10.1103/PhysRevD.86.084030. arXiv:1205.4410 [gr-qc]
- 36. J.D. Schnittman, A revised upper limit to energy extraction from a Kerr black hole. arXiv:1410.6446 [astro-ph.HE]
- E. Berti, R. Brito, V. Cardoso, Ultra-high-energy debris from the collisional Penrose process. arXiv:1410.8534 [gr-qc]
- 38. T. Piran, J. Shaham, J. Katz, High efficiency of the Penrose mechanism for particle collisions. Astrophys. J. **196**, L107 (1975)
- E. Leiderschneider, T. Piran, Super-Penrose collisions are inefficient—a comment on: black hole fireworks: ultra-high-energy debris from super-Penrose collisions. arXiv:1501.01984 [gr-qc]
- 40. S. Teukolsky, W. Press, Perturbations of a rotating black hole. III Interaction of the hole with gravitational and electromagnet ic radiation. Astrophys. J. **193**, 443–461 (1974)
- 41. Y.B. Zel'dovich, Pis'ma Zh. Eksp. Teor. Fiz. 14, 270 (1971) [JETP Lett. 14, 180 (1971)]
- 42. Y.B. Zel'dovich, Zh. Eksp. Teor. Fiz 62, 2076 (1972) [Sov. Phys. JETP 35, 1085 (1972)]
- 43. L. Di Menza, J.-P. Nicolas, Superradiance on the Reissner-Nordstrom metric. ArXiv e-prints (2014). arXiv:1411.3988 [math-ph]
- 44. M. Richartz, A. Saa, Challenging the weak cosmic censorship conjecture with charged quantum particles. Phys. Rev. **D84**, 104021 (2011). arXiv:1109.3364 [gr-qc]
- 45. S.S. Gubser, Breaking an Abelian gauge symmetry near a black hole horizon. Phys. Rev. **D78**, 065034 (2008). arXiv:0801.2977 [hep-th]
- 46. S.A. Hartnoll, C.P. Herzog, G.T. Horowitz, Building a holographic superconductor. Phys. Rev. Lett. 101, 031601 (2008). arXiv:0803.3295 [hep-th]
- 47. E. Newman, R. Penrose, An approach to gravitational radiation by a method of spin coefficients. J. Math. Phys. 3, 566–578 (1962)
- 48. S.A. Teukolsky, Rotating black holes—separable wave equations for gravitational and electromagnetic perturbations. Phys. Rev. Lett. 29, 1114–1118 (1972)

 S.A. Teukolsky, Perturbations of a rotating black hole.
 Fundamental equations for gravitational electromagnetic and neutrino field perturbations. Astrophys. J. 185, 635–647 (1973)

- W.H. Press, S.A. Teukolsky, Perturbations of a rotating black hole. II. Dynamical stability of the Kerr metric. Astrophys. J. 185, 649–674 (1973)
- B. Carter, Global structure of the Kerr family of gravitational fields. Phys. Rev. 174, 1559– 1571 (1968)
- B. Carter, Hamilton-Jacobi and Schrodinger separable solutions of Einstein's equations. Commun. Math. Phys. 10, 280 (1968)
- 53. D. Brill, P. Chrzanowski, C.M. Pereira, E. Fackerell, J. Ipser, Solution of the scalar wave equation in a kerr background by separation of variables. Phys. Rev. **D5**, 1913–1915 (1972)
- 54. S.A. Teukolsky, The Kerr metric. arXiv:1410.2130 [gr-gc]
- 55. J.N. Goldberg, A.J. Macfarlane, E.T. Newman, F. Rohrlich, E.C.G. Sudarshan, Spin s spherical harmonics and **ð**. J. Math. Phys. **8**(11), 2155–2161 (1967). http://scitation.aip.org/content/aip/journal/jmp/8/11/10.1063/1.1705135
- 56. E. Berti, V. Cardoso, M. Casals, Eigenvalues and eigenfunctions of spin-weighted spheroidal harmonics in four and higher dimensions. Phys. Rev. **D73**, 024013 (2006). arXiv:gr-qc/0511111 [gr-qc]
- 57. A.A. Starobinskij, S.M. Churilov, Amplification of electromagnetic and gravitational waves scattered by a rotating black hole. Zh. Eksp. Teor. Fiz. 65, 3–11 (1973)
- 58. A.A. Starobinskij, S.M. Churilov, Amplification of electromagnetic and gravitational waves scattered by a rotating black hole. Sov. Phys. JETP **38**, 1–5 (1973)
- 59. E. Berti, V. Cardoso, A.O. Starinets, Quasinormal modes of black holes and black branes. Classical Quantum Gravity **26**, 163001 (2009). arXiv:0905.2975 [gr-qc]
- 60. C.W. Misner, K. Thorne, J. Wheeler, *Gravitation* (Freeman, San Francisco, 1974)
- S. Hawking, J. Hartle, Energy and angular momentum flow into a black hole. Commun. Math. Phys. 27, 283–290 (1972)
- S. Chandrasekhar, The solution of Dirac's equation in Kerr geometry. R. Soc. Lond. Proc. Ser. A 349, 571–575 (1976)
- 63. D.N. Page, Dirac equation around a charged, rotating black hole. Phys. Rev. D 14, 1509–1510 (1976)
- C.H. Lee, Massive spin-1/2 wave around a Kerr-Newman black hole. Phys. Lett. B 68, 152– 156 (1977)
- B.R. Iyer, A. Kumar, Note on the absence of massive fermion superradiance from a Kerr black hole. Phys. Rev. 18, 4799–4801 (1978)
- M. Martellini, A. Treves, Absence of superradiance of a Dirac field in a Kerr background. Phys. Rev. D15, 3060–3061 (1977)
- S. Hawking, Gravitational radiation from colliding black holes. Phys. Rev. Lett. 26, 1344
 – 1346 (1971)
- 68. A. Starobinski, Amplification of waves during reflection from a rotating black hole. Zh. Eksp. Teor. Fiz. **64**, 48 (1973) [Sov. Phys. JETP **37**, 28 (1973)]
- A.A. Starobinski, S.M. Churilov, Amplification of electromagnetic and gravitational waves scattered by a rotating black hole. Zh. Eksp. Teor. Fiz. 65, 3 (1973) [Sov. Phys. JETP 38, 1 (1973)]
- 70. http://blackholes.ist.utl.pt/?page=Files
- 71. V. Cardoso, A Note on the resonant frequencies of rapidly rotating black holes. Phys. Rev. **D70**, 127502 (2004). arXiv:gr-qc/0411048 [gr-qc]
- S.L. Detweiler, Black holes and gravitational waves. III. The resonant frequencies of rotating holes. Astrophys. J. 239, 292–295 (1980)
- 73. N. Andersson, K. Glampedakis, A Superradiance resonance cavity outside rapidly rotating black holes. Phys. Rev. Lett. **84**, 4537–4540 (2000). arXiv:gr-qc/9909050 [gr-qc]
- 74. H. Yang, F. Zhang, A. Zimmerman, D.A. Nichols, E. Berti et al., Branching of quasinormal modes for nearly extremal Kerr black holes. Phys. Rev. **D87**, 041502 (2013). arXiv:1212.3271 [gr-qc]

- 75. S. Hod, Stationary resonances of rapidly-rotating Kerr black holes. Eur. Phys. J. C73, 2378 (2013). arXiv:1311.5298 [gr-qc]
- 76. S. Hod, Stationary scalar clouds around rotating black holes. Phys. Rev. **D86**, 104026 (2012). arXiv:1211.3202 [gr-qc]
- 77. S. Hod, Resonance spectrum of near-extremal Kerr black holes in the eikonal limit. Phys. Lett. **B715**, 348–351 (2012). arXiv:1207.5282 [gr-qc]
- 78. S. Hod, Quasinormal resonances of a charged scalar field in a charged Reissner-Nordstroem black-hole spacetime: a WKB analysis. Phys. Lett. **B710**, 349–351 (2012). arXiv:1205.5087 [gr-qc]
- 79. S. Hod, Algebraically special resonances of the Kerr-black-hole-mirror bomb. Phys. Rev. **D88**(12), 124007 (2013). arXiv:1405.1045 [gr-gc]
- 80. W. Unruh, Absorption cross-section of small black holes. Phys. Rev. D14, 3251–3259 (1976)
- 81. C.F. Macedo, L.C. Leite, E.S. Oliveira, S.R. Dolan, L.C. Crispino, Absorption of planar massless scalar waves by Kerr black holes. Phys. Rev. **D88**(6), 064033 (2013). arXiv:1308.0018 [gr-qc]
- 82. P. Chrzanowski, R. Matzner, V. Sandberg, M. Ryan, Zero mass plane waves in nonzero gravitational backgrounds. Phys. Rev. **D14**, 317–326 (1976)
- R. Matzner, M. Ryan, Low frequency limit of gravitational scattering. Phys. Rev. D16, 1636– 1642 (1977)
- R.A. Matzner, M.P. Ryan, Jr., Scattering of gravitational radiation from vacuum black holes. Astrophys. J. 36, 451–481 (1978)
- 85. J.A.H. Futterman, F.A. Handler, R.A. Matzner, *Scattering from Black Holes* (Cambridge University Press, Cambridge, 1988)
- 86. S.R. Dolan, Scattering and absorption of gravitational plane waves by rotating black holes. Classical Quantum Gravity 25, 235002 (2008). arXiv: 0801.3805 [gr-gc]
- 87. J.G. Rosa, Testing black hole superradiance with pulsar companions. arXiv:1501.07605 [gr-qc]
- 88. E.S. Oliveira, S.R. Dolan, L.C. Crispino, Absorption of planar waves in a draining bathtub. Phys. Rev. **D81**, 124013 (2010)
- 89. W.E. East, F.M. Ramazanoglu, F. Pretorius, Black hole superradiance in dynamical spacetime. Phys. Rev. **D89**, 061503 (2014). arXiv:1312.4529 [gr-qc]
- 90. J. Hovdebo, R.C. Myers, Black rings, boosted strings and Gregory-Laflamme. Phys. Rev. D73, 084013 (2006). arXiv:hep-th/0601079 [hep-th]
- 91. O.J. Dias, R. Emparan, A. Maccarrone, Microscopic theory of black hole superradiance. Phys. Rev. D77, 064018 (2008). arXiv:0712.0791 [hep-th]
- 92. M. Banados, C. Teitelboim, J. Zanelli, The black hole in three-dimensional space-time. Phys. Rev. Lett. 69, 1849–1851 (1992). arXiv:hep-th/9204099 [hep-th]
- 93. L. Ortiz, No superradiance for the scalar field in the BTZ black hole with reflexive boundary conditions. Phys. Rev. **D86**, 047703 (2012). arXiv:1110.2555 [hep-th]
- 94. R. Emparan, H.S. Reall, Black holes in higher dimensions. Living Rev. Relativ. 11, 6 (2008). arXiv:0801.3471 [hep-th]
- 95. S. Hawking, Black holes in general relativity. Commun. Math. Phys. 25, 152–166 (1972)
- 96. S. Hollands, A. Ishibashi, R.M. Wald, A higher dimensional stationary rotating black hole must be axisymmetric. Commun. Math. Phys. **271**, 699–722 (2007). arXiv:gr-qc/0605106 [gr-qc]
- 97. V.P. Frolov, D. Stojkovic, Quantum radiation from a five-dimensional rotating black hole. Phys. Rev. **D67**, 084004 (2003). arXiv:gr-qc/0211055 [gr-qc]
- 98. E. Jung, S. Kim, D. Park, Condition for superradiance in higher-dimensional rotating black holes. Phys. Lett. **B615**, 273–276 (2005). arXiv:hep-th/0503163 [hep-th]
- 99. E. Jung, S. Kim, D. Park, Condition for the superradiance modes in higher-dimensional rotating black holes with multiple angular momentum parameters. Phys. Lett. **B619**, 347–351 (2005). arXiv:hep-th/0504139 [hep-th]
- 100. H. Kodama, Superradiance and instability of black holes. Prog. Theor. Phys. Suppl. 172, 11–20 (2008). arXiv:0711.4184 [hep-th]

101. R. Brito, Dynamics around black holes: radiation emission and tidal effects. arXiv:1211.1679 [gr-qc]

- 102. S. Creek, O. Efthimiou, P. Kanti, K. Tamvakis, Scalar emission in the bulk in a rotating black hole background. Phys. Lett. **B656**, 102–111 (2007). arXiv:0709.0241 [hep-th]
- 103. M. Casals, S. Dolan, P. Kanti, E. Winstanley, Bulk emission of scalars by a rotating black hole. J. High Energy Phys. **0806**, 071 (2008). arXiv:0801.4910 [hep-th]
- 104. E. Jung, D. Park, Bulk versus brane in the absorption and emission: 5-D rotating black hole case. Nucl. Phys. **B731**, 171–187 (2005). arXiv:hep-th/0506204 [hep-th]
- 105. C. Harris, P. Kanti, Hawking radiation from a (4+n)-dimensional rotating black hole. Phys. Lett. **B633**, 106–110 (2006). arXiv:hep-th/0503010 [hep-th]
- 106. D. Ida, K.-Y. Oda, S.C. Park, Rotating black holes at future colliders. II. Anisotropic scalar field emission. Phys. Rev. **D71**, 124039 (2005). arXiv:hep-th/0503052 [hep-th]
- 107. S. Creek, O. Efthimiou, P. Kanti, K. Tamvakis, Greybody factors for brane scalar fields in a rotating black-hole background. Phys. Rev. **D75**, 084043 (2007). arXiv:hep-th/0701288 [hep-th]
- 108. M. Casals, P. Kanti, E. Winstanley, Brane decay of a (4+n)-dimensional rotating black hole. II. Spin-1 particles. J. High Energy Phys. 0602, 051 (2006). arXiv:hep-th/0511163 [hep-th]
- 109. R. Brito, V. Cardoso, P. Pani, Tidal effects around higher-dimensional black holes. Phys. Rev. **D86**, 024032 (2012). arXiv:1207.0504 [gr-qc]
- 110. E. Poisson, M. Sasaki, Gravitational radiation from a particle in circular orbit around a black hole. 5: black hole absorption and tail corrections. Phys. Rev. **D51**, 5753–5767 (1995). arXiv:gr-qc/9412027 [gr-qc]
- 111. E. Berti, V. Cardoso, J.P. Lemos, Quasinormal modes and classical wave propagation in analogue black holes. Phys. Rev. **D70**, 124006 (2004). arXiv:qr-qc/0408099 [qr-qc]
- 112. C. Barcelo, S. Liberati, M. Visser, Analogue gravity. Living Rev. Relativ. 8, 12 (2005). arXiv:gr-qc/0505065 [gr-qc]
- 113. C. Cherubini, F. Federici, S. Succi, M. Tosi, Excised acoustic black holes: the scattering problem in the time domain. Phys. Rev. **D72**, 084016 (2005). arXiv:gr-qc/0504048 [gr-qc]
- 114. S. Lepe, J. Saavedra, Quasinormal modes, superradiance and area spectrum for 2+1 acoustic black holes. Phys. Lett. **B617** (2005) 174–181. arXiv:gr-qc/0410074 [gr-qc]
- 115. K. Choy, T. Kruk, M. Carrington, T. Fugleberg, J. Zahn et al., Energy flow in acoustic black holes. Phys. Rev. **D73**, 104011 (2006). arXiv:gr-qc/0505163 [gr-qc]
- 116. M. Richartz, A. Prain, S. Liberati, S. Weinfurtner, Rotating black holes in a draining bathtub: superradiant scattering of gravity waves. arXiv:1411.1662 [gr-qc]
- 117. F. Federici, C. Cherubini, S. Succi, M. Tosi, Superradiance from BEC vortices: a numerical study. Phys. Rev. A73, 033604 (2006). arXiv:gr-qc/0503089 [gr-qc]
- 118. N. Ghazanfari, O.E. Mustecaplioglu, Acoustic superradiance from an optical-superradiance-induced vortex in a Bose-Einstein condensate. Phys. Rev. A89, 043619 (2014). arXiv:1401.1077 [cond-mat.quant-gas]
- 119. F. Kuhnel, C. Rampf, Astrophysical Bose-Einstein condensates and superradiance. Phys. Rev. **D90**, 103526 (2014). arXiv:1408.0790 [gr-gc]
- 120. V. Georgescu, C. Gérard, D. Häfner, Asymptotic completeness for superradiant Klein-Gordon equations and applications to the De Sitter Kerr metric. arXiv:1405.5304 [math.AP]
- 121. Z. Zhu, S.-J. Zhang, C. Pellicer, B. Wang, E. Abdalla, Stability of Reissner-Nordström black hole in de Sitter background under charged scalar perturbation. Phys. Rev. **D90**(4), 044042 (2014). arXiv:1405.4931 [hep-th]
- 122. R. Konoplya, A. Zhidenko, Charged scalar field instability between the event and cosmological horizons. Phys. Rev. **D90**, 064048 (2014). arXiv:1406.0019 [hep-th]
- 123. A. Ishibashi, R.M. Wald, Dynamics in nonglobally hyperbolic static space-times.

 3. Anti-de Sitter space-time. Classical Quantum Gravity 21, 2981–3014 (2004).

 arXiv:hep-th/0402184 [hep-th]

- 124. E. Winstanley, On classical superradiance in Kerr-Newman anti-de Sitter black holes. Phys. Rev. **D64**, 104010 (2001). arXiv:gr-gc/0106032 [gr-gc]
- 125. O.J. Dias, J.E. Santos, Boundary conditions for Kerr-AdS perturbations. J. High Energy Phys. 1310, 156 (2013). arXiv:1302.1580 [hep-th]
- 126. V. Cardoso, S.J. Dias, G.S. Hartnett, L. Lehner, J.E. Santos, Holographic thermalization, quasinormal modes and superradiance in Kerr-AdS. J. High Energy Phys. **1404**, 183 (2014). arXiv:1312.5323 [hep-th]
- 127. R. Jorge, E.S. de Oliveira, J.V. Rocha, Greybody factors for rotating black holes in higher dimensions. arXiv:1410.4590 [gr-qc]
- 128. M. Richartz, A. Saa, Superradiance without event horizons in general relativity. Phys. Rev. **D88**, 044008 (2013). arXiv:1306.3137 [gr-qc]
- 129. V. Cardoso, R. Brito, J.L. Rosa, Superradiance in stars (2015). arXiv:1505.05509 [gr-qc]
- 130. K. Glampedakis, S.J. Kapadia, D. Kennefick, Superradiance-tidal friction correspondence. Phys. Rev. **D89**(2), 024007 (2014). arXiv:1312.1912 [gr-qc]
- 131. Y.B. Zel'dovich, J. Exp. Theor. Phys. Lett. 14, 180 (1971)
- 132. N. Yunes and X. Siemens, Gravitational-wave tests of general relativity with ground-based detectors and pulsar timing-arrays. Living Rev. Relativ. **16**, 9 (2013). arXiv:1304.3473 [gr-qc]
- 133. E. Barausse, V. Cardoso, P. Pani, Can environmental effects spoil precision gravitational-wave astrophysics? Phys. Rev. **D89**, 104059 (2014). arXiv:1404.7149 [gr-qc]
- 134. E. Berti, E. Barausse, V. Cardoso, L. Gualtieri, P. Pani et al., Testing general relativity with present and future astrophysical observations. arXiv:1501.07274 [gr-qc]
- 135. P. Pani, C.F. Macedo, L.C. Crispino, V. Cardoso, Slowly rotating black holes in alternative theories of gravity. Phys. Rev. **D84**, 087501 (2011). arXiv:1109.3996 [gr-qc]
- 136. B. Kleihaus, J. Kunz, E. Radu, Rotating black holes in dilatonic Einstein-Gauss-Bonnet theory. Phys. Rev. Lett. **106**, 151104 (2011). arXiv:1101.2868 [gr-qc]
- 137. D. Psaltis, D. Perrodin, K.R. Dienes, I. Mocioiu, Kerr black holes are not unique to general relativity. Phys. Rev. Lett. **100**, 091101 (2008). arXiv:0710.4564 [astro-ph]
- 138. Y.S. Myung, Instability of rotating black hole in a limited form of f(R) gravity. Phys. Rev. **D84**, 024048 (2011). arXiv:1104.3180 [gr-qc]
- 139. Y.S. Myung, Instability of a Kerr black hole in f(R) gravity. Phys. Rev. **D88**(10), 104017 (2013). arXiv:1309.3346 [gr-qc]
- 140. T. Johannsen, D. Psaltis, A metric for rapidly spinning black holes suitable for strong-field tests of the no-hair theorem. Phys. Rev. **D83** 124015, (2011). arXiv:1105.3191 [gr-qc]
- 141. V. Cardoso, P. Pani, J. Rico, On generic parametrizations of spinning black-hole geometries. Phys. Rev. **D89**, 064007 (2014). arXiv:1401.0528 [gr-qc]
- 142. D. Bini, C. Cherubini, R.T. Jantzen, B. Mashhoon, Massless field perturbations and gravitomagnetism in the Kerr-Taub-NUT space-time. Phys. Rev. **D67**, 084013 (2003). arXiv:gr-qc/0301080 [gr-qc]
- 143. D. Bini, C. Cherubini, A. Geralico, Massless field perturbations of the spinning C metric. J. Math. Phys. 49, 062502 (2008). arXiv:1408.4593 [gr-qc]
- 144. V. Cardoso, I.P. Carucci, P. Pani, T.P. Sotiriou, Black holes with surrounding matter in scalar-tensor theories. Phys. Rev. Lett. **111**, 111101 (2013). arXiv:1308.6587 [gr-qc]
- 145. V. Cardoso, I.P. Carucci, P. Pani, T.P. Sotiriou, Matter around Kerr black holes in scalar-tensor theories: scalarization and superradiant instability. Phys. Rev. **D88**, 044056 (2013). arXiv:1305.6936 [gr-qc]
- 146. S. Chandrasekhar, V. Ferrari, On the non-radial oscillations of slowly rotating stars induced by the lense-thirring effect. Proc. R. Soc. Lond. **A433**, 423–440 (1991)
- S.L. Detweiler, Klein-Gordon equation and rotating black holes. Phys. Rev. D22, 2323–2326 (1980)
- 148. S. Hawking, Particle creation by black holes. Commun. Math. Phys. 43, 199–220 (1975)
- D.N. Page, Particle emission rates from a black hole: massless particles from an uncharged, nonrotating hole. Phys. Rev. D13, 198–206 (1976)

150. D.C. Dai, D. Stojkovic, Analytic explanation of the strong spin-dependent amplification in Hawking radiation from rotating black holes. J. High Energy Phys. **1008**, 016 (2010). arXiv:1008.4586 [gr-gc]

- 151. I. Bredberg, T. Hartman, W. Song, A. Strominger, Black hole superradiance from Kerr/CFT. J. High Energy Phys. 1004, 019 (2010). arXiv:0907.3477 [hep-th]
- 152. M. Guica, T. Hartman, W. Song, A. Strominger, The Kerr/CFT correspondence. Phys. Rev. **D80**, 124008 (2009). arXiv:0809.4266 [hep-th]
- 153. G. Compere, The Kerr/CFT correspondence and its extensions: a comprehensive review. Living Rev. Relativ. 15, 11 (2012). arXiv:1203.3561 [hep-th]
- 154. J.M. Bardeen, G.T. Horowitz, The extreme Kerr throat geometry: a vacuum analog of AdS(2) x S**2. Phys. Rev. **D60**, 104030 (1999). arXiv:hep-th/9905099 [hep-th]
- 155. A.J. Amsel, G.T. Horowitz, D. Marolf, M.M. Roberts, Uniqueness of extremal Kerr and Kerr-Newman black holes. Phys. Rev. **D81**, 024033 (2010). arXiv:0906.2367 [gr-gc]
- 156. O.J. Dias, H.S. Reall, J.E. Santos, Kerr-CFT and gravitational perturbations. J. High Energy Phys. 0908, 101 (2009). arXiv:0906.2380 [hep-th]
- 157. J.D. Bekenstein, A universal upper bound on the entropy to energy ratio for bounded systems. Phys. Rev. D23, 287 (1981)
- 158. T.K. Das, Transonic black hole accretion as analogue system. Conf. Proc. **C0405132**, 279–304 (2004). arXiv:gr-qc/0411006 [gr-qc]
- 159. T.K. Das, N. Bilic, S. Dasgupta, Black-hole accretion disc as an analogue gravity model. J. Cosmol. Astropart. Phys. **0706**, 009 (2007). arXiv:astro-ph/0604477 [astro-ph]
- 160. E. Chaverra, M.D. Morales, O. Sarbach, Quasi-normal acoustic oscillations in the Michel flow. arXiv:1501.01637 [gr-qc]

Chapter 4 Black Holes and Superradiant Instabilities

Superradiant amplification lends itself to extraction of energy from BHs, but can also be looked at as the chief cause of a number of important instabilities in BH spacetimes. Some of these instabilities lead to hairy BH solutions, whereas others extract rotational energy from the BH, spinning it down.

4.1 No Black Hole Fission Processes

One intriguing way of de-stabilizing a BH cluster using superradiance is akin to more familiar fission processes. These however can be shown—as we now do—not to occur for BH clusters. Take a cluster of rotating BHs, as in Fig. 4.1, and send in a low-frequency photon. If the cluster is appropriately built, it would seem *possible in principle* that the photon is successively amplified as it scatters off, leading to an exponential cascade. This kind of process is identical to the way fission bombs work, where neutrons play the role of our wave.

It was pointed out by Press and Teukolsky [1] that such a process could not occur for Kerr BHs, as the entire cluster would have to be contained in its own Schwarzschild radius. Let us see how this works in a generic D-dimensional setting. We take a cluster of N rotating BHs of size L, and total mass NM_{BH} , where M_{BH} is the mass of each individual BH. Assuming all the conditions are ideal, the process can only work if the mean free path l of a photon (or any other boson field) is smaller than the size of the cluster.

$$l < L. (4.1)$$

Now, the mean free path is $l = \frac{1}{n\sigma}$, where *n* is the BH number density in the cluster and σ is an absorption cross section. The absorption cross-section could be negative if a plane wave is amplified upon incidence on a rotating BH (this happens for

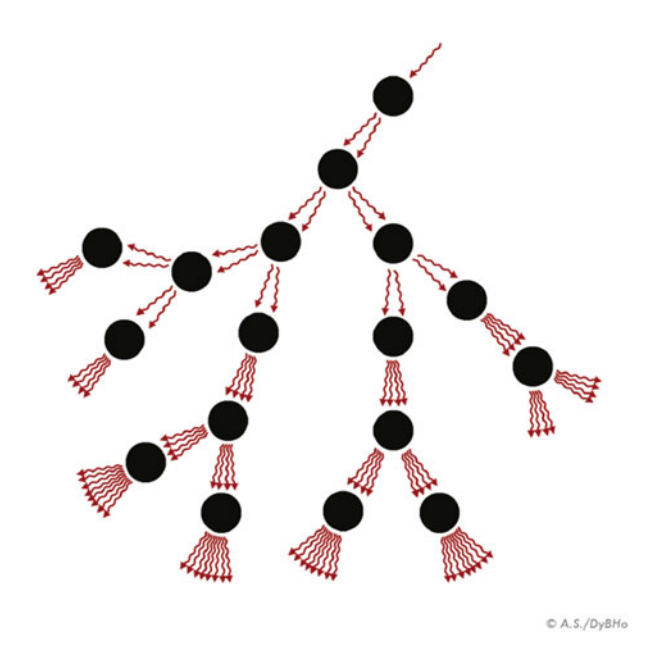


Fig. 4.1 Scheme of the hypothetical chain reaction in a cluster of rotating BHs. The incident *arrow* denotes an incident wave on the rotating BH, which is then amplified and exits with larger amplitude, before interacting with other BHs. The superradiantly scattered wave interacts with other BHs, in an exponential cascade

certain polarizations and angles of incidence only, see Sect. 3.6.6). Even in such case, it is at most of order the BH area. These two properties are very important. That the cross-section scales with the area can be seen on purely dimensional arguments and it holds true for all BH spacetimes we know of. A negative total cross-section is necessary to guarantee that whatever way the boson is scattered it will *on the average* be superradiantly amplified. In other words, we require that a plane wave is subjected to superradiance. To summarize,

$$\sigma \sim V_{D-2}r_+^{D-2},\tag{4.2}$$

where $V_{D-2} = \pi^{D/2-1}/\Gamma[D/2]$ is the volume of a unit (D-3) sphere. Thus, up to factors of order unity, the condition for fission would amount to $L^{D-2}/(Nr_+^{D-2}) < 1$ or equivalently

$$\frac{NM_{BH}}{L^{D-3}} > \frac{L}{r_{+}}$$
 (4.3)

¹Note that say, an l=m=1 mode is a sum of modes with respect to some other coordinate frame, where the following BH scatterer is sitting.

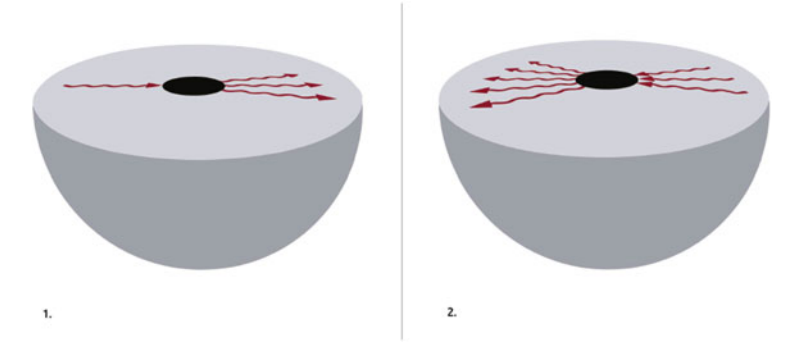


Fig. 4.2 Scheme of a confined rotating BH, and how an initially small fluctuation—the single *red arrow*—grows by successive reflections at the confining wall and amplifications by superradiance in the ergoregion

This last condition is stating that the cluster lies within its own Schwarzschild radius, making the fission process impossible even in the most idealized scenario.

4.2 Spinning Black Holes in Confining Geometries are Unstable

Fission-like processes don't work, but it was recognized early on that confinement will generically turn superradiant amplification into an instability mechanism. The idea is very simple and is depicted in Fig. 4.2: superradiance amplifies any incoming pulse, and the amplification process occurs near the ergoregion. If the pulse is now confined (say, by a perfectly reflecting mirror at some distance) it is "forced" to interact—and be amplified—numerous times, giving rise to an exponentially increasing amplitude, i.e. to an instability.

The details of the confinement are irrelevant and a simple picture in terms of a small perfect absorber immersed in a confining box can predict a number of features. A confining box supports stationary, *normal* modes. Once a small BH is placed inside, one expects that the normal modes will become quasinormal and acquire a small imaginary part, describing absorption—or amplification—at the horizon of the small BH. Thus, it seems that one can separate the two scales—BH and box size—and describe quantitatively the system in this way [2].

Normal modes supported by a box have a wavelength comparable to the box size, in other words a frequency $\omega_R \sim 1/r_0$. For small BHs, $M/r_0 \ll 1$, we then have $M\omega \ll 1$, i.e., we are in the low-frequency limit. In this limit, the equation for wave propagation can be solved via matched asymptotics [3], similar to what is discussed in Appendix B. Let \mathcal{A} denote the absorption probability at the horizon of a rotating BH (which can be computed analytically in the small frequency regime [3–

7]). By definition, a wave with initial amplitude A_0 is scattered with amplitude $A = A_0 (1 - |\mathcal{A}|^2)$ after one interaction with the BH. In the superradiant regime $|\mathcal{A}|^2 < 0$. Consider now a wave trapped inside the box and undergoing a large number of reflections. After a time t the wave interacted $N = t/r_0$ times with the BH, and its amplitude changed to $A = A_0 (1 - |\mathcal{A}|^2)^N \sim A_0 (1 - N|\mathcal{A}|^2)$. We then get

$$A(t) = A_0 \left(1 - t |\mathcal{A}|^2 / r_0 \right). \tag{4.4}$$

The net effect of this small absorption at the event horizon is to add a small imaginary part to the frequency, $\omega = \omega_R + i\omega_I$ (with $|\omega_I| \ll \omega_R$). In this limit, $A(t) \sim A_0 e^{-|\omega_I|t} \sim A_0 (1 - |\omega_I|t)$. Thus we immediately get that

$$\omega_I = |\mathcal{A}|^2 / r_0 \,. \tag{4.5}$$

For example, for a non-rotating BH [3]

$$|\mathcal{A}|^2 = 4\pi \left(\frac{M\omega_R}{2}\right)^{2+2l} \frac{\Gamma^2[1+l+s]\Gamma^2[1+l-s]}{\Gamma^2[1+2l]\Gamma^2[l+3/2]}$$
(4.6)

$$\sim (M/r_0)^{2l+2} \ll 1$$
 (4.7)

where s = 0, 2 for scalar and gravitational fields. Comparing with Eq. (4.5), we obtain

$$M\omega_I \sim -(M/r_0)^{2l+3}$$
 (4.8)

When the BH is rotating, the arguments leading to Eq. (2.47) indicate that rotation can be taken into account by multiplying the previous result by the superradiant factor $1-m\Omega/\omega$. In fact, low-frequency waves co-rotating with the BH are amplified by superradiance. Starobinsky has shown that, at least for moderate spin, the result in Eq. (4.6) still holds with the substitution [4–7]

$$\omega^{2l+2} \to (\omega - m\Omega_{\rm H})\omega^{2l+1}$$
, (4.9)

where we recall that Ω_H is the horizon angular velocity.

In other words, this intuitive picture immediately predicts that confined rotating BHs are *generically* unstable and estimates the growth rate. The dependence of the growth rate on the confining radius r_0 is estimated to be independent on the spin of the field, and this behavior is observed in a variety of systems. The details need, of course, a careful consideration of the corresponding perturbation equations; nevertheless such conclusions hold for several different scenarios [2, 8–11], as we discuss in more detail in the next sections.

4.3 Superradiant Instabilities: Time-Domain Evolutions Versus an Eigenvalue Search

At linearized level BH superradiant instabilities are associated with perturbations of a fixed BH background which grow exponentially in time. Because the background is typically stationary, a Fourier-domain analysis proves to be very convenient. In a stationary and axisymmetric background, a given perturbation $\Psi(t, r, \vartheta, \varphi)$ can be Fourier transformed as

$$\Psi(t,r,\vartheta,\varphi) = \frac{1}{2\pi} \sum_{m} \int d\omega \tilde{\Psi}_{m}(\omega,r,\vartheta) e^{-i\omega t} e^{im\varphi}, \qquad (4.10)$$

and the perturbation function $\tilde{\Psi}_m$ will satisfy a set of PDEs in the variables r and ϑ . For the special case of a Kerr BH and for most types of fields, such PDEs can be miraculously separated using spheroidal harmonics (cf. Sect. 3.6.1 and [12] for a proof of separability using Killing-Yano tensors), whereas in more generic settings other methods have to be used [13].

In any case, the system of equations for $\tilde{\Psi}_m$ together with suitable boundary conditions at the BH horizon (discussed already in Sect. 3.6.1, and more thoroughly in Section 3 in [14]) and at spatial infinity define an eigenvalue problem for the frequency ω . Due to the boundary conditions at the BH horizon and at spatial infinity, the eigenfrequencies (or quasinormal modes) are generically complex, $\omega = \omega_R + i\omega_I$ [14].

In the rest of this section we discuss various superradiant instabilities obtained by solving the corresponding perturbation equations in the frequency domain and finding the complex eigenspectrum. Through Eq. (4.10), an instability corresponds to an eigenfrequency with $\omega_I > 0$ and the instability time scale is $\tau \equiv 1/\omega_I$. In the case of superradiant modes this always occurs when the real part of the frequency satisfies the superradiant condition, e.g. $\omega_R < m\Omega_H$ for a spinning BH. Although QNMs do not form a complete basis, they correspond to poles of the corresponding Green's function, and play an important part in the time-domain problem [14], as they arise in the contour-integration of (4.10). A complementary approach consists in solving the perturbation equations directly in the time domain, by evolving an initially-small field and monitoring its energy-density as a function of time. As we will discuss, this approach has been used recently to study BH superradiance and its development. When both time-domain and frequency-domain computations are available, they yield consistent results [15, 16].

4.4 Black Holes Enclosed in a Mirror

4.4.1 Rotating Black-Hole Bombs

Closed Mirrors One of the first conceptual experiments related to BH superradiance concerns a spinning BH surrounded by a perfectly reflecting mirror [8, 17, 18]. As discussed in the previous section, confinement turns this system unstable against superradiant modes.² A perfectly reflecting wall is an artificial way of confining fluctuations, but is a useful guide to other more realistic and complex systems.

For scalars, the relevant Eq. (3.73) can be solved imposing suitable in-going or regularity boundary conditions at the horizon (discussed in Sect. 3.6.1) and a no-flux condition at the mirror boundary $r = r_m$ in Boyer-Lindquist coordinates. The latter can be realized in two different ways: either with Dirichlet $R(r_m) = 0$ (see [8] for a full analysis of this case) or Neumann $R'(r_m) = 0$ conditions for the corresponding Teukolsky master wavefunction.

The more realistic situation of electromagnetic waves trapped by a conducting spherical surface is also slightly more involved and is explained in Appendix D. The appropriate boundary conditions are that the electric field is tangent to the conductor and that the magnetic field is orthogonal to it in the mirror's frame [19, 20]. We find that the relevant boundary conditions at $r = r_m$ are

$$\partial_{r}R_{-1} = \frac{-i\Delta\left[\pm B + A_{lm} + \omega\left(a^{2}\omega - 2am + 2ir\right)\right]}{2\Delta\left(a^{2}\omega - am + r^{2}\omega\right)}R_{-1} + \frac{\left(a^{2}\omega - am + r^{2}\omega\right)\left(2ia^{2}\omega - 2iam + 2M + 2ir^{2}\omega + \partial_{r}\Delta - 2r\right)}{2\Delta\left(a^{2}\omega - am + r^{2}\omega\right)}R_{-1},$$

$$(4.11)$$

where we have defined $B = \sqrt{(\lambda + a^2\omega^2 - 2am\omega)^2 + 4ma\omega - 4a^2\omega^2}$ and R_{-1} is a radial Teukolsky function defined in Appendix D. The perturbations can be written in terms of two Newman-Penrose scalars, ϕ_2 and ϕ_0 , which are two linearly dependent complex functions. This explains the existence of two different boundary conditions, as would have been expected given the two degrees of freedom of electromagnetic fields. For a = 0 we recover the condition (D.18) when using the minus sign, while for the plus sign we recover the condition (D.19); accordingly, we label these modes as axial and polar modes, respectively.

The boundary conditions described above are only satisfied for a discrete number of QNM eigenfrequencies ω . Our results for the characteristic frequencies are

²Any initial fluctuation grows exponentially, as we argued previously, leading to an ever increasing field density and pressure inside the mirror. The exponentially increasing pressure eventually disrupts the confining mirror, leading to an "explosion," and to this system being termed a *black-hole bomb* [18].

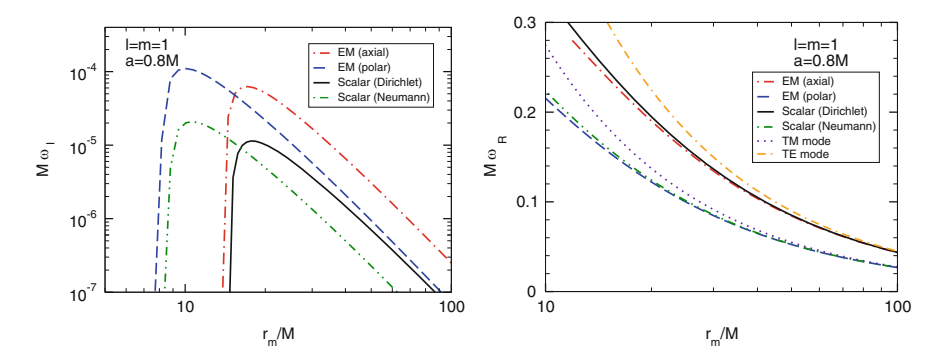


Fig. 4.3 Fundamental (n=0) QNM frequency for scalar and electromagnetic perturbations of a confined Kerr BH as a function of the mirror's location r_m , for l=m=1 and a=0.8M. For r_m larger than a critical value the modes are unstable. We show the two different polarizations for the electromagnetic BH bomb compared to the modes of a scalar field for Dirichlet and Neumann boundary conditions at the boundary. For comparison we also show the flat space transverse electric (TE) and transverse magnetic (TM) modes inside a resonant cavity, as computed in Eqs. (D.14) and (D.16) of Appendix D

shown in Fig. 4.3 for l=m=1 and a=0.8M. As the generic argument of the previous Sect. 4.2 anticipated, confined BHs develop an instability, i.e. some of the characteristic frequencies satisfy $\omega_I>0.3$ Figure 4.3 (left panel) shows that the time scale dependence on r_m is the same for electromagnetic and scalar fluctuations, as predicted in Sect. 4.2. Note that the electromagnetic growth rates $1/\omega_I$ are about one order of magnitude smaller than those of scalar fields. This is consistent with the fact that the maximum superradiant amplification factor for vector fields is approximately one order of magnitude larger than those of scalars, as shown in Fig. 3.9.

As also anticipated with the heuristic argument in the previous section, the instability time scale grows with r_m^{2l+2} and the oscillation frequency ω_R is inversely proportional to the mirror position and reduces to the flat space result when $r_m \gg M$. Thus, for very small r_m the superradiant condition $\omega < m\Omega_{\rm H}$ is violated and the superradiant instability is quenched. An analytic understanding of the onset of the instability is provided in [21]; generic analytic studies can be found in [8, 22–24]. In the limit of very large cavity radius r_m/M our results reduce to the TE and TM modes of a spherical cavity in flat space [19] (see also Appendix D).

These findings are fully corroborated by a time-domain analysis, summarized in Fig. 4.4 for the case of a scalar field with Dirichlet conditions at $r = r_m$ [15]. The exponential growth of the scalar field for rapidly spinning BHs is apparent. A full nonlinear evolution of the Einstein-Klein-Gordon system in a confining mirror was recently performed [25]; the results were promising but numerically unstable

³We recall that the time-dependence of the field is $\sim e^{-i\omega t}$, and a positive imaginary component of the frequency signals an instability.

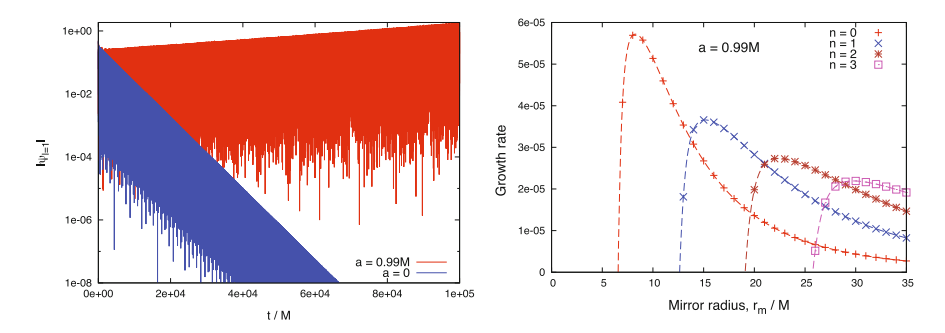


Fig. 4.4 Left: time evolution of a scalar field Ψ obeying Dirichlet conditions at some boundary, on a logarithmic scale, up to $t=10^5 M$. The envelope of the Kerr (Schwarzschild) field grows (decays) exponentially. Right: the growth rate $M\omega_l$ of the first few exponentially-growing modes, as a function of mirror radius r_m . The points show the growth rates calculated from time-domain data, using runs up to $t=10^5 M$. The lines show the growth rates found in the frequency-domain analysis [8]. From [15]

on time scales too short to observe superradiant-induced growth of the scalar, or to probe the end-state of the instability. This remains an open issue to date.

Rotating BHs surrounded by artificial mirrors were studied also in the context of higher dimensional BHs, with similar conclusions [26, 27]. Finally, as discussed in Sects. 2.4.2 and 2.5.2, realizations of effective BH metrics in the laboratory are possible through the use of acoustic setups. In this context, BH bombs were shown to be unstable on short, and possibly experimentally accessible, time scales [28]. A possible end-state of the instability are "distorted geometries", which were recently discussed at the linearized level [29]. Note however, that the boundary conditions used in both these references are very special and correspond to a highly absorbing boundary. A discussion of general boundary conditions for acoustic geometries can be found elsewhere [30].

Accretion Disks: Open Mirrors The BH bomb scenario discussed previously can serve as a model to describe astrophysical BHs surrounded by plasmas or accretion disks. Ionized matter is a good low-frequency electromagnetic waves reflector (see Sect. 4.9.1 below) and can thus play the role of the mirror (this was first realized by Teukolsky [31] and it is discussed in more detail in Sects. 4.9.1 and 5.6). A very important question which still needs clarification concerns the effectiveness of the instability in these realistic situations. The matter surrounding the BH comes under the form of thin or thick accretion disks and not as spherically shaped mirrors. Confining the field along some angular direction means forbidding low angular eigenvalue modes, implying that only higher-angular eigenvalue modes (with longer time scales, cf. Eq. (4.9)) are unstable [32, 33].

Although the geometrical constraint imposed by accretion disks does not completely quench the instability, it can be argued that absorption effects at the mirror could [33]. Consider an optimistic setup for which the electromagnetic wave is amplified by $\sim 1\%$ each time that it interacts with the BH [1]. A positive net gain

only ensues if the wall has a reflection coefficient of 99% or higher. On the other hand, this argument assumes that the mirror itself does not amplify the waves. But if it is rotating, it may too contribute to further amplification (an interesting example of amplification induced by a rotating cylinder is discussed in [34]). Clearly, further and more realistic studies need to be made before any conclusion is reached about the effectiveness of "BH bomb" mechanisms in astrophysical settings.

4.4.2 Charged Black-Hole Bombs

As shown in Sect. 3.5, charged fields can also be amplified through superradiance in a charged BH background. In complete analogy with the rotating BH bomb, one may also consider building a charged BH bomb. Charged BH bombs were studied in detail in [35, 36], both in the frequency and time-domain whereas analytic studies were done in [37, 38]. It was shown that in the limit $qQ \rightarrow \infty$ and for a mirror in the near-horizon region, the characteristic frequency follows a linear scaling $\omega_I \propto qQ/r_+$, implying that the instability growth time scale $\tau_{\rm ins} \equiv 1/\omega_I$ can be made arbitrarily small by increasing q. In [39] these results were extended to a charged massless scalar field in the background of a charged stringy black hole with mirror-like boundary conditions.

Although astrophysical BHs are thought to be neutral due to quantum effects and plasma neutralization, this system is interesting from a conceptual point of view: the very short instability time scale (as compared to the very long time scales involved in the rotating case) make it a very promising testbed for fully nonlinear studies following the development of the instability of BHs in a cavity.

4.5 Black Holes in AdS Backgrounds

Black holes in anti-de Sitter backgrounds behave as BHs in a box, as the AdS boundary is timelike and is may confine fluctuations. One way to see this is through the analysis of timelike geodesics: no timelike particle is able to reach spatial infinity, and therefore AdS backgrounds can be looked at as really a confining system. Another intuition into these spacetimes is brought about by following radial null geodesics in the geometry (3.5) with a negative cosmological constant and zero mass. According to (3.9)–(3.11), these are governed by

$$dr/dt = (r^2/L^2 + 1), (4.12)$$

where *L* is the curvature radius of AdS spacetime, related to the negative cosmological constant in the Einstein equations through

$$L^2 = -3/\Lambda . (4.13)$$

In other words, an observer at the origin measures a finite time $t = \pi L/2$ for a light ray to travel from the origin to the AdS boundary at $r = \infty$. This short result teaches us that boundary conditions at spatial infinity are crucial to determine the evolution of the system.

In view of the above, rotating or charged BHs in anti-de Sitter are expected to behave as the "BH bombs" previously described: for small BH size—relative to the AdS curvature radius—one expects superradiant instabilities, whereas for "large" BHs the resonant frequencies are too large and outside the superradiant threshold. Alternatively, slowly rotating BHs with $\Omega_H L < 1$ are expected to be stable whereas rapidly spinning BHs are expected to be unstable [40].

4.5.1 Instability of Small Kerr-AdS Black Holes and New BH Solutions

The previous arguments were shown to be correct in a series of works, starting with the proof that "large" Kerr-AdS BHs are stable [40]. Small Kerr-AdS BHs were subsequently shown to be mode-unstable against scalar-field fluctuations [9, 41, 42]. For small BHs, i.e. for $r_+/L \ll 1$, the characteristic frequencies will be a deformation of the pure-AdS spectrum $L\omega = l + 3 + 2n$ [43]. A matched asymptotic expansion method yields the eigenfrequencies [9, 42],

$$L\omega = l + 3 + 2n - i\sigma \left(\frac{l + 3 + 2n}{L} - m\Omega_{\rm H}\right) \frac{(r_+^2 + a^2)(r_+ - r_-)^{2l}}{\pi L^{2(l+1)}}, \quad (4.14)$$

where

$$\sigma = \frac{(l!)^2(l+2+n)!}{(2l+1)!(2l)!n!} \frac{2^{l+3}(2l+1+2n)!!}{(2l-1)!!(2l+1)!!(2n+3)!!} \prod_{k=1}^{l} (k^2 + 4\varpi^2), \qquad (4.15)$$

and

$$\varpi = \left(\frac{l+3+2n}{L} - m\Omega_{\rm H}\right) \frac{r_+^2 + a^2}{r_+ - r_-}.$$
 (4.16)

Here, r_- is the smallest root of Δ in (3.6) and $\Omega_{\rm H}$ was defined in (3.7). The numerical solution of the eigenvalue problem was first considered in [42] and agrees remarkably well with the analytical result (4.14). As an example we used a direct integration, shooting method to determine numerically the eigenvalues for $r_+/L=0.005$, the results are summarized in Fig. 4.5, where we also show the analytical prediction. At low rotations the imaginary component of the fundamental eigenfrequency is negative, $\omega_I < 0$, signalling a stable spacetime. As soon as the superradiance condition is satisfied, i.e., when $\omega_R < m\Omega_{\rm H}$, the superradiant

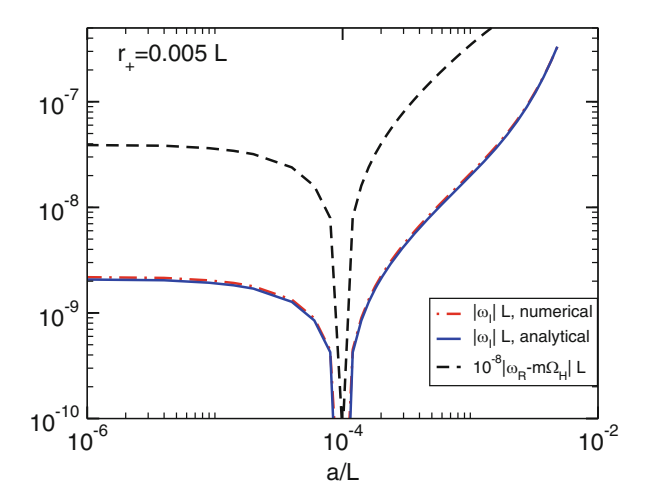


Fig. 4.5 Details of the superradiant instability against dipole (l=m=1) scalar fields. We consider a spinning Kerr-AdS BH with $r_+/L=0.005$ (in Boyer-Lindquist coordinates). The red dashed-dotted line represent numerical data points for the growth-rate ω_I , and the solid blue curve is the analytical prediction (4.14). Note that for rotation rates smaller than $a/L \sim 10^{-4}$ the perturbations become stable; as the dashed black line shows, this is also the critical point for superradiance, at which $\omega_R = m\Omega_H$. From [10]

mechanism sets in and the spacetime is unstable, $\omega_I > 0$, with an instability time scale given by $\tau \equiv 1/\omega_I$.

A numerical search of the parameter space shows that the peak growth rate for the instability is around $\omega_I \sim 3 \times 10^{-4}$ at $r_+/L \sim 0.07$ for a nearly extremal BH. For $r_+/L > 0.15$ there are no signs of unstable modes.

Gravitational perturbations can be handled in a similar way⁴; these perturbations have two degrees of freedom which have traditionally been termed gravitational vector (or Regge-Wheeler or odd) perturbations and gravitational scalar (or Zerilli or even) perturbations. For small r_+/L , a similar matched asymptotic expansion technique can be used [10]. For the lowest harmonic l=2, the characteristic frequencies satisfy

$$i(-1)^{L\tilde{\omega}+1}L^{-5}\left(r_{+}-\frac{a}{r_{+}^{2}}\right)^{5}L\tilde{\omega}\left(L^{2}\tilde{\omega}^{2}-1\right)\left(L^{2}\tilde{\omega}^{2}-4\right)\Gamma(5-2i\varpi)$$

$$+5400\left[\varepsilon+(-1)^{L\tilde{\omega}}\right]\Gamma(-2i\varpi)=0,$$
(4.17)

⁴A comprehensive discussion of the acceptable boundary conditions for gravitational fluctuations is presented in [10, 44].

where $\varepsilon=1$ describes gravitational scalar modes while $\varepsilon=-1$ represents gravitational vector modes (both with the boundary conditions corresponding to a non-deformed AdS boundary [10]). Note also that [10] uses a slightly different coordinate system with time coordinate \tilde{t} and characteristic frequency $\tilde{\omega}$. In the Boyer-Lindquist coordinates we adopt here, the characteristic frequencies are $\omega=\Sigma\tilde{\omega}$, where Σ was defined in Eq. (3.6).

An approximate analytic solution (valid in the limit $a/L \ll r_+/L \ll 1$) of the transcendental equations above is

1) Scalar modes:
$$\tilde{\omega}_{I}L \simeq \frac{16}{15\pi} \left[-\frac{3r_{+}^{6}}{L^{6}} + \frac{mar_{+}^{4}}{L^{5}} \right]$$

$$\left(1 + 15(5\gamma - 7) \frac{r_{+}^{2}}{L^{2}} \right) + \cdots, \qquad (4.18)$$
2) Vector modes: $\tilde{\omega}_{I}L \simeq \frac{96}{15\pi} \left[-\frac{4r_{+}^{6}}{L^{6}} + \frac{mar_{+}^{4}}{L^{5}} \right]$

$$\left(1 + \frac{80(5\gamma - 7)}{3} \frac{r_{+}^{2}}{L^{2}} \right) + \cdots, \qquad (4.19)$$

where $\gamma \simeq 0.577216$ is the Euler-Mascheroni constant. The overall behavior is identical to that of scalar fields. For both scalar and vector modes the imaginary part of the frequency is negative at a=0, consistent with the fact that QNMs of Schwarzschild-AdS are always damped [14, 45]. However, as a/L increases, ω_I increases. As in the previous cases, at the critical rotation where the crossover occurs, i.e. $\omega_I=0$, one has $\omega_R-m\Omega_H\simeq 0$ to within 0.01 %. For smaller rotations one has $\omega_R-m\Omega_H>0$ and for higher rotations one has $\omega_R-m\Omega_H<0$ and $\omega_I>0$. Therefore, the instability which is triggered at large rotation rates has a superradiant origin since the superradiant factor becomes negative precisely when the QNMs go from damped to unstable. These analytical matching results provide also a good testbed check to our numerics. Indeed we find that our analytical and numerical results have a very good agreement in the regime of validity of the matching analysis. This is demonstrated in Fig. 4.6 where we plot the numerical and analytical results for the fundamental l=2 scalar and vector modes.

Finally, note that the strength of the scalar or vector gravitational instabilities can be orders of magnitude higher than the strength of the same superradiant instability sourced by a scalar field perturbation [9, 42]. The maximum growth rate for the scalar and vector superradiant instability is of order $L\omega_I \sim 0.032, 0.058$ respectively at $(r_+/L, a/L) \sim (0.445, 0.589), (0.32, 0.386)$ (for further details see [10]); the peak growth rates are therefore substantially larger than those for scalar field fluctuations, as might be anticipated. Indeed the maximum growth rates are two orders of magnitude larger than in the scalar case, as might be expected from

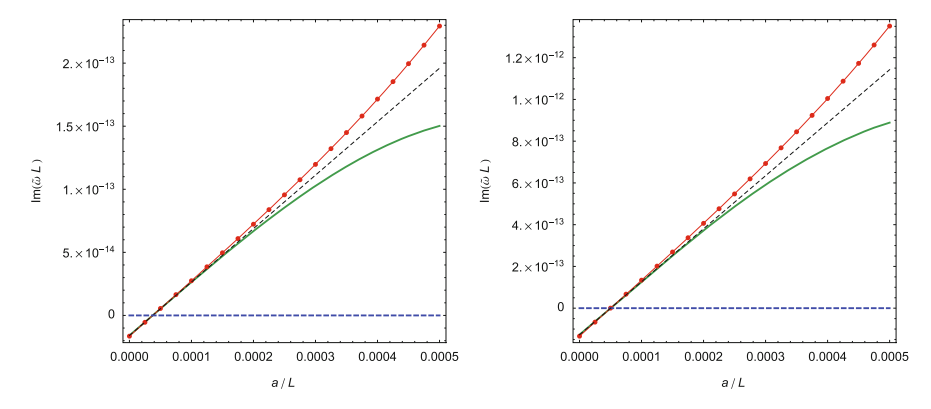


Fig. 4.6 Imaginary part of the QNM frequency as a function of the rotation parameter a/L, for fixed horizon radius $r_+/L=0.005$, for l=2 gravitational scalar (right panel) and vector modes (left panel). Here $\omega=\Sigma\tilde{\omega}$. The red dots are numerical points. The green curve is the numerical solution of the matching transcendental Eq. (4.17), while the dashed black curve is the approximated analytical solution (4.18) or (4.19) of (4.17). In both figures there is a critical rotation where $\omega_I=0$ and $\omega_R-m\Omega_{\rm H}\simeq0$ to within 0.01%. For lower rotations the QNMs are damped and with $\omega_R-m\Omega_{\rm H}>0$, while for higher rotations we have unstable superradiant modes with $\omega_R-m\Omega_{\rm H}<0$

the corresponding two orders of magnitude difference in superradiant amplification factors.

Direct evolutions in the time-domain were recently reported for scalar fields yielding instability time scales consistent with the frequency-domain analysis [46]. Finally, rigorous growth-rate estimates for generic initial data are provided in [47].

This mechanism is likely to render other rotating black objects in asymptotically AdS spacetimes unstable. One example of such objects are rotating black rings, recently discussed in [48].

Three-Dimensional BHs in AdS The only exception to this rule are (2+1)-dimensional BHs, whose spectra shares some similarities to those of Kerr BHs. Studies of the so-called rotating BTZ BH spacetime or "squashed" versions present in modified theories of gravity thereof show that these geometries are stable [49, 50]. Note that in three dimensional GR there are no gravitational degrees of freedom, and that stability results refer only to scalar or electromagnetic fluctuations.

The End-State of the Instability and New BH Solutions Small, rapidly spinning BHs in AdS are unstable. Where does the instability drives the system to? For such confining geometries, the final state cannot be a Kerr-AdS BH: energy and angular momentum conservation guarantee that the BH would have exactly the same parameters as the initial state, hence it would be unstable. Furthermore, the BH is amplifying low-frequency radiation which can not penetrate the horizon. We are thus led to the conclusion that the final state of the instability must be a rotating BH surrounded by a bosonic "cloud", generically a very dynamic spacetime due to GW emission induced by the cloud.

In certain cases, it is possible to suppress GW emission by considering contrived matter content, as it was done in [51] where the authors have explicitly constructed an AdS BH with scalar hair, albeit in five-dimensional spacetimes. The action considered includes 2 complex scalar fields in five dimensions,

$$S = \int d^5 x \sqrt{-g} \left[R + \frac{12}{L^2} - 2 \left| \nabla \vec{\Pi} \right|^2 \right], \tag{4.20}$$

with

$$\vec{\Pi} = \Pi e^{-i\omega t + i\psi} \begin{cases} \sin(\theta/2)e^{-i\phi/2} \\ \cos(\theta/2)e^{-i\phi/2} \end{cases} . \tag{4.21}$$

With the ansatz

$$ds^{2} = -fgdt^{2} + dr^{2}/f + r^{2} \left[h \left(d\psi + \frac{\cos \theta}{2} d\phi - \Omega dt \right)^{2} + \frac{d\theta^{2} + \sin^{2} \theta d\phi^{2}}{4} \right],$$
(4.22)

then all metric coefficients f, g, h, Ω and the field Ψ are real functions of a radial coordinate r. Notice that such ansatz is special in the sense that even though the scalars are dynamical, the stress-tensor

$$T_{ab} = \partial_a \vec{\Pi}^* \partial_b \vec{\Pi} + \partial_a \vec{\Pi} \partial_b \vec{\Pi}^* - g_{ab} \partial_c \vec{\Pi} \partial^c \vec{\Pi}^*, \qquad (4.23)$$

has the same symmetry as the metric. It is then possible to find five-dimensional AdS BHs with scalar hair by simply solving a set of coupled ODEs [51]. The BHs are neither stationary nor axisymmetric, but are invariant under a single Killing field which is tangent to the null generators of the horizon. These solutions can then be viewed either as the end-state of the superradiant instability, or as interpolations between (equal angular momenta) Myers-Perry-AdS BHs and rotating boson stars in AdS. In a phase diagram, these solutions bifurcate from the threshold of the superradiant instability of the original Myers-Perry BH.

More general solutions representing the end-point of superradiant instabilities, without the assumptions above, are thought to exist [41, 52]; in fact, two such solutions have recently been studied [53, 54] and they underline the role of superradiance in a vast set of physical phenomena including in the construction of novel BH solutions.

4.5.2 Charged AdS Black Holes: Spontaneous Symmetry Breaking and Holographic Superconductors

As might be anticipated, charged BHs in AdS are also unstable through superradiance, in line with what we discussed in Sect. 4.4.2 for charged BHs in a

cavity. In fact, such instability has been studied extensively in the context of the gauge-gravity duality and prompted the recent flurry of activity on so-called holographic superconductors and superfluids [55, 56]. Curiously, the connection of this phenomenon to superradiance was initially almost unnoticed, and has been realized only some years after the original proposal (see [57–59]). We present here a unified picture of this problem.

Instabilities of charged BHs in AdS have been studied in [60] under a different guise, namely with the aim to provide a holographic dual description of a spontaneous symmetry-breaking mechanism at finite temperature. Gubser [60] considered an Abelian Higgs theory in four-dimensional curved spacetime, which is given by action (3.1) with a massless Maxwell field. A solution of the theory above is a RN-AdS BH (cf. Eq. (3.4)) endowed with an electric potential $\Phi = Q/r - Q/r_+$ and a vanishing scalar field. A small scalar fluctuation on this background is governed by the Klein-Gordon equation with an effective mass term given by

$$m_{\text{eff}}^2 = -\frac{q^2 \Phi^2}{f(r)} \,, \tag{4.24}$$

where f(r) is given in Eq. (3.4) and for simplicity we have neglected the actual mass term μ_S of the scalar field, whose role is not crucial in this analysis. Thus, the effective mass squared is negative outside the horizon. If q is sufficiently large, the negative potential well can produce unstable modes. Such modes only exist when the spacetime is asymptotically AdS and have no analog in flat space.⁶ In fact, there are two different mechanisms at play [58, 63], only one of which is associated with superradiance. One (nonsuperradiant) is related to the near-horizon geometry of the extremal RN BH which is described by AdS₂. When $m_{\text{eff}}^2 < m_{\text{BL}}^2$ (where $m_{\rm BL}$ is the Breitenlohner-Freedman bound of the near-horizon AdS_2 geometry), the mode is effectively space-like and produces a tachyonic instability. Such instability also exists for non-extremal BHs although it requires larger values of q. On the other hand the second, superradiant, mechanism is related to the fact that charged scalar perturbations can be superradiantly amplified by the RN BH, the energy being trapped by the AdS boundary, which provides the arena for the instability. In fact, the linearized analysis is equivalent to that presented in Sect. 3.5. This mechanism is akin to the BH bomb and requires confinement due to the AdS boundary. Therefore, it only exists in global AdS and not for planar RN-AdS black branes [58, 59].

In the context of the gauge-gravity duality, this instability has far-reaching consequences, as it signals the onset of a phase transition towards a hairy BH

⁵As discussed in [60], the electric potential at the horizon should vanish to ensure regularity of the one-form Φdt .

⁶A similar mechanism occurs also for neutral fields with nonminimal couplings [61]. However, in that case the instability occurs also in asymptotically-flat spacetime [62] and does not have a holographic interpretation in terms of spontaneous symmetric breaking. In fact, this mechanism is akin to superradiant instabilities triggered by nonminimal couplings, as those discussed in Sect. 4.9.

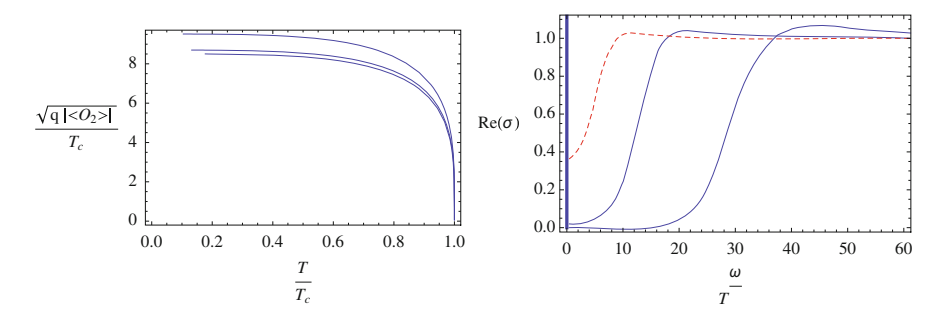


Fig. 4.7 Left panel: the scalar operator of the boundary theory dual to the Abelian Higgs model (3.1) (with massless Maxwell field) which is related to the asymptotic behavior of the scalar hair through the AdS/CFT dictionary. A hairy BH geometry branches off the RN-AdS solution and exists only below a certain critical temperature $T_c \sim \sqrt{\rho}$, where ρ is the charge density. The behavior at $T \sim T_c$ shows that the phase transition is of second order. Different curves correspond to various values of the scalar charge q. Right panel: the electric conductivity of the dual theory in the superfluid phase at various temperatures (decreasing from left to the right). A Dirac delta function appears at $\omega = 0$ and there is a frequency gap at small temperatures. From [64]

configuration that breaks the U(1) symmetry of the initial RN-AdS solution. In a quantum field theory, such spontaneous symmetry breaking (akin to the Higgs mechanism) is associated to superfluidity and the scalar condensate is associated to Cooper pairs [56, 57]. This same mechanism is at play in the Abelian Higgs model as was demonstrated in the seminal work [55] where a "holographic superconductor" was constructed as the nonlinear endstate of the superradiant instability. At small temperatures, the RN-AdS BH becomes unstable through superradiance and spontaneously develops a spherically-symmetric scalar hair. This is in agreement with our previous analysis, and only small BHs are unstable through this mechanism; in addition, planar RN-AdS black branes are stable [58]. The scalarized phase is energetically favored at low temperatures and corresponds to a nonvanishing expectation value of a scalar operator \mathcal{O}_2 living on the boundary, as shown in the left panel of Fig. 4.7.

The behavior of the scalar condensate near the critical temperature signals a second-order phase transition. Other properties of the dual phase such as the existence of a gap in the conductivity, infinite DC conductivity, the existence of Cooper-like pairs and a Meissner-like effect, can all be studied by solving the linear response of the hairy BH solutions to scalar and electromagnetic perturbations [56]. An example is presented in the right panel of Fig. 4.7, showing the conductivity of the superfluid phase.

The results in [55] triggered a flurry of activity in this field that goes well beyond the scope of this work (for a somehow outdated review see [65]). Relevant to our discussion is the analysis of [66], in which nonequilibrium processes in the holographic superfluid phase and the energy extraction from the normal phase described by the RN-AdS BH have been investigated through time evolutions. An example of such evolution is described in Fig. 4.8.

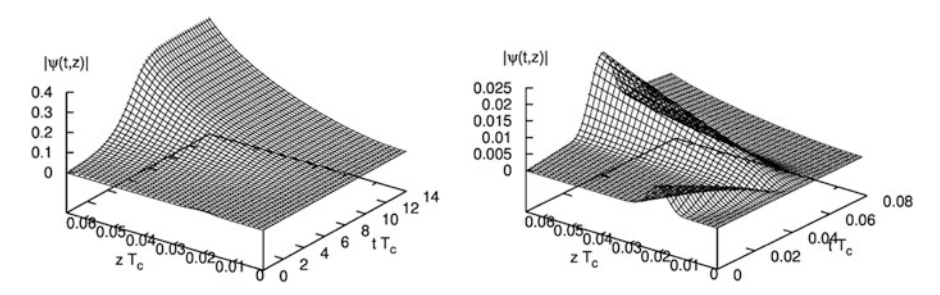


Fig. 4.8 Example of the evolution of the scalar field on (t, z)-plane starting with a perturbed RN-AdS solution in the theory. Left panel: the time interval $0 \le tT_c \le 14$ is shown, where T_c is the critical temperature for the phase transition. Because of the instability of the RN-AdS BH, the scalar density grows exponentially for $tT_c \lesssim 6$ and for $tT_c \gtrsim 6$, the scalar density approaches a stationary configuration. Right panel: the same evolution at initial times, $0 \le tT_c \le 0.08$. The wave packet is reflected by the AdS boundary at $t \simeq 0.04$ and most of it is absorbed at the BH horizon within $tT_c \lesssim 0.06$. From [66]

It is also interesting to mention the case of a charged massive fermion coupled to Einstein-Maxwell theory in AdS. As previously discussed, Pauli exclusion principle implies that fermions cannot condensate and, in turn, superradiance does not occur. From the holographic perspective, the quantum state will not have a coherent phase and the U(1) symmetry is unbroken (cf. [57] for a review). While classical fermionic instabilities are prevented, Schwinger pair production of fermions can occur for sufficiently light fermions, in analogy to the bosonic case. The result of this process is the population of a Fermi sea delimited by a Fermi surface outside the BH, giving rise to so-called "electron stars" [67] which are the (planar, AdS) cousins of astrophysical NSs.

4.6 Massive Bosonic Fields

So far we have discussed two classes of BH-bomb systems: BHs enclosed in a reflecting cavity and BHs in asymptotically AdS spacetimes. The former are highly idealized and unrealistic configurations, whereas the latter—although of great theoretical interest especially in the context of the gauge-gravity duality—are of little relevance for astrophysical BHs.

Fortunately, sometimes "nature provides its own mirrors" [8, 18]. A massive bosonic field naturally confines low-frequency radiation due to a Yukawa-like suppression $\sim e^{-\mu r}/r$ where μ is the mass term. Thus, it was suspected since the 1970s [18, 68] that superradiance triggers instabilities in spinning BH geometries.

This section is devoted to the superradiant instability of spinning BHs triggered by massive bosonic fields in asymptotically-flat spacetime, a topic that has recently flourished with numerous developments in the last few years. The busy reader will find a unified discussion of such instabilities in Sect. 4.6.5. We anticipate that

superradiant instabilities triggered by massive bosons are relevant (i.e. their time scale is sufficiently short) only when the gravitational coupling $M\mu_i \lesssim 1$. We recall that the physical mass of the fields is $m_i = \mu_i \hbar$, where i = S, V, T for scalar, vector and tensor fields, respectively. In Planck units ($G = c = \hbar = 1$), the following conversions are useful

$$1 \text{ eV} \approx 7.5 \times 10^9 M_{\odot}^{-1} \approx 5.1 \times 10^9 \text{ km}^{-1} \approx 1.5 \times 10^{15} \text{ s}^{-1}$$
. (4.25)

so that $\mu_i M \sim 0.75$ when $M \sim M_{\odot}$ and $\mu_i \sim 10^{-10}$ eV, i.e. for a ultralight bosonic field.

4.6.1 The Zoo of Light Bosonic Fields in Extensions of the Standard Model

All observed elementary particles are either fermions or bosons, according to the statistics they obey, which in turn determines whether they have half-integer or integer spin, respectively. Because superradiance does not occur for fermionic fields, here we are interested in massive bosons. All observed elementary bosons are all either massless or very massive, such as the W and Z bosons and the recently-discovered Higgs boson, whose masses are of the order $m \sim 100$ GeV. As we discuss below, the condition $\mu_i M \lesssim 1$ sets the range of mass $\hbar \mu_i$ which is phenomenologically relevant for a given BH mass M. A hypothetical boson with mass in the electronvolt range would trigger a sufficiently strong instability only for light BHs with masses $M \sim 10^{20}$ g. Although the latter could be formed in the early universe as "primordial" BHs [69–71] (see [72] for a review) and are also promising dark-matter candidates, here we focus mostly on massive BHs, i.e. those with masses ranging from a few solar masses to billions of solar masses.

Superradiant instabilities of such massive BHs require ultralight bosonic fields in order to have astrophysically relevant time scales. Such bosons are almost ubiquitous in extensions of the Standard Model of particle physics and in various extensions of GR. The prototypical example of a light boson is the Peccei-Quinn axion [73] introduced as a possible resolution for the strong CP problem in QCD, i.e. the observed suppression of CP violations in the Standard Model despite the fact that, in principle, the nontrivial vacuum structure of QCD allows for large CP violations. The Peccei-Quinn mechanism is based on a global symmetry, whose spontaneous breaking is associated to a new particle, the axion [74, 75]. The axion should acquire a small mass due to nonlinear instanton effects in QCD and its mass is theoretically predicted to be below the electronvolt scale. For a massive BH with $M \sim 5M_{\odot}$, axions with mass of the order of 10^{-11} eV would have a superradiant coupling $\mu_i M \sim 0.4$, so that superradiant instabilities are potentially important. In addition to solve the strong CP problem, light axions are also interesting candidates for cold dark matter [76, 77].

Other light bosons, such as familions [78] and Majorons [79], emerge from the spontaneous breaking of the family and lepton-number symmetries, respectively. A common characteristic of these light bosons is that their coupling to Standard-Model particles is suppressed by the energy scale that characterizes the symmetry breaking, so that it is extremely challenging to detect these fields in the laboratory. Thus, massive BHs are probably the best candidates to investigate the putative effects of light bosons in a range which is complementary to searches using cosmological observations [80].

Furthermore, a plenitude of ultralight bosons might arise from moduli compactification in string theory. In the "axiverse" scenario, multiples of light axion-like fields can populate the mass spectrum down to the Planck mass, $m_P \sim 10^{-33} \, \mathrm{eV}$, and can provide interesting phenomenology at astrophysical and cosmological scales [81].

Light bosonic fields with spin are also a generic feature of extensions of the Standard Model. For example massive vector fields ("dark photons" [82]) arise in the so-called hidden U(1) sector [83–87]. On the other hand, coupling massive spin-2 fields to gravity is a much more involved problem from a theoretical standpoint, but progress in this direction has been recently done in the context of nonlinear massive gravity and bimetric theories (cf. [88, 89] for reviews). A light massive graviton modifies the gravitational interaction at long distances and is a natural alternative to explain the accelerating expansion of the Universe.

In addition to fundamental bosonic fields, effective scalar degrees of freedom arise naturally due to nonminimal couplings or in several modified theories of gravity [90]. For example, in so-called scalar-tensor theories, the gravitational interaction is mediated by a scalar field in addition to the standard massless graviton. The no-hair theorems of GR extend to scalar-tensor gravity under certain conditions [91] so that GR BHs are also the unique vacuum, stationary solution of these theories. However, if the scalar field is massive such BHs would be unstable due to the superradiant instability. Due to a correspondence between scalar-tensor theories and theories which replace the Einstein-Hilbert term by a generic function of the Ricci curvature (so-called f(R) gravity [90]), effective massive scalar degrees of freedom are also present in these theories and trigger superradiant instabilities [92].⁷

The phenomenological implications of superradiant instabilities triggered by light bosons are discussed in Sect. 5.4, here we simply consider the mass of the boson (either m_S , m_V or m_T for spin-0, -1 and -2 particles, respectively) to be a free parameter of the model.

⁷Interestingly, in the context of f(R) gravity the effective scalar field is related to the scalar curvature of the metric, which grows exponentially through superradiance. This suggests that, at variance with the case of real massive fields in which the final state is likely a Kerr BH with lower spin (as discussed in the rest), the end-state of superradiant instabilities in f(R) gravity might be different from a Kerr BH [92]. If such theories are to satisfy the no-hair theorem [91], the end state of the instability should be a non-stationary solution.

4.6.2 Massive Scalar Fields

The simplest and best understood case of superradiant instability triggered by massive bosons is the case of a massive probe scalar field propagating on a fixed Kerr geometry. The existence of this instability was originally suggested by Damour et al. [68] and has been thoroughly investigated by several authors since then.

The linearized dynamics is governed by the massive Klein-Gordon equation

$$\left[\Box - \mu_{\rm S}^2\right]\Psi = 0\,,\tag{4.26}$$

where the D'Alembertian operator is written on the Kerr metric and μ_S is the scalar mass term (we recall that we use Planck units henceforth; the physical mass m_S of the field reads $m_S = \mu_S \hbar$). In the Teukolsky formalism [93, 94], Eq. (4.26) can be separated by use of spin-0 spheroidal wavefunctions [95] as discussed in Sect. 3.6.1 for the massless case. The ODE for the angular part is identical to the massless case after the redefinition $\omega^2 \to \omega^2 - \mu_S^2$, whereas the potential of the radial equation gets a further contribution proportional to $\mu_S^2 \Delta r^2$.

Analytical Results The crucial parameter regulating the interaction between the geometry and the massive scalar is the gravitational coupling $M\mu_S$, which is just the ratio between the gravitational radius of the BH and the Compton wavelength of the field. In the scalar case analytical results are available in the $M\mu_S \ll 1$ and $M\mu_S \gg 1$ limits.

For small $M\mu_S$, it can be shown that the eigenvalue problem admits a hydrogenic-like solution [23, 96, 97] with $\lambda \sim l(l+1)$ and

$$\omega \sim \mu_S - \frac{\mu_S}{2} \left(\frac{M\mu_S}{l+n+1} \right)^2 + \frac{i}{\gamma_{nlm}} \left(\frac{am}{M} - 2\mu_S r_+ \right) (M\mu_S)^{4l+5}, \qquad M\mu_S \ll 1,$$
(4.27)

where n=0,1,2... is analog to the principal quantum number in the hydrogen atom and γ_{nlm} is a coefficient that depends on (n,l,m); $\gamma_{011}=48$ for the dominant unstable mode [97] (this result corrects the prefactor found in the original reference, for further details we refer the reader to the appendix of [97]). Note that the QNMs are complex, $\omega=\omega_R+i\omega_I$, unless the superradiant condition is saturated. This happens when

$$a = a_{\text{crit}} \approx \frac{2\mu_S M r_+}{m} \,. \tag{4.28}$$

Because of the time dependence of the field, when $a > a_{\rm crit}$ the imaginary part of the modes is positive and the instability time scale can be defined as $\tau \equiv 1/\omega_l$. In this case, the field grows exponentially in time, $\Psi \sim e^{t/\tau}$. The instability time scale depends on the coupling $\mu_S M$, on the spin a/M and on the mode numbers (l, m, n). The strongest instability occurs for l = m = 1, n = 0 and for highly-spinning BHs.

In the same limit, $M\mu_S \ll 1$, the eigenfunctions can be written in terms of Laguerre polynomials [96, 98]

$$\psi(\mu_S, a, M, r) \propto \tilde{r}^l e^{-\tilde{r}/2} L_n^{2l+1}(\tilde{r}), \qquad (4.29)$$

and ψ becomes a universal function of the dimensionless quantity $\tilde{r} = 2rM\mu_S^2/(l+n+1)$ [99]. For the single most unstable mode, l=m=1 and n=0, the eigenfunctions simplify to $\psi \propto \tilde{r}e^{-\tilde{r}/2}$.

In the opposite regime, $M\mu_S \gg 1$, the instability is exponentially suppressed. By using a WKB analysis, Zouros and Eardley found that the shortest time scale reads [100]

$$\tau \sim 10^7 M e^{1.84 M \mu_S} \qquad M \mu_S \gg 1 \,.$$
 (4.30)

It can be shown that the super-radiant instability regime is bounded by the relation

$$\mu_{S} < \sqrt{2} \, m\Omega \,, \tag{4.31}$$

and that the upper bound can be approached arbitrarily close in the eikonal regime, $M\mu \gg 1$ [101].

Note that for a solar mass BH and a field of mass $m_S \sim 1$ eV, the parameter $M\mu_S \sim 10^{10}$ and the instability time scale is much larger than the age of the universe. Therefore, the case $M\mu_S \gg 1$ has little phenomenological relevance. Below we discuss a more interesting case, when the gravitational coupling is of order unity, $M\mu_S \lesssim 1$.

Numerical Results Exact results for any value of $M\mu_S$ and a/M can be obtained by solving the problem numerically. This was originally done in [11] and a very complete analysis of the instability can be found in [102] which used an extension of the continued-fraction method [14] to compute the unstable modes.⁸

Some representative results are displayed in Fig. 4.9, which shows ω_I as a function of the gravitational couplings for various parameters. The instability corresponds to $\omega_I > 0$, which occurs when $\omega_R < m\Omega_{\rm H}$, i.e. when the mode satisfies the superradiance condition (1.1). As expected, faster rotation leads to shorter growth timescales. Furthermore, for a given l, the mode with the faster growth rate has m = l, and clearly the axisymmetric mode with m = 0 is stable. As in the analytical case, the dominant unstable mode has l = m = 1 and n = 0. For this mode the shortest instability time scale is approximately

$$\tau_S \equiv \tau \sim 6.7 \times 10^6 M \sim \left(\frac{M}{10^6 M_\odot}\right) \text{yr}, \qquad (4.32)$$

⁸The spectrum of massive scalar perturbations of the Kerr metric contains both stable QNMs and quasibound states, which are localized near the BH [97, 102, 103]. The quasibound states are those that become unstable in the superradiant regime.

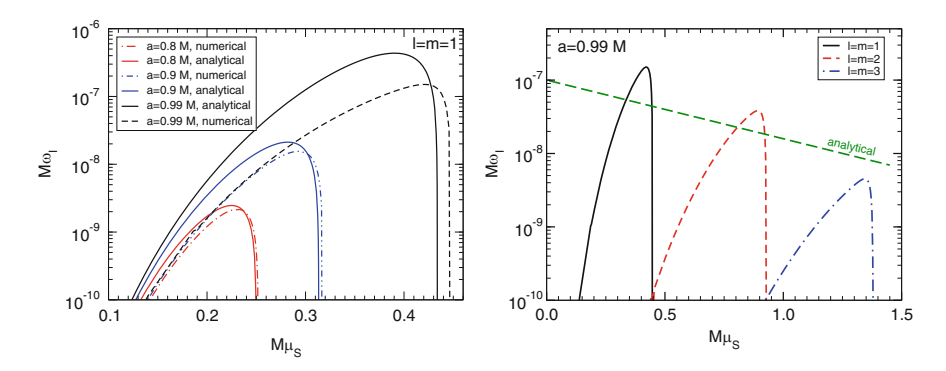


Fig. 4.9 *Left*: Superradiant instability for the fundamental (n=0) l=m=1 modes as a function of the gravitational coupling $M\mu_S$ and for various BH spin (see publicly available MATHEMATICA® notebook in Appendix A). The *dotted lines* shows Detweiler's approximation (4.27) [96] (with the coefficient corrected as in [97]), valid in the limit $M\mu_S \ll 1$. Although not shown, the instability terminates (i.e. $\omega_I \to 0$) when the superradiance condition is not satisfied. *Right*: The same for the fundamental l=m=1, l=m=2 and l=m=3 modes. The fastest growth occurs for the l=m=1 state at $M\mu_S \approx 0.42$, with a=0.999M. The *dotted line* shows Zouros and Eardley's approximation [100], valid when $M\mu \gg 1$ (cf. Eq. (4.30))

and occurs when $M\mu_S \sim 0.42$, corresponding to a light scalar field of mass

$$\mu_S \sim 0.42 M^{-1} \sim 5.6 \times 10^{-17} \left(\frac{10^6 M_{\odot}}{M} \right) \text{eV} \,.$$
 (4.33)

The exact numerical results can be used to check the validity of the analytical approximation when $\mu_S M \ll 1$. It turns out that the spectrum (4.27) and the eigenfunctions (4.29) are a valid approximation of the exact results even for moderately large coupling (roughly up to $\mu_S M \lesssim 0.2$) and even at large BH spin.

More recently, massive Klein-Gordon perturbations of Kerr BHs were also investigated through a time-domain analysis. This was done in [16] by adapting a 3+1 code, whereas subsequently an elegant decomposition in spherical harmonics was used to reduce the Klein-Gordon equation to an infinite set of hyperbolic partial differential equations for perturbations with different harmonic indices, which can then be solved with a 1+1 code [15]. The results of these works are in remarkably good agreement with the frequency-domain analysis. Furthermore, [16] provides an explanation for an apparent discrepancy between time and frequency domain calculations of the instability growth rates as obtained in [104]. This is related to an interference effect between different overtones that will be discussed in the context of massive vector fields below (cf. Fig. 4.11).

The End-State of the Instability and New BH Solutions Unlike the AdS case discussed in Sect. 4.5, massive fields can confine only low-frequency radiation. The issue of the final state of the instability is discussed in detail in Sect. 5.3. We anticipate here that—because of the no-hair theorems ensuring that axisymmetric

vacuum solutions of GR in asymptotically-flat spacetime are described by the Kerr geometry [91, 105–107]—the final state of the superradiant instability of a Kerr BH will still be a Kerr BH with smaller mass and spin. An important counterexample is provided by the hairy BHs discussed in Sect. 5.5. In that case, similarly to the AdS case, the metric remains stationary even if the scalar field oscillates in time [108]. This time dependence in the matter sector circumvents the hypothesis of the no-hair theorem and, at the same time, prevents GW emission (cf. Sect. 5.5 for details).

Massive Charged Scalars Massive charged scalars propagating on a Kerr-Newman background were studied (both analytically and numerically) in [109], which found that the instability growth rate also depends on the coupling qQ, where q and Q are the charges of the field and of the BH, respectively. For a given value of the BH spin the shortest instability time scale is comparable to that of the neutral case, although it occurs for different values of $\mu_S M$ and with $qQ \neq 0$.

Because the BH-bomb effect occurs also for minimally-coupled, charged scalar perturbations of a static, charged BH in a cavity (cf. Sect. (4.4.2)), one might be tempted to conclude that a similar instability exist also when the cavity's surface is replaced by a massive perturbation. However, unlike their rotating counterpart, asymptotically-flat charged BHs were shown to be stable against massive charged scalar perturbations. This is due to the fact that the conditions required in order to trigger the superradiant instability (existence of bound states in the superradiant regime) are incompatible [110, 111]. The same absence of superradiant instability has been recently proved for charged BHs in low-energy effective string theory [112].

4.6.3 Massive Vector Fields

While superradiant instabilities of spinning BHs against massive scalar perturbations have a relatively long history [8, 11, 18, 23, 68, 102, 113], the case of massive bosonic fields with nonvanishing spin (i.e. massive vector and tensor fields) has been investigated much more recently. This is due to technical difficulties that were only recently overcome, as we now discuss.

The equation governing massive vector (spin-1) fields is the Proca equation

$$\nabla_{\sigma} F^{\sigma \nu} = \mu_V^2 A^{\nu} \,, \tag{4.34}$$

where $F_{\mu\nu} = \partial_{\mu}A_{\nu} - \partial_{\nu}A_{\mu}$, A_{μ} is the vector potential and we will focus again on the case in which the differential operator is written on the Kerr background. Maxwell's equations are recovered when $\mu_V = m_V/\hbar = 0$, where m_V is the mass of the vector field. Note that, as a consequence of Eq. (4.34), the Lorenz condition $\nabla_{\mu}A^{\mu} = 0$ is automatically satisfied, i.e. in the massive case there is no gauge freedom and the field A_{μ} propagates 2s + 1 = 3 degrees of freedom [103].

Most studies of Proca fields on a BH geometry are restricted to the nonrotating case [103, 114–116] and clearly fail to describe the superradiant regime. The main reason is that the Proca equation (4.34) does not seem to be separable in the Kerr background by using the standard Teukolsky approach. Recently, the problem has been solved through novel semi-analytical techniques in the slow-rotation limit [97, 117] (cf. [13] for a review on the slow-rotation approximation) and through a fully numerical evolution of the Proca system [16].

In the slow-rotation approximation [13] (briefly discussed in Appendix E), the angular dependence of the perturbations can always be separated, leading to perturbation equations that can be written as a system of ODEs in the schematic form (E.7)–(E.8). This general framework also applies to the Proca system. By expanding the vector field A_{μ} in a basis of vector spherical harmonics as in Eq. (D.3) and by expanding the Kerr background to second order in the spin, 9 the Proca equation (4.34) reduces to two independent systems of ODEs [97, 117]:

$$\mathcal{D}_{\mathbf{A}} \mathbf{\Psi}_{\mathbf{A}}^{l} + \mathbf{V}_{\mathbf{A}} \mathbf{\Psi}_{\mathbf{A}}^{l} = 0, \qquad (4.35)$$

$$\mathcal{D}_{\mathbf{P}} \Psi_{\mathbf{P}}^l + \mathbf{V}_{\mathbf{P}} \Psi_{\mathbf{P}}^l = 0, \qquad (4.36)$$

where $\mathcal{D}_{A,P}$ are second order differential operators, $V_{A,P}$ are 4 × 4 and 5 × 5 matrices, respectively, and we have defined the four- and five-dimensional vectors of variables:

$$\mathbf{\Psi}_{\mathbf{A}}^{l} = (u_{(4)}^{l}, u_{(2)}^{l\pm 1}, u_{(3)}^{l\pm 1}, u_{(4)}^{l\pm 2}), \tag{4.37}$$

$$\mathbf{\Psi}_{\mathbf{P}}^{l} = (u_{(2)}^{l}, u_{(3)}^{l}, u_{(4)}^{l\pm 1}, u_{(2)}^{l\pm 2}, u_{(3)}^{l\pm 2}) \tag{4.38}$$

where the variables $u_{(i)}^l$ are proportional to a^{lm} , f^{lm} , h^{lm} and k^{lm} in Eq. (D.3). Note that the function $u_{(1)}^l$ can be obtained from the Lorenz condition once the three dynamical degrees of freedom $u_{(2)}^l$, $u_{(3)}^l$ and $u_{(4)}^l$ are known. When the spin vanishes, the equations above reduce to Proca perturbations of a Schwarzschild BH [103]. However, rotation introduces mixing between perturbations of different parity and different multipolar indices [13].

By solving the systems (4.35) and (4.36) numerically, [97, 117] found the following set of unstable modes in the small-mass limit:

$$\omega_R^2 \sim \mu_V^2 \left[1 - \left(\frac{M\mu_V}{l + n + S + 1} \right)^2 \right],$$
 (4.39)

$$M\omega_I \sim \gamma_{SI} (ma/M - 2r_+\mu_V) (M\mu_V)^{4l+5+2S},$$
 (4.40)

⁹As discussed in detail in [13, 97], a second-order calculation is needed to describe the superradiant regime in a self-consistent way, although a first-order computation turns out to be surprisingly accurate in all cases explored so far.

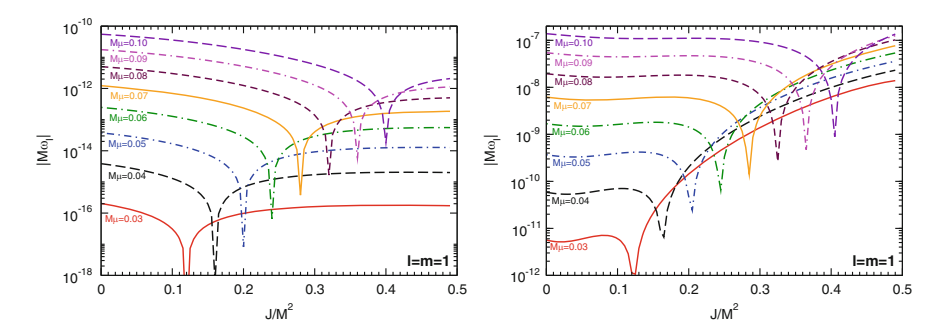


Fig. 4.10 Instability growth rate for the axial (*left panel*) and of the polar S=-1 (*right panel*) Proca modes as a function of the BH rotation rate J/M^2 for l=m=1 and several values of μ_V . The modes cross the axis and become unstable precisely when the superradiance condition, $\omega_R < m\Omega_H$ is saturated. Note that the maximum growth rate for polar modes is about three orders of magnitude larger than that for axial modes. From [97]

where $n \ge 0$ is the overtone number and S is the polarization; S = 0 for axial modes and $S = \pm 1$ for the two classes of polar modes. The coefficient γ_{Sl} depends on S and l. The results above are valid for moderately large couplings $M\mu_V \lesssim 0.2$ and are in good agreement with the analytical results, the latter are available only for the Proca axial modes [97]. Interestingly, Eq. (4.39) predicts a degeneracy for modes with the same value of l + n + S when $M\mu_V \ll 1$, which is akin to the degeneracy in the spectrum of the hydrogen atom.

Massive vector perturbations of rotating BHs are expected to induce a stronger superradiant instability than in the scalar case because, as previously discussed, superradiance is stronger for electromagnetic waves. This is confirmed by Eq. (4.40) which shows that for the dominant unstable mode (with l = m = 1, n = 0, and even parity with S = -1) the strongest instability should occur on a time scale

$$\tau \equiv \tau_V \sim \frac{M(M\mu_V)^{-7}}{\gamma_{-11}(a/M - 2\mu_V r_+)},$$
(4.41)

to be compared with the scalar case, $\tau_S \sim \frac{48M(M\mu_V)^{-9}}{a/M-2\mu_V r_+}$, cf. Eq. (4.27). Roughly speaking, the shortest instability time scale against vector polar perturbations is of order $\tau_V \sim 10^{-2} \gamma_{-11}^{-1} (M/M_\odot)$ s, i.e. some orders of magnitude shorter than in the scalar case. An example of the instability growth rate for Proca fields around spinning BHs is shown in Fig. 4.10.

The results above are valid in the slow-rotation limit. Because of the superradiance condition, $\omega_R \sim \mu_V < m\Omega_{\rm H}$, such limit also imposes that $M\mu_V$ be small. A fully-numerical analysis of the Proca equation (as well as of the massive Klein-Gordon equation) on a fixed Kerr geometry beyond the slow-rotation approximation was done in [16]. By performing a time evolution of the field equations, the exact unstable modes for spin a=0.99M were found to be in surprisingly good agreement with an extrapolation of Eqs. (4.39) and (4.40) to larger BH spin. A

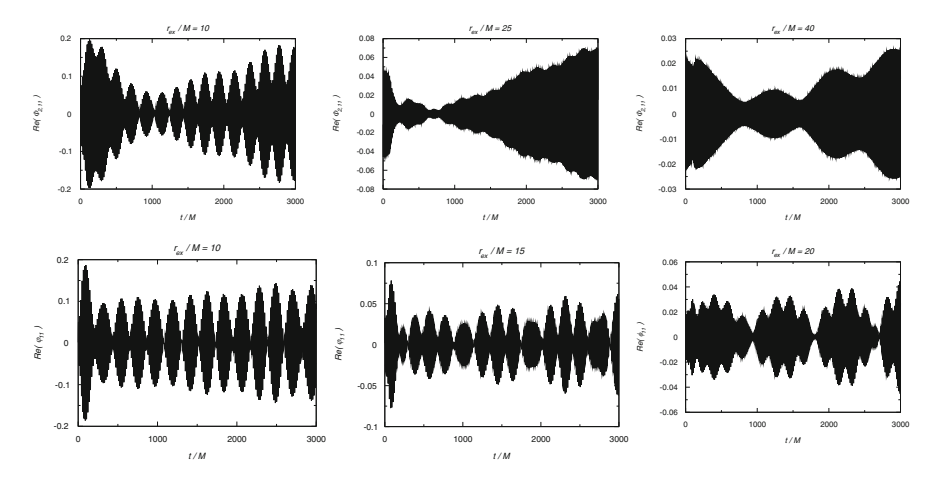


Fig. 4.11 Time evolution of the Proca field with gravitational coupling $M\mu_V=0.40$ in Kerr background with a/M=0.99, at different extraction radii. The l=m=1 mode of the Newman-Penrose scalar Φ_2 (upper panels) and of the scalar component φ (lower panels) are shown. From [16]

second interesting effect uncovered in [16] was that generic initial data excites several overtones (i.e., modes with different principal quantum number n). Because these modes all have similar frequencies ω_R and very long time scales, the overall waveform shows beating patterns [16]. An example of this effect is shown in Fig. 4.11. While the beating pattern is fully compatible with the spectrum (4.39), it also makes it difficult to extract the growth rate. Indeed, depending on the extraction radius and because of the finite time of evolution, a beating pattern can affect the estimate of the instability time scale [16].

4.6.4 Massive Tensor Fields

Massive tensor fields cannot be trivially coupled to gravity. The development of a consistent theory of massive spin-2 fields has an interesting history and we refer the reader to the recent reviews [88, 89].

At the linear level it is known, since the works of Fierz and Pauli, that there is a unique ghost- and tachyon-free mass term that preserves Lorentz invariance and describes the five polarizations of a massive spin-2 field on a flat background [118]. On a curved spacetime the most general linearized field equations describing a massive spin-2 field read

$$\begin{cases} \bar{\Box} h_{\mu\nu} + 2\bar{R}_{\alpha\mu\beta\nu} h^{\alpha\beta} - \mu_T^2 h_{\mu\nu} = 0, \\ \mu_T^2 \bar{\nabla}^{\mu} h_{\mu\nu} = 0, \\ (\mu_T^2 - 2\Lambda/3) h = 0. \end{cases}$$
(4.42)

At the linear level these equations are only consistent if we assume the background to be a vacuum solution of Einstein's equations with a cosmological constant Λ , so that $\bar{R}=4\Lambda$, $\bar{R}_{\mu\nu}=\Lambda\bar{g}_{\mu\nu}$ and barred quantities refer to the background. Interestingly, the same equations can also describe the propagation of a massive graviton in nonlinear massive gravity and in bimetric gravity in some special configurations [119]. These equations were shown to lead to a superradiant instability of Kerr BHs in these theories [119, 120]. ¹⁰

Around a Kerr BH there exist long-lived bound states which follow the same kind of hydrogenic-like scaling (4.39) and (4.40) observed for massive bosons with lower spin. In addition to these modes, a new polar dipole mode was found [119]. This mode was shown to be isolated, does not follow the same small-mass behavior and does not have any overtone. For this mode, the real part is smaller than the mass of the spin-2 field, and in the region $M\mu_T \lesssim 0.4$ is very well fitted by

$$\omega_R/\mu_T \approx 0.72(1 - M\mu_T). \tag{4.43}$$

In the limit $M\mu_T \ll 1$, and for the static case, the imaginary part was found to scale as

$$\omega_I/\mu_T \approx -(M\mu_T)^3. \tag{4.44}$$

That this mode is different is not completely unexpected since in the massless limit it becomes unphysical. This peculiar behavior seems to be the result of a nontrivial coupling between the states with spin projection S=-1 and S=0. In addition, this mode has the largest binding energy (ω_R/μ_T-1) among all couplings $M\mu_T$, much higher than the ground states of the scalar, Dirac and vector fields.

Similarly to the Proca case, also the system (4.42) does not separate on a Kerr background. To investigate the superradiant instability, Brito et al. [119] adopted a slow-rotation approximation to first order in the spin. A representative example of the unstable modes is presented in Fig. 4.12, where it is shown that the decay rate of the dipole polar mode is very large even for small couplings $M\mu_T$.

 $^{^{10}}$ In fact, even the Schwarzschild spacetime is unstable against a spherically symmetric mode in these theories. The instability of the Schwarzschild metric against massive spin-2 perturbations was first discovered in [121], where it was shown that the mass term for a massive spin-2 field can be interpreted as a Kaluza-Klein momentum of a four-dimensional Schwarzschild BH extended into a flat higher dimensional spacetime. Such "black string" spacetimes are known to be unstable against long-wavelength perturbations, a mechanism known as the Gregory-Laflamme instability [122, 123], which in turn is the analog of a Rayleigh-Plateau instability of fluids [124, 125]. Based on these results, Babichev and Fabbri [121] pointed out that massive tensor perturbations on a Schwarzschild BH in massive gravity and bimetric theories would generically give rise to a (spherically symmetric) instability. The unstable mode is absent in partially massless gravity [120] and in solutions of bimetric theories other than the bi-Schwarzschild solution [126]. The former case corresponds to the Higuchi bound $\mu_T^2 = 2\Lambda/3$, so that the scalar equation in (4.42) becomes an identity and the scalar modes does not propagate.

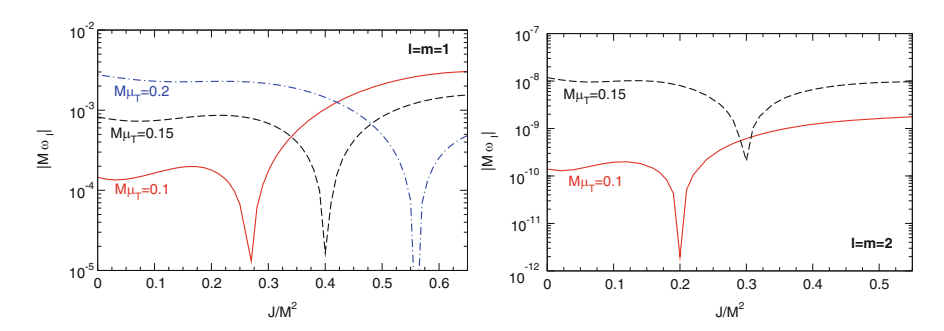


Fig. 4.12 Absolute value of the imaginary part of the polar quasibound modes as a function of the BH rotation rate a/M to first order in the spin for different values of l and m and different values of the mass coupling $\mu_T M$. Left panel: polar dipole mode for l=m=1. Right panel: polar mode l=m=2, S=-2. For any mode with $m\geq 0$, the imaginary part crosses the axis and become unstable when the superradiance condition $\omega_R < m\Omega_H$ is met. From [119]

Indeed, the time scale for this unstable mode is [119]

$$\tau_T \sim \frac{M(M\mu_T)^{-3}}{\gamma_{\text{polar}}(a/M - 2r_+\omega_R)},$$
(4.45)

where $\gamma_{polar} \sim \mathcal{O}(1)$. This time scale is four orders of magnitude shorter than the corresponding Proca field instability and, in fact, it is the shortest instability time scale of a four dimensional, asymptotically-flat GR BH known to date.

4.6.5 A Unified Picture of Superradiant Instabilities of Massive Bosonic Fields

The results presented in the previous sections for spin-0, spin-1 and spin-2 fields suggest the following unified picture describing the superradiant instability of massive bosonic fields around a spinning BH. For any bosonic field propagating on a spinning BH, there exists a set of quasibound states whose frequency satisfies the superradiance condition $\omega_R < m\Omega_{\rm H}$. This modes are localized at a distance from the BH which is governed by the Compton wavelength $1/\mu$ and decay exponentially at large distances. In the small gravitational coupling limit, $M\mu \ll 1$ (where μ denotes the mass of the field), the spectrum of these modes resembles that of the hydrogen atom:

$$\omega_R/\mu \sim 1 - \frac{(M\mu)^2}{2(j+1+n)^2},$$
(4.46)

where j = l + S is the total angular momentum of the state with spin projections $S = -s, -s + 1, \dots, s - 1, s, s$ being the spin of the field. For a given l and n, the total angular momentum j satisfies the quantum mechanical rules for addition of angular momenta, $|l - s| \le j \le l + s$, and the spectrum is highly degenerate.

In the nonspinning case, the decay rate of these modes is well described by

$$\omega_I/\mu \propto -(M\mu)^{\eta} \qquad \eta = 4l + 2S + 5. \tag{4.47}$$

In the spinning case, the imaginary part of the modes in the small $M\mu$ limit is described by the equation above with an extra factor $(2r_+\mu - ma/M)$, which changes the sign of the imaginary part in the superradiant regime. Indeed, when $\omega_R < m\Omega_H$ the imaginary part becomes positive and ω_I corresponds to the growth rate of the field ($\tau \equiv \omega_I^{-1}$ being the instability time scale).

According to Eq. (4.47), the shortest instability time scale occurs for l=1 and S=-1. The only exception to the scaling (4.46) and (4.47) is given by the dipole polar mode of a spin-2 field, whose frequency is given by Eq. (4.43) and the scaling of the imaginary part is similar to Eq. (4.47) but with $\eta=3$.

Despite the recent progress in understanding these instabilities, so far only the massive spin-0 case is fully understood [11, 16, 102] and further work is needed to reach the same level of understanding for higher-spin fields. Massive spin-1 instabilities are known in detail to second order in the BH spin [97, 117]. Beyond the slow-rotation approximation, the only work dealing with Proca instability of highly-spinning Kerr BHs is of numerical nature [16]. The case of massive spin-2 fields is even less explored, because only first-order computations in the spin are available [119]. We believe the progress made in recent years and the wide theoretical and phenomenological interest in light bosons (cf. Sect. 5.4) should serve as an extra motivation to explore these instabilities further.

4.7 Black Holes Immersed in a Magnetic Field

Magnetic fields can also confine radiation and work as "natural" mirrors. Strong magnetic fields are believed to exist around astrophysical BHs, mainly supported by accretion disks. Realistic astrophysical BHs are in general very complex systems which involve the coupling of gravity to the surrounding accretion disk and magnetic field. However some approximate solutions have been found that can give an accurate qualitative, and in some cases quantitative, description of stationary magnetized BH solutions.

The first approximate solution to be found describes a test uniform magnetic field in a Kerr background [127]. In addition to this solution, there exists a class of exact "Ernst" solutions of the Einstein–Maxwell equations, which describe BHs immersed in a uniform magnetic field [128]. These solutions are not asymptotically flat. At infinity the Ernst solutions resemble another solution of the Einstein–Maxwell found by Melvin [129, 130] and further studied by Thorne [131],

describing a uniform magnetic field held together by its own gravitational pull. Much like AdS spacetime which behaves as a covariant box for perturbations (cf. Sect. 4.5), the Melvin solution also admits normal modes [2], because the asymptotic boundary of the Melvin solution is able to confine perturbations. The model introduced in Sect. 4.2 then predicts that a rotating BH immersed in this spacetime should be superradiantly unstable.

Similarly to massive vector and tensor perturbations of a Kerr background (cf. Sect. 4.6), perturbations do not separate in the Ernst backgrounds. Due to this difficulty, up to date no study of the gravito-electromagnetic perturbation of this solution has been performed. However scalar field perturbations have been studied by several authors [2, 132-134]. This was first done in [132], who found that in a $Br \ll 1$ expansion (with B being the magnetic field strength and r the radial coordinate, both in geometric units) the massless scalar field equation (4.26) is separable and is equivalent to a massive scalar perturbation propagating on a Schwarzschild or Kerr metric with an effective mass $\mu_{\text{eff}} = Bm$, where m is the field's azimuthal number. This was further developed in [133, 134] who showed that the magnetic field triggers the same superradiant instability associated to massive fields. However, this approximation becomes inaccurate at distances comparable to or larger than $\sim 1/B$. To handle the problem of non-separability, Brito et al. [2] used a slow-rotation approximation (cf. Sect. 4.6.3) and methods introduced in [15] to study in full detail scalar perturbations of the Ernst solutions without any approximation in the magnetic field strength B. In particular, they studied perturbations around the most generic of these solutions, a magnetized version of the Kerr-Newman metric, and found that in this background, the mode spectrum reads

$$\omega_R \sim [0.75n + 1.2m + 0.25l + 0.7] B + \mathcal{O}(B^3),$$
(4.48)

$$\omega_l M \sim \gamma \left(am/M - \frac{2\omega_R r_+}{1 + 8B^2 M^2 - 16B^4 M^4} \right) (BM)^{2(l+1)}$$
 (4.49)

This estimate was computed including Wald's result for the charge induction [127] caused by the magnetic field, which implies that to have a vanishing total electric charge at infinity a rotating BH should acquire a non-zero charge q=-2aMB. It is clear that the instability time scale can be orders of magnitude smaller than the one estimated using the $Br\ll 1$ approximation of [132–134], in terms of an effective mass $\mu_{\rm eff}=Bm$ (cf. Eq. (4.27)). An example of the instability growth rate for the Kerr–Newman–Ernst BH is shown in Fig. 4.13.

The model presented in Sect. 4.2 suggests that magnetized Kerr–Newman BHs should also be unstable against gravito-electromagnetic perturbations. The same model predicts that the instability growth rate should follow the same scaling as scalar perturbations (4.49). Moreover, since superradiant extraction is more efficient for gravitational and electromagnetic perturbations (cf. Sect. 3.6.5) we expect them to trigger a slightly stronger instability. This generic instability of BHs surrounded

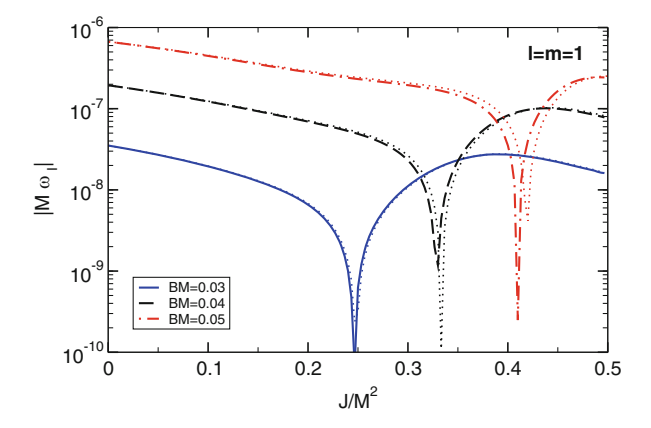


Fig. 4.13 Imaginary part of the fundamental modes of a Kerr-Newman-Ernst BH with Wald's charge q=-2aMB, computed at second order in the rotation, as a function of the BH rotation J/M^2 , for l=m=1, and different values of the magnetic field. The *dotted thinner lines* correspond to a magnetized BH without charge q=0. The only effect of the charge is to change the superradiance threshold. From [2]

by magnetic fields can be used to impose intrinsic limits on the strength of magnetic fields around rotating BHs as we discuss in more detail in Sect. 5.7.

4.8 Superradiant Instability of Black Holes Surrounded by Conducting Rings

An interesting toy model of superradiant-triggered energy extraction in astrophysical systems was proposed by Press [135]. As depicted in Fig. 4.14, the model consists of two coaxial rings, the inner of which is resistive and rotates around the common axis of symmetry, whereas the outer one is a conductor (which we take to be nonspinning for simplicity). The astrophysical analog of such toy model (right panel of Fig. 4.14) is obtained by replacing the inner ring by a Kerr BH, the event horizon playing the role of the rotating resistor.¹¹

In the two-ring model, the electric field is computed by solving Maxwell equations in terms of retarded potentials [19, 135]. The key point of the derivation is to recognize that Ohm's law $J = \sigma E_{\varphi}$ (where J, σ and E are the electric current on the ring, the conductivity and the φ component of the electric field, respectively) must be applied in the matter rest frame of each ring element. Using Lorentz

¹¹The membrane paradigm assigns an electrical resistance of \sim 377 Ohm to the horizon [136].

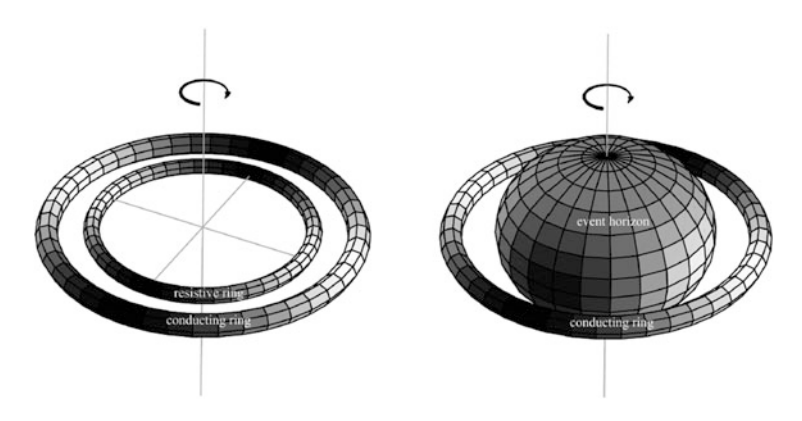


Fig. 4.14 *Left*: Table-top model for superradiant amplification by two conducting rings. The inner resistive ring rotates at relativistic speed, whereas the outer ring is a conductor and might be nonrotating. Rotational energy is extracted from the resistive ring and may be larger than radiative losses to infinity, yielding exponential growth of the stored field energy. *Shading* shows schematically the location of positive and negative charge in an m=2 unstable mode. *Right*: the conjectured BH analog of the table-top model, where the resistive rotating ring is replaced by a Kerr BH. *Shading* shows the charge density on the ring, and the image charge density on the horizon. From [135]

transformations into the inner rotating ring frame yields

$$J_1^{'\hat{\varphi}} = \sigma E^{'\hat{\varphi}} \quad \rightarrow \quad \gamma \left(1 - \frac{m\Omega}{\omega}\right) J_1 = \sigma E_1^{\hat{\varphi}},$$
 (4.50)

where a prime denotes the ring rest frame, the hatted index is the orthonormal tetrad component [135], γ is the Lorentz factor associated to the inner ring angular velocity Ω , i.e. $\gamma = (1-v^2)^{-1/2}$ where v is the linear velocity. Note the superradiant factor emerging in the equation above when Ohm's law is written in the inertial frame.

4.9 Nonminimal Interactions

Nonminimal couplings can produce effective mass terms in the perturbation equations and confine radiation, thus giving rise to superradiant instabilities akin to the ones discussed above for massive bosonic fields. Here we discuss two representative examples: (a) spinning BHs surrounded by a plasma, and (b) instabilities in a modified theory of gravity.

4.9.1 Plasma-Triggered Superradiant Instabilities

Consider a spinning BH surrounded by a plasma. If the total mass of the surrounding matter is sufficiently small, its gravitational backreaction is negligible and the background spacetime is uniquely described by the Kerr metric. In this configuration even standard photons interacting with the plasma acquire an effective mass given (in Planck units) by the plasma frequency [137, 138]

$$\omega_p = \sqrt{\frac{4\pi e^2 n}{m_e}},\tag{4.51}$$

where n is the electron density and m_e and e are the electron mass and charge, respectively. As a consequence of the modified dispersion relation, Maxwell equations within the plasma in flat spacetime read

$$\nabla_{\sigma} F^{\sigma \nu} = \omega_{\rm p}^2 A^{\nu} \,. \tag{4.52}$$

The equation above is also valid in curved spacetime as long as the background is slowly varying compared to ω_p^{-1} and the density gradient is small compared to the gravitational field [138].

When the plasma density is constant and homogeneous, Eq. (4.52) coincides with Proca equation (4.34), where the plasma frequency can be identified with the mass of the vector field. More generically, the plasma density might have a nontrivial radial and angular profile. In this case the instability can be investigated semi-analytically by using the methods developed in [13, 117] or by a fully numerical analysis.

Superradiant instabilities triggered by plasma were analyzed in [139], where it was shown that they are relevant only for small primordial BHs in the early universe, as discussed in detail in Sect. 5.6.

4.9.2 Spontaneous Superradiant Instabilities in Scalar-Tensor Theories

As discussed in Sect. 3.12.1, the presence of matter may drastically affect the superradiant amplification of scalar waves in scalar-tensor theories [140, 141]. Indeed, the Klein-Gordon equation for a massless scalar field acquires an effective, spacetime-dependent mass term $\mu_{\rm eff}$ proportional to the trace of the stress-energy tensor.

When $\mu_{\rm eff}^2 > 0$, a "spontaneous superradiant instability" might be present for rotating BHs, similarly to the case of massive Klein-Gordon fields previously discussed. Focusing on separable solutions of the Klein-Gordon equation with $\Phi = \Psi(r)S(\vartheta)e^{-i\omega t + im\varphi}$, [140, 141] found that if the (trace of the stress-energy

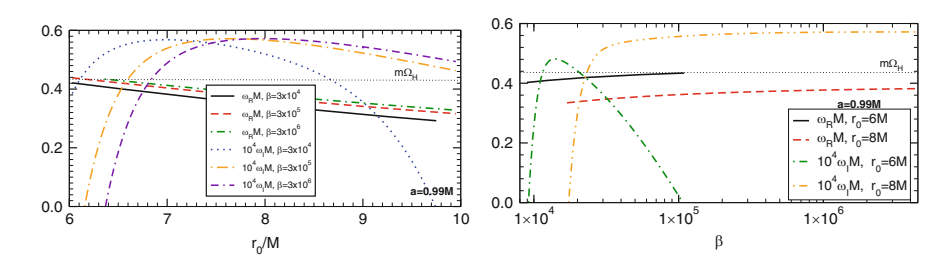


Fig. 4.15 Superradiant instability for a matter profile characterized by Eq. (4.53) with $\mu_0 = 0$, $\mathcal{F} = 0$ and $\mathcal{G} = \Theta[r - r_0]\beta(r - r_0)/r^3$, where β parametrizes the strength of the scalar-tensor coupling. For large β the system behaves as a BH enclosed in a cavity with radius r_0 . Curves are truncated when the modes become stable. From [140]

tensor of the) matter profile has the general form

$$T(r,\vartheta) \sim 2 \frac{\mathcal{F}(\vartheta) + \mathcal{G}(r)}{a^2 + 2r^2 + a^2 \cos 2\vartheta},$$
(4.53)

then the scalar acquires an effective mass $\mu_{\rm eff}^2 \sim \mu_0^2 + T$, and the Klein-Gordon equation is separable, where μ_0 is the original, constant, mass of the scalar [140, 141]. In this case, the scalar perturbations reduce to the following coupled system of equations:

$$\begin{split} &\frac{(\sin\vartheta S')'}{\sin\vartheta} + \left[a^2 \left(\omega^2 - \mu_0^2 \right) \cos^2\vartheta - \frac{m^2}{\sin^2\vartheta} - \mathcal{F} + \lambda \right] S = 0, \\ &\Delta \frac{d}{dr} \left(\Delta \frac{d\Psi}{dr} \right) + \left[K^2 - \Delta \left(\mathcal{G} + r^2 \mu_0^2 + \lambda \right) \right] \Psi = 0 \,, \end{split}$$

where Δ , K and λ have been defined in Sect. 3.6.1, whereas μ_0 is a "bare" mass that will be set to zero in the following, because we are interested in an effective mass term that vanishes at large distances.

A representative case is summarized in Fig. 4.15 for a matter profile characterized by $\mu_0=0$, $\mathcal{F}=0$ and $\mathcal{G}=\Theta[r-r_0]\beta(r-r_0)/r^3$, where β parametrizes the strength of the scalar-tensor coupling. Even though the effective mass term vanishes at large distances, the instability is akin to the original BH bomb, i.e. a spinning BH enclosed by a mirror located at $r=r_0$: as discussed in Sect. 4.4, for small r_0 there is no instability, as the natural frequencies of this system scale like $1/r_0$ and are outside the superradiant regime. It is clear from Fig. 4.15 that this is a superradiant phenomenon, as the instability is quenched as soon as one reaches the critical superradiance threshold. At fixed large r_0/M , and for any sufficiently large β , the instability time scale ω_I^{-1} is roughly constant. In agreement with the simpler BH bomb system, a critical β corresponds to a critical barrier height which is able to reflect radiation back. After this point increasing β further is equivalent to a further increase of the height of the barrier and has no effect on the instability.

Although spontaneous superradiant instabilities seem to be a generic feature of scalar-tensor theories [141], so far they have been investigated only through the ansatz (4.53), i.e. when the equations are separable. Further investigation is necessary in order to understand realistic configurations such as accretion disks. In that case, methods such as those used in [15, 16, 97, 117] would be required.

Finally, spontaneous superradiant instabilities of Kerr-de Sitter BHs in scalartensor theories and the role of a positive cosmological constant were recently investigated [142].

4.10 Kaluza-Klein Mass: Superradiant Instabilities in Higher Dimensions

For higher-dimensional BH spacetimes, instabilities are the rule rather than the exception. For example, black strings and black branes are unstable against long wavelength modes along the flat dimension. This is known as the Gregory-Laflamme instability [122, 143] (see also Sect. 4.6 for the relation between this instability and the instability of the Kerr BH family against massive spin-2 fluctuations [119, 121]). As another example, for $D \ge 6$ dimensions where no upper bound on the rotation of Myers-Perry BHs exists, a Gregory-Laflamme-like instability renders ultra-spinning BHs unstable [144–148]. Besides these instabilities, it was shown that spinning black branes in D = d + n dimensions (and black strings for the particular case n = 1) are unstable against massless bosonic fields due to a superradiant instability when d = 4 [11, 149]. Spinning black branes in D = 4 + n have the form

$$ds^2 = ds_{\text{Kerr}}^2 + dx^j dx_j, \quad (j = 1, 2, ..., n),$$
 (4.54)

where Kerr stands for the 4D Kerr geometry given in (3.5) with $\Lambda=0$. With the ansatz $\Psi=e^{-i\omega t+im\varphi+i\mu_jx^j}S_{0lm}(\vartheta)\psi(r)$, the *massless* Klein-Gordon equation (4.26) in the background (4.54) results in the decoupled Teukolsky equations for a scalar field with effective mass $\mu_S^2\equiv\sum_i\mu_i^2$. Thus the propagation of massless fields around this geometry is equivalent to the propagation of a massive field in the vicinity of the 4D Kerr BH, the mass of field being played by the "Kaluza-Klein" momenta along the flat dimensions. Since Kerr BHs are unstable against massive bosonic fields, the black brane (4.54) is also unstable. Surprisingly it was found that this is only true if d=4 [11]. For d>4 there is no stable bound orbits for massive particles [150], which in terms of wave propagation means that there is no well in the effective potential, and thus there are no (quasi)-bound states. As discussed in Sect. 4.6, this is a fundamental property needed to trigger the superradiant instability. Similar arguments were used to show that large doubly

spinning black rings in $D = 5 [151]^{12}$ are unstable. That this geometry must be unstable was realized from the fact that in the large-radius limit they reduce to boosted Kerr black strings, which are unstable due to the reasons stated above. The superradiant instability for massive scalar fields around boosted Kerr black strings was recently studied [154].

4.11 Ergoregion Instability

We argued in Sect. 3.3.4 that the standard Penrose process and superradiance from spinning BHs are two distinct phenomena: the former only requires the existence of an ergoregion, whereas the latter requires the existence of a horizon. For stationary and axisymmetric BHs, this distinction is superfluous because the existence of an ergoregion implies that of a horizon (cf. proof in Sect. 3.1.5). However, an interesting effect occurs for those geometries that possess an ergoregion but not a horizon: the so-called *ergoregion instability* [155]. The mechanism is simple: a negative-energy fluctuation in the ergoregion is forced to travel outwards; at large distances only positive-energy states exist, and energy conservation implies that the initial disturbance gives rise to a positive fluctuation at infinity plus a larger (negative-energy) fluctuation in the ergoregion. Repetition of the process leads to a cascading instability. The only way to prevent such cascade from occurring is by absorbing the negative energy states, which BHs do efficiently (and hence Kerr BHs are stable against massless fields), but horizonless objects must then be unstable. ¹³

This instability was discovered by Friedman while studying ultracompact slowly-rotating stars with an ergoregion [155, 158], with subsequent work quantitatively describing the unstable modes for a scalar field propagating on a slowly-rotating metric in the large-l limit [159]. This approach has been extended in subsequent work [160–162]. Most notably, [160] extended the analysis to the case of small multipoles (l, m), finding that the instability time scale is much shorter. Finally, [163] studied axial gravitational modes (but again only to first order in the spin), by neglecting the coupling to polar modes that arises in the slow-rotation limit. They find that the time scale can be of the order of the seconds/minutes depending on the compactness of the star. A discussion of these results and their connection to the CFS instability and the r-mode instability is given in Sect. 5.

However, these works are based on an initial assumption which is not fully consistent, because they consider a slowly-rotating, perfect-fluid star including some terms to second order in the rotation but neglecting others (see below). Although

¹²Black rings have topology $S^1 \times S^{D-3}$ unlike Myers-Perry BHs which have topology S^{D-2} . The first 5D black ring was found by Emparan and Reall [152, 153].

¹³The only exception to this rule and argument may occur if the ergoregion extends all the way to infinity as in certain non-asymptotically flat geometries [156, 157]; we thank Óscar Dias for drawing our attention to this point.

this approximation is expected to be reliable for very compact stars [159], no consistent treatment of the ergoregion instability has been developed to date. Below, based on recent developments in the study of perturbations of slowly rotating spacetimes [13, 97, 164, 165], we give the first fully-consistent treatment of this problem.

4.11.1 Ergoregion Instability of Rotating Objects: A Consistent Approach

The technical details of this computation are given in Appendix E and in a publicly available MATHEMATICA[®] notebook (cf. Appendix A). Our starting point is the line element (E.2). To second order in the spin, the ergosphere condition $g_{tt} = 0$ becomes

$$e^{\nu}(1+2h_0) = [r^2\varpi^2\sin^2\vartheta + e^{\nu}h_2(3\sin^2\vartheta - 2)]. \tag{4.55}$$

The solution to Eq. (4.55) is topologically a torus. Thus, to characterize the ergoregion it is necessary to include the second-order terms h_0 and h_2 . All previous analysis of the ergoregion instability neglected such terms, based on the fact that for a very compact object $e^{\nu} \sim 0$ and the terms proportional to h_0 and h_2 should be subdominant relative to the term proportional to ϖ^2 . However, it is easy to show that this approach would give the wrong result for the ergosphere. For example, in the particular case of a Kerr BH, Eq. (4.55) is solved by

$$r_{\rm ergo} = 2M - \frac{a^2}{4M}\cos 2\vartheta + \mathcal{O}\left(\frac{a^4}{M^4}\right),\tag{4.56}$$

which agrees with the exact result to second order in the spin. ¹⁴ On the other hand, neglecting the second-order terms h_0 and h_2 in Eq. (4.55) would give the wrong result, $r_{\rm ergo} = 2M \left(1 + \frac{a^2}{2M^2} \sin^2 \vartheta\right) + \mathcal{O}\left(\frac{a^4}{M^4}\right)$, i.e. the ergoregion would always be larger than the Schwarzschild radius, in clear contrast with the correct result (4.56). Clearly, computing the ergoregion of slowly-rotating spacetimes requires to go at least to second order in the rotation. The formalism to construct slowly-rotating geometries has been developed by Hartle & Thorne and is described in Appendix E. The ergoregion of a compact rotating star, computed by solving Einstein's equations to second order in the angular momentum and using Eq. (4.55), is shown in Fig. 4.16.

In Fig. 4.17, we show the size of the ergoregion for a constant-density star (whose metric in the static case is given in Eqs. (F.2) and (F.3)) for the consistent second-

¹⁴Note that the metric (E.2) is not written in Boyer-Lindquist coordinates, so the ergoregion location does not coincide with that given in Eq. (3.14).

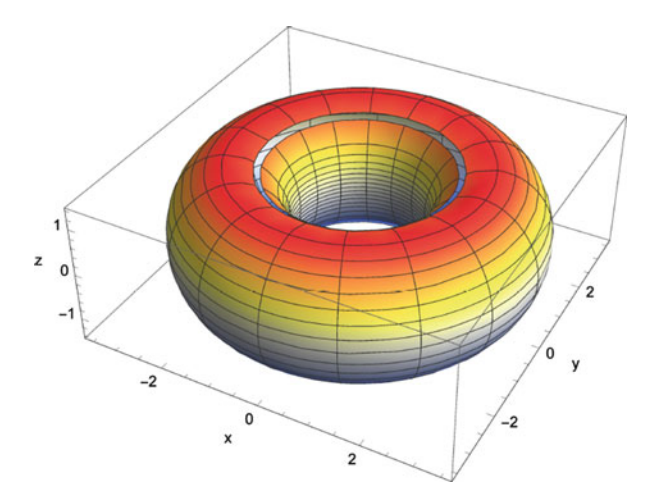


Fig. 4.16 The toroidal ergoregion of a NS with APR equation of state and spinning at the mass-shedding limit, $\Omega = \Omega_K \equiv \sqrt{M/R^3}$, for a mass slightly above the maximum value (to be compared with Fig. 3.2 for a Kerr BH). The coordinates (x, y, z) are Cartesian-like coordinates obtained from (r, ϑ, φ) of the line element (E.2)

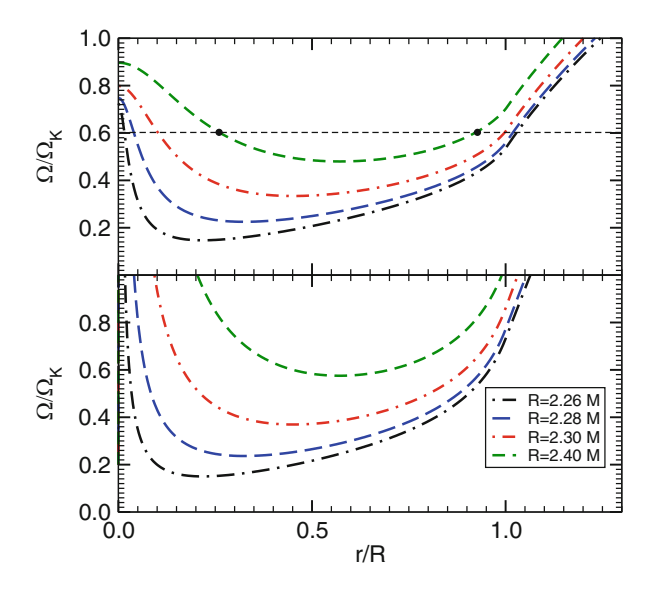


Fig. 4.17 Size of the ergoregion on the equatorial plane of a constant-density star with various compactnesses for the consistent second-order case (top panel) and for the inconsistent case obtained neglecting h_0 and h_2 in Eq. (4.56) (bottom panel). For a given rotational frequency Ω and a given compactness, the boundaries of the ergoregion are the intersections between the corresponding curve and the horizontal line. For example in the consistent case with R=2.40M and $\Omega \sim 0.6\Omega_K$, the ergoregion extends between the two black markers, $0.25 \lesssim r/R \lesssim 0.95$

order case (top panel) and for the inconsistent case obtained neglecting h_0 and h_2 in Eq. (4.56) (bottom panel). For a given rotational frequency Ω , the boundaries of the ergoregion are the intersections between each curve and the horizontal line. The two cases can differ substantially, especially as the compactness decreases. In particular, two striking differences appear: (a) in the consistent case the ergoregion extends to the center of the star, while it disappears in the inconsistent case, and (b) in the consistent case the ergoregion can extend well beyond the radius of the star. Overall, the inconsistent result tends to underestimate the size of the ergoregion.

The spectrum of perturbations of spinning geometries is generically involved, due the coupling between modes with opposite parity and different harmonic index *l*. Nonetheless, within a slow-rotation approach, certain classes of perturbations can be studied consistently by neglecting such couplings [13, 97, 164, 166]. For example, for perturbations of a perfect-fluid star to first order in the spin, the following master equation can be derived:

$$\frac{d^{2}\Psi}{dr_{*}^{2}} + \left[\omega^{2} - 2m\omega\varpi - e^{\nu}\left(\frac{l(l+1)}{r^{2}} + \eta\frac{2M(r)}{r^{3}} + 4\pi(P-\rho)\right)\right]\Psi(r) = 0,$$
(4.57)

where $dr/dr_* = e^{(\nu-\lambda)/2}$ and $\eta = -3$, 1 for gravitational-axial and probe-scalar perturbations, respectively. For an ultracompact star with an ergoregion, the former and the latter perturbations were studied in [163] and [159, 160], respectively, finding a family of unstable modes. ¹⁵ The instability growth rate increases with the spin of the object, is typically maximum for l = m = 1 modes, and is also larger for gravitational perturbations than for scalar modes.

Nonetheless, our previous analysis shows that—to treat the ergoregion instability consistently—one has to include a background geometry to second-order in the spin. Here we consider the simplest case of a probe scalar field that propagates on the background of a spinning NS. The perturbation equations to second order in the spin are derived in Appendix E, the final result is the master equation

$$\frac{d^2\Psi}{dr_{**}^2} + \left[\omega^2 - 2m\omega\varpi - V\right]\Psi(r) = 0, \qquad (4.58)$$

where

$$V = e^{\nu} \left(\frac{l(l+1)}{r^2} + \frac{2M(r)}{r^3} + 4\pi(P - \rho) + V_2(\omega) \right), \tag{4.59}$$

and V_2 is a second-order quantity in the spin that is a cumbersome function of the background metric coefficients appearing in (E.2), of the pressure P and the density ρ , and of their derivatives. Indeed, because V_2 contains second radial derivatives

¹⁵We remark that [159, 160] studied scalar perturbations propagating in the toy-model metric (4.60).

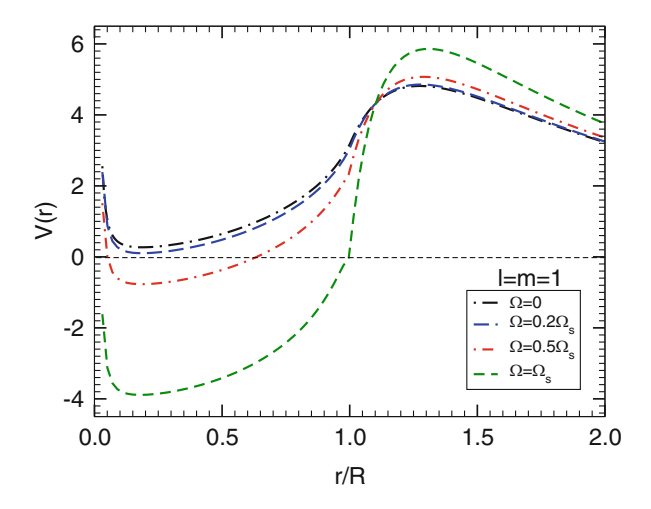


Fig. 4.18 The potential V for $\omega=0$ as defined in Eq. (4.59) for a constant-density spinning star with $R\sim 2.26M$ for different values of the angular velocity. As the mass-shedding limit $\Omega\to\Omega_K$ is approached, the potential develops a deeper negative well. Note that V becomes negative only because of second-order corrections and is positive when $\Omega=0$, although its minimum almost crosses the real axis, giving rise to long-lived modes in the nonspinning case, cf. Sect. 4.11.2

of ρ , solving the corresponding eigenvalue problem is quite challenging. For this reason, here we consider a constant-density star which simplifies the problem considerably. The effective potential V for this case is shown in Fig. 4.18 for various spin rates.

We have solved the eigenvalue problem associated to Eq. (4.58) on the background of a constant-density spinning star to second order in the angular velocity. The background problem is solved in the interior by requiring continuity of the metric functions at the star radius R.¹⁶ For the scalar perturbations, the fact that $\rho = \rho_c = \text{const}$ in the interior and $\rho = 0$ in the exterior produces discontinuities in V at the star's radius, which can be taken into account by suitable junction conditions for the derivative of the scalar field. At the stellar radius we impose $\psi_- = \psi_+$ and $\partial_r \psi_+ = \partial_r \psi_- - \Delta V \psi_-/(1 - 2M/r)^2$, where $\Delta V = V_+ - V_-$ and we defined $A_{\pm} = \lim_{\epsilon \to 0} A(R \pm \epsilon)$.

The fundamental modes of the system are shown in Fig. 4.19 for a constantdensity star with ultrahigh compactness, $R \sim 2.26M$, whose effective potential is shown in Fig. 4.18. We present both first-order and second-order computations. As expected, these two cases are in agreement with each other for small angular velocities, but they are dramatically different when $\Omega \gtrsim 0.1\Omega_K$. Indeed, while the modes remain stable to first order in the spin, they become unstable to second

¹⁶Note that, because of the absence of Birkhoff theorem in the spinning case, the exterior geometry is not a slowly-spinning Kerr metric.

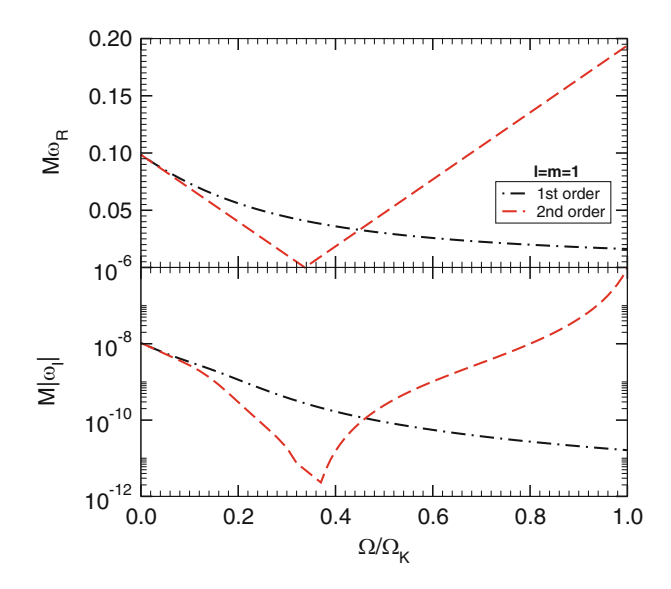


Fig. 4.19 Real and imaginary parts of the fundamental l=m=1 mode for a constant-density star with ultrahigh compactness, $R\sim 2.26M$, as a function of the angular velocity of the star normalized by the mass shedding limit. Note that the vertical axis of the *bottom plot* shows the absolute value of ω_I and is in a log scale. The first order result fails to capture the instability ($\omega_I>0$, rightmost part of the plots) because in this case the background geometry does not possess an ergoregion. To second order, the threshold of the instability corresponds to a zero crossing of both ω_R and ω_I , see text for details

order. Interestingly, the threshold of the instability corresponds (within numerical accuracy) to a zero crossing also of the *real* part of the mode. In Fig. 4.19, we focus only on $\omega_R > 0$ by exploiting the symmetry of the field equations under $m \to -m$ and $\omega \to -\omega$.

The fact that the second-order terms play such an important role in the stability analysis can be understood by the fact that the ergoregion of the spacetime appears only at the second order. Indeed, while our results are generically in qualitative agreement with previous analysis [159–163], it is important to note that in all cases the latter have been obtained by including *some* (but not all) second-order terms. Should all second-order terms be neglected, no unstable mode would be found. The results in Fig. 4.19 represent the first fully-consistent computation of the ergoregion instability for a spinning compact star. The phenomenology of this instability is discussed in detail in Sect. 5.8.1.

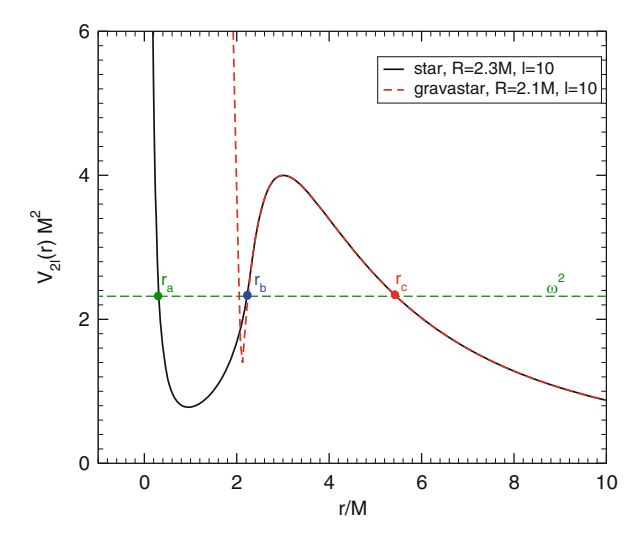


Fig. 4.20 Examples of the potential governing linear perturbations of a static ultracompact star. The *black solid line* and the *red dashed line* correspond to l=10 gravitational axial perturbations of a uniform star with R=2.3M and of a gravastar with R=2.1M, respectively

4.11.2 Ergoregion Instability and Long-Lived Modes

The underlying origin of the ergoregion instability is the existence of long-lived modes in ultracompact spacetimes in the static limit; these modes are very slowly damped and can become unstable when rotation is included. This has been first discussed in the eikonal limit [159] and it has been recently put on a firmer basis in [167].

Such long-lived modes exist in ultracompact spacetimes which possess a light ring (i.e. an unstable circular orbit as in the Schwarzschild case) but not a horizon [167, 168]. The reason for that is explained in Fig. 4.20 (cf. also Fig. 4.18 above), which shows the effective potential (F.1) (cf. Appendix F for details) corresponding to two models of static ultracompact objects: a constant-density star with compactness $M/R \sim 0.435$ (black solid curve) and of a thin-shell gravastar¹⁷ with compactness $M/R \sim 0.476$ (dashed red curve), respectively. Because the radius of these objects is smaller than the light-ring location of the external Schwarzschild spacetime, r = 3M, the effective potential develops a maximum at that location. Furthermore, the centrifugal potential near the center of these objects is responsible for the existence of a further *stable* null circular orbit in the object's

¹⁷Thin-shell gravastars [169] are discussed in Sect. 5.8.2 in the context of so-called "BH mimickers".

¹⁸Other regular geometries which possess a light-ring are the perfect-fluid stellar objects with multiple necks discussed in [170–172].

interior. This corresponds to the minimum shown in Fig. 4.20, where the long-lived modes are localized [167]. These modes (sometimes dubbed "s-modes" in the context of ultracompact stars [166]) are computed in the WKB approximation in Appendix F and they agree quite well with exact numerical results (cf. Fig. F.1 and [167]).

The dependence of the frequency and damping time of these long-lived modes to instability as functions of the spin in connection to the ergoregion has been first discussed in [159], which considers an approximate line element

$$ds^{2} = -F(r)dt^{2} + B(r)dr^{2} + r^{2}d\theta^{2} + r^{2}\sin^{2}\theta(d\phi - \varpi(r)dt)^{2}.$$
 (4.60)

Although not being a solution of Einstein's equations coupled to a fluid, this metric should approximate the exact geometry describing a spinning star in the case of slow rotation and high compactness, as we discussed. In such approximate metric, the ergoregion is defined by

$$\varpi(r)\sin\theta > \frac{\sqrt{F(r)}}{r}$$
. (4.61)

In the eikonal limit, the Klein-Gordon equation in the background (4.60) can be written in the form [159]

$$\psi'' + m^2 \frac{B}{F} (\bar{\omega} + V_+)(\bar{\omega} + V_-) \psi = 0, \qquad (4.62)$$

where $\bar{\omega} = \omega/m$ is a rescaled frequency, m is the azimuthal number associated to the axisymmetry of the background, and

$$V_{\pm} = -\varpi \pm \frac{\sqrt{F}}{r},\tag{4.63}$$

are the effective potentials that describe the motion of (counter-rotating for the plus sign and co-rotating for the minus sign) null geodesics in the equatorial plane of the geometry (4.60).

Now, the boundary of the ergoregion (if it exists) corresponds to two real roots of $V_+ = 0$ and $V_+ < 0$ inside the ergoregion. Because $V_+ \to +\infty$ at the center and attains a positive finite value in the exterior, it is clear that the ergoregion must contain a point in which V_+ displays a (negative) local minimum. This simple argument shows the important result that the presence of an ergoregion in a horizonless object implies the existence of *stable* counter-rotating photon orbits [167].

Furthermore, Eq. (4.62) supports unstable modes, whose computation is briefly presented in Appendix F in the WKB approximation. In the eikonal limit, the instability time scale depends exponentially on the azimuthal number,

$$\tau_{\rm ergo} \sim 4\alpha e^{2\beta m},$$
(4.64)

where α and β are two positive constants [159] (cf. Appendix F). The instability can be understood from the fact that the corresponding modes are localized near the stable photon orbit, which is situated within the ergosphere, and are confined within the star. This confinement provides the arena for the instability to grow through the negative-energy states that are allowed within the ergoregion [173]. Likewise, this argument also explains why spinning BHs—that also possess a light ring and an ergoregion—are linearly stable, because the presence of the horizon forbids the existence of trapped modes.

4.11.3 Ergoregion Instability in Fluids

In the context of acoustic geometries introduced in Sect. 2.4.2 and expanded in Sects. 2.5.2 and 3.9, sound waves propagate in moving fluids as a massless scalar field in curved spacetime, with an effective geometry dictated by the background fluid flow. There are simple acoustic setups with instabilities that can be framed in the language of curved spacetime as ergoregion instabilities [30].

Let us focus again on the two-dimensional fluid flow of Sect. 3.9, but consider a specific flow with vanishing radial speed (A = 0 in Eq. (3.133)), the so-called the *hydrodynamic vortex*, whose line element is

$$ds^{2} = -c^{2} \left(1 - \frac{C^{2}}{c^{2}r^{2}} \right) dt^{2} + dr^{2} - 2Cdtd\theta + r^{2}d\theta^{2} + dz^{2}.$$
 (4.65)

This effective spacetime presents an ergoregion with outer boundary at $r_{\text{ergo}} = C/c$, which coincides with the circle at which the (absolute value of the) background flow velocity equals the speed of sound c. Henceforth we set the speed of the sound equal to unity (c = 1).

The *background* velocity diverges at the origin as 1/r, signaling a physically singular behavior. Possible experimental setups can be mimicked by imposing boundary conditions at a finite position $r = r_{\min}$, the precise form of which depend on the specific experimental apparatus. Assume therefore that an infinitely long cylinder of radius r_{\min} is placed at the center of our coordinate system. The cylinder is made of a certain material with acoustic impedance Z [174]. Low-impedance materials correspond to Dirichlet-type boundary conditions on the master variable (see Sect. 2.5.2) and, for completeness, we also consider Neumann-type conditions [30]).

Together with Sommerfeld conditions at large distance, the problem is an eigenvalue problem for the possible frequencies, the solution of which is shown in Fig. 4.21 for a specific cylinder position at $r_{\rm min}=0.3$ as a function of rotation rate C. Notice that our generic arguments in favor of an ergoregion instability predict that the geometry is unstable as long as the cylinder position is within the ergosurface. In other words, as long as C>0.3. Figure 4.21 shows that indeed the large-m threshold of the instability asymptotes to C=0.3, as can be seen from Fig. 4.21, and as

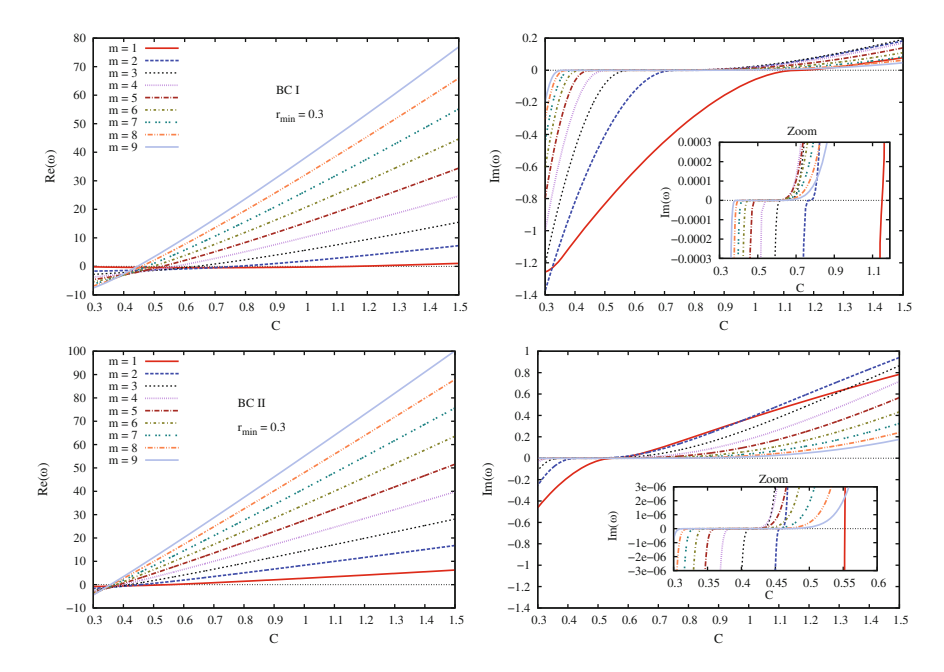


Fig. 4.21 Real (*left*) and imaginary (right) components of the fundamental QNM frequencies, plotted as a function of C, for $r_{min} = 0.3$ and different values of m. The $top\ plots$ correspond to Dirichlet-like boundary conditions, whereas the *bottom plots* correspond to Neumann-like boundary conditions. Note the striking similarity with Fig. 4.19. From [30]

anticipated from our discussion. The striking similarity between Figs. 4.21 and 4.19 is also remarkable. Indeed, in this analog geometry we recover all the qualitative features previously discussed for ultracompact stars. In particular, in both cases at the threshold for the instability the frequency of the mode has a zero crossing and the imaginary part of the mode has an inflection point. Further insights into the onset of the instability were derived in [175].

The results also indicate (cf. Fig. 4.21) that all modes m > 5 are unstable for $r_{\min} = 0.3$ and circulation C = 0.5. Moreover, at fixed inner boundary location r_{\min} and fixed m the instability gets stronger for larger C, as might also be anticipated. All the numerical results fully support the statement that the presence of an ergoregion without event horizon gives rise to instabilities. A complementary facet of the instability is shown in snapshots of the evolution, as those depicted in Fig. 4.22. These snapshots compare the evolution of a stable (C = 0.5) and unstable (C = 1.5) configuration, both for m = 2, and show clearly how the instability develops inside the ergoregion and close to the inner boundary at $r_{\min} = 0.3$. Notice the scale in the last snapshot, and how the field decays in space but grows in time.

As might be expected in a centuries-old field, similar instabilities were reported decades ago in fluid dynamics, within that specific field's language. Broadbent and Moore have conducted a thorough study of stability of rotating fluids, but imposing

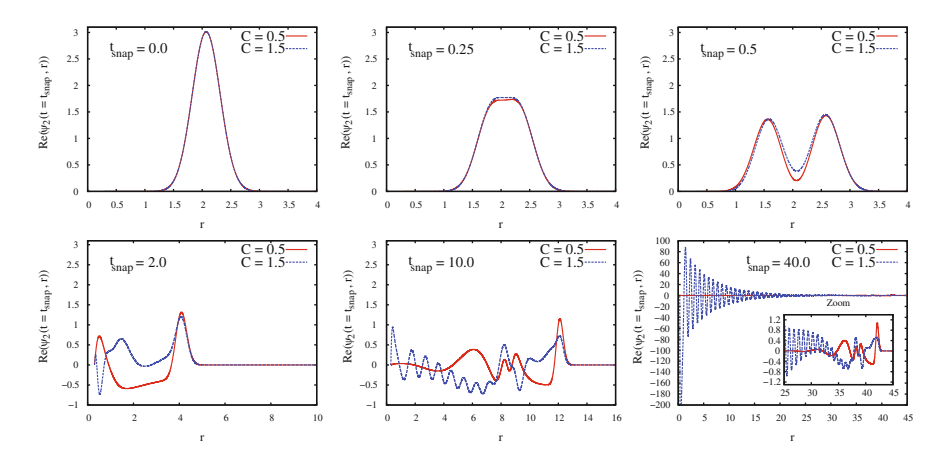


Fig. 4.22 Snapshots of the radial profiles of $\text{Re}(\psi_m(t,r))$ for azimuthal number m=2, circulations C=0.5 (stable case) and C=1.5 (unstable case). Dirichlet-like boundary conditions are imposed at $r_{\min}=0.3$. From [30]

slightly different boundary conditions [176]. In line with our findings, they uncover an instability for compressible fluids related also to sound wave amplification (note that incompressible fluids were also analyzed by Lord Kelvin and were found to be marginally stable [177]). The evidence that the hydrodynamic vortex is an unstable system and that the instabilities are directly related to the existence of an ergoregion together with the absence of an event horizon agrees with the prediction in [155]. This confirmation further strengthens the similarities between effective spacetimes in fluids and BHs.

4.11.4 Ergoregion Instability and Hawking Radiation

As we mentioned in Sect. 3.13, string theory has made great progress in understanding the microphysics of BHs. In particular, for certain (nearly) supersymmetric BHs, one is able to show that the Bekenstein-Hawking entropy $S_{\rm BH} = A/4$, as computed in the strongly-coupled supergravity description, can be reproduced in a weakly-coupled *D*-brane description as the degeneracy of the relevant microstates [178]. The AdS/CFT correspondence [179–181] allows further insights into these issues by providing a dictionary relating the geometric description of the physics in the near-horizon region with the physics of a dual conformal field theory. In particular, the AdS/CFT indicates that Hawking evaporation should be a unitary process, in keeping with the basic tenets of quantum theory. The discussion of BHs in the context of the AdS/CFT correspondence makes it evident that the path integral over geometries in the bulk may include multiple saddle-points, i.e., several classical supergravity solutions [182]. Another point that was realized early on is that the

geometric description of individual microstates would not have a horizon [183]. These ideas were incorporated by Mathur and colleagues in a radical revision of the stringy description of BHs, the "fuzzball" proposal [184, 185]. They argue that each of the CFT microstates corresponds to a separate spacetime geometry with no horizon. The BH is dual to an ensemble of such microstates and so the BH geometry only emerges in a coarse-grained description which "averages" over the BH microstate geometries.

In a fuzzball microstate the spacetime ends just outside the horizon (because compact directions "cap-off" [185]) thus avoiding issues like the information paradox in BH physics. However, it seemingly introduces an unexpected problem: if the horizon is not the traditional one, how is it possible to recover traditional BH thermodynamics like the Hawking radiation rate? Surprisingly, for the few microstates known explicitly—which rotate and possess an ergoregion—it was shown that the Hawking radiation rate can be *exactly* reproduced from the ergoregion instability [186, 187] (because these effective geometries have no horizon, spin will in general give rise to an ergoregion hence an instability [188]).

4.12 Black-Hole Lasers and Superluminal Corrections to Hawking Radiation

A completely different, semi-classical realization of the BH-bomb mechanism was put forward in [189]. In this model, one considers Hawking radiation from a geometry with an outer and an inner horizon and in the presence of high-energy modifications that change the dispersion relation $\omega(k)$ of photons at high frequencies. ¹⁹

For a geometry with a single (event) horizon, Hawking radiation is rather insensitive to high-energy modifications, producing the classical thermal spectrum [190] at frequencies much lower than the new scale. However, in the presence of two horizons and if the dispersion relation is superluminal, the negative-energy partners of Hawking quanta are able to bounce back and return to the outer horizon on a superluminal trajectory. Indeed, the origin of the laser effect can be attributed to the closed trajectories followed by the negative Killing frequency partners of Hawking quanta, which can bounce between the two horizons due to the modified dispersion relation. If the quanta are fermions, they suppress Hawking radiation, whereas if they are bosons they stimulate a secondary emission which is correlated to the original radiation, unlike in the usual Hawking effect. The process sustains itself as in the BH-bomb mechanism (and, in fact, as in the stimulated emission of a laser), the role of the mirror being played by the ergoregion between the two horizons

¹⁹The example considered in [189] was inspired by analogue BH models and, as should be clear from Sect. 2.4.2, the geometry only plays the role of a spectator. The laser effect occurs in analogue models as well as in true, gravitational BHs (for example, in the RN geometry).

which allows for superluminal bouncing trajectories with negative energies (see [189] for details). A thorough mode analysis of the BH laser effect shows that it is described in terms of frequency eigenmodes that are spatially bound. The spectrum contains a discrete and finite set of complex frequency modes which appear in pairs and which encode the laser effect [191, 192]. Related, zero-frequency "undulation" modes were dealt with in [193, 194].

The BH laser is a dynamical instability, the origin of which can be traced back to the negative energy states behind the outer horizon, and which work in fact as an ergoregion for the modes "living" there. One can then naturally associate the BH laser instability with a superradiant instability [191, 192].

4.13 Black Holes in Lorentz-Violating Theories: Nonlinear Instabilities

A related instability is thought to occur for BHs in Lorentz-violating theories [195, 196]. In these theories, BH solutions can exist (see e.g. [197–199] or a recent overview [90]) with multiple, nested horizons, one for each maximal speed of propagation in the theory. Each horizon traps the corresponding species of field excitations. Consider two particles, with different propagation speeds, and therefore two horizons. In this framework, the region between the two horizons is classically accessible to the faster particle and it is a classically inaccessible ergoregion for the slower one. If these particles are now allowed to interact gravitationally, it is *possible* that an energy transfer occurs from the slower to the faster particle, resulting in a nonlinear ergoregion instability. Hints of nonlinear instabilities were discussed in [196], but it is not clear whether they are related to this particular mechanism.

4.14 Open Issues

Superradiant (or "BH bomb") instabilities are a fascinating and rapidly growing topic. Here we list some of the most urgent open questions related to this problem.

• Despite the recent progress in understanding superradiant instabilities of spinning BHs triggered by massive bosons, the results for vector and tensor perturbations are not complete. Massive spin-1 instabilities were investigated in detail only to second order in the BH spin [97, 117]. To date the only work dealing with the Proca instability of highly-spinning Kerr BH is [16]. For massive spin-2 fields, only first-order computations in the spin are available [119] and no estimates for highly-spinning BHs have been derived yet.

4.14 Open Issues 145

• It was recently shown that RN-dS BHs are unstable under spherically-symmetric charged scalar perturbations [200, 201]. Given the fact that asymptotically flat RN BHs are stable against these perturbations, this is a quite surprising and still not very well understood result. In [201] it was shown that a necessary condition for the instability to occur is that the field's frequency ω_R satisfies:

$$\frac{qQ}{r_c} < \omega_R < \frac{qQ}{r_+} \,. \tag{4.66}$$

This is exactly the superradiant condition for this spacetime (cf. Eq. (3.136)), which suggests that the instability is of superradiant nature. However, it was also found that not all the superradiant modes are unstable and only the monopole l=0 suffers from this instability. The instability only occurs at small values of the coupling $qQ\lesssim 1$, as long as $qQ\gg \mu M$, where μ is the mass of the scalar field, and disappears when $\Lambda\to 0$. The end-state of the instability is still an open-problem, but the fact that the system is not confined, unlike in the RN-AdS case (see Sect. 4.5.2), makes it likely that the instability will extract charge and mass from the BH, evolving to a stable region in the parameter space.

- Recently, Shibata and Yoshino found that rapidly singly-spinning higher-dimensional BHs with spherical topology are unstable against non-axisymmetric perturbations (the so-called "bar"—mode instability) [205, 206] in D = 5, 6, 7, 8 dimensions (see also [207]). This was extended to equal angular momenta Myers-Perry BHs in odd dimensions in [208] and analytically studied in the large-D limit in [209]; these unstable BHs will emit gravitational radiation and consequently spin down and decrease their mass [206]. The area theorem (cf. Sect. 3.2) then requires that the unstable modes should satisfy the superradiant condition (1.1), which indicates that the instability is of superradiant nature. However not all the superradiant modes are unstable and unlike the superradiant instability discussed in this section, this instability is not due to confinement. A complete comprehension of the physical mechanism behind this instability is still an open problem.
- An interesting open question is the effect of rotation in the *outer* disk of
 the two-ring model discussed in Sect. 4.8, for example to investigate possible
 resonant effects when both rings are spinning. Likewise, the BH analog of the
 two-ring model proposed by Press [135], namely a Kerr BH surrounded by a
 conductive disk—in particular whether such system is unstable or not, and on
 which timescales—has not been studied yet.

²⁰Higher dimensional RN-dS were shown to be unstable in $D \ge 7$ dimensions against gravito-electromagnetic perturbations [202–204]. However this instability is of different nature.

- One of the important missing studies concerns a detailed investigation of the ergoregion instability of ultracompact spinning NSs or other compact objects. Rapidly or (consistently built, see Sect. 4.11.1) slowly-spinning stars are all basically uncharted territory. Gravitational perturbations of slowly-spinning NSs can, in principle, be computed by extending recently-developed perturbative methods to second order in the spin (including the star structure [210] and its perturbations [13, 164, 165]).
- Massive fermions near a Kerr BH form bound states that, rather than inducing an instability as in the bosonic case, condense and form a Fermi sea which extends outside the ergosphere [211]. This analysis has been performed in the WKB limit and hints at possible important nonlinear effects in the behavior of fermion fields. Whether or not such systems can trigger superradiant instabilities at the nonlinear level is unclear. In a different but related vein, Matsas and da Silva [212] opened the possibility of overspinning a RN BH by quantum tunneling; such possibility was later argued to be ruled out, and that cosmic censorship conjecture is actually respected in this situation [213]. The physical mechanism is a quantum version of superradiance, which protects the integrity of the BH horizon by spontaneously emitting low-energy ($\omega < m\Omega$) fermions. The final destiny of charged BHs is still unclear, as quantum effects may still play an important role [214] (and references therein).
- As we discussed in Sect. 4.7, BHs in strong magnetic fields are unstable. Because
 these are confining geometries, the lesson from AdS spacetimes (see Sect. 4.5.1)
 implies that non-axially symmetric BH solutions should exist. These would be
 interesting to construct, even if only numerically.
- One of the most exciting open issues is the detection of rotational superradiance.
 As we proposed in the context of the acoustic BH bomb discussed in Sect. 2.5.2, there are compelling setups for experimental realizations, both in the acoustic regime and in the electromagnetic regime.
- An intriguing mechanism to trigger instabilities in astrophysical systems concerns the ergoregion instability in *fluids*, such as accretion disks around gravitational BHs. In an analogue description, sound waves in these systems are described by an effectively-curved background geometry [215–217]. When the accretion disk velocity surpasses the local *sound* speed, an acoustic ergoregion appears, presumably giving rise to ergoregion instabilities. As far as we are aware, these phenomena have not been explored.
- We mentioned in Sect. 4.13 that nonlinear ergoregion instabilities are thought to occur for BHs with multiple horizons in Lorentz-violating theories. Explicit examples do not exist yet.
- Superradiance of self-interacting fields, or fields with nontrivial dispersion relations have hardly been explored, with a noteworthy (but one-spatial dimensional) toy-model [218].

References

 S. Teukolsky, W. Press, Perturbations of a rotating black hole, III—interaction of the hole with gravitational and electromagnet ic radiation. Astrophys. J. 193, 443–461 (1974)

- 2. R. Brito, V. Cardoso, P. Pani, Superradiant instability of black holes immersed in a magnetic field. Phys. Rev. **D89**, 104045 (2014). arXiv:1405.2098 [gr-qc]
- 3. V. Cardoso, M. Cavaglia, L. Gualtieri, Hawking emission of gravitons in higher dimensions: Non-rotating black holes. J. High Energy Phys. **0602**, 021 (2006). arXiv:hep-th/0512116 [hep-th]
- 4. A.A. Starobinskij, Amplification of waves reflected from a rotating "black hole". Zhurnal Eksperimentalnoi i Teoreticheskoi Fiziki **64**, 48–57 (1973)
- A.A. Starobinskij, Amplification of waves reflected from a rotating "black hole". Sov. Phys.-JETP 37, 28–32 (1973)
- A.A. Starobinskij, S.M. Churilov, Amplification of electromagnetic and gravitational waves scattered by a rotating black hole. Zhurnal Eksperimentalnoi i Teoreticheskoi Fiziki 65, 3–11 (1973)
- 7. A.A. Starobinskij, S.M. Churilov, Amplification of electromagnetic and gravitational waves scattered by a rotating black hole. Sov. Phys.-JETP 38, 1–5 (1973)
- 8. V. Cardoso, O.J. Dias, J.P. Lemos, S. Yoshida, The Black hole bomb and superradiant instabilities. Phys. Rev. **D70**, 044039 (2004). arXiv:hep-th/0404096 [hep-th]
- 9. V. Cardoso, O.J. Dias, Small Kerr-anti-de Sitter black holes are unstable. Phys. Rev. **D70**, 084011 (2004). arXiv:hep-th/0405006 [hep-th]
- V. Cardoso, S.J. Dias, G.S. Hartnett, L. Lehner, J.E. Santos, Holographic thermalization, quasinormal modes and superradiance in Kerr-AdS. J. High Energy Phys. 1404, 183 (2014). arXiv:1312.5323 [hep-th]
- 11. V. Cardoso, S. Yoshida, Superradiant instabilities of rotating black branes and strings. J. High Energy Phys. **0507**, 009 (2005). arXiv:hep-th/0502206 [hep-th]
- 12. E.G. Kalnins, W. Miller, G.C. Williams, Killing-yano tensors and variable separation in kerr geometry. J. Math. Phys. **30**(10), 2360-2365 (1989)
- 13. P. Pani, Advanced Methods in Black-Hole Perturbation Theory. Int. J. Mod. Phys. A28, 1340018 (2013). arXiv:1305.6759 [gr-gc]
- 14. E. Berti, V. Cardoso, A.O. Starinets, Quasinormal modes of black holes and black branes. Classical and Quantum Gravity **26**, 163001 (2009). arXiv:0905.2975 [gr-qc]
- 15. S.R. Dolan, Superradiant instabilities of rotating black holes in the time domain. Phys. Rev. **D87**, 124026 (2013). arXiv:1212.1477 [gr-qc]
- 16. H. Witek, V. Cardoso, A. Ishibashi, U. Sperhake, Superradiant instabilities in astrophysical systems. Phys. Rev. **D87**, 043513 (2013). arXiv:1212.0551 [qr-qc]
- 17. Y.B. Zel'dovich, Zh. Eksp. Teor. Fiz **62**, 2076 (1972) [Sov.Phys. JETP **35**, 1085 (1972)]
- W.H. Press, S.A. Teukolsky, Floating orbits, superradiant scattering and the black-hole bomb. Nature 238, 211–212 (1972)
- 19. J.D. Jackson, Classical Electrodynamics, 3rd edn. Wiley, New York (1999)
- 20. A.R. King, Black-hole magnetostatics. Math. Proc. Camb. Philos. Soc. 81, 149 (1977)
- S. Hod, Onset of superradiant instabilities in the composed Kerr-black-holemirror bomb. Phys. Lett. B736, 398–402 (2014)
- 22. S. Hod, O. Hod, Analytic treatment of the black-hole bomb. Phys. Rev. **D81**, 061502 (2010). arXiv:0910.0734 [gr-qc]
- 23. J. Rosa, The extremal black hole bomb. J. High Energy Phys. 1006, 015 (2010). arXiv:0912.1780 [hep-th]
- 24. S. Hod, O. Hod, Comment on 'The Extremal black hole bomb'. arXiv:0912.2761 [gr-qc]
- H. Witek, V. Cardoso, C. Herdeiro, A. Nerozzi, U. Sperhake, et al., Black holes in a box: towards the numerical evolution of black holes in AdS. Phys. Rev. D82, 104037 (2010). arXiv:1004.4633 [hep-th]

- J.-P. Lee, Superradiance by mini black holes with mirror. J. High Energy Phys. 1201, 091 (2012). arXiv:1107.5641 [hep-ph]
- 27. A.N. Aliev, Superradiance and black hole bomb in five-dimensional minimal ungauged supergravity. J. Cosmol. Astropart. Phys. 11, 029 (2014). arXiv:1408.4269 [hep-th]
- E. Berti, V. Cardoso, J.P. Lemos, Quasinormal modes and classical wave propagation in analogue black holes. Phys. Rev. D70, 124006 (2004). arXiv:gr-qc/0408099 [gr-qc]
- C.L. Benone, L.C.B. Crispino, C. Herdeiro, E. Radu, Acoustic clouds: standing sound waves around a black hole analogue. Phys. Rev. D91(10), 104038 (2015). doi:10.1103/PhysRevD.91.104038. arXiv:1412.7278 [gr-qc]
- 30. L.A. Oliveira, V. Cardoso, L.C.B. Crispino, Ergoregion instability: the hydrodynamic vortex. Phys. Rev. **D89**, 124008 (2014). arXiv:1405.4038 [qr-qc]
- S.A. Teukolsky, Perturbations of a rotating black hole. Ph.D. thesis, California Institute of Technology, 1973.
- 32. M.H.P.M. Van Putten, Science **284**, 115 (1999)
- 33. A.N. Aguirre, On the superradiance of spin 1 waves in an equatorial wedge around a Kerr hole. Astrophys. J. **529**, L9 (2000). arXiv:astro-ph/9910403 [astro-ph]
- 34. J.D. Bekenstein, M. Schiffer, The many faces of superradiance. Phys. Rev. **D58**, 064014 (1998). arXiv:gr-qc/9803033 [gr-qc]
- 35. C.A.R. Herdeiro, J.C. Degollado, H.F. Rnarsson, Rapid growth of superradiant instabilities for charged black holes in a cavity. Phys. Rev. **D88**, 063003 (2013). arXiv:1305.5513 [gr-qc]
- 36. J.C. Degollado, C.A.R. Herdeiro, Time evolution of superradiant instabilities for charged black holes in a cavity. Phys. Rev. **D89**, 063005 (2014). arXiv:1312.4579 [gr-qc]
- 37. S. Hod, Analytic treatment of the charged black-hole-mirror bomb in the highly explosive regime. Phys. Rev. **D88**(6), 064055 (2013). arXiv:1310.6101 [gr-qc]
- 38. R. Li, J.-K. Zhao, Y.-M. Zhang, Superradiant instability of D-dimensional Reissner-Nordström black hole mirror system. Commun. Theor. Phys. **63**(5), 569–574 (2015). doi:10.1088/0253-6102/63/5/569. arXiv: 1404.6309 [gr-qc]
- R. Li, J. Zhao, Numerical study of superradiant instability for charged stringy black hole-mirror system. Phys. Lett. B740, 317–321 (2015). doi:10.1016/j.physletb.2014.12.007. arXiv:1412.1527 [gr-qc]
- 40. S. Hawking, H. Reall, Charged and rotating AdS black holes and their CFT duals. Phys. Rev. **D61**, 024014 (2000). arXiv:hep-th/9908109 [hep-th]
- 41. V. Cardoso, O.J. Dias, S. Yoshida, Classical instability of Kerr-AdS black holes and the issue of final state. Phys. Rev. **D74**, 044008 (2006). arXiv:hep-th/0607162 [hep-th]
- 42. N. Uchikata, S. Yoshida, T. Futamase, Scalar perturbations of Kerr-AdS black holes. Phys. Rev. **D80**, 084020 (2009).
- C. Burgess, C. Lutken, Propagators and effective potentials in anti-de sitter space. Phys. Lett. B153, 137 (1985).
- 44. O.J. Dias, J.E. Santos, Boundary Conditions for Kerr-AdS Perturbations. J. High Energy Phys. 1310, 156 (2013). arXiv:1302.1580 [hep-th]
- 45. V. Cardoso, J.P. Lemos, Quasinormal modes of Schwarzschild anti-de Sitter black holes: Electromagnetic and gravitational perturbations. Phys. Rev. **D64**, 084017 (2001). arXiv:gr-qc/0105103 [gr-qc]
- 46. V. Cardoso, G. Khanna, Black holes in anti-de Sitter spacetime: quasinormal modes, tails, and flat spacetime. Phys. Rev. **D91**(2), 024031 (2015). doi:10.1103/PhysRevD.91.024031. arXiv:1501.00977 [gr-gc]
- 47. Y. Shlapentokh-Rothman, Exponentially growing finite energy solutions for the Klein-Gordon equation on sub-extremal Kerr spacetimes. Commun. Math. Phys. **329**, 859–891 (2014). arXiv:1302.3448 [gr-qc]
- 48. P. Figueras, S. Tunyasuvunakool, Black rings in global anti-de Sitter space. J. High Energy Phys. 1503, 149 (2015). doi:10.1007/JHEP03(2015)149. arXiv:1412.5680 [hep-th]

 D. Birmingham, I. Sachs, S.N. Solodukhin, Conformal field theory interpretation of black hole quasinormal modes. Phys. Rev. Lett. 88, 151301 (2002). arXiv:hep-th/0112055 [hep-th]

- 50. H.R.C. Ferreira, Stability of warped AdS3 black holes in Topologically Massive Gravity under scalar perturbations. Phys. Rev. D87(12), 124013 (2013). arXiv:1304.6131 [gr-qc]
- O.J. Dias, G.T. Horowitz, J.E. Santos, Black holes with only one Killing field. J. High Energy Phys. 1107, 115 (2011). arXiv:1105.4167 [hep-th]
- 52. V. Cardoso, O.J. Dias, J.V. Rocha, Phase diagram for non-axisymmetric plasma balls. J. High Energy Phys. 1001, 021 (2010). arXiv:0910.0020 [hep-th]
- 53. N. Iizuka, A. Ishibashi, K. Maeda, A rotating hairy AdS₃ black hole with the metric having only one Killing vector field (2015). arXiv:1505.00394 [hep-th]
- 54. O.J.C. Dias, J.E. Santos, B. Way, Black holes with a single Killing vector field: black resonators (2015). arXiv:1505.04793 [hep-th]
- 55. S.A. Hartnoll, C.P. Herzog, G.T. Horowitz, Building a Holographic Superconductor. Phys. Rev. Lett. 101, 031601 (2008). arXiv:0803.3295 [hep-th]
- 56. S.A. Hartnoll, Lectures on holographic methods for condensed matter physics. Classical and Quantum Gravity 26, 224002 (2009). arXiv:0903.3246 [hep-th]
- 57. S.A. Hartnoll, Horizons, holography and condensed matter, in *Black Holes in Higher Dimensions*, ed. by G. Horowitz (Cambridge University Press, Cambridge, 2010). arXiv:1106.4324 [hep-th]
- 58. O.J. Dias, P. Figueras, S. Minwalla, P. Mitra, R. Monteiro, et al., Hairy black holes and solitons in global AdS_5 . J. High Energy Phys. 1208, 117 (2012). arXiv:1112.4447 [hep-th]
- P. Basu, J. Bhattacharya, S. Bhattacharyya, R. Loganayagam, S. Minwalla, et al., Small Hairy Black Holes in Global AdS Spacetime. J. High Energy Phys. 1010, 045 (2010). arXiv:1003.3232 [hep-th]
- 60. S.S. Gubser, Breaking an Abelian gauge symmetry near a black hole horizon. Phys. Rev. D78, 065034 (2008). arXiv:0801.2977 [hep-th]
- 61. M. Cadoni, G. D'Appollonio, P. Pani, Phase transitions between Reissner-Nordstrom and dilatonic black holes in 4D AdS spacetime. J. High Energy Phys. 1003, 100 (2010). arXiv:0912.3520 [hep-th]
- 62. S.S. Gubser, Phase transitions near black hole horizons. Classical and Quantum Gravity 22, 5121–5144 (2005). arXiv:hep-th/0505189 [hep-th]
- O.J. Dias, R. Monteiro, H.S. Reall, J.E. Santos, A Scalar field condensation instability of rotating anti-de Sitter black holes. J. High Energy Phys. 1011, 036 (2010). arXiv:1007.3745 [hep-th]
- 64. S.A. Hartnoll, C.P. Herzog, G.T. Horowitz, Holographic superconductors. J. High Energy Phys. 0812, 015 (2008). arXiv:0810.1563 [hep-th]
- G.T. Horowitz, Introduction to Holographic Superconductors. Lect. Notes Phys. 828, 313–347 (2011). arXiv:1002.1722 [hep-th]
- 66. K. Murata, S. Kinoshita, N. Tanahashi, Non-equilibrium Condensation Process in a Holographic Superconductor. J. High Energy Phys. 1007, 050 (2010). arXiv:1005.0633 [hep-th]
- 67. S.A. Hartnoll, A. Tavanfar, Electron stars for holographic metallic criticality. Phys. Rev. **D83**, 046003 (2011). arXiv:1008.2828 [hep-th]
- 68. T. Damour, N. Deruelle, R. Ruffini, On quantum resonances in stationary geometries. Lett. Nuovo Cimento 15, 257–262 (1976)
- 69. S. Hawking, Gravitationally collapsed objects of very low mass. Mon. Not. R. Astron. Soc. **152**, 75 (1971)
- 70. Y.B. Zel'Dovich, I.D. Novikov, The hypothesis of cores retarded during expansion and the hot cosmological model. Astron. Zh. 43, 758 (1966)
- B.J. Carr, S.W. Hawking. Black holes in the early universe. Mon. Not. R. Astron. Soc. 168, 399–416 (1974)
- 72. B. Carr, K. Kohri, Y. Sendouda, J. Yokoyama, New cosmological constraints on primordial black holes. Phys. Rev. **D81**, 104019 (2010). arXiv:0912.5297 [astro-ph.CO]

- R.D. Peccei, H.R. Quinn, CP. Phys. Rev. Lett. 38, 1440–1443 (1977). http://link.aps.org/doi/ 10.1103/PhysRevLett.38.1440
- 74. S. Weinberg. A new light boson? Phys. Rev. Lett. **40**, 223–226 (1978)
- 75. F. Wilczek, Problem of strong p and t invariance in the presence of instantons. Phys. Rev. Lett. 40, 279–282 (1978)
- 76. M. Fairbairn, R. Hogan, D.J.E. Marsh, Unifying inflation and dark matter with the Peccei-Quinn field: observable axions and observable tensors. Phys. Rev. **D91**(2), 023509 (2015). doi:10.1103/PhysRevD.91.023509. arXiv:1410.1752 [hep-ph]
- 77. D.J.E. Marsh, D. Grin, R. Hlozek, P.G. Ferreira, Tensor detection severely constrains axion dark matter. Phys. Rev. Lett. 113, 011801 (2014). arXiv:1403.4216 [astro-ph.CO]
- 78. F. Wilczek, Axions and family symmetry breaking. Phys. Rev. Lett. 49, 1549–1552 (1982).
- Y. Chikashige, R. Mohapatra, R. Peccei, Are there real goldstone bosons associated with broken lepton number? Phys. Lett. B 98(4), 265–268 (1981). http://www.sciencedirect.com/ science/article/pii/0370269381900113
- 80. R. Hlozek, D. Grin, D.J.E. Marsh, P.G. Ferreira, A search for ultralight axions using precision cosmological data. Phys. Rev. **D91**(10), 103512 (2015). doi:10.1103/PhysRevD.91.103512. arXiv:1410.2896 [astro-ph.CO]
- 81. A. Arvanitaki, S. Dimopoulos, S. Dubovsky, N. Kaloper, J. March-Russell, String axiverse. Phys. Rev. D81, 123530 (2010). arXiv:0905.4720 [hep-th]
- 82. L. Ackerman, M.R. Buckley, S.M. Carroll, M. Kamionkowski, Dark matter and dark radiation. Phys. Rev. **D79**, 023519 (2009). arXiv:0810.5126 [hep-ph]
- M. Goodsell, J. Jaeckel, J. Redondo, A. Ringwald, Naturally light hidden photons in LARGE volume string compactifications. J. High Energy Phys. 0911, 027 (2009). arXiv:0909.0515 [hep-ph]
- 84. J. Jaeckel, A. Ringwald, The low-energy Frontier of particle physics. Ann. Rev. Nucl. Part. Sci. 60, 405–437 (2010). arXiv:1002.0329 [hep-ph]
- 85. P.G. Camara, L.E. Ibanez, F. Marchesano, RR photons. J. High Energy Phys. **1109**, 110 (2011). arXiv:1106.0060 [hep-th]
- 86. A.S. Goldhaber, M.M. Nieto, Photon and graviton mass limits. Rev. Mod. Phys. **82**, 939–979 (2010). arXiv:0809.1003 [hep-ph]
- 87. J. Hewett, H. Weerts, R. Brock, J. Butler, B. Casey, et al., in *The Proceedings of the 2011 Workshop on Fundamental Physics at the Intensity Frontier* (2011). arXiv:1205.2671 [hep-ex]
- 88. K. Hinterbichler, Theoretical aspects of massive gravity. Rev. Mod. Phys. **84**, 671–710 (2012). arXiv:1105.3735 [hep-th]
- 89. C. de Rham, Massive gravity. Living Rev. Rel. 17, 7 (2014). arXiv:1401.4173 [hep-th]
- 90. E. Berti, E. Barausse, V. Cardoso, L. Gualtieri, P. Pani, et al., Testing general relativity with present and future astrophysical observations. arXiv:1501.07274 [gr-qc]
- 91. T.P. Sotiriou, V. Faraoni, Black holes in scalar-tensor gravity. Phys. Rev. Lett. 108, 081103 (2012). arXiv:1109.6324 [gr-qc]
- J. Hersh, R. Ove, Instability of the Kerr solution of fourth order gravity. Phys. Lett. B156, 305 (1985)
- 93. S.A. Teukolsky, Rotating black holes—separable wave equations for gravitational and electromagnetic perturbations. Phys. Rev. Lett. 29, 1114–1118 (1972)
- S.A. Teukolsky, Perturbations of a rotating black hole.
 Fundamental equations for gravitational electromagnetic and neutrino field perturbations. Astrophys. J. 185, 635–647 (1973)
- 95. E. Berti, V. Cardoso, M. Casals, Eigenvalues and eigenfunctions of spin-weighted spheroidal harmonics in four and higher dimensions. Phys. Rev. **D73**, 024013 (2006). arXiv:gr-qc/0511111 [gr-qc]
- S.L. Detweiler, Klein-Gordon equation and rotating black holes. Phys. Rev. D22, 2323–2326 (1980)

97. P. Pani, V. Cardoso, L. Gualtieri, E. Berti, A. Ishibashi, Perturbations of slowly rotating black holes: massive vector fields in the Kerr metric. Phys. Rev. **D86**, 104017 (2012). arXiv:1209.0773 [gr-qc]

- 98. H. Yoshino, H. Kodama, Gravitational radiation from an axion cloud around a black hole: superradiant phase. Prog. Theor. Exp. Phys. **2014**, 043E02 (2014). arXiv:1312.2326 [gr-qc]
- 99. R. Brito, V. Cardoso, P. Pani, Black holes as particle detectors: evolution of superradiant instabilities. arXiv:1411.0686 [gr-gc]
- T. Zouros, D. Eardley, Instabilities of massive scalar perturbations of a rotating black hole. Ann. Phys. 118, 139–155 (1979)
- 101. S. Hod, On the instability regime of the rotating Kerr spacetime to massive scalar perturbations. Phys. Lett. **B708**, 320–323 (2012). arXiv:1205.1872 [gr-gc]
- 102. S.R. Dolan, Instability of the massive Klein-Gordon field on the Kerr spacetime. Phys. Rev. **D76**, 084001 (2007). arXiv:0705.2880 [gr-qc]
- 103. J.G. Rosa, S.R. Dolan, Massive vector fields on the Schwarzschild spacetime: quasinormal modes and bound states. Phys. Rev. **D85**, 044043 (2012). arXiv:1110.4494 [hep-th]
- 104. M.J. Strafuss, G. Khanna, Massive scalar field instability in Kerr spacetime. Phys. Rev. **D71**, 024034 (2005). arXiv:gr-qc/0412023 [gr-qc]
- 105. S. Hawking, G. Ellis, *The Large Scale Structure of Space-Time*. Cambridge University Press, Cambridge (1973)
- 106. M. Heusler, The Uniqueness theorem for rotating black hole solutions of selfgravitating harmonic mappings. Classical and Quantum Gravity 12, 2021–2036 (1995). arXiv:gr-qc/9503053 [gr-qc]
- 107. A.A.H. Graham, R. Jha, Stationary black holes with time-dependent scalar fields. Phys. Rev. **D90**, 041501 (2014). arXiv:1407.6573 [gr-qc]
- 108. C.A.R. Herdeiro, E. Radu, Kerr black holes with scalar hair. Phys. Rev. Lett. 112, 221101 (2014). arXiv:1403.2757 [gr-qc]
- 109. H. Furuhashi, Y. Nambu, Instability of massive scalar fields in Kerr-Newman space-time. Prog. Theor. Phys. 112, 983–995 (2004). arXiv:gr-qc/0402037 [gr-qc]
- 110. S. Hod, Stability of the extremal Reissner-Nordstroem black hole to charged scalar perturbations. Phys. Lett. **B713**, 505–508 (2012). arXiv:1304.6474 [gr-gc]
- S. Hod, No-bomb theorem for charged Reissner-Nordstroem black holes. Phys. Lett. B718, 1489–1492 (2013)
- 112. C.-Y. Zhang, S.-J. Zhang, B. Wang, Charged scalar perturbations around Garfinkle-Horowitz-Strominger black holes. arXiv:1501.03260 [hep-th]
- 113. V. Cardoso, S. Chakrabarti, P. Pani, E. Berti, L. Gualtieri, Floating and sinking: the imprint of massive scalars around rotating black holes. Phys. Rev. Lett. **107**, 241101 (2011). arXiv:1109.6021 [gr-gc]
- 114. D. Gal'tsov, G. Pomerantseva, G. Chizhov, Behavior of massive vector particles in a Schwarzschild field. Sov. Phys. J. 27, 697–700 (1984)
- 115. C. Herdeiro, M.O. Sampaio, M. Wang, Hawking radiation for a Proca field in D-dimensions. Phys. Rev. **D85**, 024005 (2012). arXiv:1110.2485 [gr-qc]
- 116. R. Konoplya, Massive vector field perturbations in the Schwarzschild background: stability and unusual quasinormal spectrum. Phys. Rev. **D73**, 024009 (2006). arXiv:qr-qc/0509026 [qr-qc]
- 117. P. Pani, V. Cardoso, L. Gualtieri, E. Berti, A. Ishibashi, Black hole bombs and photon mass bounds. Phys. Rev. Lett. 109, 131102 (2012). arXiv:1209.0465 [gr-qc]
- 118. M. Fierz, W. Pauli, On relativistic wave equations for particles of arbitrary spin in an electromagnetic field. Proc. R. Soc. Lond. **A173**, 211–232 (1939)
- 119. R. Brito, V. Cardoso, P. Pani, Massive spin-2 fields on black hole spacetimes: instability of the Schwarzschild and Kerr solutions and bounds on the graviton mass. Phys. Rev. **D88**, 023514 (2013). arXiv:1304.6725 [gr-qc]

- 120. R. Brito, V. Cardoso, P. Pani, Partially massless gravitons do not destroy general relativity black holes. Phys. Rev. **D87**, 124024 (2013). arXiv:1306.0908 [gr-gc]
- 121. E. Babichev, A. Fabbri, Instability of black holes in massive gravity. Classical and Quantum Gravity 30, 152001 (2013). arXiv:1304.5992 [gr-qc]
- 122. R. Gregory, R. Laflamme, Black strings and p-branes are unstable. Phys. Rev. Lett. 70, 2837–2840 (1993). arXiv:hep-th/9301052 [hep-th]
- 123. H. Kudoh, Origin of black string instability. Phys. Rev. **D73**, 104034 (2006). arXiv:hep-th/0602001 [hep-th]
- 124. V. Cardoso, O.J. Dias, Rayleigh-Plateau and Gregory-Laflamme instabilities of black strings. Phys. Rev. Lett. 96, 181601 (2006). arXiv:hep-th/0602017 [hep-th]
- 125. J. Camps, R. Emparan, N. Haddad, Black brane viscosity and the Gregory-Laflamme instability. J. High Energy Phys. 1005, 042 (2010). arXiv:1003.3636 [hep-th]
- 126. E. Babichev, A. Fabbri, Stability analysis of black holes in massive gravity: a unified treatment. Phys. Rev. **D89**, 081502 (2014). arXiv:1401.6871 [gr-qc]
- 127. R.M. Wald, Black hole in a uniform magnetic field. Phys. Rev. D10, 1680–1685 (1974)
- 128. F.J. Ernst, Black holes in a magnetic universe. J. Math. Phys. 17(1), 54–56 (1976). http://scitation.aip.org/content/aip/journal/jmp/17/1/10.1063/1.522781.
- 129. M. Melvin, Pure magnetic and electric geons. Phys. Lett. 8, 65–70 (1964)
- M. Melvin, Dynamics of cylindrical electromagnetic universes. Phys. Rev. 139, B225–B243 (1965)
- 131. K.S. Thorne, Absolute stability of Melvin's magnetic universe. Phys. Rev. 139, B244–B254 (1965)
- D. Galtsov, V. Petukhov, Black hole in an external magnetic field. Zh. Eksp. Teor. Fiz. 74, 801–818 (1978)
- 133. R. Konoplya, R. Fontana, Quasinormal modes of black holes immersed in a strong magnetic field. Phys. Lett. **B659**, 375–379 (2008). arXiv:0707.1156 [hep-th]
- 134. R. Konoplya, Magnetic field creates strong superradiant instability. Phys. Lett. **B666**, 283–287 (2008). arXiv:0801.0846 [hep-th]
- 135. W.H. Press, Table-top model for black hole electromagnetic instabilities, in *Frontiers Science Series 23: Black Holes and High Energy Astrophysics*, ed. by H. Sato, N. Sugiyama, p. 235 (1998)
- 136. K.S. Thorne, R. Price, D. Macdonald, *Black Holes: The Membrane Paradigm*. Yale University Press, New Haven (1986)
- 137. A.G. Sitenko, Electromagnetic Fluctuations in Plasma. Academic, New York (1976)
- 138. R. Kulsrud, A. Loeb, Dynamics and gravitational interaction of waves in nonuniform media. Phys. Rev. **D45**, 525–531 (1992)
- 139. P. Pani, A. Loeb, Constraining primordial black-hole bombs through spectral distortions of the cosmic microwave background. Phys. Rev. **D88**, 041301 (2013). arXiv:1307.5176 [astro-ph.CO]
- 140. V. Cardoso, I.P. Carucci, P. Pani, T.P. Sotiriou, Black holes with surrounding matter in scalar-tensor theories. Phys. Rev. Lett. 111, 111101 (2013). arXiv:1308.6587 [gr-qc]
- 141. V. Cardoso, I.P. Carucci, P. Pani, T.P. Sotiriou, Matter around Kerr black holes in scalar-tensor theories: scalarization and superradiant instability. Phys. Rev. **D88**, 044056 (2013). arXiv:1305.6936 [gr-qc]
- 142. C.-Y. Zhang, S.-J. Zhang, B. Wang, Superradiant instability of Kerr-de Sitter black holes in scalar-tensor theory. J. High Energy Phys. 1408, 011 (2014). arXiv:1405.3811 [hep-th]
- 143. R. Gregory, R. Laflamme, The Instability of charged black strings and p-branes. Nucl. Phys. **B428**, 399–434 (1994). arXiv:hep-th/9404071 [hep-th]
- 144. R. Emparan, R.C. Myers, Instability of ultra-spinning black holes. J. High Energy Phys. 0309, 025 (2003). arXiv:hep-th/0308056 [hep-th]
- 145. O.J. Dias, P. Figueras, R. Monteiro, J.E. Santos, R. Emparan, Instability and new phases of higher-dimensional rotating black holes. Phys. Rev. **D80**, 111701 (2009). arXiv:0907.2248 [hep-th]

146. O.J. Dias, P. Figueras, R. Monteiro, H.S. Reall, J.E. Santos, An instability of higher-dimensional rotating black holes. J. High Energy Phys. **1005**, 076 (2010). arXiv:1001.4527 [hep-th]

- 147. O.J. Dias, P. Figueras, R. Monteiro, J.E. Santos, Ultraspinning instability of rotating black holes. Phys. Rev. **D82**, 104025 (2010). arXiv:1006.1904 [hep-th]
- 148. O.J. Dias, R. Monteiro, J.E. Santos, Ultraspinning instability: the missing link. J. High Energy Phys. 1108, 139 (2011). arXiv:1106.4554 [hep-th]
- 149. V. Cardoso, J.P. Lemos, New instability for rotating black branes and strings. Phys. Lett. **B621**, 219–223 (2005). arXiv:hep-th/0412078 [hep-th]
- 150. V. Cardoso, A.S. Miranda, E. Berti, H. Witek, V.T. Zanchin, Geodesic stability, Lyapunov exponents and quasinormal modes. Phys. Rev. **D79**, 064016 (2009). arXiv:0812.1806 [hep-th]
- 151. O.J. Dias, Superradiant instability of large radius doubly spinning black rings. Phys. Rev. **D73**, 124035 (2006). arXiv:hep-th/0602064 [hep-th]
- 152. R. Emparan, H.S. Reall, A rotating black ring solution in five-dimensions. Phys. Rev. Lett. 88, 101101 (2002). arXiv:hep-th/0110260 [hep-th]
- 153. R. Emparan, H.S. Reall, Black rings. Classical and Quantum Gravity 23, R169 (2006). arXiv:hep-th/0608012 [hep-th]
- 154. J.G. Rosa, Boosted black string bombs. J. High Energy Phys. **1302**, 014 (2013). arXiv:1209.4211 [hep-th]
- 155. J.L. Friedman, Ergosphere instability. Commun. Math. Phys. 63(3), 243–255 (1978). http://projecteuclid.org/euclid.cmp/1103904565
- 156. O.J. Dias, H.S. Reall, J.E. Santos, Kerr-CFT and gravitational perturbations. J. High Energy Phys. 0908, 101 (2009). arXiv:0906.2380 [hep-th]
- 157. O.J. Dias, J.E. Santos, M. Stein, Kerr-AdS and its near-horizon geometry: perturbations and the Kerr/CFT correspondence. J. High Energy Phys. **1210**, 182 (2012). arXiv:1208.3322 [hep-th]
- A. Vilenkin, Exponential amplification of waves in the gravitational field of ultrarelativistic rotating body. Phys. Lett. B78, 301–303 (1978)
- 159. N. Comins, B.F. Schutz, On the ergoregion instability. Proc. R. Soc. Lond. Ser. A **364**(1717), 211–226 (1978). http://www.jstor.org/stable/79759.
- 160. S. Yoshida, Y. Eriguchi, Ergoregion instability revisited—a new and general method for numerical analysis of stability. Mon. Not. R. Astron. Soc. 282 (Sept., 1996) 580–586.
- 161. V. Cardoso, P. Pani, M. Cadoni, M. Cavaglia, Ergoregion instability of ultracompact astrophysical objects. Phys. Rev. **D77**, 124044 (2008). arXiv:0709.0532 [gr-qc]
- 162. C.B. Chirenti, L. Rezzolla, On the ergoregion instability in rotating gravastars. Phys. Rev. **D78**, 084011 (2008). arXiv:0808.4080 [gr-qc]
- 163. K.D. Kokkotas, J. Ruoff, N. Andersson, The w-mode instability of ultracompact relativistic stars. Phys. Rev. **D70**, 043003 (2004). arXiv:astro-ph/0212429 [astro-ph]
- 164. Y. Kojima, Equations governing the nonradial oscillations of a slowly rotating relativistic star. Phys. Rev. D46, 4289–4303 (1992)
- 165. Y. Kojima, Normal modes of relativistic stars in slow rotation limit. Astrophys. J. 414, 247–253 (1993)
- 166. S. Chandrasekhar, V. Ferrari, On the non-radial oscillations of slowly rotating stars induced by the lense-thirring effect. Proc. R. Soc. Lond. **A433**, 423–440 (1991)
- 167. V. Cardoso, L.C.B. Crispino, C.F.B. Macedo, H. Okawa, P. Pani, Light rings as observational evidence for event horizons: long-lived modes, ergoregions and nonlinear instabilities of ultracompact objects. Phys. Rev. D90, 044069 (2014). arXiv:1406.5510 [gr-qc]
- 168. J. Keir, Slowly decaying waves on spherically symmetric spacetimes and an instability of ultracompact neutron stars. arXiv:1404.7036 [gr-gc]
- 169. P.O. Mazur, E. Mottola, Gravitational condensate stars: an alternative to black holes. arXiv:gr-qc/0109035 [gr-qc]
- 170. M. Karlovini, K. Rosquist, L. Samuelsson, Constructing stellar objects with multiple necks. Classical and Quantum Gravity 18, 817-832 (2001). arXiv:gr-qc/0009079 [gr-qc]

- 171. M. Karlovini, K. Rosquist, L. Samuelsson, Ultracompact stars with multiple necks. Mod. Phys. Lett. A17, 197–204 (2002). arXiv:gr-qc/0009073 [gr-qc]
- 172. M. Karlovini, K. Rosquist, L. Samuelsson, Compact stellar objects with multiple neck optical geometries. Ann. Phys. **9SI**, 149 (2000). arXiv:gr-qc/0002045 [gr-qc]
- 173. J.L. Friedman, Ergosphere instability. Commun. Math. Phys. 63, 243-255 (1978)
- 174. M. Lax, H. Feshbach, Absorption and scattering for impedance f on spheres and circular cylinders. J. Acoust. Soc. Am. **20**, 108 (1948)
- 175. S. Hod, Onset of superradiant instabilities in the hydrodynamic vortex model. Phys. Rev. **D90**, 027501 (2014). arXiv:1405.7702 [gr-qc]
- E.G. Broadbent, D.W. Moore, Acoustic destabilization of vortices. Philos. Trans. R. Soc. Lond. A290, 353 (1979)
- 177. L. Kelvin, On the vibrations of a columnar vortex. Philos. Mag. 10 (1880) 155-168.
- 178. A. Strominger, C. Vafa, Microscopic origin of the Bekenstein-Hawking entropy. Phys. Lett. **B379**, 99-104 (1996). arXiv:hep-th/9601029 [hep-th]
- 179. J.M. Maldacena, The large N limit of superconformal field theories and supergravity. Adv. Theor. Math. Phys. 2, 231–252 (1998). arXiv:hep-th/9711200
- 180. S.S. Gubser, I.R. Klebanov, A.M. Polyakov, Gauge theory correlators from non-critical string theory. Phys. Lett. **B428**, 105–114 (1998). arXiv:hep-th/9802109
- 181. E. Witten, Anti-de Sitter space and holography. Adv. Theor. Math. Phys. 2, 253–291 (1998). arXiv:hep-th/9802150
- 182. E. Witten, Anti-de Sitter space, thermal phase transition, confinement in gauge theories. Adv. Theor. Math. Phys. 2, 505–532 (1998). arXiv:hep-th/9803131 [hep-th]
- 183. R.C. Myers, Pure states don't wear black. Gen. Rel. Grav. 29, 1217-1222 (1997). arXiv:gr-qc/9705065 [gr-qc]
- 184. S.D. Mathur, The Fuzzball proposal for black holes: an elementary review. Fortsch. Phys. 53, 793–827 (2005). arXiv:hep-th/0502050 [hep-th]
- 185. S.D. Mathur, Fuzzballs and black hole thermodynamics. arXiv:1401.4097 [hep-th]
- 186. B.D. Chowdhury, S.D. Mathur, Radiation from the non-extremal fuzzball. Classical and Quantum Gravity 25, 135005 (2008). arXiv:0711.4817 [hep-th]
- 187. B.D. Chowdhury, S.D. Mathur, Pair creation in non-extremal fuzzball geometries. Classical and Quantum Gravity 25, 225021 (2008). arXiv:0806.2309 [hep-th]
- 188. V. Cardoso, O.J. Dias, J.L. Hovdebo, R.C. Myers, Instability of non-supersymmetric smooth geometries. Phys. Rev. **D73**, 064031 (2006). arXiv:hep-th/0512277 [hep-th]
- 189. S. Corley, T. Jacobson, Black hole lasers. Phys. Rev. **D59**, 124011 (1999). arXiv:hep-th/9806203 [hep-th]
- 190. S. Hawking, Particle creation by black holes. Commun. Math. Phys. 43, 199–220 (1975)
- 191. A. Coutant, R. Parentani, Black hole lasers, a mode analysis. Phys. Rev. D81, 084042 (2010). arXiv:0912.2755 [hep-th]
- 192. A. Coutant, On the phenomenology of quantum gravity: stability properties of Hawking radiation in the presence of ultraviolet violation of local Lorentz invariance. arXiv:1405.3466 [hep-th]
- 193. A. Coutant, A. Fabbri, R. Parentani, R. Balbinot, P. Anderson, Hawking radiation of massive modes and undulations. Phys. Rev. **D86**, 064022 (2012). arXiv:1206.2658 [gr-gc]
- 194. A. Coutant, R. Parentani, Undulations from amplified low frequency surface waves. Phys. Fluids 26, 044106 (2014). arXiv:1211.2001 [physics.flu-dyn]
- 195. C. Eling, B.Z. Foster, T. Jacobson, A.C. Wall, Lorentz violation and perpetual motion. Phys. Rev. D75, 101502 (2007). arXiv:hep-th/0702124 [HEP-TH]
- 196. D. Blas, S. Sibiryakov, Horava gravity versus thermodynamics: the black hole case. Phys. Rev. **D84**, 124043 (2011). arXiv:1110.2195 [hep-th]
- 197. D. Giannios, Spherically symmetric, static spacetimes in TeVeS. Phys. Rev. **D71**, 103511 (2005). arXiv:gr-qc/0502122 [gr-qc]
- 198. C. Eling, T. Jacobson, Black holes in einstein-aether theory. Classical and Quantum Gravity 23, 5643–5660 (2006). arXiv:gr-qc/0604088 [gr-qc]

199. E. Barausse, T.P. Sotiriou, Black holes in Lorentz-violating gravity theories. Classical and Quantum Gravity 30, 244010 (2013). arXiv:1307.3359 [gr-qc]

- 200. Z. Zhu, S.-J. Zhang, C. Pellicer, B. Wang, E. Abdalla, Stability of Reissner-Nordstrm black hole in de Sitter background under charged scalar perturbation. Phys. Rev. D90(4), 044042 (2014). arXiv:1405.4931 [hep-th]
- 201. R. Konoplya, A. Zhidenko, Charged scalar field instability between the event and cosmological horizons. Phys. Rev. **D90**, 064048 (2014). arXiv:1406.0019 [hep-th]
- 202. R. Konoplya, A. Zhidenko, Instability of higher dimensional charged black holes in the de-Sitter world. Phys. Rev. Lett. **103**, 161101 (2009). arXiv:0809.2822 [hep-th]
- 203. V. Cardoso, M. Lemos, M. Marques, On the instability of Reissner-Nordstrom black holes in de Sitter backgrounds. Phys. Rev. **D80**, 127502 (2009). arXiv:1001.0019 [gr-qc]
- 204. R. Konoplya, A. Zhidenko, Instability of D-dimensional extremally charged Reissner-Nordstrom(-de Sitter) black holes: extrapolation to arbitrary D. Phys. Rev. **D89**(2), 024011 (2014). arXiv:1309.7667 [hep-th]
- 205. M. Shibata, H. Yoshino, Nonaxisymmetric instability of rapidly rotating black hole in five dimensions. Phys. Rev. **D81**, 021501 (2010). arXiv:0912.3606 [gr-qc]
- 206. M. Shibata, H. Yoshino, Bar-mode instability of rapidly spinning black hole in higher dimensions: numerical simulation in general relativity. Phys. Rev. D81, 104035 (2010). arXiv:1004.4970 [gr-qc]
- 207. O.J.C. Dias, G.S. Hartnett, J.E. Santos, Quasinormal modes of asymptotically flat rotating black holes. Classical Quantum Gravity 31(24), 245011 (2014). doi:10.1088/0264-9381/31/24/245011. arXiv:1402.7047 [hep-th]
- 208. G.S. Hartnett, J.E. Santos, Non-axisymmetric instability of rotating black holes in higher dimensions. Phys. Rev. **D88**, 041505 (2013). arXiv:1306.4318 [gr-qc]
- 209. R. Emparan, R. Suzuki, K. Tanabe, Instability of rotating black holes: large D analysis. J. High Energy Phys. **1406**, 106 (2014). arXiv:1402.6215 [hep-th]
- J.B. Hartle, Slowly rotating relativistic stars.
 Equations of structure. Astrophys. J. 150, 1005–1029 (1967)
- 211. T. Hartman, W. Song, A. Strominger, The Kerr-Fermi sea. arXiv:0912.4265 [hep-th]
- 212. G.E. Matsas, A.R. da Silva, Overspinning a nearly extreme charged black hole via a quantum tunneling process. Phys. Rev. Lett. **99**, 181301 (2007). arXiv:0706.3198 [gr-gc]
- 213. S. Hod, Return of the quantum cosmic censor. Phys. Lett. **B668**, 346–349 (2008). arXiv:0810.0079 [gr-qc]
- 214. M. Richartz, A. Saa, Challenging the weak cosmic censorship conjecture with charged quantum particles. Phys. Rev. **D84**, 104021 (2011). arXiv:1109.3364 [gr-qc]
- 215. T.K. Das, Transonic black hole accretion as analogue system. Conf. Proc. **C0405132**, 279–304 (2004). arXiv:gr-qc/0411006 [gr-qc]
- 216. T.K. Das, N. Bilic, S. Dasgupta, Black-hole accretion disc as an analogue gravity model. J. Cosmol. Astropart. Phys. **0706**, 009 (2007). arXiv:astro-ph/0604477 [astro-ph]
- 217. E. Chaverra, M.D. Morales, O. Sarbach, Quasinormal acoustic oscillations in the Michel flow. Phys Rev. **D91**(10), 104012 (2015). doi:10.1103/PhysRevD.91.104012. arXiv:1501.01637 [gr-qc]
- 218. M. Richartz, A. Prain, S. Weinfurtner, S. Liberati, Superradiant scattering of dispersive fields. Classical and Quantum Gravity 30, 085009 (2013). arXiv:1208.3601 [gr-qc]

Chapter 5 Black Hole Superradiance in Astrophysics

BHs are one of the most striking predictions of Einstein's GR and, in fact, they are predicted by any relativistic theory of gravity [1]. Since Schmidt's identification of the first quasar [2], large consensus in the astronomy community has mounted that nearly any galactic center harbors a supermassive BH and that compact objects with mass above $\sim 3M_{\odot}$ as found in some low-mass X-ray binaries should be BHs (we discuss some alternatives to this paradigm in Sect. 5.8.2 below). Indeed, strong evidence exists that astrophysical BHs with masses ranging from few solar masses to billions of solar masses are abundant objects.

GR's uniqueness theorems imply a very strong prediction: all isolated, vacuum BHs in the Universe are described by the two-parameter Kerr family. Not only this implies that BHs are perfect testbeds for strong-gravity effects due to their simplicity, but it also means that observing any deviation from this "Kerr paradigm"—a goal within the reach of upcoming GW [3–8] and electromagnetic [9, 10] facilities—would inevitably imply novel physics beyond GR.

A special feature of vacuum stationary GR solutions is their *axisymmetry* [11]. This simplifies the treatment of superradiant instabilities considerably, as it excludes mixing between modes with different azimuthal number *m*. Finally, the equivalence principle guarantees that gravity couples universally to matter. Altogether, these properties imply that any prediction based on gravitational effects of extra fields around BHs should be very solid.

5.1 Superradiance and Relativistic Jets

Relativistic jets emitted by astrophysical sources are one of the most interesting and mysterious phenomena in our Universe. The most powerful jets are seen in active galactic nuclei (AGNs), and are believed to be the result of accretion of matter by supermassive BHs [12]. AGNs are the most powerful sources in the

Universe, making it very hard to conceive viable models for their production without invoking very compact objects. Although the first AGNs (such as quasars and radio galaxies) were discovered four decades ago, the engine powering these events is still largely unknown. The energy needed for the acceleration of these relativistic outflows of matter is widely believed to either come from gravitational binding energy and/or from the object's rotational energy. In the first case, accretion of matter onto the BH leads to a transfer of gravitational binding energy to particles which are tossed away along the rotational axis of the BH (see e.g. [13] for such a process). Other mechanisms, akin to superradiance or to the Penrose process, make use of the rotational energy of the BH. This is the case of the Blandford-Znajek (BZ) mechanism [14] which occurs for BHs immersed in magnetic fields (see also e.g. [15, 16] for a discussion on the relationship between the BZ mechanism and superradiance or the Penrose process). In this mechanism the magnetic field lines, which are anchored in the accretion disk, are twisted due to the frame dragging effect near the rotating BH (see Sect. 3.1.3), thus increasing the magnetic flux. Similar to the Earth-Moon system discussed in Sect. 2.6, due to dissipative effects, this can lead to energy transfer from the BH to the magnetic field [17]. This energy is then used to accelerate the surrounding plasma and to power a jet collimated along the BH rotational axis. In general both the accretion process and the BZ mechanism might contribute to the energy released in the jets, making it difficult to prove from numerical simulations that the latter mechanism is at work, but recent general relativistic magnetohydrodynamic (GRMHD) simulations seem to indicate that this is indeed the case [16, 18-20].

5.1.1 Blandford-Znajek Process

In the BZ solution a Kerr BH is considered to be immersed in a stationary axisymmetric force-free magnetosphere [14]. In [14] it was argued that in analogy with what happens in pulsars, a rotating BH would trigger an electron-positron pair cascade just outside the accretion disk and the horizon where the plasma is rarefied, establishing an approximately force-free magnetosphere. In Fig. 5.1 we depict the region where this force-free magnetosphere is localized plus the other regions that characterize the magnetosphere. Region (FF) is where the transfer of energy takes place. This energy is then deposited in region (A) where particles are accelerated.

¹A condition for this to happen is that initially there is a small electric field component parallel to the magnetic field (note that this is a Lorentz invariant condition). In [21], this was shown to occur for rotating BHs immersed in a magnetic field.

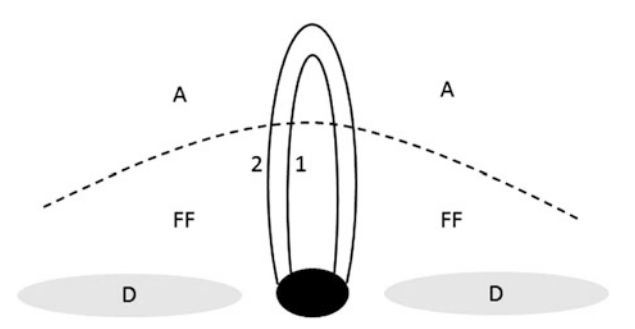


Fig. 5.1 Pictorial description of the magnetosphere surrounding a BH in the BZ mechanism. The *solid lines* denote electric equipotential surfaces. The magnetosphere is composed of three different regions: a region (D) which includes the accretion disk and the horizon, where the field is degenerate, i.e., the electric field is perpendicular to the magnetic field, but not force-free. This last condition is required for these regions to be able to anchor the magnetic field; a region (FF) where the field is force-free. In this region the current flows along equipotential surfaces; an acceleration region (A) in which the field is neither degenerate nor force free. In region (A) the equipotential surfaces close up, and the energy extracted from the BH is used to accelerate charged particles. In regions (D) and (A) the current can flow across the equipotential surfaces. Reproduction of figure from [17]

To describe the force-free magnetosphere, in addition to Maxwell's equations with a source

$$\nabla_{\nu}F^{\mu\nu} = \frac{J^{\mu}}{\epsilon_0},\tag{5.1}$$

the electromagnetic field must satisfy the following three conditions

$$F_{\mu\nu}J^{\nu} = 0$$
, ${}^*F^{\mu\nu}F_{\mu\nu} = 0$, $F_{\mu\nu}F^{\mu\nu} > 0$, (5.2)

where ${}^*F^{\mu\nu}\equiv \frac{1}{2}\epsilon^{\mu\nu\rho\sigma}F_{\rho\sigma}$ is Maxwell's tensor dual (we use the definition $\epsilon^{\mu\nu\rho\sigma}\equiv \frac{1}{\sqrt{-g}}E^{\mu\nu\rho\sigma}$ where $E^{\mu\nu\rho\sigma}$ is the totally anti-symmetric Levi-Civita symbol with $E^{0123}=1$), ϵ_0 is the vacuum permittivity and J^μ is the current generated by the electron-positron plasma. The first condition implies—assuming that the vector potential has the same symmetries (axisymmetry and stationarity) than the BH spacetime—that the magnetic field lines lie along surfaces of constant A_{φ} . On the other hand, if the second condition is satisfied but not the third one can always find a local inertial frame where the electromagnetic field is purely electric. From these equations, it also follows that one can define a function $\Omega_{\rm EM}(r,\vartheta)$ as

$$\Omega_{\rm EM}(r,\vartheta) = -\frac{A_{t,r}}{A_{\varphi,r}} = -\frac{A_{t,\vartheta}}{A_{\varphi,\vartheta}},\tag{5.3}$$

which can be interpreted as being the "angular velocity" of the electromagnetic field as will become clear below.

The field equations must also be supplemented with appropriate boundary conditions at the horizon and at infinity. At the horizon it was shown in [22] that regularity implies (assuming A_{φ} to be finite)

$$\frac{\Delta \sin \vartheta}{\rho^2} F_{r\vartheta} = \frac{2Mr_+ (\Omega_{\rm EM} - \Omega_{\rm H})}{r_+^2 + a^2 \cos^2 \vartheta} A_{\varphi,\vartheta}(r_+,\vartheta), \qquad (5.4)$$

where in the force-free approximation, $F_{r\vartheta}$ can be shown to be a function of A_{φ} only. On the other hand, the boundary conditions at infinity are not unique but they can be chosen, e.g., by matching the field to known flat-space solutions.

The factor $\Omega_{EM} - \Omega_H$ appearing in the boundary conditions above [compare it with the superradiant condition (1.1)] already suggests that stationary axisymmetric solutions of the inhomogeneous Maxwell's equations (5.1) in a Kerr background are akin to a superradiance-like process. In fact the conserved radial electromagnetic energy and angular momentum fluxes at the horizon are given by [14]

$$\delta E_{\text{hole}}^{r} \equiv -T_{\mu}^{\ r} \xi_{(t)}^{\mu} = \Omega_{\text{EM}} (\Omega_{\text{EM}} - \Omega_{\text{H}}) \left(\frac{A_{\varphi, \vartheta}}{r_{+}^{2} + a^{2} \cos^{2} \vartheta} \right)^{2} (r_{+}^{2} + a^{2}) \epsilon_{0}, \tag{5.5}$$

$$\delta J_{\text{hole}}^r \equiv T_{\mu}^{\ r} \xi_{(\varphi)}^{\mu} = \frac{\delta E_{\text{hole}}^r}{\Omega_{\text{TM}}},\tag{5.6}$$

and thus when $0 < \Omega_{\rm EM} < \Omega_{\rm H}$ there is a net radial negative energy and angular momentum flux $\delta E^r_{\rm hole} < 0$, $\delta J^r_{\rm hole} < 0$ at the horizon, i.e., energy and angular momentum are extracted from the BH. From Eq. (5.6) one sees that the function $\Omega_{\rm EM}$ can indeed be interpreted as the "angular velocity" of the electromagnetic field.

By deriving specific solutions for the electromagnetic field, it is possible to construct the function Ω_{EM} through Eq. (5.3) explicitly. Particularly important are the split monopole, and the paraboidal magnetic field solutions found perturbatively in the slowly-rotating limit [14]. In these cases, $\Omega_{EM} = \Omega_H/2$ and $\Omega_{EM} \approx 0.38\Omega_H$, respectively (see e.g. [23] for a recent summary of these solutions and also [24–27] for recent exact solutions found around extreme Kerr BHs). Recently [28] studied the linear stability of the monopole solution and their results suggest that the solution is mode stable. In fact, force-free simulations (e.g. [15, 29–32]) and recent GRMHD simulations seem to indicate that magnetic fields generated by accretion disks have large split monopole components [18–20] suggesting that the BZ mechanism should occur in fully dynamical setups.

5.1.2 Blandford-Znajek Process and the Membrane Paradigm

The understanding of the physics behind the BZ mechanism was at the origin of a new paradigm to describe BHs, the so-called membrane paradigm. This paradigm uses a 3 + 1 spacetime decomposition in which the BH event horizon is regarded as a two-dimensional surface residing in a three-dimensional space, while the region inside the horizon is "thrown away" from the picture since it is causally disconnected from any observer outside the horizon.² This surface can be shown to behave as an electrically charged viscous fluid with finite surface electrical resistivity, entropy and temperature. In this picture the interaction of the membrane with the rest of the Universe is then governed by well-known physical laws for the horizon's fluid, such as the Navier-Stokes equation, Ohm's law, tidal force equations and the laws of thermodynamics. Originally all quantities were computed in the ZAMO frame (see Sect. 3.1) in relation to which electric and magnetic fields are defined and physical laws are formulated, although the membrane paradigm has also been reformulated in a covariant form in [33]. For stationary (or static) BH spacetimes the membrane paradigm is fully equivalent to the standard spacetime approach as long as one is only interested in physics occurring outside the horizon. The teleological nature of the paradigm makes it more challenging to study time-dependent problems although some cases involving weakly perturbed non-stationary spacetimes have successfully been studied [34]. For astrophysical purposes this paradigm has been quite successful to describe and understand relativistic phenomena in BH spacetimes (see [34] for a pedagogical introduction and a compilation of works which led to the full formulation of the membrane paradigm. See also [33] for a derivation of the membrane paradigm starting from an action principle).

In the membrane paradigm, one can understand how the BZ mechanism works through an analogy with the tidal acceleration effect (see Sect. 2.6) [17]. Taking an infinitesimal tube of magnetic flux $\delta\psi$ in the force-free region (for example a tube with walls given by surfaces 1 and 2 of Fig. 5.1) and which intersects the hole, it is possible to show that the torque exerted by the membrane on this tube is [17]

$$-\frac{d\delta J}{dt} = \frac{\Omega_{\rm H} - \Omega_{\rm EM}}{4\pi} g_{\varphi\varphi} B_{\perp} \delta \psi , \qquad (5.7)$$

where B_{\perp} is the magnetic field perpendicular to the membrane as seen by the ZAMO's observer and $g_{\varphi\varphi}$ is to be taken at the horizon. The power transmitted

²The use of a 3 + 1 spacetime decomposition was mainly useful to write the equations in a more familiar form for the astrophysics community. In fact most of the work done in this area in the last decades has been done using this formalism. Recently the GR community has regained interest in the subject and some remarkable effort has been done to develop a fully covariant theory of force-free magnetospheres around rotating BHs [23].

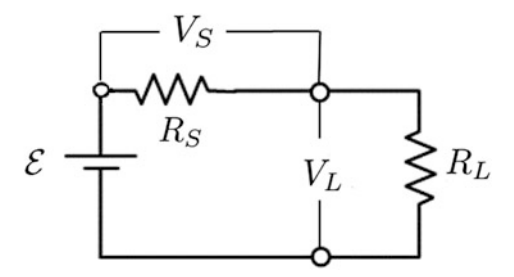


Fig. 5.2 Circuit analogy of the BZ mechanism in which a battery transfers energy to a load. A battery of electromotive force \mathcal{E} with internal resistance R_S drives a current I through the load resistance R_L (which could be for example an electric light). Maximum power transfer is attained when $R_L = R_S$

to the flux tube due to this torque is then

$$P = -\Omega_{\rm EM} \frac{d\delta J}{dt} = \Omega_{\rm EM} \frac{\Omega_{\rm H} - \Omega_{\rm EM}}{4\pi} g_{\varphi\varphi} B_{\perp} \delta \psi . \tag{5.8}$$

This torque and power are transmitted through the tube up to region A, where angular momentum gets gradually deposited into charged particles. A direct comparison with Eqs. (2.66) and (2.67) shows that from the point of view of the ZAMO's observer this is indeed a analogous process to tidal acceleration, and thus completely analogous to superradiance.

The membrane picture also suggests an analogy between the BZ mechanism and the circuit of Fig. 5.2, in which energy is transferred from a battery (the BH) to a load (the acceleration region A) [17]. The current flowing along the resistance R_S produces a potential drop V_S , while at R_L it produces a potential drop V_L such that the electromotive force of the battery is given by $\mathcal{E} = V_S + V_L$. From Ohm's law the current I flowing along the circuit is given by

$$I = \frac{\mathcal{E}}{R_S + R_L},\tag{5.9}$$

while the power dissipated in the load is given by

$$P_L = I^2 R_L = \frac{\mathcal{E}^2}{R_S^2 / R_L + 2R_S + R_L} \,. \tag{5.10}$$

On the other hand the efficiency of this process, defined by the ratio of the power dissipated in the load to the total power generated by the source, reads

$$\eta = \frac{1}{R_S/R_L + 1} \,. \tag{5.11}$$

Although the efficiency has its maximum when $R_L \gg R_S$, the maximum power output at the load is obtained when $R_L = R_S$. Note that in this case only half of the energy is really transferred to the load, the other half being dissipated as heat due to the source internal resistance. On the other hand, if $R_L \ll R_S$, then most of the power output is dissipated as heat at the source, whereas if $R_L \gg R_S$ the current I generated at the source will be very low and thus the power transferred to the load will be very small, even though the efficiency will tend to 100 %.

In the BZ process case, the current flowing from surface 1 to 2 of Fig. 5.1 in the horizon membrane's produces a potential drop δV_H due the membrane internal resistance R_H , given by [17]

$$\delta V_H = I \delta R_H = \frac{(\Omega_{\rm H} - \Omega_{\rm EM}) \delta \psi}{2\pi}, \qquad (5.12)$$

where δR_H is related to R_H through [17]

$$\delta R_H = R_H \frac{\delta \psi}{4\pi^2 g_{\varphi\varphi} B_\perp} \,. \tag{5.13}$$

The potential drop in region A can be thought as being due to a resistance δR_A , and it can be shown to be given by [17]

$$\delta V_A = I \delta R_A = \frac{\Omega_{\rm EM} \delta \psi}{2\pi} \,, \tag{5.14}$$

where it is assumed that the acceleration region A is sufficiently far away such that frame dragging effects are negligible. Using Eqs. (5.12), (5.13) and (5.14), the ratio between the potentials in the acceleration region and at the horizon are then given by

$$\frac{\delta V_A}{\delta V_H} = \frac{\delta R_A}{\delta R_H} = \frac{1}{\Omega_{\rm H}/\Omega_{\rm EM} - 1} \,. \tag{5.15}$$

By comparison with Eq. (5.11), one can define the efficiency of the BZ mechanism by $\eta = \Omega_{\rm EM}/\Omega_{\rm H}$ [14].³ The sum of the potential drops is equal to the total electromotive force $\mathcal{E} = \delta V_H + \delta V_A$ around a closed loop that passes along the horizon from surface 1 to 2, then up the surface 2 poloidally to the region A in which it crosses to surface 1 again and then back down to the horizon. Thus, the total

³This is not to be confused with the jet efficiency, defined by $\eta_{\rm jet} = \langle L_{\rm jet} \rangle / \langle \dot{M} \rangle$ where $\langle L_{\rm jet} \rangle$ is the time-average jet luminosity and $\langle \dot{M} \rangle$ is the time-average rate of matter accretion by the BH. Recently, efficiencies up to $\eta_{\rm jet} \sim 300 \%$ have been obtained in GRMHD simulations [16, 18, 19, 35] which is a strong indication that the BZ mechanism is at work.

current I and the total power transmitted P to the acceleration region are given by

$$I = \frac{\mathcal{E}}{\delta R_A + \delta R_H} = \frac{1}{2} \left(\Omega_{\rm H} - \Omega_{\rm EM} \right) g_{\varphi\varphi} B_{\perp} \delta \psi , \qquad (5.16)$$

$$P = \delta R_A I^2 = \Omega_{\rm EM} \frac{(\Omega_{\rm H} - \Omega_{\rm EM})}{4\pi} g_{\varphi\varphi} B_{\perp} \delta \psi . \tag{5.17}$$

Maximum power transmission then implies $\Omega_{\rm EM}=\Omega_{\rm H}/2$. From Eq. (5.15), this happens when $R_A=R_H$ and $\delta V_A=\delta V_H$, which corresponds to the condition obtained from the circuit analogy. In [17] it was argued that the configuration $\Omega_{\rm EM}=\Omega_{\rm H}/2$ would be likely to be achieved in a dynamical setup due to the backreaction of charged particles onto the field lines. In fact recent GRMHD simulations seem to obtain $\Omega_{\rm EM}/\Omega_{\rm H}\approx 0.3-0.4$, in agreement with this analysis [19, 20].

A key ingredient for this analogy to work is to understand the physical origin behind the electromotive force \mathcal{E} driving the current I. The membrane paradigm suggests an analogy with Faraday's unipolar inductor. Consider a rotating conducting disk, which can be idealized as a perfect conductor, immersed in a uniform magnetic field perpendicular to the rotational axis of the disk. Due to the rotational motion of the disk through the magnetic field there is a radial Lorentz force on the free charges in the disk, which in turn produces a potential difference between the center and the boundary of the disk. On the other hand, due to the magnetic field, this current feels a Lorentz force opposite to the rotational motion of the disk, producing a reaction torque on the conductor which will make it slow down in analogy with the BZ mechanism. Completing this circuit with a wire attached at the boundary and the center of the disk, one can effectively use the disk as a battery. This is in fact the mechanism behind the electromotive force developed by rotating magnetized stars [36, 37] and planets [38]. However, as was pointed out in [15, 29] the membrane paradigm suggests that the horizon plays a similar role to the surface of a magnetized rotating star, hiding the role played by the ergosphere. Unlike the surface of a disk in which an electromotive force can indeed drive an electric current, Einstein's equivalence principle tells us that the BH horizon is not a physical surface where electrics current can flow.⁴ In [29] the author showed that inside the ergoregion there are no stationary axisymmetric solution of the Einstein-Maxwell equations, describing a electromagnetic field supported by a remote source, that satisfy both the second and third conditions of Eq. (5.2) along the magnetic field lines (see also [40, 41]). This implies that near a rotating BH there are no stationary solutions with a completely screened electric field. This is in fact a purely gravitational effect caused by the dragging of inertial frames near the BH. Although the force-free approximation is for all purposes a good approximation

⁴However from the point of view of *BH complementarity* introduced in [39], the membrane is real as long as the observers remain outside the horizon, but fictitious for observers who jump inside the BH. Since neither observer can verify a contradiction between each other, the two are complementary in the same sense of the wave-particle duality.

for the magnetosphere near a rotating BH, it fails to predict that current sheets must form inside the ergoregion, where a strong enough unscreened electric field perpendicular to the magnetic field must persist in order to sustain the potential drop along the magnetic field lines. On the other hand, in the region where the force-free approximation holds, it is the residual component of the electric field parallel to the magnetic field that drives the poloidal currents [29].

We should stress that although the ergoregion is necessary for the BZ mechanism to occur, the circuit and tidal acceleration analogies make it clear that *dissipation* is also a fundamental ingredient. However the precise mechanism behind this dissipation, and whether it is due to the horizon or the plasma surrounding the BH, is unclear and still a matter of debate.

5.2 Superradiance, CFS Instability, and r-Modes of Spinning Stars

Another important astrophysical process that bears some resemblance with superradiant phenomena is the Chandrasekhar-Friedman-Schutz (CFS) instability of spinning NSs driven by gravitational radiation. This instability was discovered by Chandrasekhar in 1970 while studying Maclaurin spheroids [42]. In 1978, Friedman and Schutz extended the analysis to the case of compressible, perfect-fluid stars and explained the instability in an elegant way [43]. In fact, such instability is very generic and occurs whenever a mode that is retrograde in a frame corotating with the star appears as prograde to a distant inertial observer (see [44–46] and references therein).

The mechanism for the instability is depicted in Fig. 5.3. In the left panel we show a stable configuration: a fluid perturbation of a static star with phase velocity ω/m moving counter-clockwise. Within our axis conventions, this perturbation carries a positive angular momentum and also emits positive angular momentum through GWs. The angular momentum emitted in GWs has to be subtracted by that of the perturbation, whose amplitude consequently decreases. However, a drastically different picture emerges when the star rotates (right panel of Fig. 5.3). In such case the sign of the angular momentum carried by GWs depends only on the relative motion of the perturbation with respect to the laboratory frame, whereas the sign of the angular momentum of the perturbation depends only on the motion of the mode relative to the star. Therefore, as the star rotates faster and faster in clockwise direction, the counter-clockwise mode starts rotating more slowly as viewed from the laboratory frame, decreasing the rate of angular momentum emission in GWs, but not its intrinsic angular momentum, which remains roughly the same as in the nonrotating case. For some critical angular velocity, the phase velocity of the mode will vanish and the mode will freeze relative to the laboratory (as shown in the right panel of Fig. 5.3). For a slightly higher stellar rotation rate, the initially counterclockwise mode rotates in the *clockwise* sense, thus emitting *negative* angular

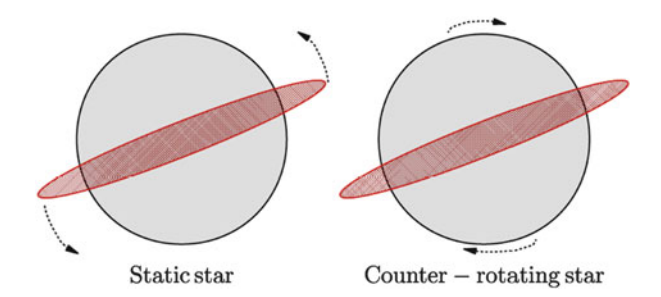


Fig. 5.3 Illustration of the CFS instability as seen from the laboratory frame. In the *left panel* a bar-like mode of the fluid in a static star rotates counter-clockwise. This perturbation tends to increase the angular momentum of the star. Because the perturbation carries away positive angular momentum through GWs, it also reduces its amplitude. In the *right panel* the star rotates clockwise (with rotational axis perpendicular to the plane of the figure) such that, in the laboratory frame, the phase velocity of the mode vanishes and so does the emission of GWs. For a slightly higher stellar spin, the mode would appear to rotate *clockwise* and it would emit GWs with *negative* angular momentum. This negative value is subtracted from the (positive) angular momentum of the perturbation, which therefore increases in amplitude. The larger the perturbation grows, the larger is the angular momentum radiated in GWs, thus producing a positive feedback

momentum through GWs. This emission has to be compensated by an *increase* of the (positive) angular momentum of the perturbation, which therefore increases in amplitude. The larger the perturbation grows, the larger is the angular momentum radiated in GWs, and the instability ensues. The instability evolves on a secular timescale, extracting angular momentum from the star via GW emission, unless it is suppressed by other mechanisms, such as viscosity.

This qualitative picture already shows some similarity with the fact that superradiant modes within the ergoregion appear to be prograde to a distant inertial observer but are in fact retrograde in a frame corotating with the BH. To put this in more quantitative terms, let us consider Newtonian stars within the Lagrangian perturbation framework developed in [43]. We consider a normal mode (i.e. ignoring GW dissipation) of the star in the form $\xi = \hat{\xi} e^{-i(\omega t - m\varphi)}$. In such case, the canonical energy and angular momentum of the mode are related as [43, 45]

$$E_c = -\frac{\omega}{m} J_c, \qquad (5.18)$$

which resembles Eq. (3.23), as expected for the perturbation of an axisymmetric object. When the star rotates with angular velocity $\Omega > 0$, the canonical angular momentum must also satisfy the inequality [43, 45]

$$\frac{\omega - m\Omega - \Omega}{m} \le \frac{J_c/m^2}{\langle \hat{\xi}, \rho \hat{\xi} \rangle} \le \frac{\omega - m\Omega + \Omega}{m}, \tag{5.19}$$

where ρ is the fluid density and the angular parenthesis denote the inner product over the volume of the star. The equation above shows that, in the static $\Omega \to 0$ limit, corotating modes (with $\omega/m > 0$) must have $J_c > 0$, whereas counter-rotating modes have $J_c < 0$. From Eq. (5.18), this implies $E_c > 0$ and therefore the modes are stable. However, when the star rotates in the opposite direction relative to the mode phase velocity, an initially counter-rotating mode can become corotating as discussed before. When this happens E_c can change sign and the mode becomes unstable when $\omega \leq m\Omega$ (in the laboratory frame), with the inequality saturated for marginally stable modes. Therefore, it is clear that the CFS instability requires the existence of modes satisfying the superradiant condition (1.1).

The relativistic framework to study this instability was developed in a series of papers during the 1970s [43, 47, 48], the crucial additional ingredient being the emission of GWs generated by fluid and spacetime perturbations of the star. These works confirmed the Newtonian analysis, finding that a mode becomes unstable at the point where its phase velocity vanishes in the inertial frame, i.e. when $\omega/m = \Omega$ (see [44, 45] for some reviews on the important of the CFS instability in astrophysics).

The r-Mode Instability of Rotating Stars Some axial fluid modes of static, Newtonian stars (as well as the axial gravitational modes of relativistic stars) are degenerate at zero frequency. Therefore, even in the nonrotating case such modes are marginally stable towards the CFS instability. As soon as rotation is turned on, these *r-modes* become unstable for arbitrarily small rotation rates [49] (cf. [50] for a review).

To first order in the stellar spin, the frequency of the r-modes in the inertial frame reads

$$\omega = m\Omega \left(1 - \frac{2}{l(l+1)} \right). \tag{5.20}$$

Therefore, modes with positive phase velocity, $\omega/m > 0$, relative to the laboratory frame have always a *negative* phase velocity $\omega/m - \Omega < 0$ in the star comoving frame for any value of l and Ω (the special case of l = 1 fluid perturbations is marginally stable to first order in the spin). This is confirmed by the canonical energy of these modes which, to first order in Ω , reads [45]

$$E_c = A(\omega + m\Omega)(\omega - m\Omega), \qquad (5.21)$$

where A > 0 is a constant depending on the amplitude of the modes, the harmonic index l and on the stellar density. Therefore, to first order in the spin the instability occurs when $\omega < m\Omega$, i.e. when the superradiant condition (1.1) holds. Such analogy remains valid also to second order in Ω in the large-l limit.

5.3 Evolution of Superradiant Instabilities: Gravitational-Wave Emission and Accretion

We saw that quantum or classical fluctuations of *any* massive bosonic field can trigger a superradiant instability of the Kerr metric, whose time scale τ can be extremely short. For a BH with mass M, the shortest instability time scale is $\tau \sim \left(\frac{M}{10^6 M_{\odot}}\right)$ yr for a ultralight scalar [51–55], and shorter for vector [53, 54, 56] and tensor fields [55] for which superradiance is more efficient (cf. Sect. 4.6).

Little is known about the nonlinear development of the superradiant instability. However, by analyzing the energy and angular momentum fluxes through the BH horizon, it is reasonable to expect that a nonspherical bosonic cloud would grow near the BH on a time scale τ , extracting energy and angular momentum until superradiance stops and the cloud is slowly re-absorbed by the BH and dissipated through GW emission⁵ [54, 57–61]. During the evolution, the BH acquires an effective "hair" as pictorially depicted in Fig. 5.4.

Although (at least for a real, stationary scalar field) the no-hair theorems [62–65] guarantee that the final state of the instability has to be a Kerr BH with lower spin, it is important to understand the time scales involved in this process, because a scalar cloud surviving for cosmological times would be practically indistinguishable from a full-fledged hairy BH and would have various important consequences.

In recent years superradiant instabilities have been used to turn astrophysical BHs into effective particle detectors, by using the fact that putative ultralight bosons (cf. Sect. 4.6.1) would make such massive BHs superradiantly unstable, in

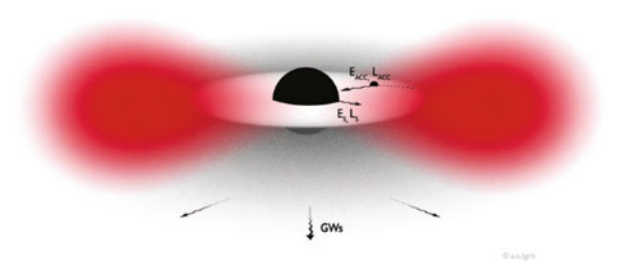


Fig. 5.4 Pictorial description of a bosonic cloud around a spinning BH in a realistic astrophysical environment. The BH loses energy E_S and angular momentum L_S through superradiant extraction of scalar waves and emission of GWs, while accreting gas from the disk, which transports energy $E_{\rm ACC}$ and angular momentum $L_{\rm ACC}$. Notice that accreting material is basically in free fall after it reaches the innermost stable circular orbit. A scalar cloud would be localized at a distance $\sim 1/M\mu_S^2 > 2M$

⁵This expectation is also supported by the proof given in Sect. 3.5.2, where we showed that—when backreaction effects are taken into account—superradiance of charged fields does indeed extract mass and charge away from the BH.

disagreement with current observations of spinning BHs. This exciting possibility is discussed in Sect. 5.4. However, before venturing in the astrophysical implications of superradiant instabilities, we need to assess whether or not the linearized analysis previously presented is reliable. Indeed, essentially all previous works on superradiant instabilities were based on a linearized analysis, neglecting backreaction and other competitive effects—such as GW emission and gas accretion—which can have an impact on the development of the process.

5.3.1 Scalar Clouds Around Spinning Black Holes

This issue was recently addressed by performing a quasi-adiabatic, fully-relativistic evolution of the superradiant instability of a Kerr BH triggered by a massive scalar field, including the effect of GW emission and of gas accretion [60]. The starting point of the analysis is the action (3.1) with vanishing gauge field, so that the model describes a (generically complex) massive scalar field minimally coupled to gravity.

Following the development of the instability in a fully nonlinear evolution is extremely challenging because of the time scales involved: $\tau_{\rm BH} \sim M$ is the light-crossing time, $\tau_S \sim 1/\mu_S$ is the typical oscillation period of the scalar cloud and $\tau \sim M/(M\mu_S)^9$ is the instability time scale in the small- $M\mu_S$ limit. As previously discussed, in the most favorable case for the instability, $\tau \sim 10^6 \tau_S$ is the minimum evolution time scale required for the superradiant effects to become noticeable. Thus, current nonlinear evolutions (which typically last at most $\sim 10^3 \tau_S$ [58]) have not yet probed the development of the instability, nor the impact of GW emission. However, in such configuration the system is suitable for a *quasiadiabatic approximation*: over the dynamical time scale of the BH the scalar field can be considered almost stationary and its backreaction on the geometry can be neglected as long as the scalar energy is small compared to the BH mass [60].

At leading order, the geometry is described by the Kerr spacetime and the scalar evolves in this fixed background. For small mass couplings $M\mu_S$, the spectrum of the scalar perturbations admits the hydrogenic-like solution (4.27), whereas the eigenfunctions are given in Eq. (4.29) [66, 67]. The eigenfunction peaks at [57, 68]

$$r_{\text{cloud}} \sim \frac{(l+n+1)^2}{(M\mu_S)^2} M,$$
 (5.22)

and thus extends well beyond the horizon, where rotation effects can be neglected. The analytical result is a good approximation to the numerical eigenfunctions for moderately large couplings, $\mu_S M \lesssim 0.2$, even at large BH spin [60].

In the quasi-adiabatic approximation (and focusing on the l=m=1 fundamental mode), the cloud is stationary and described by

$$\Psi = A_0 \tilde{r} e^{-\tilde{r}/2} \cos(\varphi - \omega_R t) \sin \vartheta , \qquad (5.23)$$

where the amplitude A_0 can be expressed in terms of the mass M_S of the scalar cloud through [60]

$$A_0^2 = \frac{3}{4\pi \mathcal{I}_2} \left(\frac{M_S}{M} \right) (\mu_S M)^4. \tag{5.24}$$

5.3.2 Gravitational-Wave Emission from the Bosonic Condensate

A nonspherical monochromatic cloud as in Eq. (5.23) will emit GWs with frequency $2\pi/\lambda \sim 2\omega_R \sim 2\mu_S$, the wavelength λ being in general *smaller* than the size of the source, $r_{\rm cloud}$. Thus, even though the cloud is nonrelativistic, the quadrupole formula does not apply because the emission is incoherent [57, 60, 61, 67]. However, due to the separation of scales between the size of the cloud and the BH size for $\mu_S M \ll 1$, the GW emission can be analyzed taking the source to lie in a nonrotating (or even flat [67]) background.

By performing a fully relativistic analysis within the Teukolsky formalism, [60] found that the energy and angular-momentum fluxes of gravitational radiation emitted from the cloud read

$$\dot{E}_{\rm GW} = \frac{484 + 9\pi^2}{23040} \left(\frac{M_S^2}{M^2}\right) (M\mu_S)^{14}, \tag{5.25}$$

$$\dot{J}_{\rm GW} = \frac{1}{\omega_R} \dot{E}_{\rm GW} \,. \tag{5.26}$$

This result has been obtained for small values of the coupling $M\mu_S$ and by neglecting spin effects, i.e. by considering a Schwarzschild background. The latter is a well-motivated assumption, because the cloud is localized away from the horizon, when spin effects are negligible. The energy flux above is in agreement with a previous analysis [67] except for a different prefactor in Eq. (5.25) due to the fact that [60] considered a Schwarzschild background, whereas [67] considered a flat-metric approximation. This analytical result is an *upper bound* relative to the exact numerical flux, the latter being valid for any μ_S and any BH spin [67]. Therefore, using Eq. (5.25) to estimate the energy loss in GWs is a very conservative assumption, since the GW flux is generically smaller.

5.3.3 Gas Accretion

Astrophysical BHs are not in isolation but surrounded by matter fields in the form of gas and plasma. On the one hand, addition of mass and angular momentum to the BH

via accretion competes with superradiant extraction. On the other hand, a slowly-rotating BH which does not satisfy the superradiance condition might be spun up by accretion and might become superradiantly unstable precisely *because* of angular momentum accretion. Likewise, for a light BH whose coupling parameter $\mu_S M$ is small, superradiance might be initially negligible but it can become important as the mass of the BH grows through gas accretion. It is therefore crucial to include accretion in the treatment of BH superradiance.

Brito et al. [60] considered a very conservative and simple model in which mass accretion occurs at a fraction of the Eddington rate (see e.g. [69]):

$$\dot{M}_{ACC} \equiv f_{Edd} \dot{M}_{Edd} \sim 0.02 f_{Edd} \frac{M(t)}{10^6 M_{\odot}} M_{\odot} \text{yr}^{-1}$$
 (5.27)

The formula above assumes an average value of the radiative efficiency $\eta \approx 0.1$, as required by Soltan-type arguments, i.e. a comparison between the luminosity of active galactic nuclei and the mass function of BHs [12, 70]. The Eddington ratio for mass accretion, $f_{\rm Edd}$, depends on the details of the accretion disk surrounding the BH and it is at most of the order unity for quasars and active galactic nuclei, whereas it is typically much smaller for quiescent galactic nuclei (e.g. $f_{\rm Edd} \sim 10^{-9}$ for SgrA*). If we assume that mass growth occurs via accretion through Eq. (5.27), the BH mass grows exponentially with e-folding time given by a fraction $1/f_{\rm Edd}$ of the Salpeter time scale

$$\tau_{\text{Salpeter}} = \frac{\sigma_T}{4\pi m_p} \sim 4.5 \times 10^7 \text{ yr}, \qquad (5.28)$$

where σ_T is the Thompson cross section and m_p is the proton mass. Therefore, the minimum time scale for the BH spin to grow via gas accretion is roughly $\tau_{\rm ACC} \sim \tau_{\rm Salpeter}/f_{\rm Edd} \gg \tau_{\rm BH}$ and also in this case the adiabatic approximation is well justified.

Regarding the evolution of the BH angular momentum through accretion, [60] made the conservative assumption that the disk lies on the equatorial plane and extends down to the innermost stable circular orbit (ISCO). If not, angular momentum increase via accretion is suppressed and superradiance becomes (even) more dominant. Ignoring radiation effects,⁶ the evolution equation for the spin reads [72]

$$\dot{J}_{\rm ACC} \equiv \frac{L(M,J)}{E(M,J)} \dot{M}_{\rm ACC} \,, \tag{5.29}$$

⁶In the absence of superradiance the BH would reach extremality in finite time, whereas radiation effects set an upper bound of $a/M \sim 0.998$ [71]. To mimic this upper bound in a simplistic way, a smooth cutoff in the accretion rate for the angular momentum can be introduced [60]. This cutoff merely prevents the BH to reach extremality and does not play any role in the evolution.

where $L(M,J) = 2M/(3\sqrt{3}) \left(1 + 2\sqrt{3r_{\rm ISCO}/M - 2}\right)$ and $E(M,J) = \sqrt{1 - 2M/3r_{\rm ISCO}}$ are the angular momentum and energy per unit mass, respectively, of the ISCO of the Kerr metric, located at $r_{\rm ISCO} = r_{\rm ISCO}(M,J)$ in Boyer-Lindquist coordinates.

5.3.4 Growth and Decay of Bosonic Condensates Around Spinning Black Holes

The evolution of the cloud is governed by a simple set of differential equations [60]. Energy and angular momentum conservation requires that

$$\dot{M} + \dot{M}_S = -\dot{E}_{\rm GW} + \dot{M}_{\rm ACC} \,, \tag{5.30}$$

$$\dot{J} + \dot{J}_S = -\frac{1}{\mu_S} \dot{E}_{GW} + \dot{J}_{ACC},$$
 (5.31)

where M_S and J_S are the mass and the angular momentum of the scalar cloud, we have neglected the subdominant contributions of the mass of the disk and of those GWs that are absorbed at the horizon, and we have approximated the local mass and angular momentum by their ADM counterparts. The latter approximation is valid as long as backreaction effects are small, as we discuss below. The system is closed by two further equations

$$\dot{M} = -\dot{E}_S + \dot{M}_{ACC} \,, \tag{5.32}$$

$$\dot{J} = -\frac{1}{\mu_S} \dot{E}_S + \dot{J}_{ACC} \,,$$
 (5.33)

which describe the superradiant extraction of energy and angular momentum and the competitive effects of gas accretion at the BH horizon. In the equations above we have introduced the scalar energy flux that is extracted from the horizon through superradiance,

$$\dot{E}_S = 2M_S \omega_I \,, \tag{5.34}$$

where $M\omega_I = \frac{1}{48}(a/M - 2\mu_S r_+)(M\mu_S)^9$ for the l=m=1 fundamental mode. These equations assume that the scalar cloud is not directly (or only very weakly) coupled to the disk.

Representative results for the evolution of the system are presented in Fig. 5.5 where we consider the scalar-field mass $\mu_S = 10^{-18} \,\mathrm{eV}$ and mass accretion near the Eddington rate, $f_{\rm Edd} = 0.1$. We consider two cases: (I) the left set of plots corresponds to a BH with initial mass $M_0 = 10^4 M_{\odot}$ and initial spin $J_0/M_0^2 = 0.5$, whereas (II) the right set of plots corresponds to $M_0 = 10^7 M_{\odot}$ and $J_0/M_0^2 = 0.8$.

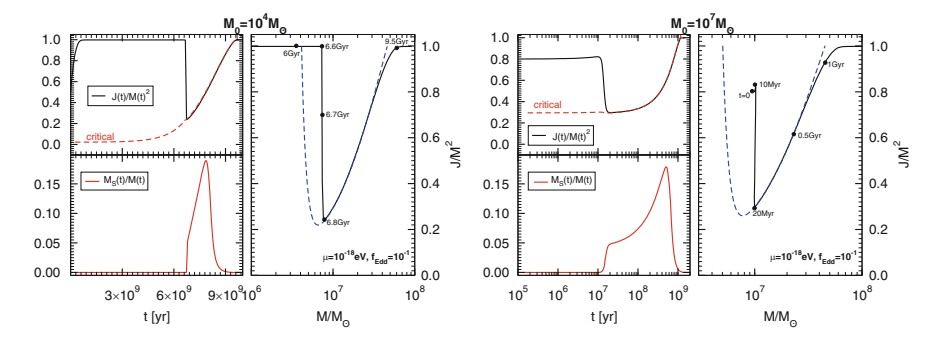


Fig. 5.5 Evolution of the BH mass and spin and of the scalar cloud due to superradiance, accretion of gas and emission of GWs. The two sets of plots show two different cases. In Case I (left set) the initial BH mass $M_0=10^4M_\odot$ and the initial BH spin $J_0/M_0^2=0.5$. The BH enters the instability region at about $t\sim 6$ Gyr, when its mass $M\sim 10^7M_\odot$ and its spin is quasi-extremal. The set of plots on the right shows Case II, in which $M_0=10^7M_\odot$ and $J_0/M_0^2=0.8$, and the evolution starts already in the instability region for this scalar mass $\mu=10^{-18}$ eV. For both cases, the left top panels show the dimensionless angular momentum J/M^2 and the critical superradiant threshold $a_{\rm crit}/M$ [cf. Eq. (4.28)]; the left bottom panels show the mass of the scalar cloud M_S/M (note the logarithmic scale in the x-axis for Case II); and the right panels show the trajectory of the BH in the Regge plane [57] during the evolution. The dashed blue line denotes the depleted region as estimated by the linearized analysis, i.e. it marks the threshold at which $\tau \sim \tau_{\rm ACC}$

In Case I, superradiance is initially negligible because $\mu_S M_0 \sim 10^{-4}$ and superradiant extraction is suppressed. Thus, the system evolves mostly through gas accretion, reaching extremality $(J/M^2 \sim 0.998)$ within the time scale $\tau_{ACC} \sim 10\tau_{Salpeter}$. At about $t \sim 6$ Gyr, the BH mass is sufficiently large that the superradiant coupling $\mu_S M$ becomes important. This corresponds to the BH entering the region delimited by a dashed blue curve in the Regge plane [57] shown in Fig. 5.5 for Case I. At this stage superradiance becomes effective very quickly: a scalar cloud grows exponentially near the BH (left bottom panel), while mass and angular momentum are extracted from the BH (left top panel). This abrupt phase lasts until the BH spin reaches the critical value a_{crit}/M [cf Eq. (4.28)] and superradiance halts. Because the initial growth is exponential, the evolution does not depend on the initial mass and initial spin of the scalar cloud as long as the latter are small enough, so that in principle also a quantum fluctuation would grow to a sizeable fraction of the BH mass in finite time.

Before the formation of the scalar condensate, the evolution is the same regardless of GW emission and the only role of accretion is to bring the BH into the instability window. After the scalar growth, the presence of GW dissipation and accretion produces two effects: (1) the scalar condensate loses energy through the emission of GWs, as shown in the left bottom panel of Fig. 5.5 [the signatures of this GW emission are discussed in Sect. 5.4.2 below]; (2) gas accretion returns to increase the BH mass and spin.

However, because accretion restarts in a region in which the superradiance coupling $\mu_S M$ is nonnegligible, the "Regge trajectory" $J(t)/M(t)^2 \sim a_{\rm crit}/M$ [cf.

Eq. (4.28)] is an attractor for the evolution and the BH "stays on track" as its mass and angular momentum grow. For Case I, this happens between $t \sim 6.8\,\mathrm{Gyr}$ and $t \sim 9.5\,\mathrm{Gyr}$, i.e. the Regge trajectory survives until the spin reaches the critical value $J/M^2 \sim 0.998$ and angular momentum accretion saturates.

A similar discussion holds true also for Case II, presented in the right set of plots in Fig. 5.5. In this case, the BH starts already in the instability regime, its spin grows only very little before superradiance becomes dominant, and the BH angular momentum is extracted in about 10 Myr. After superradiant extraction, the BH evolution tracks the critical value $a_{\rm crit}/M$ while the BH accretes over a time scale of 1 Gyr.

5.3.5 Superradiant Instabilities Imply No Highly-Spinning Black Holes

While GW emission is always too weak to affect the evolution of the BH mass and spin (nonetheless being responsible for the decay of the scalar condensate as shown in Fig. 5.5), accretion plays a more important role. From Fig. 5.5, it is clear that accretion produces two effects. First, for BHs which initially are not massive enough to be in the superradiant instability region, accretion brings them to the instability window by feeding them mass as in Case I. Furthermore, when $J/M^2 \rightarrow a_{\rm crit}/M$ the superradiant instability is exhausted, so that accretion is the only relevant process and the BH inevitably spins up again. This accretion phase occurs in a very peculiar way, with the dimensionless angular momentum following the trajectory $J/M^2 \sim a_{\rm crit}/M$ over very long time scales.

Therefore, a very solid prediction of BH superradiance is that supermassive BHs would move on the Regge plane following the bottom-right part of the superradiance threshold curve. The details of this process depend on the initial BH mass and spin, on the scalar mass μ_S and on the accretion rate. A relevant problem concerns the *final* BH state at the time of observation; namely, given the observation of an old BH and the measurement of its mass and spin, would these measurements be compatible with the evolution depicted in Fig. 5.5?

This problem is addressed in Fig. 5.6, which shows the final BH mass and spin in the Regge plane [57] (i.e. a BH mass-spin diagram) for $N=10^3$ Monte Carlo evolutions. We consider a scalar field mass $\mu=10^{-18}\,\mathrm{eV}$ and three different accretion rates $f_{\rm Edd}$ (defined as the fraction of mass accretion rate relative to the Eddington limit) and, in each panel, we superimpose the bounds derived from the linearized analysis, i.e. the threshold line when the instability time scale equals the accretion time scale (cf. Sect. 5.4 below for details). As a comparison, in the same plot we include the experimental points for the measured mass and spin of some supermassive BHs listed in [73].

Various comments are in order. First, it is clear that the higher the accretion rate the better the agreement with the linearized analysis. This seemingly counter-

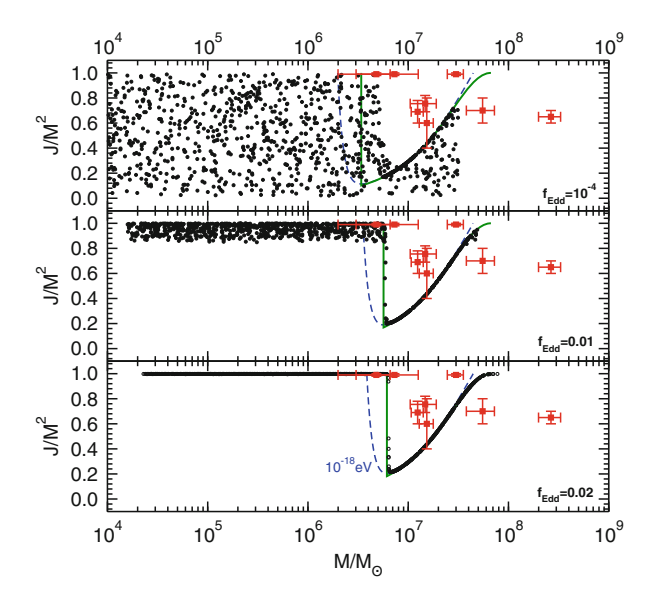


Fig. 5.6 The final BH mass and spin in the Regge plane for initial data consisting of $N=10^3$ BHs with initial mass and spin randomly distributed between $\log_{10} M_0 \in [4,7.5]$ and $J_0/M_0^2 \in [0.001,0.99]$. The BH parameters are then extracted at $t=t_F$, where t_F is distributed on a Gaussian centered at $\bar{t}_F \sim 2 \times 10^9$ yr with width $\sigma = 0.1\bar{t}_F$. We considered $\mu_S = 10^{-18}$ eV. The *dashed blue line* is the prediction of the linearized analysis obtained by comparing the superradiant instability time scale with the accretion time scale, $\tau \approx \tau_{\text{Salpeter}}/f_{\text{Edd}}$, whereas the *solid green line* denotes the region defined through Eq. (5.35). Old BHs do not populate the region above the *green threshold curve*. The experimental points with error bars refer to the supermassive BHs listed in [73]

intuitive result can be understood by the fact that higher rates of accretion make it more likely to find BHs that have undergone a superradiant instability phase over our observational time scales. In fact, for high accretion rates it is very likely to find supermassive BHs precisely on the "Regge trajectory" [57] given by $J/M^2 \sim a_{\rm crit}/M$ [cf. Eq. (4.28)].

Furthermore, for any value of the accretion rate, we always observe a depleted region (a "hole") in the Regge plane [57], which is not populated by old BHs. While the details of the simulations might depend on the distribution of initial mass and spin, the qualitative result is very solid and is a generic feature of the evolution. For the representative value $\mu_S = 10^{-18}\,\mathrm{eV}$ adopted here, the depleted region is incompatible with observations [73]. Similar results would apply for different values of μ_S in a BH mass range such that $\mu_S M \lesssim 1$. Therefore, as discussed

⁷Note that, through Eq. (5.27), the mass accretion rate only depends on the combination $f_{\rm Edd}M$, so that a BH with mass $M=10^6M_{\odot}$ and $f_{\rm Edd}\sim10^{-3}$ would have the same accretion rate of a smaller BH with $M=10^4M_{\odot}$ accreting at rate $f_{\rm Edd}\sim10^{-1}$. Because this is the only relevant scale for a fixed value of $μ_SM$, in our model the evolution of a BH with different mass can be obtained from Fig. 5.5 by rescaling $f_{\rm Edd}$ and $μ_S$.

in [53, 55, 57] and reviewed in Sect. 5.4 below, observations of massive BHs with various masses can be used to rule out various ranges of the boson-field mass μ_s .

Finally, Fig. 5.6 suggests that when accretion and GW emission are properly taken into account, the holes in the Regge plane are smaller than what naively predicted by the relation $\tau \approx \tau_{ACC}$, i.e. by the dashed blue curve in Fig. 5.6. Indeed, a better approximation for the depleted region is [60]

$$\frac{J}{M^2} \gtrsim \frac{a_{\rm crit}}{M} \sim 4\mu M \quad \cup \quad M \gtrsim \left(\frac{96}{\mu^{10} \tau_{\rm ACC}}\right)^{1/9},$$
 (5.35)

whose boundaries are shown in Fig. 5.6 by a solid green line. These boundaries correspond to the threshold value $a_{\rm crit}$ [cf. Eq. (4.28)] for superradiance and to a BH mass which minimizes the spin for which $\tau \approx \tau_{\rm ACC}$, for a given μ [56]. As shown in Fig. 5.6, the probability that a BH populates this region is strongly suppressed as the accretion rate increases.

5.3.6 Summary of the Evolution of Superradiant Instabilities

Because the results of [60] play an important role for the discussion of the next sections, it is relevant to summarize here the main features of the evolution of superradiant instabilities:

- The sole role of GW emission is to dissipate the dipolar bosonic cloud that forms as a result of the instability, but it does not have a significant effect on the evolution of the BH parameters. Nevertheless, such GW emission has a very peculiar signature, as discussed in Sect. 5.4.2 in the context of GW tests of bosonic clouds around spinning massive BHs.
- The mass of the cloud remains a sizeable fraction of the BH total mass over cosmological times, so that such systems can be considered as (quasi)-stationary hairy BHs for any astrophysical purpose.
- Nonetheless, the energy-density in the scalar field is negligible because the cloud typically extends over very large distances. Therefore, the geometry is very well described by the Kerr metric during the entire evolution. The prospects of imagining deviations from Kerr due to superradiantly-produced bosonic clouds in the electromagnetic band [9, 10] are low, but such systems are a primary source for observations aiming at testing the Kerr hypothesis through GW detection [4–8] [cf. Sect. 5.4.2 for a discussion].
- The role of gas accretion is twofold. On the one hand, accretion competes against superradiant extraction of mass and angular momentum. On the other hand accretion might produce the optimal conditions for superradiance, for example by increasing the BH spin before the instability becomes effective or by "pushing" the BH into the instability region in the Regge plane.

- The Monte Carlo simulations of [60] confirm that a very generic prediction of BH superradiant instabilities is the existence of holes in the Regge plane. For mass accretion near the Eddington rate, such depleted regions are very well described by Eq. (5.35), which refines the estimate obtained just by comparing the instability time scale against a typical accretion time scale (cf. Sect. 5.4 below). A more sophisticated analysis—including radiative effects and the geometry of the disk—would be important to refine the bounds previously derived [53, 55, 57, 74].
- Although the instability is strongly suppressed for higher multipoles, the first few (l,m) modes (and not only the dipole with l=m=1) can contribute to the depleted region in the Regge plane [57]. Because the superradiance condition depends on the azimuthal number m, for certain parameters it might occur that the modes with l=m=1 are stable, whereas the modes with l=m=2 are unstable, possibly with a superradiant extraction stronger than accretion. When this is the case, the depleted region of the Regge plane is the union of various holes [57], as shown in Fig. 5.8 below.

5.4 Astrophysical Black Holes as Particle Detectors

The "BH bomb" instabilities presented in Sect. 4 have important astrophysical implications that arise from the surprising connections between strong-field gravity and particle physics. One generic prediction of these instabilities is that—over the superradiance time scale—isolated, massive BHs should not spin above the superradiant threshold. In other words, superradiant instabilities set an upper bound on the BH spin which is smaller than the theoretical Kerr bound for the absence of naked singularities. Another prediction is a peculiar emission of GWs through various channels, as discussed below. These effects have been recently investigated in the contexts of testing stringy axions and ultralight scalars [57, 60, 67, 74–76] (these bounds being complementary to those coming from cosmological observations [77, 78]), to derive bounds on light vector fields [53] and on the mass of the graviton [55].

In this section we present an overview on this problem. As previously discussed, for a bosonic field of mass μ , the only parameter regulating the strength of the gravitational coupling to a BH of mass M is the dimensionless combination μM . The instability is maximum when $\mu M \sim 1$, i.e. when the Compton wavelength of the bosonic field is roughly comparable to the size of the BH. However, the details of the process depend on the nature of the bosonic field. As discussed in Sect. 4, for a given coupling μM the instability time scale is shorter for bosonic fields with spin due to spin-spin interactions.

5.4.1 Bounds on the Mass of Bosonic Fields from Gaps in the Regge Plane

A very generic and solid prediction of BH superradiant instabilities is the existence of holes in the Regge plane, as discussed in Sect. 5.3. Indeed, the estimates for the instability time scale, together with reliable spin measurements for massive BHs, can be used to impose stringent constraints on the allowed mass range of ultralight bosons [53, 55, 57, 76]. These bounds follow from the requirement that astrophysical spinning BHs should be stable, in the sense that the superradiant instability time scale τ should be larger than some observational threshold. For isolated BHs we can take the observational threshold to be the age of the Universe, $\tau_{\text{Hubble}} = 1.38 \times 10^{10} \text{ yr. However, for supermassive BHs we may worry about}$ possible spin growth due to mergers with other BHs and/or accretion. The most likely mechanism to produce fastly-spinning BHs is prolonged accretion [79]. Therefore, a conservative assumption to estimate the astrophysical consequences of the instability is to compare the superradiance time scale to the minimum time scale over which accretion could spin up the BH. Thin-disk accretion can increase the BH spin from a=0 to $a\approx M$ with a corresponding mass increase by a factor $\sqrt{6}$ [72]. For simplicity we assume that mass growth occurs via accretion at the Eddington limit, so that the BH mass grows exponentially with e-folding time given by the Salpeter time scale (5.28).

In order to quantify the dependence of the boson mass bounds on the mass and spin of supermassive BHs, in Fig. 5.7 we show exclusion regions in the BH Regge plane. More precisely, using the results derived in Sect. 4, we plot contours corresponding to an instability time scale of the order of the Salpeter time for four different masses of the bosonic field and considering the unstable mode with the largest growth rate. From top to bottom, the three panels refer to a spin-0, spin-1 and spin-2 field, respectively. The plot shows that observations of supermassive BHs with $10^5 M_{\odot} \lesssim M \lesssim 10^{10} M_{\odot}$ spinning above a certain threshold would exclude a wide range of boson-field masses. Because superradiance is stronger for bosonic fields with spin, the exclusion windows are wider as the spin of the field increases, and they also extend almost down to $J \sim 0$ in the case of spin-1 and spin-2 bosons. This latter feature is important because current spin measurements might be affected by large systematics.

Nonetheless, it's clear from Fig. 5.7 that almost any supermassive BH spin measurement would exclude a considerable range of masses. Similar exclusion plots exist in the region $M_{\odot} \lesssim M \lesssim 10^5 M_{\odot}$ for larger values of μ . Indeed, the only parameter that regulates the instability is the combination μM . Thus, the best bound comes from the most massive BHs for which spin measurements are reliable, e.g. the BH candidate Fairall 9 [80].

Using these arguments, from the analysis of [53, 55, 57] we can obtain the following bounds⁸:

$$m_S \lesssim 5 \times 10^{-20} \text{eV} \cup m_S \gtrsim 10^{-11} \text{eV},$$
 (5.36)

$$m_V \lesssim 5 \times 10^{-21} \text{eV} \cup m_V \gtrsim 10^{-11} \text{eV},$$
 (5.37)

$$m_T \lesssim 5 \times 10^{-23} \text{eV} \cup m_T \gtrsim 10^{-11} \text{eV},$$
 (5.38)

for the mass of ultralight scalar, vector and tensor fields, respectively. Note that, for a single BH observation, superradiant instabilities can only exclude a *window* in the mass range of the fields, as shown in Fig. 5.7. Nonetheless, by combining different

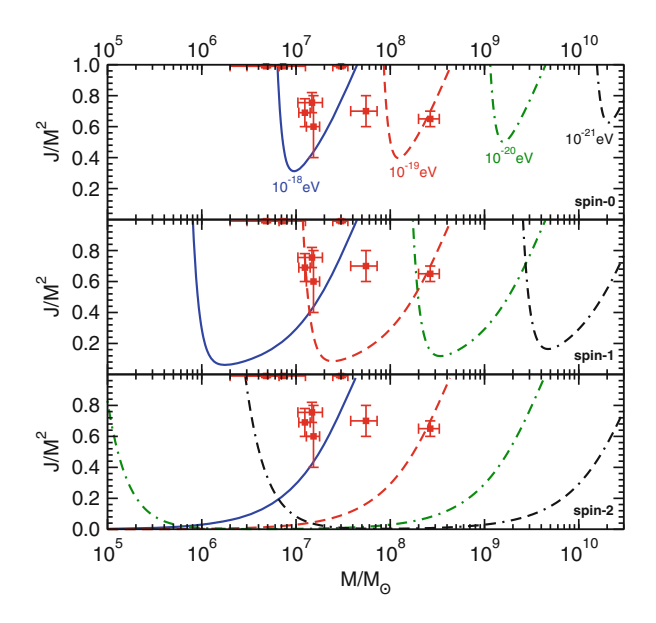


Fig. 5.7 Contour plots in the BH Regge plane [57] corresponding to an instability time scale shorter than τ_{Salpeter} for different values of the boson field mass $\mu\hbar$ and for the most unstable modes. Top, middle and bottom panels show the case of scalar (spin-0), vector (spin-1) and tensor (spin-2) massive fields. The experimental points (with error bars) refer to the supermassive BHs listed [73]. Supermassive BHs lying above each of these curves would be unstable on an observable time scale, and therefore each point rules out a range of the boson field masses. Note that the rightmost part of each curve is universal, $a \sim a_{\text{crit}}$ [cf. Eq. (4.28)], i.e. it does not depend on the spin of the field

⁸These bounds were obtained using a linearized analysis. By including the effects of GW emission and gas accretion, [60] shows that the linearized prediction should be corrected by Eq. (5.35), cf. Fig. 5.6 and discussion in Sect. 5.3. Nonetheless, such corrections would not affect the order of magnitude of these constraints. In [76], the authors estimate the statistical and systematic errors affecting these bounds, finding exclusions regions at approximately 2σ and 1σ for stellar-mass and supermassive BHs, respectively.

BH observations in a wide range of BH masses and assuming⁹ that spinning BHs exist in the entire mass range $M_{\odot} \lesssim M \lesssim 10^9 M_{\odot}$, one is able to constrain the range above, where the lower bound comes from the lightest massive BHs (with $M \approx 5 M_{\odot}$), whereas the upper bound comes from the heaviest supermassive BHs for which spin measurements are reliable. If the largest known supermassive BHs with $M \simeq 2 \times 10^{10} M_{\odot}$ [82, 83] were confirmed to have nonzero spin, we could get even more stringent bounds.

For each BH observation, the upper limit comes from the fact that when $M\mu \ll 1$ the time scale grows with some power of $1/(\mu M)$ and eventually the instability is ineffective on astrophysical time scales. The lower limit comes from the fact that the instability exists only when the superradiant condition is satisfied, and this imposes a constraint on μ for a given azimuthal number m.¹⁰ Indeed, the rightmost part of the curves shown in Fig. 5.7 for fixed μ is universal and arises from saturation of the superradiant condition, $a \sim a_{\rm crit}$, where $a_{\rm crit}$ is given in Eq. (4.27). Such condition does not depend on the spin of the field, and this explains why the upper bounds in Eqs. (5.36)–(5.38) are the same for scalar, vector and tensor fields.

As discussed above, higher multipoles might also be relevant and modes with (say) l=m=2 can be unstable in regions of the Regge plane where the dipolar l=m=1 mode is not superradiant. This is depicted in Fig. 5.8 for a QCD axion, which is described by the action (3.1) for a real scalar with no gauge field, $\mu_S=0$ and supplemented by the axion self-potential

$$U(\Psi) = f_a^2 \mu_a^2 \left[1 - \cos\left(\frac{\Psi}{f_a}\right) \right], \tag{5.39}$$

where μ_a is the axion mass¹¹ and f_a is the axion decay constant, which depends on the model but it is typically of the order of the GUT scale, $f_a \approx 10^{16}$ GeV.

Under certain conditions, the constraint (5.38) on massive spin-2 fields also applies to massive gravitons propagating on a Kerr BH [55], and sets a stringent bound on the mass of the graviton [84]. Similarly, the bound (5.37) on massive spin-1 fields might also be translated in a bound on the photon mass [53], although in this case the coupling between photons and accreting matter might quench the instability (see [53] for a discussion). A more rigorous analysis should be performed to assess whether plasma interactions can affect the bounds discussed above in the case of massive photons.

⁹Recently, the first detection of intermediate-mass BHs was reported [81], suggesting the BH mass spectrum might be populated continuously from few solar masses to billions of solar masses.

 $^{^{10}}$ As m increases, larger values of μ are allowed in the instability region and virtually any value of μ gives some unstable mode in the eikonal $(l, m \gg 1)$ limit. However, the instability is highly suppressed as l increases so that, in practice, only the first few allowed values of l = m correspond to an effective instability.

¹¹By expanding the potential (5.39) when $\Psi \ll f_a$, the nonlinearities can be neglected and the sine-Gordon potential reduces to a mass term for a Klein-Gordon field.

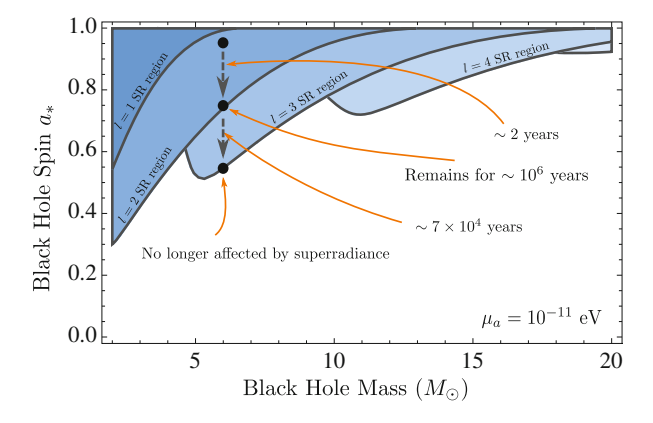


Fig. 5.8 Holes in the Regge plane for a QCD axion with mass $\mu_a=10^{-11}\,\mathrm{eV}$ and decay constant $f_a=6\times10^{17}\,\mathrm{GeV}$ for various multipoles $(l=1,\ldots,5)$. Shaded regions correspond to BH parameters which would result in spindown within $10^6\,\mathrm{yr}$. The description refers to a representative evolution of a BH with $M=6M_\odot$ and initial spin a/M=0.95. From [76]

5.4.2 Gravitational-Wave Signatures and Bosenova

Upcoming precise spin measurements of massive BHs [9, 10] will be useful to refine the bounds discussed above. However, a very different phenomenology can be probed through detection of GWs that are possibly emitted by bosonic clouds around spinning BHs [57, 60, 76]. The GW phenomenology of superradiance has mostly focused on axions and the discussion of this section will be mainly specialized to these fields, although essentially all the results are valid for a generic massive scalar field. When the specific analysis applies to a generic massive scalar, we will denote its mass by μ_S , whereas μ_a and f_a will specifically refer to axions as in Eq. (5.39).

As discussed in [57, 75, 76], a bosonic condensate around a spinning BH as the one depicted in Fig. 5.4 would emit GWs through three different channels, which are discussed below.

Axion Annihilation A nonspherical cloud anchored to a spinning BH [cf. Eq. (5.23)] would possess a quadrupole moment and would emit GWs. In a particle-like description of the interaction, such waves can be interpreted as arising from the annihilation of the scalar field to produce gravitons [57]. As previously discussed, the wavelength of such radiation would be in general smaller than the size of the source. Thus, even when the cloud is extended over large distances and is nonrelativistic, the quadrupole formula does not apply because the emission is incoherent [57, 60, 67]. A detailed relativistic computation has been recently performed in [67], finding that the emitted GW flux for the l multipole scales as

$$\dot{E}_{\rm GW} \propto \left(\frac{M_S}{M}\right)^2 (\mu_S M)^{4l+10} \,. \tag{5.40}$$

This result is formally valid only when $\mu_S M \ll 1$, but it approximates the exact results reasonably well also for moderately large values of the coupling. In fact, it can be considered as an upper bound for the exact flux that has to be computed numerically by solving the Teukolsky equation [60, 67]. This radiation is *monochromatic* with frequency

$$f_{\rm ann} \sim 10 \,\mathrm{kHz} \left(\frac{\mu_S \hbar}{10^{-11} \,\mathrm{eV}} \right) \,,$$
 (5.41)

and is therefore associated to a very peculiar signal. By estimating the annihilation rate and the occupation number of a single axion level, [76] computed the GW strain¹² of this signal and discussed the prospect for detection with the Advanced LIGO/Virgo experiments [4, 5] and with an eLISA-like mission [85]. Although the frequency of the signal (5.41) is independent from the BH mass, in practice $\mu_S M \lesssim 1$ for the axion occupation number to grow sufficiently fast through superradiance. Thus, ground-based detectors would be sensitive to stellar-mass BHs, whereas space-based detectors are sensitive to signatures of axionic clouds around supermassive BHs. The expected number of events estimated in [76] for these two cases is shown in Fig. 5.9. Using recent mass distributions for stellar BHs and supermassive BHs, [76] estimated an event rate as large as $\mathcal{O}(10^5)$, assuming axions

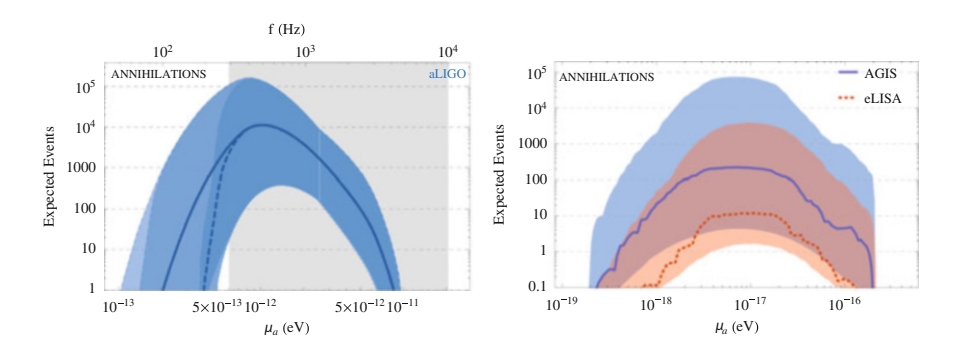


Fig. 5.9 Expected number of axion annihilation events observable with aLIGO/aVirgo [4, 5] (*left panel*) and for space-based detectors AGIS and eLISA [85] as a function of the axion mass. Each event in the left (resp. right) panel can last thousands (resp. millions) of years. In the *left panel*, the vertical shaded region is disfavored by BH spin measurements assuming the QCD axion coupling strength. Each of the three bands corresponds to cutting off the BH mass distribution at a maximum mass of $\{30, 80, 160\}M_{\odot}$ (*dark, medium*, and *light blue*, respectively) including optimistic and pessimistic estimates of astrophysical uncertainties. In the *right panel*, the *shaded bands* bracket the optimistic and pessimistic estimates. See [76] for details

¹²The GW strain is $h = \sqrt{4P/(d^2\omega^2)}$, for a source emitting power *P* at angular frequency ω and at distance *d* away from the detector. In the formalism of [76], the power *P* can be computed in terms of transition rate Γ and occupation number *N*, the former depends on the emission process, whereas the latter depends on superradiance.

with masses in the optimal range for a given BH exist. The range of axion masses that is detectable is complementary to that excluded by BH spin measurements (cf. Sect. 5.4).

Level Transitions Because the scalar condensate has a hydrogenic-like spectrum [cf. Eq. (4.27)], GW emission can occur from level transitions between states with same harmonic indices (l, m) but different overtone numbers n, similarly to photon emission through atomic transitions. This process occurs when the growth rate of some n > 0 mode is stronger than that of the fundamental n = 0, as this can happen for high values of (l, m) [57] (a detailed analysis of this effect is presented in [61]). The frequency of the emitted graviton is given by the frequency difference between the excited (n > 0) state and the ground (n = 0) state,

$$\omega_{\text{trans}} \sim \frac{\mu_S}{2} (M \mu_S)^2 \left(\frac{1}{n_g^2} - \frac{1}{n_e^2} \right),$$
 (5.42)

and the corresponding wavelength is usually much longer than the size of the system. Therefore, in this case the quadrupole formula is valid [57]. In this approximation, the single axion transition rate reads [76]

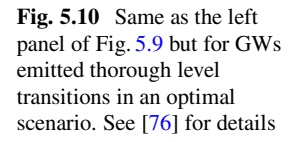
$$\Gamma_t \sim \mathcal{O}(10^{-6} \div 10^{-8}) \frac{(\mu_s M)^9}{M} \,.$$
 (5.43)

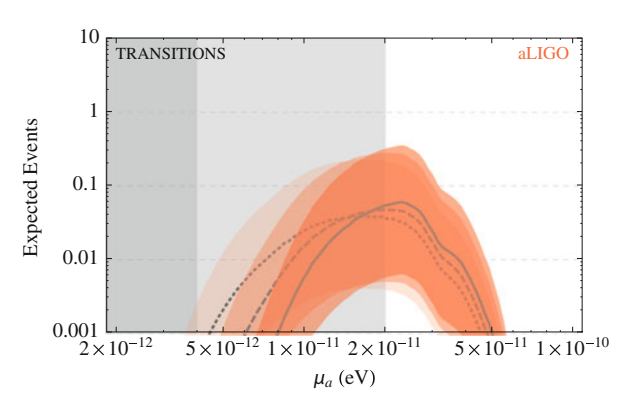
Although this is usually tiny, the GW strain is enhanced by the occupation number of the two levels, which grow exponentially through superradiance. Also in this case the signal is monochromatic. For the dominant transition, the typical frequency is

$$f_{\text{trans}} \sim 13 \text{Hz} \left(\frac{\mu_S \hbar}{10^{-11} \text{ eV}} \right)^3 \left(\frac{M}{5 M_{\odot}} \right),$$
 (5.44)

which falls in the sensitivity bands of advanced ground-based detectors for an axion with mass about 10^{-11} eV around a stellar-mass BH with $M \sim 5 M_{\odot}$, whereas it falls within eLISA milliHerz band for an axion with mass about 10^{-15} eV around a supermassive BH with $M \sim 10^5 M_{\odot}$. The number of axion transition events for aLIGO/aVirgo as estimated in [76] is shown in Fig. 5.10. For space-based detectors, the peak of sensitivity falls in the range of intermediate-mass BHs, for which precise mass distributions are lacking. This affects the event estimates, but it is promising that the reach radius for axion transition signals of a eLISA-like detector would extend up to hundred megaparsec [76].

GW Bursts from Bosenova Explosions When nonlinear terms are taken into account, novel effects in the scalar condensate might arise. For example, axion-like fields described by the sine-Gordon potential (5.39) would collapse when the mass of the axion cloud $M_S \approx 1600(f_a/m_P)^2 M$, with m_P being the Planck mass [74, 75]. This process was dubbed "bosenova" in analogy with a similar





phenomenon occurring in condensed-matter systems. For sufficiently strong self-interactions ($f_a \ll m_{\rm P}$) this can happen during the superradiant growth and before extracting all the BH spin as allowed by the superradiant condition. For example, if f_a corresponds to the GUT scale, $f_a \approx 10^{16}\,{\rm GeV}$, the bosenova occurs when $M_S \gtrsim 0.16M$. As shown in the evolutions presented Sect. 5.3, the scalar cloud can typically attain such fraction of the BH mass under conservative assumptions (cf. Fig. 5.5 and [60]), and therefore the effects of bosenova can have interesting phenomenological applications.

During the bosenova, a fraction of the cloud energy is absorbed by the BH, whereas the majority of the rest is emitted in a GW burst, leaving just a small fraction of the cloud bound to the BH [57, 74, 75]. This reduces the size of the cloud and the effects of nonlinearities. After the first collapse, the cloud is replenished through superradiance until the next bosenova possibly occurs (assuming the conditions are such that nonlinearities can become important before superradiant extraction is exhausted). This superradiance-bosenova cycle repeats until all available BH spin is exhausted. Thus, at variance with annihilation and level transition, the signal from bosenova explosions is a *periodic* emission of bursts, whose separation depends on the fraction of the cloud which remains bound to the BH after each subsequent collapse.

The typical frequency of a single burst is [74–76]

$$f_{\rm bn} \sim 30 \,\mathrm{Hz} \left(\frac{16 r_{\rm cloud}}{t_{\rm bn}}\right) \left(\frac{\mu_a M}{0.4 l}\right)^2 \left(\frac{10 M_{\odot}}{M}\right),$$
 (5.45)

where $t_{\rm bn}$ is the infall time and $r_{\rm cloud}$ is the characteristic size of the cloud as given in Eq. (5.22). For example, a typical bosenova burst from a $10M_{\odot}$ BH would last approximately 1 ms and, as the result of multiple subsequent explosions, there can be various spikes separated by a quiet period of approximately 300s [76]. A

quadrupole estimate of the GW strain for such signal yields [74–76]

$$h \sim 10^{-21} \left(\frac{\text{kpc}}{d}\right) \left(\frac{\epsilon}{0.05}\right) \left(\frac{16r_{\text{cloud}}}{t_{\text{bn}}}\right)^2 \left(\frac{\mu_a M}{0.4l}\right) \left(\frac{M}{10M_{\odot}}\right) \left(\frac{f_a}{f_a^{\text{max}}}\right)^2, \quad (5.46)$$

where ϵ is the fraction of the cloud falling into the BH (typically $\epsilon \approx 5\%$ [75]), f_a^{max} is the largest coupling for which bosenova occurs and d is the distance of the source from the detector.

Finally, [86] have modeled the dynamics of the axion cloud by a simple cellular automaton, showing that the process exhibits self-organized criticality.

5.4.3 Floating Orbits

When the bosonic field is coupled to matter, new effects related to stimulated emission may be triggered, modifying the inspiral dynamics of compact binaries [87–89]. Figure 5.11 illustrates one such process: a point particle of mass m_p orbits a supermassive BH on a quasi-circular orbit of Boyer-Lindquist radius r_0 . The point particle is coupled to a scalar field through the trace of its stress-energy tensor \mathcal{T} , yielding the equation of motion for the scalar field,

$$\left[\Box - \mu_s^2\right] \Phi = \alpha \mathcal{T} \,. \tag{5.47}$$

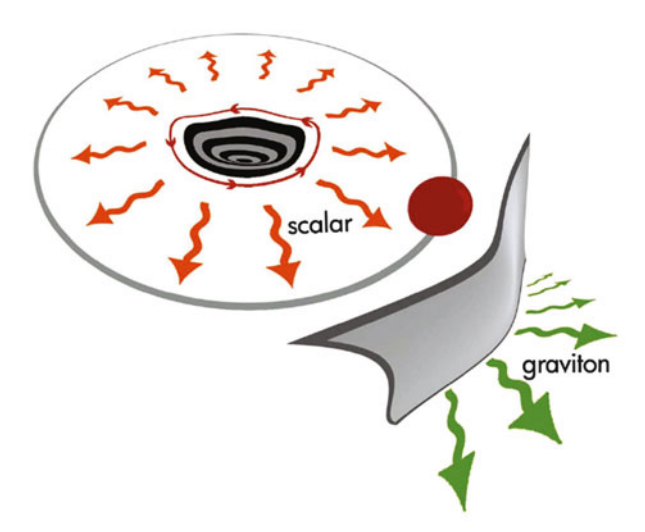


Fig. 5.11 Pictorial description of floating orbits. An orbiting body excites superradiant scalar modes close to the BH horizon which are prevented from escaping to infinity due to their being massive (represented by the *gray* "wall"). Since the scalar field is massive, the flux at infinity consists solely of gravitational radiation. From [87]

the coupling α is related to the specific theory under consideration [87, 90]. Within a perturbation framework, for small masses m_p the scalar field Φ is small and its backreaction in the geometry can be neglected. In other words, the particle follows a geodesic in the spacetime of a rotating BH, emitting scalar and gravitational waves of frequency proportional to the orbital frequency of the circular geodesic.

The power emitted as gravitational radiation can be estimated with the use of the quadrupole formula to be $\dot{E}_{\infty}^g = 32/5 \left(r_0/M\right)^{-5} m_p^2/M^2$. This is the power at spatial infinity in the low-frequency regime, the flux through the horizon being negligible for large orbital radii. The scalar flux at infinity can be computed in the low-frequency regime,

$$\dot{E}_{\infty}^{s} = \frac{\alpha^{2} M^{2}}{12\pi} \frac{\left(1 - \mu_{s}^{2} r_{0}^{3} / M\right)^{3/2}}{r_{0}^{4}} m_{p}^{2} \Theta(\Omega_{p} - \mu_{s}), \qquad (5.48)$$

where $\Theta(x)$ is the Heaviside function. As expected, for orbital radii large enough that the orbital frequency $\Omega_p < \mu_s$, scalar radiation is quenched at spatial infinity. However, we learned in Sect. 4.6 that the Kerr spacetime admits the existence of *superradiant* resonances at

$$\omega_{\text{res}}^2 = \mu_s^2 - \mu_s^2 \left(\frac{\mu_s M}{l+1+n}\right)^2, \quad n = 0, 1, \dots$$
 (5.49)

Thus, one might expect enhanced scalar flux at the horizon close to these resonances. Indeed, Fig. 5.12 shows that the flux of (scalar) energy at the horizon is greatly enhanced close to these resonances. We can estimate the peak flux close to

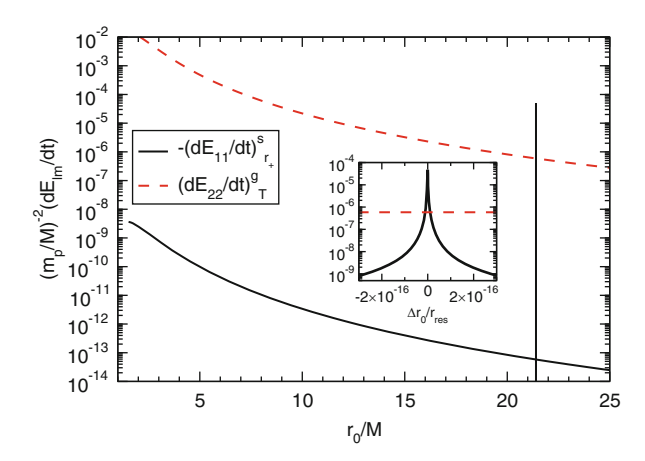


Fig. 5.12 Dominant fluxes of scalar and gravitational energy (l=m=1 and l=m=2, respectively) for $\mu_s M=10^{-2}$, $\alpha=10^{-2}$ and a=0.99M. The *inset* is a zoom around resonance. From [87]

the resonant frequencies for large distances and for l = m = 1,

$$\dot{E}_{r+}^{s,\text{peak}} \sim -\frac{3\alpha^2 \sqrt{\frac{r_0}{M}} m_p^2 M}{16\pi r_+ (M^2 - a^2) \left(\frac{a}{2r_+} - (\frac{M}{r_0})^{3/2}\right) \mathcal{F}},$$
(5.50)

with $\mathcal{F} = 1 + 4P^2$. The scalar flux at the horizon *grows* in magnitude with r_0 and it is negative, due to superradiance, at sufficiently large distances.

Thus, for any $\mu_s M \ll 1$, there exists a frequency $\omega_{\rm res} \lesssim \mu_s$ for which the total flux $\dot{E}_{\infty}^s + \dot{E}_{r_+}^s + \dot{E}_{\infty}^g + \dot{E}_{r_+}^g = 0$, because the negative scalar flux at the horizon is large enough to compensate for the other positive contributions. These points are called *floating orbits*, because an energy balance argument suggests that at these locations the small point particle does not inspiral (neither inwards nor outwards). All the energy lost at infinity under GWs is provided entirely by the rotational energy of the BH. Under ideal conditions, floating would stop only when the peak of the scalar flux at the horizon is too small to compensate for the gravitational flux, $|\dot{E}^g| > |\dot{E}_{\rm peak}^s|$.

Floating orbits are not possible in GR [91]. Thus, they are a smoking-gun of new physics; the orbital frequency at which the particle stalls exactly matches the mass of the putative fundamental field, making BHs ideal self-tuned "particle detectors". The existence of floating orbits manifests itself in a sizeable and detectable dephasing of gravitational waves, with respect to pure GR waveforms [69, 87–89].

5.5 Are Black Holes in the Universe of the Kerr Family?

A series of works established what is now known as uniqueness theorems in GR: regular, stationary BHs in Einstein-Maxwell theory are extremely simple objects, being characterized by three parameters only: mass, angular momentum and electric charge [92–96]. Because of quantum and classical discharge effects, astrophysical BHs are thought to be neutral to a very good approximation [14, 36, 37, 69, 97]. Therefore the geometry of astrophysical BHs in GR is simply described by the two-parameter Kerr metric (3.5). On the other hand, NSs—the most compact, nonvacuum objects that exist—cannot be more massive than $\sim 3M_{\odot}$ [98]; taken together, these two results imply that any observation of a compact object with mass larger than $\sim 3M_{\odot}$ must belong to the Kerr family. Therefore tests of strong-field gravity targeting BH systems aim at verifying the "Kerr hypothesis" in various ways [1].

We saw already that when (electro-vacuum) GR is enlarged to include minimally coupled, massive scalar fields, Kerr BHs may become superradiantly unstable, cf. Sect. 4.6. For *real* scalars, this leads to a bosonic cloud around the BH, whose nonzero quadrupole moment results in periodic GW emission. Thus, the end-state is thought to be a Kerr BH with lower spin [54, 58, 59], as dictated by the uniqueness theorems. The analysis presented in the Sect. 5.3 confirms this picture [60].

5.5.1 Circumventing the No-Hair Theorem with Complex Scalars

However, there is a subtle way of circumventing the hypothesis of the uniqueness theorem. Namely, the scalar field could be time dependent but in such a way that the geometry remains stationary. This requires that the stress-energy tensor of the scalar field shares the same symmetries of the metric, similarly to the AdS case discussed in Sect. 4.5.1. Having such stationary configuration is impossible for a single real scalar field, but for a *complex* scalar field with time dependence $\Psi(t, \mathbf{x}) = e^{-i\omega t}\psi(\mathbf{x})$, it is possible precisely when the frequency saturates the superradiant condition (1.1), i.e. when

$$\omega = m\Omega_{\rm H} \,. \tag{5.51}$$

This is easily seen from the analytic formula (4.27) together with the flux result (3.79). Consequently, there is no scalar field flux through the horizon as long as (5.51) is obeyed and the field is allowed to be complex.

we provide details on their construction, discussing properties of the ansatz, the field equations, the boundary conditions and the numerical strategy.

This argument suggests the existence of asymptotically-flat rotating BHs with complex scalar hair. In fact, the argument parallels the discussion of hairy solutions in asymptotically AdS spacetimes, discussed in Sect. 4.5.1. Such solutions in asymptotically flat spacetimes were indeed found and studied in the limit that the BH is extremal [99, 100]. The solutions in full generality were found in [101], while a detailed discussion on their construction and physical properties can be found in [102]. The ultimate physical reason for the existence of a stationary geometry endowed with an oscillating scalar field is that GW emission is halted due to cancellations in the stress-energy tensor, which becomes independent on the time and azimuthal variables, thus avoiding GW emission and consequent angular momentum losses.

The fact that the condition (5.51) for the existence of hairy BHs lies precisely at the threshold of the superradiant condition (1.1) arises from the fact that *real* frequency bound states are possible if and only if Eq. (5.51) is satisfied. The hairy BHs found in [101] can be thought of as nonlinear extensions of the linear bound states, when the backreaction of the scalar condensate on the metric is included (see also [103]).

The minimally coupled hairy solutions are described by the following ansatz [101]

$$ds^{2} = e^{2F_{1}} \left(\frac{dR^{2}}{N} + R^{2} d\theta^{2} \right) + e^{2F_{2}} R^{2} \sin^{2} \vartheta (d\varphi - W dt)^{2} - e^{2F_{0}} N dt^{2} ,$$

$$\Psi = \phi(r, \vartheta) e^{i(m\varphi - \omega t)} ,$$
(5.52)

where $N \equiv 1 - R_H/R$, the parameter R_H being the location of the event horizon. The five functions of (R, ϑ) , F_0, F_1, F_2, N, ϕ , are obtained by solving numerically a system of nonlinear, coupled PDEs, with appropriate boundary conditions that ensure both asymptotic flatness and regularity at the horizon; the latter requirement implies condition (5.51).

The solutions form a five-parameter family described by the ADM mass M, the ADM angular momentum J, the Noether scalar charge Q (which roughly measures the amount of scalar hair outside the horizon), and by two discrete parameters: the azimuthal harmonic index m and the node number n of the scalar field [101]. One may regard n=0 as the fundamental configuration and $n \ge 1$ as excited states. Remarkably, these solutions interpolate between a Kerr BH when $q \equiv Q/2J = 0$ and a rotating boson stars [104, 105] when q=1. The latter are (horizonless) gravitating solitons, that are discussed in Sect. 5.8.2 in the context of so-called "BH mimickers". Because the scalar charge Q is a free parameter, the solutions found in [101] corresponds to hairy spinning BHs with primary hair (in contrast to BH solutions with secondary hair, in which the scalar charge is fixed in terms of other parameters, such as the mass [1]).

Figure 5.13 shows the parameter space for the ground-state (n = 0) solutions with m = 1 [101]. Interestingly, uniqueness in the (M, J) subspace is broken because there is a region in which hairy BHs and the Kerr solution coexist with the same values of mass and angular momentum. However, no two solutions were found with the same (M, J, q) [101]. In the region of nonuniqueness, hairy BHs

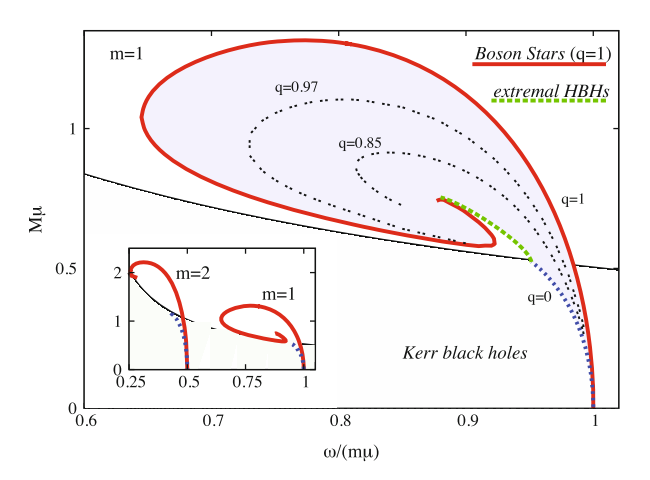


Fig. 5.13 The M- ω parameter space of hairy BHs with a complex scalar field for n=0 and m=1. These solutions exist in the *shaded blue region*. The *black solid curve* corresponds to extremal Kerr BHs and nonextremal Kerr BHs exist below it. For $q \equiv Q/2J = 0$, the domain of existence connects to Kerr solutions (*dotted blue line*). For q=1, hairy BHs reduce to boson stars (*red solid line*). The final line that delimits the domain of existence of the hairy BHs (*dashed green line*) corresponds to extremal BHs, i.e. with BHs with zero temperature. The *inset* shows the boson star curves for m=1,2. Units in the axes are normalized to the scalar field mass μ . Adapted from [101]

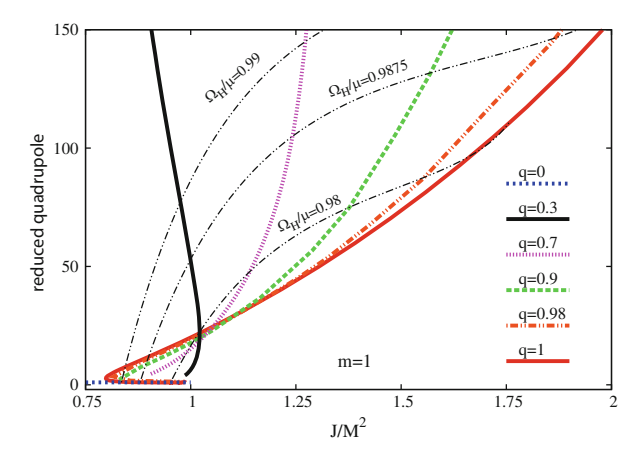


Fig. 5.14 Quadrupole moment of a hairy BH normalized by its Kerr value for the same mass and angular momentum and as a function of the dimensionless spin J/M^2 . Several lines of constant $\Omega_{\rm H}$ (dashed black) and $q \equiv Q/2J$ are displayed. From [101]

have *larger* entropy than the corresponding Kerr BHs. Therefore, the former cannot decay into the latter adiabatically.

As found in [101], the quadrupole moment and the angular frequency at the ISCO can differ significantly for hairy BHs, as compared to the standard Kerr values. This is shown in Fig. 5.14

In fact, in one corner of the parameter space these solutions can be interpreted as Kerr BHs perturbed by a small scalar field (and whose quadrupole moment is close to that of Kerr), whereas in the opposite corner they describe a small BH within a large boson star. In the latter case the properties of the solutions are resemble those of a stellar configuration rather than those of a BH.

Finally, hairy BHs have a richer structure of ergoregions than Kerr. For example, besides the ergosphere of Kerr-like configurations (cf. Fig. 3.2) also *ergosaturn* can form in a certain region of parameter space [106].

Nonlinear, hairy solutions were also extended to encompass rotating, charged geometries [68] whereas in [107, 108] these solutions were constructed and analyzed analytically at linear level.

5.5.2 Other Hairy Solutions and the Role of Tidal Dissipation

Generalizations were soon found that encompass hairy BHs with self-interacting scalar fields. For example, in [109] the authors studied a complex massive scalar field with quartic plus hexic self-interactions, dubbed nonlinear *Q*-clouds. Without the self-interactions, it reduces to the hairy solutions just described and correspond to zero modes of the superradiant instability. Non-linear *Q*-clouds, on the other

hand, are also in synchronous rotation with the BH horizon; but they exist on a twodimensional subspace, delimited by a minimal horizon angular velocity and by an appropriate existence line, wherein the nonlinear terms become irrelevant and the Qcloud reduces to a linear cloud. Thus, Q-clouds provide an example of scalar bound states around Kerr BHs which, generically, are not zero modes of the superradiant instability. Note that self-interaction terms only become important in the nonlinear regime: accordingly, it could be anticipated that nonlinear solutions exist (where the nonlinear terms play the role of an effective mass term) despite not corresponding to any superradiant bound state in the linear regime.

Other hairy solutions were also found in higher dimensional, asymptotically flat spacetime [110]; the construction parallels that of AdS spacetime (see Sect. 4.5.1 and [111]) and consists on finding rotating BHs with scalar hair and a regular horizon, within five dimensional Einstein's gravity minimally coupled to a complex, massive scalar field doublet. They are described by their mass M, two equal angular momenta and a conserved Noether charge Q, measuring the scalar hair. For vanishing horizon size the solutions reduce to five dimensional boson stars. In the limit of vanishing Noether charge density, the scalar field becomes pointwise arbitrarily small and the geometry becomes, locally, arbitrarily close to that of a specific set of Myers-Perry BHs (the higher-dimensional versions of the Kerr solution [112]); but there remains a global difference with respect to the latter, manifest in a finite mass gap. Thus, the scalar hair never becomes a linear perturbation of the Myers-Perry geometry. This is a qualitative difference when compared to Kerr BHs with scalar hair [101]. Whereas the existence of the latter can be anticipated in linear theory, from the existence of scalar bound states on the Kerr geometry (i.e. scalar clouds), the hair of these Myers-Perry BHs is intrinsically nonlinear.

An aspect that deserves to be highlighted is condition (5.51) for stationary solutions, which holds even when the hairy solution cannot easily be mapped onto a linearly, superradiantly unstable spacetime. This condition is tightly connected to tidal dissipation, in turn associated with superradiance, as we explained in Sect. 2.6 (see also [113, 114]). In summary, if the scalar "cloud" does not obey Eq. (5.51), tidal forces (of gravitational or other nature) will act and the system cannot possibly be in equilibrium. This fact is reminiscent of the phenomenon of "tidal locking" that occurs, for instance, in the Earth-Moon system [113].

5.5.3 Formation of Hairy Solutions and Bounds on Bosonic Fields

In parallel with the open problem of stability of the hairy BHs discussed above, a relevant question is the mechanism of formation of such solutions. Formation scenarios based on collapse or Jeans-like instability arguments are hard to devise. Indeed, if the collapsing matter does not possess any scalar charge, it is reasonable

to expect that collapse would form a Kerr BH, which might eventually migrate towards a hairy BH solution through superradiant amplification of a scalar-field fluctuation. However, as we discussed in Sect. 5.3, should these solutions arise from a superradiant instability of the Kerr metric, the energy-density of the scalar field is negligible and the geometry would be very well described by the Kerr solution [60]. In other words, superradiant instabilities require a Kerr BH to start with, and they can at most produce "light" scalar clouds, i.e. condensates which backreact very weakly on the geometry. The physical reason is that superradiance can only extract a finite amount of mass from the BH (at most 29 % of the initial BH mass [115]), and therefore the scalar cloud can only grow to a limited value. Although it is unlikely that configurations that deviate considerably from Kerr can arise from the evolution of initially isolated Kerr BHs, they may arise as the end-state of some other initial conditions, most likely involving a large scalar field environment; for instance they could arise from the collapse of ordinary stars inside a large boson-star environment.

Finally, the putative existence of hairy BH solutions as the end-state of the superradiant instability does *not* invalidate any of the results of Sects. 5.3 or 5.4. The reason is of course that hairy BHs lie along the $\omega = m\Omega \sim \mu$ line. In other words, for a Kerr BH to evolve towards a hairy BH it will necessarily loose angular momentum, in the same way as Kerr BHs do, and as taken into account in Sect. 5.3.

5.6 Plasma Interactions

Already in his PhD thesis, Teukolsky proposed that plasmas could be used as mirrors to trigger superradiant instabilities [116, 117]. Because the frequency of amplified radiation is much smaller than the plasma frequency ω_p^{-1} (cf Eq. (4.51)) of the interstellar medium, photons scattered by a BH in vacuum would be reflected by a spherically-symmetric plasma distribution.

This process was recently analyzed in [118] [cf. Sect. 4.9.1]. If the background is slowly-varying relative to the plasma time scale ω_p^{-1} and the density gradients are small compared to the gravitational field, then [119] the relevant dynamical equation is given by Eq. (4.52), which is equivalent to the Proca equation (4.34) when the plasma is homogeneous. In this simple case the plasma frequency ω_p can be identified with the mass μ_V of the vector field and all the results discussed for Proca fields around a Kerr BH can be directly applied [118]. In a more realistic situation the plasma will have an inhomogeneous distribution due to the local gravitational field near the BH, e.g., the density would peak at a few Schwarzschild radii whereas it would be negligible near the horizon. In this case a detailed model for matter distribution is necessary for a quantitative assessment, although preliminary computations show that the frequency and the time scale of the instability are insensitive to local inhomogeneities near the horizon [118]. As an example of superradiance stimulated amplification in a realistic setting, [120] studied superradiant confinement in a toroidal magnetosphere around a Kerr BH,

5.6 Plasma Interactions 193

arguing that the repeated amplification of EM (with time scales of the order of the second for stellar-mass BHs) might be a model for periodic γ -ray bursts.

This class of plasma-triggered superradiant instabilities are also relevant for small primordial BHs in the early universe [121]. When formed at redshift *z*, such BHs are surrounded by a mean cosmic electron density,

$$n = n_0 (1+z)^3 \approx 220 \,\mathrm{cm}^{-3} \left(\frac{1+z}{10^3}\right)^3$$
, (5.53)

which translates to a time-dependent plasma frequency through Eq. (4.51). Because the cosmological evolution occurs on a much longer time scale than the BH evolution, we can adopt an adiabatic approximation and treat n as constant during the energy extraction phase at a given z.

In order for the superradiance instability to be effective at a given redshift z, the instability time scale must be much shorter than the cosmological evolution time scale. By comparing the time scale (4.41) (with l=m=1 and after identifying $\mu_S=\omega_p$) with the age of the Universe $\tau_{\rm age}$ as a function of redshift, we show in Fig. 5.15 the Regge plane for primordial BHs with mass in the range $10^{-9}M_{\odot} < M < M_{\odot}$ for three representative redshift values. Similarly to the previous cases, at any plotted z, BHs located above the corresponding curve are unstable due to superradiant instability with $\tau < \tau_{\rm age}$. It is easy to derive an upper bound on the BH mass corresponding to the portion of the Regge plane where superradiant instability

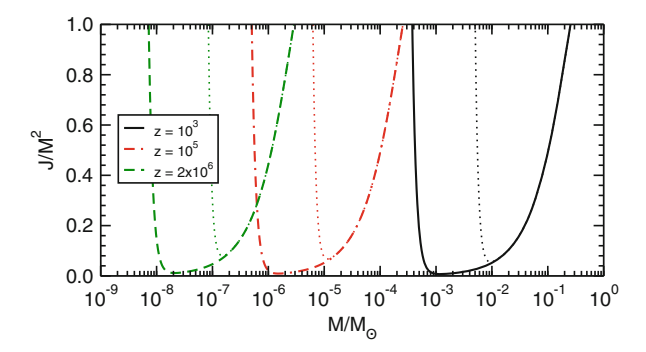


Fig. 5.15 Contour plots in the BH Regge plane [56, 57] corresponding to a plasma-triggered instability of a primordial BH whose time scale is shorter than the age of the universe at a given redshift, assuming a mean cosmic gas density (5.53). *Thick* and *thin curves* correspond to polar and axial modes, respectively [56]. In both families, the rightmost part of each curve is described by $J/M^2 \sim 4M\omega_p$. Roughly speaking, primordial BHs in the mass range $7 \times 10^{-9} M_{\odot} < M < 0.2 M_{\odot}$ go through a cosmic era (at some redshift $10^3 < z < 2 \times 10^6$) when the superradiant instability is effective. From [118]

starts becoming effective. This reads [118]

$$\frac{M}{M_{\odot}} \lesssim 0.19 \frac{a}{M} \left(\frac{1+z}{10^3}\right)^{-3/2}$$
 (5.54)

In other words, a primordial BH with mass M and spin a satisfying the relation above will pass through an epoch at redshift z when the mean gas density is such that the superradiant instability is effective.

As previously discussed, a spinning BH could lose most of its rotational energy over a short time scale as a result of the superradiant instability. Because the threshold curves shown in Fig. 5.15 extend almost down to $J \sim 0$, a single primordial BH will essentially lose all its initial angular momentum, whereas its mass loss reads [118]

$$\frac{\Delta M}{M} \approx \frac{a\omega_R}{1 - 2a\omega_R} \approx 10^{-3} \frac{a}{M} \left(\frac{1+z}{10^3}\right)^{3/2} \left(\frac{M}{10^{-3}M_{\odot}}\right),$$
(5.55)

where in the last step we assumed $(M/M_{\odot}) \ll 2 \times 10^5 (1+z)^{-3/2}$. According to this estimate, in the linear approximation the efficiency of the energy extraction at $z \sim 10^5$ for $M \sim 10^{-4} M_{\odot}$ is roughly $a/M \times 20 \%$.

Primordial BHs are intensively investigated as a possible solution of the dark matter problem (see e.g. [121] for a review). In [118], it was argued that as the plasma density declines due to cosmic expansion, the superradiance energy (5.55) is released and dissipated in the cosmic microwave background through Coulomb collisions. By evaluating the resulting spectral distortions of the cosmic microwave background in the redshift range $10^3 \lesssim z \lesssim 2 \times 10^6$, and by using the existing COBE/FIRAS data [122], competitive upper limits on the fraction of dark matter that can be associated with spinning primordial BHs in the mass range $10^{-8} M_{\odot} \lesssim M \lesssim 0.2 M_{\odot}$ were obtained, as shown in Fig. 5.16.

5.7 Intrinsic Limits on Magnetic Fields

In Sect. 4.7 we showed that rotating BHs immersed in a magnetic field are unstable against superradiant modes. In complete analogy with the discussion of Sects. 5.3 and 5.4, due to this instability, the energy density of the radiation in the region $r \lesssim 1/B$, with B the magnetic field strength, would grow exponentially in time at the expense of the BH angular momentum, with the end state being a spinning BH with a spin set by the superradiant threshold. This implies an upper bound on the spin of magnetized BHs, again leading to holes in the BH Regge plane (cf.

¹³As was pointed out in [124], for the (unrealistic) Ernst metric in which radiation cannot escape, the end state is most likely a rotating BH in equilibrium with the outside radiation, similarly to

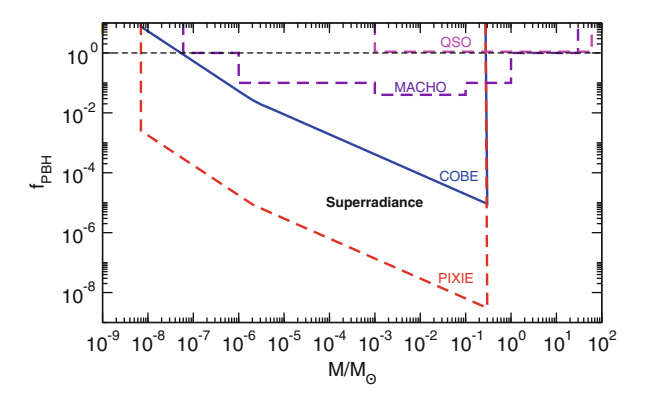


Fig. 5.16 Upper limits on the mass fraction of dark matter in primordial BHs with masses in the range $10^{-9} M_{\odot} < M < 10^2 M_{\odot}$. The *solid blue curve* is the theoretical constraint derived in this paper using COBE/FIRAS data [122]. The *dashed red line* is the expected limit from the proposed PIXIE experiment [123]. The limits from superradiant instabilities are plotted for maximally-spinning primordial BHs, and scale roughly as the inverse of the average spin parameter weighted by the initial BH spin distribution. The limits from other methods are adopted from [121]. See [118] for details

Sect. 5.3). This was used in [124] to put intrinsic limits on magnetic fields around astrophysical BHs.

In Fig. 5.17 we show the BH Regge plane with contour curves corresponding to an instability time scale $1/\omega_I$, given by Eq. (4.49), of the order of the Salpeter time. Since the contours extend almost up to $J/M^2 \sim 0$, one interesting consequence of these results is that essentially *any* observation of a spinning supermassive BH (even with spin as low as $J/M^2 \sim 0.1$) would provide some constraint on B. However, these observations can possibly exclude only very large values of B. For example a putative observation of a supermassive BH with $M \sim 10^9 M_{\odot}$ and $J/M^2 \gtrsim 0.5$ can potentially exclude the range $10^7 \text{Gauss} \lesssim B \lesssim 10^9 \text{Gauss}.^{14}$

Although these results are only valid when $B/B_M \lesssim 1$, this limit includes the most interesting region of the parameter space. Indeed, the strongest magnetic fields around compact objects observed in the Universe are of the order of 10^{13} – 10^{15} Gauss [125] and, in natural units, this value corresponds to $B/B_M \sim 10^{-6}$ – 10^{-4} . For astrophysical BHs, a reference value for the largest magnetic field that can be supported in an accretion disk is given by $B \sim 4 \times 10^8 \, (M/M_\odot)^{-1/2}$ Gauss [126] so that the approximation $B \ll B_M$ is well justified.

the asymptotically AdS case discussed in Sect. 4.5.1. However, in realistic situations part of the radiation will escape to infinity, reducing the BH spin (see discussion below).

¹⁴The strength of the magnetic field can be measured defining the characteristic magnetic field $B_M=1/M$ associated to a spacetime curvature of the same order of the horizon curvature. In physical units this is given by $B_M\sim 2.4\times 10^{19}\,(M_\odot/M)$ Gauss.

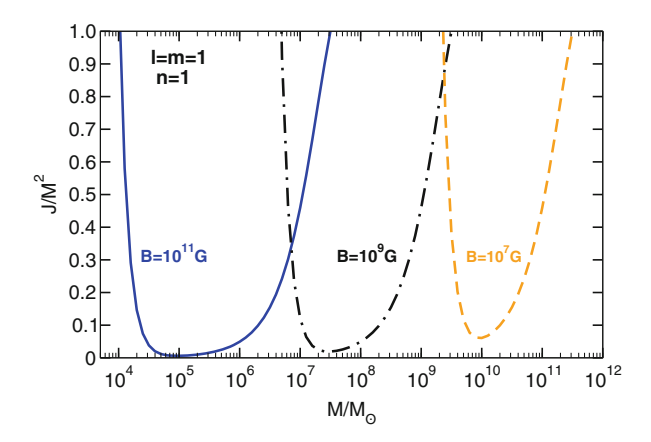


Fig. 5.17 Contour plots in the BH Regge plane corresponding to an instability time scale shorter than $\tau_{\text{Salpeter}} \sim 4.5 \times 10^7 \,\text{yr}$ for different values of the magnetic field strength B for modes with l=m=n=1. BHs lying above each of these curves would be unstable on an observable time scale. The threshold lines are obtained using Eq. (4.49) in the range $10^{-4} \lesssim B/B_M \lesssim 1$. From [124]

The main caveat of these bounds is that they were obtained using the Ernst metric which, as we discussed in Sect. 4.7, is not asymptotically flat, but instead describes a BH immersed in a magnetic field which is supported by some form of matter at infinity. In most realistic models it is expected that the Ernst metric is a relatively good approximation for the geometry of astrophysical BHs only up to a cutoff distance associated with the matter distribution. Considering that the accretion disk is concentrated near the innermost stable circular orbit, this would imply that these results can be trusted only when $B/B_M \gtrsim 0.1$ [124], which is a very large value for typical massive BHs. On the other hand, the Ernst metric is more accurate to describe configurations in which the disk extends much beyond the gravitational radius, as is the case in various models (cf. [69, 127]). In this case, however, the magnetic field will not be uniform and the matter profile has to be taken into account. While the simplistic analysis of [124] can provide the correct order of magnitude for the instability, a more refined study is needed to assess the validity of these results in the full range of B.

5.8 Phenomenology of the Ergoregion Instability

The ergoregion instability discussed in Sect. 4.11 has important phenomenological implications. Indeed, building on the results by Friedman [128] that a horizonless object with an ergoregion is unstable, a series of more recent works [129–134] have established that this instability rules out extremely compact NSs and various exotic alternatives to BHs.

5.8.1 Ergoregion Instability of Ultracompact Stars

As shown in Fig. 4.19, the time scale of the ergoregion instability of a compact spinning star can be as short as $\tau_{\rm ER} \sim 10^7 M$ (although this requires an extrapolation to $\Omega \sim \Omega_K$ beyond the slowly-rotating regime). For a compact star with $M \approx 1.4 M_{\odot}$, this corresponds to a short time scale of the order of seconds. A relevant question concerns the dependence of the instability on the compactness of the star and on its equation of state. A representative example is shown in Fig. 5.18, which presents the frequency and time scale of the fundamental l=m=1 mode as functions of the stellar compactness R/M for a constant-density star, whose pressure is given in terms of the constant density in Eq. (F.4).

The instability time scale grows very rapidly as the compactness decreases and the l=m=1 mode turns stable at $R\approx 2.35M$. This result is valid to second order in the spin, a consistent treatment was described in Sect. 4.11.1. On the other hand, by neglecting some of the second-order terms in the perturbations equations, various works have explored the dependence of the time scale on l, m and on the stellar compactness. Yoshida and Eriguchi have presented a detailed analysis [136], showing that various l=m modes can become unstable. The WKB analysis by Comins and Schutz [135] shows that in the eikonal $(l=m\to\infty)$ limit an unstable mode appears precisely when an ergoregion is formed, although the time scale is

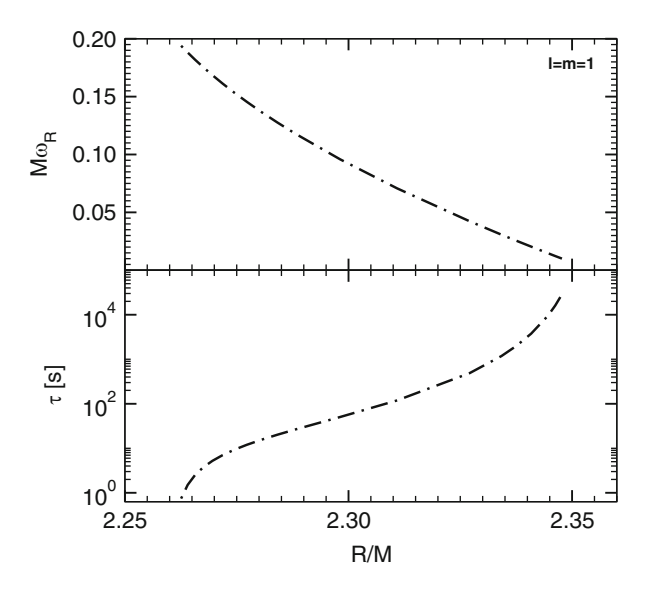


Fig. 5.18 The frequency (top panel) and the time scale (bottom panel) of the fundamental l=m=1 unstable mode of a constant-density NS as functions of the stellar compactness R/M. The l=m=1 mode turns stable at about $R\sim 2.35M$. Although not shown, higher multipoles with $l=m\gg 1$ will remain unstable until $R\lesssim 3M$ [135, 136] (cf. also Fig. 4.21 where higher unstable multipoles are shown in a different system.)

exponentially long, cf. Eq. (4.64). This is also confirmed by our previous analysis of the ergoregion instability in analog-gravity system, see Fig. 4.21. Clearly, the instability is phenomenologically relevant only if the associated time scale is shorter than the age of the star. In addition, the compactness of a NS is bounded from above by the requirement that the speed of sound in the stellar interior is smaller than the speed of light. This causality bound translates into the lower constraint $R \gtrsim 3M$ [137, 138] on the NS radius. This seems to exclude the ergoregion instability because, as we have shown, the latter is associated with long-lived modes which exist only for ultracompact stars with $R \lesssim 3M$ in the nonspinning limit.¹⁵ Furthermore, causality also constrains the maximum angular velocity of a spinning NS [140], thus disfavoring the formation of an ergoregion. However, it is likely that an ergoregion forms for NSs whose radius is larger than 3M if the star is fastlyspinning. In this case a theoretical bound on the NS compactness—based on the fact that the fastest millisecond pulsars cannot be unstable to the ergoregion instability on dynamical time scales—could be more stringent than the causality bound. It would be interesting to compute the instability time scale for a realistic, fastlyspinning NS model and check whether the ergoregion instability can exclude some allowed region of the mass-radius-spin parameter space. A systematic study in this direction is still lacking.

5.8.2 Supporting the Black-Hole Paradigm: Instabilities of Black-Hole Mimickers

BHs in GR have a remarkable property: being vacuum solutions of Einstein's field equations they do not depend on any external scale and, therefore, can exist in any size (or, equivalently, with any mass). Compact objects as compact and massive as BHs but that do not possess an event horizon go under the generic name of "BH mimickers" (see, e.g., [141]). Notwithstanding, ordinary matter—even when in extreme conditions—cannot support the enormous self-gravity of a massive and ultracompact object. For example, NSs—the densest material objects known in the Universe—cannot sustain masses larger than $^{16} \approx 3 M_{\odot}$. Therefore, supporting the self-gravity of a BH mimicker requires (at least!) exotic matter, this is the price to pay to avoid dealing with event horizons.

¹⁵Recently, [139] showed that long-lived modes necessarily exist for matter configurations whose trace of the stress-energy tensor is positive (or zero). For a perfect-fluid star, this requires $P > \rho/3$, where P and ρ are the NS pressure and density. This is an extreme configuration which is unlike to exist in ordinary stars, but it might occur in other models of ultracompact objects, as those discussed in Sect. 5.8.2.

¹⁶Even constant-density NSs have a maximum compactness which is smaller than the BH limit M/R = 1/2. Inspection of Eq. (F.2) shows that $M/R \le 4/9$ to ensure regularity of the geometry. More realistic equations of state yield a maximum mass and a maximum compactness.

There are at least two strong motivations to study BH mimickers as alternative to ordinary BHs. First, despite the growing evidence in favor of the BH paradigm, a definite proof that massive compact objects are endowed with an event horizon is still lacking. The observation—or lack thereof—of a surface would be bulletproof indication that compact dark objects have star-like properties or are instead BHs (see e.g. [142]). Such tests are extremely challenging to perform in the optical window and, in fact, some claims exist [143] that performing these tests might even be intrinsically impossible. However, these tests might become available with the advent of GW astronomy: the oscillation modes of BHs have a very precise and well-known structure, which can be tested against observations [144–146], while the presence of a surface should be imprinted also on the GWs generated during the merger of two objects [147–149] (but see [69, 134] for a discussion). Secondly, the applications of the superradiant instabilities discussed in Sect. 5.4 assume that massive compact objects are BHs, whose event horizon allows for superradiant scattering. Therefore, it is important to understand whether BH mimickers are viable alternatives, in order to quantify the generality of the bounds previously discussed. In this section, we show that BH mimickers are associated with various instabilities, which make these objects unlikely to form in realistic scenarios, thus giving further theoretical support to the BH paradigm.

BH Mimickers Because the pressure of ordinary matter cannot sustain ultracompact massive objects, BH mimickers have to rely on different support mechanisms. Among the most popular alternatives are [141]:

- *Boson stars* made up of fundamental self-interacting scalar fields that are prevented from gravitational collapse through the Heinsenberg uncertainty principle (for reviews on the subject see [150–152]). Bosons stars can be as compact as a NS and as massive as the BH candidate at the center of our galaxy [148, 152]. These compact objects can be classified according to the scalar potential in the Klein-Gordon Lagrangian [148, 151, 153]. Similarly to ordinary compact stars, boson stars are linearly stable below a critical mass [152, 153].
- Gravitational condensate stars (or *gravastars* [154]) are proposed as the end state of a quantum phase transition in the vicinity of the would-be BH horizon. The latter is effectively replaced by a transition layer and the BH interior by a segment of de Sitter space [155]. The effective negative pressure of the de Sitter interior contributes to sustain the self-gravity of the object for any compactness. In the static case these models have been shown to be thermodynamically [154] and dynamically [149, 156, 157] stable for reasonable equations of state.
- Superspinars are BH-like objects described by the Kerr metric with spin parameter exceeding the Kerr bound, a > M. In these models, the region containing naked singularities and closed timelike curves of the super-extreme Kerr geometry is excised or assumed to be modified by, say, stringy corrections [129, 130, 158].
- Wormholes are regular geometries which—at least in the context of BH mimickers—are described by $ds_{\text{wormhole}}^2 = ds_{\text{Kerr}}^2 + \epsilon \delta g_{ab} dx^a dx^b$, where $\epsilon \ll 1$ parametrizes the deviations from the Kerr metric. Under certain assumptions on

 δg_{ab} , the geometry describes a horizonless object with an excision at distance $\mathcal{O}(\epsilon)$ from the would-be horizon [159]. Traversable wormholes require exotic matter or divergent stress tensors [160], thus some ultra-stiff matter is assumed close to the would-be horizon.

Ergoregion Instabilities Spinning BH mimickers can develop an ergoregion and become unstable, similarly to ultracompact stars as previously discussed. The ergoregion instability of various boson-star and gravastar models has been studied in detail in [129], showing that unstable modes generically exist (see also [132] for a detailed discussion in the case of gravastars). While gravastars have been studied only in the slowly rotating limit, numerical solutions of highly-spinning boson stars are available. For a given compactness of the order of $M/R \sim 1/2$, gravastars and boson stars develop an ergoregion when spinning above a certain threshold. As for ultracompact stars, also in this case the instability arises from long-lived modes that exist when these objects possess a light-ring, which typically happens when $R \lesssim 3M$ in the nonspinning limit.

The ergoregion instability of superspinars and Kerr-like wormholes was studied in [130], showing that similar results hold. Because in this case the exact form of the geometry is unknown, the stability analysis has been performed by imposing Dirichlet boundary conditions at the excision surface at $r = r_0$. The latter should approximate the boundary conditions required by a hard surface at the would-be horizon location. A detailed analysis of the instability of superspinars, including different boundary conditions and various configurations, was performed in [131]. An example of such unstable modes is presented in Fig. 5.19. The instability turns out to be effective in a significant region of the two-dimensional parameter space

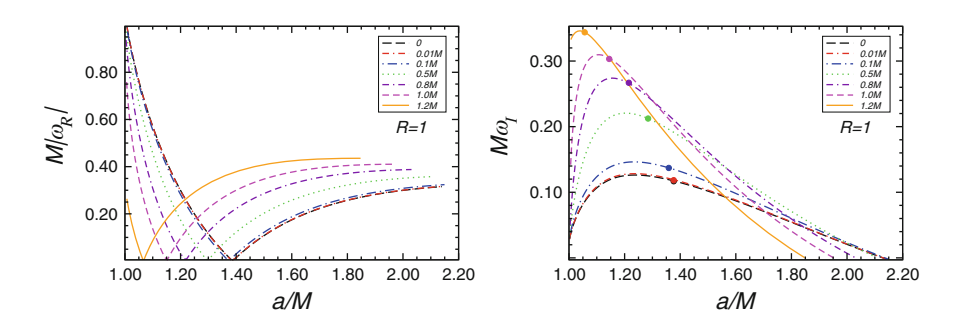


Fig. 5.19 Real (left panel) and imaginary (right panel) part of unstable l=m=2 gravitational modes of a superspinar as a function of the spin parameter, a/M, for several fixed values of the surface location r_0 where Dirichlet conditions (i.e., perfect reflectivity $\mathcal{R}=\mathcal{I}$) are imposed. See [131] for details

¹⁷The angular momentum of a boson star is quantized [152]; this prevents performing a standard slow-rotation approximation.

 $(a/M, r_0/M)$. The most effective instability at low rotation rates corresponds to the l=m=2 fundamental mode, but when $a \sim M$ and $r_0 \sim M$ unstable modes with m=0 also exist. In this case, the instability is related to the existence of stable polar null circular orbits in the spacetime [131]. Finally, when $r_0/M < 0$, a third family of m=0 modes exists, which is probably related to the existence of naked singularities and closed timelike curves.

Nonlinear Instability The ergoregion instability requires an ultracompact object to rotate above a certain critical spin, what happens when these objects are slowly rotating or almost static? Recently, a new mechanism has been put forward which could exclude any ultracompact BH mimicker on the grounds that such an object would be nonlinearly unstable [133]. This nonlinear instability is associated to the longlived modes discussed above [134]. Being trapped between the center of the object and the light ring, and being localized near a second, stable null geodesic, these modes may become unstable under fragmentation via a "Dyson-Chandrasekhar-Fermi' mechanism [161–163] at the nonlinear level. To understand this mechanism, it is illustrative to inspect the eigenfunctions of the linearized problem. An example is shown in Fig. 5.20 for the case of a ultracompact star (qualitatively similar results hold for other BH mimickers). As the multipolar index l increases, the eigenfunctions becomes more and more elongated along the radial direction. If we assume for simplicity that the perturbations are axisymmetric (m = 0), these elongated, long-lived modes are unstable against the same "Dyson-Chandrasekhar-Fermi" mechanism that affects thin cylinders or rings of matter [161–164]. The minimum growth time scale of this instability scales as $\tau_{DCF} \sim \delta \rho^{-1/2}$, where $\delta \rho$ is the density fluctuation. The requirement that nonlinearities take over is that $\tau_{\rm DCF}$ be much smaller than the lifetime of linear fluctuations. Because the latter grows exponentially with l [cf. Eq. (4.64)], it is easy to show that fragmentation becomes important already at moderately small values of l even for $\delta \rho / \rho \sim 10^{-16}$ or smaller [134].

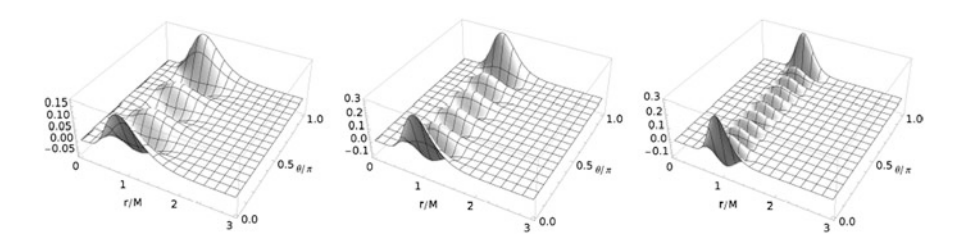


Fig. 5.20 Scalar eigenfunctions of a static, ultracompact star with radius R = 2.3M for m = 0 and l = 6, 10, 20 (from *left* to the *right*). The eigenfunctions have a typical width that scales as l^{-1} in the angular direction and a width in the radial direction that depends on the model, but typically ranges between $l^{-0.4} - l^{-0.8}$. Therefore, the "aspect ratio" of the perturbation $\sim l^{0.6} - l^{0.2}$ grows in the large-l limit and the perturbation becomes more and more elongated along the radial direction. See [134] for details

The fragmentation of the linear eigenfunction leads to a configuration which consists on a spherically symmetric core surrounded by droplets of the star fluid, whose sizes are much smaller than that of the original object [134] (see also nonlinear results for fragmentation of black strings [165]). It is easy to see that these smaller droplets, although of the same material as the original star, are much less compact because they are much smaller and are therefore expected to be themselves stable. Likewise, the core of the star is also less compact and stable. On longer time scales, these droplets re-arrange and fall into the core, and the process continues. The dynamical picture looks like that of a "boiling" fluid, and radiates a nonnegligible amount of radiation. Exact calculations have not been performed yet but, if this scenario is correct, a sizable fraction of the object's initial mass can disperse to infinity, possibly reducing the compactness of the final object to values which no longer allow for the existence of light rings. In an alternative scenario, nonlinear interactions over the ultralong lifetime of the unstable modes may lead to the formation of small BHs close to the stable light ring [134].

Light Rings Imply Black Holes To summarize, ultracompact objects with $R \lesssim 3M$ are plagued by various instabilities. When these objects are spinning sufficiently fast they suffer from the ergoregion instability and, even when they are only slowly spinning or static, long-lived modes trapped by the light-ring can become unstable at the nonlinear level. In the latter case, the instability can lead to fragmentation (thus reducing the object's compactness) or to gravitational collapse (thus forming a BH). In both cases, the instability can be sufficiently strong to be dynamically effective. As recently pointed out [139], exotic matter configurations with T > 0 are necessarily characterized by the existence of long-lived modes. Altogether, these results give further theoretical support to the BH hypothesis: the mere observation of a light ring—a much simpler task than the observation of the event horizon, and something that is within the reach of upcoming facilities [9, 10, 166]—would be conclusive evidence for the existence of BHs.

5.9 Open Issues

- The role of the horizon in the BZ mechanism is still unclear and whether it is
 necessary for the process to occur is still a matter of debate. In fact, some recent
 numerical simulations [41] seem to indicate that the ergosphere alone is sufficient
 for the process to occur.
- As was pointed out in [167], recent GRMHD simulations studying the BZ mechanism suggest that the magnetosphere leading to BH jets has a large split-monopole component [18–20]; however a simple explanation for why the system tends to this solution is still missing.
- Recent numerical simulations suggest that BHs carrying linear momentum [168] and coalescing BH–BH or BH–NS binary systems can also power jets [169].

5.9 Open Issues 203

Although some work has been done to understand the mechanism behind these jets [170, 171], a complete theoretical understanding is still needed.

- In the context of the BH analog of the two-ring model discussed in Sect. 4.8, it is important to understand whether such mechanism (or extensions therein) can be used to power gamma-ray burst, as discussed in [172]. More in general, a purely-superradiant model for gamma-ray burst production has not yet been developed.
- The stability of the hairy solutions discussed in Sect. 5.5 remains an urgent open issue; all the hairy solutions have ergoregions [106] and it is likely that in part of the parameter space these solutions will be simply rotating too fast and will themselves be unstable against an ergoregion instability, discussed in Sect. 4.11. Indeed, as discussed above, fastly-spinning boson stars are unstable due to the ergoregion instability, whereas Kerr BHs are not. Since the hairy solutions found in [106] interpolate between these two geometries, it is reasonable to expect that there exists some critical value of the scalar charge above which the solution is unstable. All this remains to be proven.
- The GW phenomenology of massive bosons with spin remains to be investigated.
 Specifically, more detailed computations of the superradiant rates for massive vector and tensor fields are needed. Likewise, the role of nonlinearities for these fields (e.g. generalizations of the bosenova collapse [57, 74, 75]) have not been explored yet.
- More in general, the impact of nonlinearities on the bounds discussed in Sect. 5.4
 has not been fully explored. Nonlinearities might slow down or even saturate the
 superradiant growth of bosonic clouds, thus making the constraints derived from
 BH superradiance less stringent. On the other hand, nonlinear effects similar to
 the bosenova [74, 75] can provide novel smoking guns for bosonic condensates
 around astrophysical BHs.
- Floating orbits are not possible with massless fields [91], and have so far been discussed only in the context of massive scalars where the spacetime itself is unstable (cf. Sect. 5.4.3). Outstanding issues are related to (1) the existence of floating orbits for other massive fields; (2) the existence of this effect for stable spacetimes; (3) understanding floating for eccentric orbits or its dependence on the size of the floating body.
- Plasma-triggered superradiant instabilities have been studied in [118] but mostly
 for homogeneous configurations. It would be interesting to extend such analysis
 to more realistic matter profiles around a spinning BH, for example by extending
 perturbative [173] or fully-numerical [54] methods (see [120] for a related
 analysis).
- As mentioned above, a systematic study of the ergoregion instability in realistic
 models of spinning NSs is still lacking. It would be interesting to compute the
 time scale and check whether the instability can be used to rule out some region
 of the NS mass-radius-spin parameter space.

Wormholes are interesting alternatives to the BH paradigm. Traversable wormholes are predicted in GR for matter that violates the null energy condition [160]. When rotating, such objects are expected to be unstable because of the ergoregion instability, but a detailed computation, together with a discussion of possible astrophysical implications, is not available yet.

References

- 1. E. Berti, E. Barausse, V. Cardoso, L. Gualtieri, P. Pani et al., Testing general relativity with present and future astrophysical observations. Topical Rev. Classical Quantum Gravity (2015). arXiv:1501.07274 [gr-gc]
- 2. M. Schmidt, 3C 273: a star-like object with large red-shift. Nature 197, 1040 (1963)
- S. Doeleman, J. Weintroub, A.E. Rogers, R. Plambeck, R. Freund et al., Event-horizon-scale structure in the supermassive black hole candidate at the Galactic Centre. Nature 455, 78 (2008). arXiv:0809.2442 [astro-ph]
- 4. Ligo Scientific Collaboration, http://www.ligo.org/
- 5. Virgo, http://www.ego-gw.it
- 6. Kagra: large-scale cryogenic gravitational wave telescope project, http://www.gwcenter.icrr.u-tokyo.ac.jp/en/
- 7. Einstein Telescope (2008), http://www.et-gw.eu/
- 8. eLISA, https://www.elisascience.org/
- 9. R.-S. Lu, A.E. Broderick, F. Baron, J.D. Monnier, V.L. Fish, S.S. Doeleman, V. Pankratius, Imaging the supermassive black hole shadow and jet base of m87 with the event horizon telescope. Astrophys. J. **788**(2), 120 (2014). http://www.stacks.iop.org/0004-637X/788/i=2/a=120
- 10. F. Eisenhauer, G. Perrin, W. Brandner, C. Straubmeier, A. Richichi et al., GRAVITY: getting to the event horizon of Sgr A*, in Society of Photo-Optical Instrumentation Engineers (SPIE) Conference Series, Vol. 7013 of Society of Photo-Optical Instrumentation Engineers (SPIE) Conference Series, July 2008. arXiv:0808.0063.
- 11. S. Hawking, Black holes in general relativity. Commun. Math. Phys. 25, 152–166 (1972)
- 12. D. Lynden-Bell, Galactic nuclei as collapsed old quasars. Nature 223, 690 (1969)
- R. Blandford, D. Payne, Hydromagnetic flows from accretion discs and the production of radio jets. Mon. Not. R. Astron. Soc. 199, 883 (1982)
- R. Blandford, R. Znajek, Electromagnetic extractions of energy from Kerr black holes. Mon. Not. R. Astron. Soc. 179, 433–456 (1977)
- S. Komissarov, Blandford-Znajek mechanism versus Penrose process. J. Korean Phys. Soc. 54, 2503–2512 (2009). arXiv:0804.1912 [astro-ph]
- J.P. Lasota, E. Gourgoulhon, M. Abramowicz, A. Tchekhovskoy, R. Narayan, Extracting black-hole rotational energy: the generalized Penrose process. Phys. Rev. D89, 024041 (2014). arXiv:1310.7499 [gr-qc]
- D. MacDonald, K. Thorne, Black-hole electrodynamics an absolute-space/universal-time formulation. Mon. Not. R. Astron. Soc. 198, 345–383 (1982)
- A. Tchekhovskoy, J.C. McKinney, R. Narayan, General relativistic modeling of magnetized jets from accreting black holes. J. Phys. Conf. Ser. 372, 012040 (2012). arXiv:1202.2864 [astro-ph.HE]
- J.C. McKinney, A. Tchekhovskoy, R.D. Blandford, General relativistic magnetohydrodynamic simulations of magnetically choked accretion flows around black holes. Mon. Not. R. Astron. Soc. 423, 3083 (2012). arXiv:1201.4163 [astro-ph.HE]

References 205

 R.F. Penna, R. Narayan, A. Sadowski, General relativistic magnetohydrodynamic simulations of Blandford-Znajek jets and the membrane paradigm. Mon. Not. R. Astron. Soc. 436, 3741 (2013). arXiv:1307.4752 [astro-ph.HE]

- 21. R.M. Wald, Black hole in a uniform magnetic field. Phys. Rev. D10, 1680–1685 (1974)
- 22. R.L. Znajek, Black hole electrodynamics and the Carter tetrad. Mon. Not. R. Astron. Soc. 179, 457–472 (1977)
- S.E. Gralla, T. Jacobson, Spacetime approach to force-free magnetospheres. Mon. Not. R. Astron. Soc. 445, 2500 (2014). arXiv:1401.6159 [astro-ph.HE]
- A. Lupsasca, M.J. Rodriguez, A. Strominger, Force-free electrodynamics around extreme Kerr black holes. J. High Energy Phys. 1412, 185 (2014). arXiv:1406.4133 [hep-th]
- A. Lupsasca, M.J. Rodriguez, Exact solutions for extreme black hole magnetospheres (2014). arXiv:1412.4124 [hep-th]
- F. Zhang, H. Yang, L. Lehner, Towards an understanding of the force-free magnetosphere of rapidly spinning black holes. Phys. Rev. D90(12), 124009 (2014). arXiv:1409.0345 [astro-ph.HE]
- 27. H. Li, C. Yu, J. Wang, Z. Xu, Force-free magnetosphere on near-horizon geometry of near-extreme Kerr black holes (2014). arXiv:1403.6959 [gr-qc]
- 28. H. Yang, F. Zhang, Stability of force-free magnetospheres. Phys. Rev. **D90**(10), 104022 (2014). arXiv:1406.4602 [astro-ph.HE]
- 29. S. Komissarov, Electrodynamics of black hole magnetospheres. Mon. Not. R. Astron. Soc. 350, 407 (2004). arXiv:astro-ph/0402403 [astro-ph]
- 30. J.C. McKinney, General relativistic force-free electrodynamics: a new code and applications to black hole magnetospheres. Mon. Not. R. Astron. Soc. 367, 1797–1807 (2006). arXiv:astro-ph/0601410 [astro-ph]
- 31. A. Tchekhovskoy, J.C. McKinney, R. Narayan, Simulations of ultrarelativistic magnetodynamic jets from Gamma-ray burst engines. Mon. Not. R. Astron. Soc. 388, 551 (2008). arXiv:0803.3807 [astro-ph]
- 32. C. Palenzuela, T. Garrett, L. Lehner, S. L. Liebling, Magnetospheres of black hole systems in force-free plasma. Phys. Rev. **D82**, 044045 (2010). arXiv:1007.1198 [gr-qc]
- 33. M. Parikh, F. Wilczek, An Action for black hole membranes. Phys. Rev. **D58**, 064011 (1998). arXiv:gr-qc/9712077 [gr-qc]
- K.S. Thorne, R. Price, D. Macdonald, Black Holes: The Membrane Paradigm (Yale University Press, New Haven, 1986)
- 35. A. Tchekhovskoy, R. Narayan, J.C. McKinney, Efficient generation of jets from magnetically arrested accretion on a rapidly spinning black hole. Mon. Not. R. Astron. Soc. 418, L79–L83 (2011). arXiv:1108.0412 [astro-ph.HE]
- 36. P. Goldreich, W.H. Julian, Pulsar electrodynamics. Astrophys. J. 157, 869 (1969)
- 37. M. Ruderman, P. Sutherland, Theory of pulsars: polar caps, sparks, and coherent microwave radiation. Astrophys. J. 196, 51 (1975)
- 38. P. Goldreich, D. Lynden-Bell, Io, a jovian unipolar inductor. Astrophys. J. 156, 59–78 (1969)
- 39. L. Susskind, L. Thorlacius, J. Uglum, The stretched horizon and black hole complementarity. Phys. Rev. **D48**, 3743–3761 (1993). arXiv:hep-th/9306069 [hep-th]
- 40. K. Toma, F. Takahara, Electromotive force in the Blandford-Znajek process. Mon. Not. R. Astron. Soc. 442, 2855 (2014). arXiv:1405.7437 [astro-ph.HE]
- 41. M. Ruiz, C. Palenzuela, F. Galeazzi, C. Bona, The Role of the ergosphere in the Blandford-Znajek process. Mon. Not. R. Astron. Soc. 423, 1300–1308 (2012). arXiv:1203.4125 [gr-qc]
- 42. S. Chandrasekhar, Solutions of two problems in the theory of gravitational radiation. Phys. Rev. Lett. 24, 611–615 (1970)
- J.L. Friedman, B.F. Schutz, Lagrangian perturbation theory of nonrelativistic fluids. Astrophys. J. 221, 937–957 (1978)
- 44. N. Stergioulas, Rotating stars in relativity. Living Rev. Relativ. 6, 3 (2003). arXiv:gr-qc/0302034 [gr-qc]

- 45. N. Andersson, G. Comer, Relativistic fluid dynamics: physics for many different scales. Living Rev. Relativ. 10, 1 (2007). arXiv:qr-qc/0605010 [qr-qc]
- 46. J.L. Friedman, N. Stergioulas, *Rotating Relativistic Stars* (Cambridge University Press, Cambridge, 2013)
- 47. J.L. Friedman, B.F. Schutz, On the stability of relativistic systems. Astrophys. J. **200**, 204–220 (1975)
- J. Friedman, B.F. Schutz, Secular instability of rotating Newtonian stars. Astrophys. J. 222, 281 (1978)
- N. Andersson, A New class of unstable modes of rotating relativistic stars. Astrophys. J. 502, 708–713 (1998). arXiv:gr-qc/9706075 [gr-qc]
- 50. N. Andersson, K.D. Kokkotas, The R mode instability in rotating neutron stars. Int. J. Mod. Phys. **D10**, 381–442 (2001). arXiv:gr-gc/0010102 [gr-gc]
- 51. V. Cardoso, S. Yoshida, Superradiant instabilities of rotating black branes and strings. J. High Energy Phys. **0507**, 009 (2005). arXiv:hep-th/0502206 [hep-th]
- 52. S.R. Dolan, Instability of the massive Klein-Gordon field on the Kerr spacetime. Phys. Rev. **D76**, 084001 (2007). arXiv:0705.2880 [gr-qc]
- 53. P. Pani, V. Cardoso, L. Gualtieri, E. Berti, A. Ishibashi, Black hole bombs and photon mass bounds. Phys. Rev. Lett. 109, 131102 (2012). arXiv:1209.0465 [gr-qc]
- 54. H. Witek, V. Cardoso, A. Ishibashi, U. Sperhake, Superradiant instabilities in astrophysical systems. Phys. Rev. **D87**, 043513 (2013). arXiv:1212.0551 [gr-qc]
- 55. R. Brito, V. Cardoso, P. Pani, Massive spin-2 fields on black hole spacetimes: instability of the Schwarzschild and Kerr solutions and bounds on the graviton mass. Phys. Rev. **D88**, 023514 (2013). arXiv:1304.6725 [gr-qc]
- 56. P. Pani, V. Cardoso, L. Gualtieri, E. Berti, A. Ishibashi, Perturbations of slowly rotating black holes: massive vector fields in the Kerr metric. Phys. Rev. **D86**, 104017 (2012). arXiv:1209.0773 [gr-qc]
- 57. A. Arvanitaki, S. Dubovsky, Exploring the string axiverse with precision black hole physics. Phys. Rev. **D83**, 044026 (2011). arXiv:1004.3558 [hep-th]
- H. Okawa, H. Witek, V. Cardoso, Black holes and fundamental fields in numerical relativity: initial data construction and evolution of bound states. Phys. Rev. D89, 104032 (2014). arXiv:1401.1548 [gr-qc]
- 59. V. Cardoso, Black hole bombs and explosions: from astrophysics to particle physics. Gen. Relativ. Gravit. 45, 2079–2097 (2013). arXiv:1307.0038 [gr-qc]
- R. Brito, V. Cardoso, P. Pani, Black holes as particle detectors: evolution of superradiant instabilities. Focus Iss. Classical Quantum Gravity (2015, in press). arXiv:1411.0686 [gr-qc]
- 61. H. Yoshino, H. Kodama, Bosenova and Axiverse (2015). arXiv:1505.00714 [gr-qc]
- 62. S. Hawking, G. Ellis, *The Large Scale Structure of Space-Time* (Cambridge University Press, Cambridge, 1973)
- 63. M. Heusler, The Uniqueness theorem for rotating black hole solutions of self-gravitating harmonic mappings. Classical Quantum Gravity 12, 2021–2036 (1995). arXiv:gr-qc/9503053 [gr-qc]
- 64. T.P. Sotiriou, V. Faraoni, Black holes in scalar-tensor gravity. Phys. Rev. Lett. **108**, 081103 (2012). arXiv:1109.6324 [gr-qc]
- 65. A.A.H. Graham, R. Jha, Stationary black holes with time-dependent scalar fields. Phys. Rev. **D90**, 041501 (2014). arXiv:1407.6573 [gr-qc]
- S.L. Detweiler, Klein-Gordon equation and rotating black holes. Phys. Rev. D22, 2323–2326 (1980)
- 67. H. Yoshino, H. Kodama, Gravitational radiation from an axion cloud around a black hole: superradiant phase. PTEP **2014**, 043E02 (2014). arXiv:1312.2326 [gr-gc]
- C.L. Benone, L.C. Crispino, C. Herdeiro, E. Radu, Kerr-Newman scalar clouds. Phys. Rev. D90(10), 104024 (2014). arXiv:1409.1593 [gr-qc]
- 69. E. Barausse, V. Cardoso, P. Pani, Can environmental effects spoil precision gravitational-wave astrophysics? Phys. Rev. **D89**, 104059 (2014). arXiv:1404.7149 [gr-qc]

- 70. A. Soltan, Masses of quasars. Mon. Not. R. Astron. Soc. **200**, 115–122 (1982)
- K.S. Thorne, Disk accretion onto a black hole.
 Evolution of the hole.. Astrophys. J. 191, 507–520 (1974)
- 72. J.M. Bardeen, Kerr metric black holes. Nature **226**, 64–65 (1970)
- 73. L. Brenneman, C. Reynolds, M. Nowak, R. Reis, M. Trippe, et al., The spin of the supermassive black hole in NGC 3783. Astrophys. J. 736, 103 (2011). arXiv:1104.1172 [astro-ph.HE]
- 74. H. Kodama, H. Yoshino, Axiverse and black hole. Int. J. Mod. Phys. Conf. Ser. 7, 84-115 (2012). arXiv:1108.1365 [hep-th]
- 75. H. Yoshino, H. Kodama, Bosenova collapse of axion cloud around a rotating black hole. Prog. Theor. Phys. 128, 153–190 (2012). arXiv:1203.5070 [gr-qc]
- 76. A. Arvanitaki, M. Baryakhtar, X. Huang, Discovering the QCD axion with black holes and gravitational waves. Phys. Rev. **D91**, 084011 (2015). arXiv:1411.2263 [hep-ph]
- 77. B. Bozek, D.J.E. Marsh, J. Silk, R.F.G. Wyse, Galaxy UV-luminosity function and reionisation constraints on axion dark matter (2014). arXiv:1409.3544 [astro-ph.CO]
- 78. R. Hlozek, D. Grin, D.J.E. Marsh, P.G. Ferreira, A search for ultra-light axions using precision cosmological data. Phys. Rev. **D91**, 103512 (2015). arXiv:1410.2896 [astro-ph.CO]
- 79. E. Berti, M. Volonteri, Cosmological black hole spin evolution by mergers and accretion. Astrophys. J. **684**, 822–828 (2008). arXiv:0802.0025 [astro-ph]
- 80. S. Schmoll, J. Miller, M. Volonteri, E. Cackett, C. Reynolds et al., Constraining the spin of the black hole in fairall 9 with Suzaku. Astrophys. J. **703**, 2171–2176 (2009). arXiv:0908.0013 [astro-ph.HE]
- D.R. Pasham, T.E. Strohmayer, R.F. Mushotzky, A 400-solar-mass black hole in the galaxy M82. Nature 513, 74–76 (2014)
- 82. N.J. McConnell, C.-P. Ma, K. Gebhardt, S.A. Wright, J.D. Murphy et al., Two ten-billion-solar-mass black holes at the centres of giant elliptical galaxies. Nature 480, 215 (2011). arXiv:1112.1078 [astro-ph.CO]
- 83. N.J. McConnell, C.-P. Ma, J.D. Murphy, K. Gebhardt, T.R. Lauer et al., Dynamical measurements of black hole masses in four brightest cluster galaxies at 100 Mpc. Astrophys. J. 756, 179 (2012). arXiv:1203.1620 [astro-ph.CO]
- Particle Data Group Collaboration, K. Olive et al., Review of particle physics. Chin. Phys. C38, 090001 (2014)
- 85. P. Amaro-Seoane et al., eLISA: astrophysics and cosmology in the millihertz regime (2012). arXiv:1201.3621 [astro-ph]
- 86. G. Mocanu, D. Grumiller, Self-organized criticality in boson clouds around black holes. Phys. Rev. **D85**, 105022 (2012). arXiv:1203.4681 [astro-ph.CO]
- 87. V. Cardoso, S. Chakrabarti, P. Pani, E. Berti, L. Gualtieri, Floating and sinking: the Imprint of massive scalars around rotating black holes. Phys. Rev. Lett. **107**, 241101 (2011). arXiv:1109.6021 [gr-qc]
- 88. N. Yunes, P. Pani, V. Cardoso, Gravitational waves from quasicircular extreme massratio inspirals as probes of scalar-tensor theories. Phys. Rev. **D85**, 102003 (2012). arXiv:1112.3351 [gr-qc]
- 89. J. Alsing, E. Berti, C.M. Will, H. Zaglauer, Gravitational radiation from compact binary systems in the massive Brans-Dicke theory of gravity. Phys. Rev. **D85**, 064041 (2012). arXiv:1112.4903 [gr-gc]
- 90. V. Cardoso, I.P. Carucci, P. Pani, T.P. Sotiriou, Black holes with surrounding matter in scalar-tensor theories. Phys. Rev. Lett. 111, 111101 (2013). arXiv:1308.6587 [gr-qc]
- 91. S.J. Kapadia, D. Kennefick, K. Glampedakis, Do floating orbits in extreme mass ratio binary black holes exist? arXiv:1302.1016 [gr-qc]
- 92. J.D. Bekenstein, Black hole hair: 25-years after (1996). arXiv:gr-qc/9605059 [gr-qc]
- 93. B. Carter, Has the black hole equilibrium problem been solved? arXiv:gr-qc/9712038 [gr-qc]

- 94. M. Heusler, Stationary black holes: uniqueness and beyond. Living Rev. Relativ. 1, 6 (1998)
- 95. P.T. Chrusciel, J.L. Costa, M. Heusler, Stationary black holes: uniqueness and beyond. Living Rev. Relativ. 15, 7 (2012). arXiv:1205.6112 [gr-gc]
- 96. D. Robinson, *The Kerr Spacetime: Rotating Black Holes in General Relativity* (Cambridge University Press, Cambridge, 2009)
- 97. G. Gibbons, Vacuum polarization and the spontaneous loss of charge by black holes. Commun. Math. Phys. 44, 245–264 (1975)
- 98. C.E. Rhoades Jr., R. Ruffini, Maximum mass of a neutron star. Phys. Rev. Lett. 32, 324–327 (1974)
- 99. S. Stationary scalar clouds around rotating black holes. Phys. Rev. **D86**, 104026 (2012). arXiv:1211.3202 [gr-qc]
- 100. S. Hod, Stationary resonances of rapidly-rotating Kerr black holes. Eur. Phys. J. C73, 2378 (2013). arXiv:1311.5298 [gr-qc]
- 101. C.A.R. Herdeiro, E. Radu, Kerr black holes with scalar hair. Phys. Rev. Lett. 112, 221101 (2014). arXiv:1403.2757 [gr-qc]
- 102. C. Herdeiro, E. Radu, Construction and physical properties of Kerr black holes with scalar hair (2015). arXiv:1501.04319 [gr-qc]
- 103. C.A.R. Herdeiro, E. Radu, A new spin on black hole hair. Int. J. Mod. Phys. **D23**, 1442014 (2014). arXiv:1405.3696 [gr-qc]
- 104. S. Yoshida, Y. Eriguchi, Rotating boson stars in general relativity. Phys. Rev. D56, 762–771 (1997)
- 105. B. Kleihaus, J. Kunz, M. List, Rotating boson stars and Q-balls. Phys. Rev. D72, 064002 (2005). arXiv:gr-qc/0505143 [gr-qc]
- 106. C. Herdeiro, E. Radu, Ergo-spheres, ergo-tori and ergo-Saturns for Kerr black holes with scalar hair. Phys. Rev. **D89**, 124018 (2014). arXiv:1406.1225 [gr-qc]
- 107. S. Hod, Kerr-Newman black holes with stationary charged scalar clouds. Phys. Rev. **D90**, 024051 (2014). arXiv:1406.1179 [gr-qc]
- 108. S. Hod, Rotating black holes can have short bristles. Phys. Lett. **B739**, 196 (2014). arXiv:1411.2609 [gr-qc]
- 109. C. Herdeiro, E. Radu, H. Runarsson, Non-linear *Q*-clouds around Kerr black holes. Phys. Lett. **B739**, 302–307 (2014). arXiv:1409.2877 [gr-qc]
- 110. Y. Brihaye, C. Herdeiro, E. Radu, Myers?Perry black holes with scalar hair and a mass gap. Phys. Lett. **B739**, 1–7 (2014). arXiv:1408.5581 [gr-qc]
- 111. O.J. Dias, G.T. Horowitz, J.E. Santos, Black holes with only one Killing field. J. High Energy Phys. 1107, 115 (2011). arXiv:1105.4167 [hep-th]
- 112. R.C. Myers, M. Perry, Black holes in higher dimensional space-times. Ann. Phys. 172, 304 (1986)
- 113. V. Cardoso, P. Pani, Tidal acceleration of black holes and superradiance. Classical Quantum Gravity 30, 045011 (2013). arXiv:1205.3184 [gr-gc]
- 114. R. Brito, V. Cardoso, P. Pani, Tidal effects around higher-dimensional black holes. Phys. Rev. **D86**, 024032 (2012). arXiv:1207.0504 [gr-qc]
- 115. M.C. Begelman, Accreting black holes, in *Proceedings of the 26th Solvay Conference on Physics: "Astrophysics and Cosmology"*, World Scientific, 2014, ed. by R. Blandford, A. Sevrin (to be published). arXiv:1410.8132 [astro-ph.HE]
- 116. S.A. Teukolsky, Perturbations of a rotating black hole. Ph.D. thesis, California Institute of Technology (1973)
- 117. W.H. Press, S.A. Teukolsky, Floating orbits, superradiant scattering and the black-hole bomb. Nature 238, 211–212 (1972)
- 118. P. Pani, A. Loeb, Constraining primordial black-hole bombs through spectral distortions of the cosmic microwave background. Phys. Rev. **D88**, 041301 (2013). arXiv:1307.5176 [astro-ph.CO]
- R. Kulsrud, A. Loeb, Dynamics and gravitational interaction of waves in nonuniform media. Phys. Rev. D45, 525–531 (1992)

120. M.H. Van Putten, Superradiance in a torus magnetosphere around a black hole. Science **284**(5411), 115–118 (1999)

- 121. B. Carr, K. Kohri, Y. Sendouda, J. Yokoyama, New cosmological constraints on primordial black holes. Phys. Rev. **D81**, 104019 (2010). arXiv:0912.5297 [astro-ph.CO]
- 122. D. Fixsen, E. Cheng, J. Gales, J.C. Mather, R. Shafer et al., The cosmic microwave background spectrum from the full COBE FIRAS data set. Astrophys. J. 473, 576 (1996). arXiv:astro-ph/9605054 [astro-ph]
- 123. A. Kogut, D. Fixsen, D. Chuss, J. Dotson, E. Dwek et al., The primordial inflation explorer (PIXIE): a nulling polarimeter for cosmic microwave background observations. JCAP 1107, 025 (2011). arXiv:1105.2044 [astro-ph.CO]
- 124. R. Brito, V. Cardoso, P. Pani, Superradiant instability of black holes immersed in a magnetic field. Phys. Rev. **D89**, 104045 (2014). arXiv:1405.2098 [gr-gc]
- 125. Data taken from the McGill online magnetar catalog, www.physics.mcgill.ca/~pulsar/magnetar/main.html
- 126. M.J. Rees, Black hole models for active galactic nuclei. Annu. Rev. Astron. Astrophys. 22(1), 471–506 (1984)
- 127. M.A. Abramowicz, P.C. Fragile, Foundations of black hole accretion disk theory. Living Rev. Relativ. 16, 1 (2013). http://www.livingreviews.org/lrr-2013-1
- 128. J.L. Friedman, Ergosphere instability. Commun. Math. Phys. **63**(3), 243–255 (1978). http://www.projecteuclid.org/euclid.cmp/1103904565
- 129. V. Cardoso, P. Pani, M. Cadoni, M. Cavaglia, Ergoregion instability of ultracompact astrophysical objects. Phys. Rev. **D77**, 124044 (2008). arXiv:0709.0532 [gr-gc]
- 130. V. Cardoso, P. Pani, M. Cadoni, M. Cavaglia, Instability of hyper-compact Kerr-like objects. Classical Quantum Gravity 25, 195010 (2008). arXiv: 0808.1615 [gr-qc]
- 131. P. Pani, E. Barausse, E. Berti, V. Cardoso, Gravitational instabilities of superspinars. Phys. Rev. **D82**, 044009 (2010). arXiv:1006.1863 [qr-qc]
- 132. C.B. Chirenti, L. Rezzolla, On the ergoregion instability in rotating gravastars. Phys. Rev. **D78**, 084011 (2008). arXiv:0808.4080 [gr-qc]
- 133. J. Keir, Slowly decaying waves on spherically symmetric spacetimes and an instability of ultracompact neutron stars (2014). arXiv:1404.7036 [gr-qc]
- 134. V. Cardoso, L.C.B. Crispino, C.F.B. Macedo, H. Okawa, P. Pani, Light rings as observational evidence for event horizons: long-lived modes, ergoregions and nonlinear instabilities of ultracompact objects. Phys. Rev. **D90**, 044069 (2014). arXiv:1406.5510 [gr-qc]
- 135. N. Comins, B.F. Schutz, On the ergoregion instability. Proc. R. Soc. Lond. A Math. Phys. Sci. 364(1717), 211–226 (1978). http://www.istor.org/stable/79759
- 136. S. Yoshida, Y. Eriguchi, Ergoregion instability revisited a new and general method for numerical analysis of stability. Mon. Not. R. Astron. Soc. 282, 580–586 (1996)
- J.M. Lattimer, M. Prakash, D. Masak, A. Yahil, Rapidly rotating pulsars and the equation of state. Astrophys. J. 355, 241–254 (1990)
- 138. N.K. Glendenning, First order phase transitions with more than one conserved charge: consequences for neutron stars. Phys. Rev. **D46**, 1274–1287 (1992)
- 139. S. Hod, Self-gravitating field configurations: the role of the energy-momentum trace. Phys. Lett. **B739**, 383 (2014). arXiv:1412.3808 [gr-gc]
- 140. S. Koranda, N. Stergioulas, J.L. Friedman, Upper limit set by causality on the rotation and mass of uniformly rotating relativistic stars. Astrophys. J. **488**, 799 (1997). arXiv:astro-ph/9608179 [astro-ph]
- 141. P. Pani, Applications of black hole perturbation theory. Eur. Phys. J. Plus 127, 67 (2012)
- 142. R. Narayan, Black holes in astrophysics. New J. Phys. 7, 199 (2005). arXiv:gr-qc/0506078 [gr-qc]
- 143. M.A. Abramowicz, W. Kluzniak, J.-P. Lasota, No observational proof of the black hole event-horizon. Astron. Astrophys. **396**, L31–L34 (2002). arXiv:astro-ph/0207270 [astro-ph]

- 144. E. Berti, V. Cardoso, C.M. Will, On gravitational-wave spectroscopy of massive black holes with the space interferometer LISA. Phys. Rev. **D73**, 064030 (2006). arXiv:gr-qc/0512160 [gr-qc]
- 145. E. Berti, V. Cardoso, A.O. Starinets, Quasinormal modes of black holes and black branes. Classical Quantum Gravity **26**, 163001 (2009). arXiv:0905.2975 [gr-qc]
- 146. E. Berti, V. Cardoso, Supermassive black holes or boson stars? Hair counting with gravitational wave detectors. Int. J. Mod. Phys. **D15**, 2209–2216 (2006). arXiv:qr-qc/0605101 [gr-qc]
- 147. M. Kesden, J. Gair, M. Kamionkowski, Gravitational-wave signature of an inspiral into a supermassive horizonless object. Phys. Rev. **D71**, 044015 (2005). arXiv:astro-ph/0411478 [astro-ph]
- 148. C.F. Macedo, P. Pani, V. Cardoso, L.C. Crispino, Into the lair: gravitational-wave signatures of dark matter. Astrophys. J. 774, 48 (2013). arXiv:1302.2646
- 149. P. Pani, E. Berti, V. Cardoso, Y. Chen, R. Norte, Gravitational wave signatures of the absence of an event horizon. I. Nonradial oscillations of a thin-shell gravastar. Phys. Rev. **D80**, 124047 (2009). arXiv:0909.0287 [gr-qc]
- 150. P. Jetzer, Boson stars. Phys. Rep. 220, 163–227 (1992)
- 151. F. Schunck, E. Mielke, General relativistic boson stars. Classical Quantum Gravity **20**, R301–R356 (2003). arXiv:0801.0307 [astro-ph]
- 152. S.L. Liebling, C. Palenzuela, Dynamical boson stars. Living Rev. Relativ. 15, 6 (2012). arXiv:1202.5809 [gr-qc]
- 153. C.F. Macedo, P. Pani, V. Cardoso, L.C.B. Crispino, Astrophysical signatures of boson stars: quasinormal modes and inspiral resonances. Phys. Rev. **D88**(6), 064046 (2013). arXiv:1307.4812 [gr-qc]
- 154. P.O. Mazur, E. Mottola, Gravitational condensate stars: an alternative to black holes (2001). arXiv:gr-qc/0109035 [gr-qc]
- 155. P.O. Mazur, E. Mottola, Gravitational vacuum condensate stars. Proc. Natl. Acad. Sci. **101**, 9545–9550 (2004). arXiv:gr-qc/0407075 [gr-qc]
- 156. M. Visser, D.L. Wiltshire, Stable gravastars: an Alternative to black holes? Classical Quantum Gravity 21, 1135–1152 (2004). arXiv:gr-qc/0310107 [gr-qc]
- 157. C.B. Chirenti, L. Rezzolla, How to tell a gravastar from a black hole. Classical Quantum Gravity 24, 4191–4206 (2007). arXiv:0706.1513 [gr-qc]
- 158. E.G. Gimon, P. Horava, Astrophysical violations of the Kerr bound as a possible signature of string theory. Phys. Lett. **B672**, 299–302 (2009). arXiv:0706.2873 [hep-th]
- 159. E. Teo, Rotating traversable wormholes. Phys. Rev. **D58**, 024014 (1998). arXiv:gr-qc/9803098 [gr-qc]
- 160. M. Visser, Lorentzian Wormholes: From Einstein to Hawking (AIP Press, American Institute of Physics, Woodbury, 1995)
- 161. F.W. Dyson, The potential of an anchor ring. Philos. Trans. R. Soc. 184, 43 (1893)
- 162. F.W. Dyson, The potential of an anchor ring. Philos. Trans. R. Soc. 184A, 1041 (1893)
- 163. S. Chandrasekhar, E. Fermi, Problems of gravitational stability in the presence of a magnetic field. Astrophys. J. **118**, 116 (1953)
- 164. V. Cardoso, L. Gualtieri, Equilibrium configurations of fluids and their stability in higher dimensions. Classical Quantum Gravity 23, 7151–7198 (2006). arXiv:hep-th/0610004 [hep-th]
- 165. L. Lehner, F. Pretorius, Black strings, low viscosity fluids, violation of cosmic censorship. Phys. Rev. Lett. 105, 101102 (2010). arXiv:1006.5960 [hep-th]
- 166. T. Johannsen, Photon rings around Kerr and Kerr-like black holes. Astrophys. J. 777, 170 (2013)
- 167. R.F. Penna, Black hole Meissner effect and Blandford-Znajek jets. Phys. Rev. **D89**(10), 104057 (2014). arXiv:1403.0938 [astro-ph.HE]
- 168. D. Neilsen, L. Lehner, C. Palenzuela, E.W. Hirschmann, S.L. Liebling et al., Boosting jet power in black hole spacetimes. Proc. Natl. Acad. Sci. 108, 12641-12646 (2011). arXiv:1012.5661 [astro-ph.HE]

169. C. Palenzuela, L. Lehner, S.L. Liebling, Dual jets from binary black holes. Science **329**, 927 (2010). arXiv:1005.1067 [astro-ph.HE]

- 170. M. Lyutikov, Schwarzschild black holes as unipolar inductors: expected electromagnetic power of a merger. Phys. Rev. **D83**, 064001 (2011). arXiv:1101.0639 [astro-ph.HE]
- 171. S.T. McWilliams, J. Levin, Electromagnetic extraction of energy from black hole-neutron star binaries. Astrophys. J. **742**, 90 (2011). arXiv:1101.1969 [astro-ph.HE]
- 172. W.H. Press, Table-top model for black hole electromagnetic instabilities, in *Frontiers Science Series 23: Black Holes and High Energy Astrophysics*, ed. by H. Sato, N. Sugiyama (Universal Academic Press, Groningen, 1998), p. 235
- 173. P. Pani, Advanced methods in black-hole perturbation theory. Int. J. Mod. Phys. A28, 1340018 (2013). arXiv:1305.6759 [gr-gc]

Chapter 6 Conclusions and Outlook

Energy extraction through superradiance is ubiquitous in physics and appears in essentially any dissipative system under different guises. In fact, we have discussed how superradiance can be understood in simple kinematical terms. In flat spacetime the most common superradiant phenomenon is Cherenkov emission, but many classical and quantum systems can be turned into superradiant amplificators. Sound and surface waves can be amplified in a variety of settings that could be easily devised in the laboratory.

In gravitational theories, superradiance is intimately connected to tidal acceleration, even at Newtonian level. Relativistic gravitational theories predict the existence of BHs, gravitational vacuum solutions whose event horizon behaves as a oneway viscous membrane. This allows superradiance to occur in BH spacetimes, and to extract energy from vacuum even at the classical level. When semiclassical effects are taken into account, superradiance occurs also in static configurations, as in the case of Hawking radiation from a Schwarzschild BH. The efficiency of superradiant scattering of GWs by a spinning (Kerr) BH can be larger than 100 % and this phenomenon is deeply connected to other important mechanisms associated to spinning compact objects, such as the Penrose process, the ergoregion instability, the Blandford-Znajek effect, and the CFS instability. Rotational superradiance might be challenging to observe in the laboratory, but its BH counterpart is associated with a number of interesting effects and instabilities, which may leave an observational imprint. We have presented a unified treatment of BH superradiant phenomena including charged BHs, higher dimensions, nonasymptotically flat spacetimes, analog models of gravity and theories beyond GR.

An important point of our analysis is the role played by the event horizon and by the ergoregion in energy-extraction processes, such as superradiance, tidal acceleration and the Penrose process. Extraction of energy and angular-momentum requires dissipation and the latter is provided by the event horizon. It is often assumed that the ergosphere (allowing negative energy states in its interior) is responsible for energy amplification. While this is largely true, the ergoregion alone

is not sufficient, the crucial role being played by the event horizon. Interestingly, the distinction between ergoregion and horizon is superfluous because, as we have shown, the existence of an event horizon in stationary and axisymmetric spacetimes implies that of an ergoregion, so the two effects (dissipation and negative-energy states) are indissolubly connected to each other.

One of the most interesting applications of BH superradiance is the possibility of tapping the amplified radiation through various mechanisms of confinement, thus producing a "BH bomb" instability. We have discussed various of such confining mechanisms, including reflecting surfaces, AdS boundaries, massive fields, magnetic fields and other nonminimal interactions. In the AdS case, superradiant instabilities of charged BHs provide a holographic dual description of a spontaneous symmetry-breaking mechanism at finite temperature, and are associated with a phase transition between RN-AdS BHs and a novel hairy BH which is the ground state at low temperatures.

The study of superradiant instabilities triggered by light bosons has flourished in recent years, because of the exciting connections between BH superradiance and particle physics. We have provided a unified picture of the state-of-the-art in this field and have described the evolution of these instabilities in a Kerr BH. Superradiant instabilities of massive bosons have important phenomenological effects, being associated to very peculiar electromagnetic and GW emission from astrophysical BHs. The effects we have discussed (formation of bosonic condensates near spinning BHs, lack of highly-spinning BHs, emission of peculiar monochromatic GWs and dipolar scalar waves) are currently investigated to constrain ultralight bosons arising in various extensions of the Standard Model, to rule out dark-matter candidates, and to study various astrophysical effects in the strong-curvature regime.

Furthermore, we have discussed novel hairy BH solutions that branch off the superradiant threshold in the AdS case and in the asymptotically-flat case with massive complex scalars. These solutions can be interpreted as the nonlinear extension of linear bound states of frequency saturating the superradiant condition (1.1), and give rise to stationary hairy BHs that interpolate between Kerr BHs and regular solutions without a horizon. These hairy BHs evade the no-hair theorem of GR and might play an important role in astrophysical tests of the Kerr hypothesis.

BH superradiance has been discovered more than 40 years ago, but it is nowadays more alive than ever. Not only new exciting theoretical developments have been recently discovered, but it is likely that upcoming electromagnetic and GW facilities will allow us to observe the effects of BH superradiance directly in the near future, thus providing a new tool to test gravitational interactions and particle physics in curved spacetime. Among the most urgent open problems are the fully nonlinear evolution of the superradiant instability, the stability of hairy BHs, electromagnetic and GW tests of bosonic condensates around massive BHs, observing superradiance in analog-gravity models in the laboratory, understanding completely the holographic dual of superradiant states and their microscopic description.

Appendix A List of Publicly Available Codes

The numerical and analytical methods used in this work have been implemented in ready-to-be-used MATHEMATICA[®] notebooks, which are publicly available [1]. Here we give a short description of them:

- **superradiance charge.nb**: Amplification factors of the superradiant scattering of a charged wave off a spherically-symmetric or a slowly-rotating BH with generic metric.
- **superradiance spin.nb**: Amplification factors of the superradiant scattering of a neutral bosonic wave of generic spin off a Kerr BH, obtained by solving the Teukolsky equations.
- Kerr massive scalar bound states.nb: solves the eigenspectrum of unstable modes of a Kerr BH under massive scalar perturbations through Leaver's continued fraction method.
- HartleThorne.nb: (a) computes and solves Einstein's equations for a rotating self-gravitating perfect-fluid to second order in the spin and (b) derives in detail the procedure to separate the Klein-Gordon equation in this background.

Some data presented in the main text are also available on the webpage [1]. For example, the data files contained in the file **superradiance spin.nb** provide the dependence of the amplification factor $Z_{slm}(\omega)$ for a Kerr BH in the entire parameter space. The number of digits in the tables is not indicative of the precision; our tests indicate a precision of roughly one part in 10^5 .

Appendix B

Analytic Computation of the Amplification Coefficients

In this section we compute the cross section of a Kerr BH for generic spin. We will follow [2, 3]. We assume that the Compton wavelength of the particle is much bigger than the gravitational size of the BH, i.e., $\omega M \ll 1$. We also consider the slowly rotating regime $a\omega \ll 1$.

To solve the radial equation (3.73) we use a matching procedure, dividing the spacetime in two overlapping regions, the near-region $r - r_+ \ll 1/\omega$, and the farregion $M \ll r - r_+$.

Changing variables to

$$x = \frac{r - r_{+}}{r_{+} - r_{-}} \,, \tag{B.1}$$

Eq. (3.73) is approximately given by

$$x(1+x)^{2} \frac{d^{2}R}{dx^{2}} + (s+1)x(x+1)(2x+1)\frac{dR}{dx} + \left[k^{2}x^{4} + 2iskx^{3} - \lambda x(x+1) - isQ(2x+1) + Q^{2}\right]R = 0,$$
 (B.2)

where
$$Q = \frac{\omega - m\Omega_{\rm H}}{4\pi T_H}$$
, $4\pi T_H = (r_+ - r_-)/r_+^2$ and $k = \omega (r_+ - r_-)$.

(i) Near-Region Solution In this region we consider $kx \ll 1$ such that Eq. (B.2) is then approximately given by

$$x(1+x)^{2} \frac{d^{2}R}{dx^{2}} + (s+1)x(x+1)(2x+1)\frac{dR}{dx} + \left[Q^{2} - isQ(2x+1) - \lambda x(x+1)\right]R = 0.$$
 (B.3)

The most general solution to Eq. (B.3), satisfying the ingoing boundary condition is given by

$$R = A_1 x^{-s-iQ} (x+1)^{-s+iQ} F(\alpha, \beta, \gamma, -x), \qquad (B.4)$$

$$\gamma = 1 - s - 2iQ, \tag{B.5}$$

$$\alpha = -l - s \,, \tag{B.6}$$

$$\beta = l - s + 1. \tag{B.7}$$

The large x behavior is

$$R \sim A_1 \left[x^{l-s} \frac{\Gamma(\gamma)\Gamma(\beta - \alpha)}{\Gamma(\gamma - \alpha)\Gamma(\beta)} + x^{-l-1-s} \frac{\Gamma(\gamma)\Gamma(\alpha - \beta)}{\Gamma(\alpha)\Gamma(\gamma - \beta)} \right]. \tag{B.8}$$

(ii) Far-Region Solution In the asymptotic region Eq. (B.2) is approximately given by

$$\frac{d^2R}{dx^2} + \frac{2(1+s)}{x}\frac{dR}{dx} + \left(k^2 + \frac{2isk}{x} - \frac{\lambda}{x^2}\right)R = 0,$$
 (B.9)

The solution of this equation can be written in terms of the confluent hypergeometric function

$$R = C_1 e^{-ikx} x^{l-s} U(l-s+1, 2l+2, 2ikx) + C_2 e^{-ikx} x^{-l-s-1} U(-l-s, -2l, 2ikx).$$
 (B.10)

Expanding for small $kx \ll 1$, we obtain

$$R \sim C_1 x^{l-s} + C_2 x^{-l-s-1}$$
 (B.11)

Matching (B.8) and (B.11) we get

$$C_1 = A_1 \frac{\Gamma(1 - s - 2iQ)\Gamma(2l + 1)}{\Gamma(l - s + 1)\Gamma(l + 1 - 2iQ)},$$
(B.12)

$$C_2 = A_1 \frac{\Gamma(1 - s - 2iQ)\Gamma(-1 - 2l)}{\Gamma(-l - 2iQ)\Gamma(-l - s)}.$$
 (B.13)

When $r \to \infty$ and in the low-frequency limit, the solution of (3.73) behaves as

$$R_{slm} \sim \mathcal{I}_s \frac{e^{-i\omega r}}{r} + \mathcal{R}_s \frac{e^{i\omega r}}{r^{2s+1}}, \text{ as } r \to \infty.$$
 (B.14)

To compute the fluxes at infinity, we must relate the C_1 and C_2 with \mathcal{I}_s and \mathcal{R}_s . Expanding (B.10) at infinity and matching to (B.14) we find

$$\mathcal{I}_{s} = \frac{1}{\omega} \left[k^{l+1+s} \frac{C_{2}(-2i)^{l+s} \Gamma(-2l)}{\Gamma(-l+s)} + k^{s-l} \frac{C_{1}(-2i)^{s-l-1} \Gamma(2l+2)}{\Gamma(l+s+1)} \right], \quad (B.15)$$

$$\mathcal{R}_{s} = \omega^{-2s-1} \left[k^{l+1+s} \frac{C_{2}(2i)^{l-s} \Gamma(-2l)}{\Gamma(-l-s)} + k^{s-l} \frac{C_{1}(2i)^{-l-s-1} \Gamma(2l+2)}{\Gamma(l-s+1)} \right]. \quad (B.16)$$

To obtain the fluxes one can use the trick proposed in [4]: solve Eq. (3.73) replacing s by -s, with the asymptotic behavior of R_{-slm} given by

$$R_{-slm} \sim \mathcal{I}_{-s} \frac{e^{-i\omega r}}{r} + \mathcal{R}_{-s} \frac{e^{i\omega r}}{r^{-2s+1}}$$
 (B.17)

Making use of the symmetries of the radial equation,

$$R_{slm\omega}(r) = (-1)^m R_{sl-m-\omega}^*(r) ,$$

 $R_{slm\omega}^*(r) = \Delta^{-s} R_{-slm\omega}(r) ,$ (B.18)

the absorption coefficient can then be computed using

$$Z_{slm} = \frac{dE_{\text{out}}}{dE_{\text{in}}} - 1 = \left| \frac{\mathcal{R}_s \mathcal{R}_{-s}}{\mathcal{I}_s \mathcal{I}_{-s}} \right| - 1.$$
 (B.19)

After some algebra one finally finds (3.102) (see also the Appendix of [4] for details).

Appendix C

Angular Momentum and Energy

Consider a stationary and axially symmetric spacetime with Killing vector fields $\xi^{\mu}_{(t)} \equiv \partial^{\mu} t$ and $\xi^{\mu}_{(\varphi)} \equiv \partial^{\mu} \varphi$. For a stress-energy tensor $T_{\mu\nu}$ the conserved energy flux vector is given by

$$\epsilon^{\mu} = -T^{\mu}_{\ \nu} \xi^{\nu}_{(t)} \,, \tag{C.1}$$

and the conserved angular momentum flux vector by

$$l^{\mu} = T^{\mu}_{\ \nu} \xi^{\nu}_{(\alpha)} \,. \tag{C.2}$$

Thus over a hypersurface $\mathbf{d}\Sigma_{\mu}$ the energy and angular momentum fluxes are

$$\delta E = \epsilon^{\mu} \mathbf{d} \Sigma_{\mu} \,, \qquad \delta J = l^{\mu} \mathbf{d} \Sigma_{\mu} \,. \tag{C.3}$$

Over a spherical surface $\mathbf{d}\Sigma_{\mu} \equiv n_{\mu}r^2dtd\Omega$, where n_{μ} is the radial outgoing normal vector to the surface, we then have

$$\frac{\delta J}{\delta E} = -\frac{T_{\varphi}^r}{T_t^r}.$$
 (C.4)

Considering a scalar field $\Phi(t, r, \vartheta, \varphi) = f(r, \vartheta)e^{-i\omega t + im\varphi}$ with the scalar stress-energy tensor

$$T_{\mu\nu} = \Phi_{,\mu}\Phi_{,\nu} - \frac{1}{2}g_{\mu\nu}\Phi_{\alpha}\Phi^{\alpha},$$
 (C.5)

one finds

$$\frac{\delta J}{\delta E} = \frac{m}{\omega} \,. \tag{C.6}$$

This applies for generic fields (photons, gravitons, ...) as can be seen, by using the electromagnetic stress-energy tensor or using the effective stress-energy tensor for linearized gravitational waves [5]. We can also see it using the following simple argument [6]. At infinity the wave is composed of many quanta each with energy $E = \hbar \omega$ and angular momentum in the φ direction $J = \hbar m$. Thus the ratio of the total angular momentum to the total energy carried by the wave across a sphere must be m/ω .

C.1 Energy and Angular Momentum Fluxes at the Horizon

The energy flux at the horizon, as measured at infinity, is given by

$$\delta E_{\text{hole}} = -T_{\mu}^{\ \nu} \xi_{(t)}^{\mu} d^3 \Sigma_{\nu} , \qquad (C.7)$$

where $\xi^{\mu}_{(t)} \equiv \partial^{\mu} t$ is the time Killing vector of the Kerr metric and Σ_{μ} is the 3-surface element of the hole given by

$$d^{3}\Sigma_{\mu} = n_{\mu} 2Mr_{+} \sin \vartheta d\vartheta d\varphi dt, \qquad (C.8)$$

with the normal vector n_{μ} in the inward direction. Likewise we can define a conserved angular momentum flux associated with the axial Killing vector $\xi^{\mu}_{(\varphi)} \equiv \partial^{\mu}\varphi$,

$$\delta J_{\text{hole}} = T_{\mu}{}^{\nu} \xi^{\mu}_{(\omega)} d^{3} \Sigma_{\nu} \,. \tag{C.9}$$

On the horizon we have

$$n^{\mu} = \xi^{\mu}_{(t)} + \Omega_{\rm H} \xi^{\mu}_{(\varphi)},$$
 (C.10)

thus for any wave that enters the BH we obtain

$$\frac{d^2 E_{\text{hole}}}{dt d\Omega} - \Omega_{\text{H}} \frac{d^2 J_{\text{hole}}}{dt d\Omega} = 2M r_+ T^{\mu\nu} n_\mu n_\nu \,. \tag{C.11}$$

Because of energy conservation, an angular momentum increment δJ is related to an energy increment $\delta E \equiv \delta M$ by Eq. (3.23) [6]. Inserting this in (C.11) gives

$$\frac{d^2 E_{\text{hole}}}{dt d\Omega} = \frac{\omega}{k_H} 2M r_+ T^{\mu\nu} n_\mu n_\nu . \tag{C.12}$$

Appendix D

Electromagnetic Fluctuations Around a Rotating Black Hole Enclosed in a Mirror

Consider the evolution of a Maxwell field in a Schwarzschild background with metric given by

$$ds^{2} = -f(r)dt^{2} + \frac{dr^{2}}{f(r)} + r^{2}(d\vartheta^{2} + \sin^{2}\vartheta d\varphi^{2}),$$
 (D.1)

where, f(r) = 1 - 2M/r and M is the BH mass. The perturbations are governed by Maxwell's equations:

$$F^{\mu\nu}_{;\nu} = 0 \quad , F_{\mu\nu} = A_{\nu,\mu} - A_{\mu,\nu} \,,$$
 (D.2)

where a comma stands for ordinary derivative and a semi-colon for covariant derivative. Since the background is spherically symmetric, we can expand A_{μ} in four-dimensional vector spherical harmonics (see [7]):

$$A_{\mu}(t,r,\vartheta,\varphi) = \sum_{l,m} \left[\begin{pmatrix} 0\\0\\a^{lm}(t,r)\bar{\mathbf{S}}_{lm} \end{pmatrix} + \begin{pmatrix} f^{lm}(t,r)Y_{lm}\\h^{lm}(t,r)Y_{lm}\\k^{lm}(t,r)\bar{\mathbf{Y}}_{lm} \end{pmatrix} \right], \tag{D.3}$$

with the vector spherical harmonics given by,

$$\bar{\mathbf{Y}}_{lm}^{\mathsf{T}} = \left(\partial_{\vartheta} Y_{lm}, \partial_{\varphi} Y_{lm}\right), \quad \bar{\mathbf{S}}_{lm}^{\mathsf{T}} = \left(\frac{1}{\sin \vartheta} \partial_{\varphi} Y_{lm}, -\sin \vartheta \, \partial_{\vartheta} Y_{lm}\right), \tag{D.4}$$

and where Y_{lm} are the usual scalar spherical harmonics, m is the azimuthal number and l the angular quantum number. The first term in the right-hand side has parity $(-1)^{l+1}$, and the second term has parity $(-1)^{l}$. We shall call the former the axial modes and the latter the polar modes.

Upon defining

$$\Upsilon^{lm} = \frac{r^2}{l(l+1)} \left(\partial_t h^{lm} - \partial_r f^{lm} \right) , \qquad (D.5)$$

and inserting (D.3) into Maxwell's equations (D.2), and after some algebra, we get the following system of equations

$$\frac{\partial^2 a^{lm}(t,r)}{\partial r_*^2} + \left[-\frac{\partial^2}{\partial t^2} - V(r) \right] a^{lm}(t,r) = 0, \qquad (D.6)$$

$$\frac{\partial^2 \Upsilon^{lm}(t,r)}{\partial r_*^2} + \left[-\frac{\partial^2}{\partial t^2} - V(r) \right] \Upsilon^{lm}(t,r) = 0, \qquad (D.7)$$

$$V = f \frac{l(l+1)}{r^2} \,. \tag{D.8}$$

If we assume a time dependence a^{lm} , $\Upsilon^{lm} \propto e^{-i\omega t}$, the equation for electromagnetic perturbations of the Schwarzschild geometry takes the form

$$\frac{\partial^2 \Psi}{\partial r_{*}^2} + \left[\omega^2 - V\right] \Psi = 0, \qquad (D.9)$$

where the tortoise coordinate is defined through $dr/dr^* = f(r)$, $\Psi = a^{lm}$ for axial modes and $\Psi = \Upsilon$ for polar modes. The potential V appearing in Eq. (D.9) is given by Eq. (D.8).

Let us now assume we have a spherical conductor at $r=r_m$. The conditions to be satisfied are then that the electric/magnetic field as seen by an observer at rest with respect to the conductor has no tangential/parallel components, $E_{\vartheta} \propto F_{\vartheta t} = 0$, $E_{\varphi} \propto F_{\varphi t}$, $B_r \propto F_{\varphi \vartheta} = 0$. This translates into

$$\partial_t a^{lm}(t, r_m) = 0$$
, $f^{lm}(t, r_m) - \partial_t k^{lm}(t, r_m) = 0$. (D.10)

Using Maxwell's equations (D.2), we get the relation

$$f^{lm}(t,r_m) - \partial_t k^{lm}(t,r_m) = \frac{f}{l(l+1)} \partial_r \left(r^2 \partial_r f^{lm} - r^2 \partial_t h^{lm} \right). \tag{D.11}$$

Finally, using Eq. (D.5) we get

$$\partial_r \Upsilon = 0. \tag{D.12}$$

In other words, the boundary conditions at the surface $r=r_m$ are $\Psi=0$ and $\partial_r \Psi=0$ for axial and polar perturbations respectively. This can be used to easily

compute the electromagnetic modes inside a resonant cavity in flat space. Taking M = 0 in Eq. (D.9) we find the exact solution

$$\Psi = \sqrt{r} \left[C_1 J_{l+1/2}(r\omega) + C_2 Y_{l+1/2}(r\omega) \right],$$
 (D.13)

where C_i are constants and $J_n(r\omega)$ and $Y_n(r\omega)$ are Bessel functions of the first and second kind, respectively. Imposing regularity at the origin r=0 implies $C_2=0$. The Dirichlet boundary condition $\Psi=0$ at $r=r_m$, which can easily be shown to correspond to the *transverse electric* modes (modes with $E_r=0$) [8], then gives

$$\omega_{\text{TE}} = \frac{j_{l+1/2,n}}{r_m} \,, \tag{D.14}$$

where $j_{l+1/2,n}$ are the zeros of the Bessel function $J_{l+1/2}$ and n is a non-negative integer. On the other hand the eigenfrequencies for the Neumann boundary condition $\partial_r \Psi = 0$, which corresponds to the *transverse magnetic* modes (modes with $B_r = 0$) [8], can be computed solving

$$\left\{\partial_r \left[\sqrt{r} J_{l+1/2}(r\omega) \right] \right\}_{r=r_m} = \frac{(l+1) J_{l+1/2}(r_m \omega) - r_m \omega J_{l+3/2}(r_m \omega)}{\sqrt{r_m}} = 0.$$
(D.15)

Defining $\tilde{j}_{l+1/2,n}$ as being the zeroes of $\partial_r \left[\sqrt{r_m} J_{l+1/2}(r_m \omega) \right]$ we find

$$\omega_{\text{TM}} = \frac{\tilde{j}_{l+1/2,n}}{r_m} \,. \tag{D.16}$$

The eigenfrequencies for l=1 and n=0 are shown in Fig. 4.3 where we see that when $r_m \gg M$, the real part of the quasinormal frequencies of a BH enclosed in a mirror asymptotically reduces to the flat space result. One can write down a relation between the Regge-Wheeler function Ψ [9–11] and the Teukolsky radial function R (cf. Eq. (3.72)) given by

$$\frac{\Psi}{r(r^2 - 2Mr)^{s/2}} = \left(r\sqrt{\Delta}\right)^{|s|} \mathcal{D}_{-}^{|s|} \left(r^{-|s|}R\right), \ s < 0,$$

$$\frac{\Psi}{r(r^2 - 2Mr)^{s/2}} = \left(\frac{r}{\sqrt{\Delta}}\right)^s \mathcal{D}_{+}^s \left[\left(\frac{r^2 - 2Mr}{r}\right)^s R\right], \ s > 0, \tag{D.17}$$

where $\mathcal{D}_{\pm}=d/dr\pm i\omega/f$. Using these relations and Teukolsky's radial equation (3.73), one finds that the Dirichlet and the Neumann boundary conditions for Ψ , correspond to the Robin boundary conditions for the radial function R given respectively by

$$\partial_r R_{-1} = \frac{r - 2M + ir^2 \omega}{r(r - 2M)} R_{-1}, \qquad (D.18)$$

$$\partial_r R_{-1} = \frac{r\omega[2M + r(-1 - ir\omega)] - il(l+1)(2M - r)}{(2M - r)r^2\omega} R_{-1}.$$
 (D.19)

After having understood the nonrotating case, below we turn to the rotating case. The main difficulty relies in describing the electromagnetic physical quantities in terms of the Newman-Penrose quantities. We will show that doing so, will allow us to generalize the conditions (D.18) and (D.19).

Newman-Penrose Approach In the Newman-Penrose formalism, the electromagnetic field is characterized by three complex scalars from which one can obtain the electric and magnetic field. The details of this procedure are not important for us here so we refer the reader to [12]. In the frame of a ZAMO observer (cf. Sect. 3.1), the relevant electric and magnetic field components read [12]

$$\begin{split} E_{(\vartheta)} &= \left[\frac{\Delta^{1/2} (r^2 + a^2)}{\sqrt{2} \rho^* A^{1/2} (r^2 + a^2 \cos^2 \vartheta)} \left(\frac{\phi_0}{2} - \frac{\phi_2}{\rho^2 \Delta} \right) + \text{c.c.} \right] - \frac{2a \Delta^{1/2}}{A^{1/2}} \sin \vartheta \, \text{Im}(\phi_1) \,, \\ E_{(\varphi)} &= \left[-i \Delta^{1/2} \rho \left(\frac{\phi_0}{2\sqrt{2}} + \frac{\phi_2}{\sqrt{2} \rho^2 \Delta} \right) + \text{c.c.} \right] \,, \\ B_{(r)} &= \left[\frac{a \sin \vartheta}{\sqrt{2} \rho A^{1/2}} \left(\phi_2 - \Delta \rho^2 \frac{\phi_0}{2} \right) + \text{c.c.} \right] + 2 \frac{r^2 + a^2}{A^{1/2}} \text{Im}(\phi_1) \,, \end{split} \tag{D.20}$$

where $\rho = -(r - ia\cos\vartheta)^{-1}$, $A = (r^2 + a^2)^2 - a^2\Delta\sin^2\vartheta$ and $\Delta = r^2 - 2Mr + a^2$. If we assume a conducting spherical surface surrounding the BH at $r = r_m$, then Maxwell's equations require that $E_{(\vartheta)} = E_{(\varphi)} = B_{(r)} = 0$ at $r = r_m$ and we are left with the boundary conditions at the conductor:

$$\operatorname{Re}\left(\rho\Phi_{0}\right) = \frac{\operatorname{Re}\left(\rho\Phi_{2}\right)}{\Delta}, \quad \operatorname{Im}\left(\rho\Phi_{0}\right) = -\frac{\operatorname{Im}\left(\rho\Phi_{2}\right)}{\Delta}, \quad \operatorname{Im}(\phi_{1}) = 0, \quad (D.21)$$

where we defined $\Phi_0=\phi_0$ and $\Phi_2=2\rho^{-2}\phi_2$. This can be simplified to

$$\rho \Phi_0 = \frac{\rho^* \Phi_2^*}{\Lambda} \,. \tag{D.22}$$

We use the decomposition

$$\Phi_{0} = e^{-i\omega t + im\varphi} R_{slm\omega} S_{slm\omega}(\vartheta) \pm e^{i\omega t - im\varphi} R_{sl-m-\omega} S_{sl-m-\omega}(\vartheta), \qquad (D.23)$$

$$\Phi_{2} = e^{-i\omega t + im\varphi} R_{-slm\omega} S_{-slm\omega}(\vartheta) \pm e^{i\omega t - im\varphi} R_{-sl-m-\omega} S_{-sl-m-\omega}(\vartheta), \qquad (D.24)$$

where the plus and minus signs stand for different polarizations, while the radial and the angular function, R and S, satisfy Teukolsky's Eqs. (3.73) and (3.74), respectively. The functions $R_{s=1}$ can be written as a linear combination of $R_{s=-1}$,

and $S_{s=-1}$ can be written as a linear combination of $S_{s=1}$ and its derivative through the Starobinski-Teukolsky identities [13–15]

$$\mathcal{D}_0 \mathcal{D}_{0-1} R = B R_1, \quad \mathcal{L}_0 \mathcal{L}_1 S_1 = B S_{-1},$$
 (D.25)

where $B = \sqrt{(\lambda + a^2\omega^2 - 2am\omega)^2 + 4ma\omega - 4a^2\omega^2}$ and the linear operators are given by

$$\mathcal{D}_0 = \partial_r - i\frac{K}{\Delta}, \quad \mathcal{L}_n = \partial_\vartheta + m\csc\vartheta - a\omega\sin\vartheta + n\cot\vartheta.$$
 (D.26)

Furthermore, from Teukolsky's equations one can derive the following identities [9]

$$R_{slm\omega}^* = (-1)^m R_{sl-m-\omega}, \quad S_{slm\omega}^* = (-1)^m S_{-sl-m-\omega}.$$
 (D.27)

Finally, using (D.23), (D.27) and (D.25) we find that the boundary conditions (D.22) can be written as the following conditions for the two polarizations:

$$\partial_{r}R_{-1} = \frac{-i\Delta\left[\pm B + A_{lm} + \omega\left(a^{2}\omega - 2am + 2ir\right)\right]}{2\Delta\left(a^{2}\omega - am + r^{2}\omega\right)}R_{-1} + \frac{\left(a^{2}\omega - am + r^{2}\omega\right)\left(2ia^{2}\omega - 2iam + 2M + 2ir^{2}\omega + \partial_{r}\Delta - 2r\right)}{2\Delta\left(a^{2}\omega - am + r^{2}\omega\right)}R_{-1},$$
(D.28)

which is the result shown in Sect. 4. Note that to for a=0 we recover the condition (D.18) when using the minus sign, while for the plus sign we recover the condition (D.19).

Appendix E

Hartle-Thorne Formalism for Slowly-Rotating Spacetimes and Perturbations

In this Appendix we summarize the formalism originally developed by Hartle and Thorne [16] to construct slowly-rotating stars and that developed by Kojima [17, 18] to include generic nonspherical perturbations (see also [19, 20] for extensions and [21] for a review.).

E.1 Background

Let us start by considering the most general stationary axisymmetric spacetime (we also assume circularity, see Sect. 3.1.5 and [22])

$$ds_0^2 = g_{tt}dt^2 + g_{rr}dr^2 + 2g_{t\varphi}dtd\varphi + g_{\vartheta\vartheta}d\vartheta^2 + g_{\varphi\varphi}d\varphi^2, \qquad (E.1)$$

where g_{tt} , g_{rr} , $g_{t\varphi}$, $g_{\vartheta\vartheta}$ and $g_{\varphi\varphi}$ are functions of r and ϑ only. Assuming slow rotation, we construct a perturbative expansion in the angular momentum J (or in some other parameter linear in J, which characterizes the rotation rate). To second order in rotation, the metric above can be expanded as [16]

$$d\tilde{s}^{2} = -e^{\nu} \left[1 + 2\epsilon^{2} \left(h_{0} + h_{2} P_{2} \right) \right] dt^{2} + \frac{1 + 2\epsilon^{2} (m_{0} + m_{2} P_{2}) / (r - 2M)}{1 - 2M / r} dr^{2} + r^{2} \left[1 + 2\epsilon^{2} (\nu_{2} - h_{2}) P_{2} \right] \left[d\vartheta^{2} + \sin^{2} \vartheta \left(d\varphi - \epsilon \varpi dt \right)^{2} \right], \tag{E.2}$$

where $P_2 = P_2(\cos \vartheta) = (3\cos^2 \vartheta - 1)/2$ is a Legendre polynomial. The radial functions ν and M are of zeroth order in rotation, ϖ is of first order, and h_0 , h_2 , m_0 , m_2 , ν_2 are of second order.

We consider a perfect fluid coupled to gravity with a barotropic equation of state $P = P(\rho)$, where P and ρ are the pressure and the density of the fluid, respectively. Under an infinitesimal rotation both P and ρ transform as scalars. As shown in [16,

23], in order to perform a valid perturbative expansion it is necessary to transform the radial coordinate in such a way that the deformed density in the new coordinates coincides with the unperturbed density at the same location. It can be shown that this transformation is formally equivalent to working in the original coordinates but expanding the pressure and the density as

$$P \equiv P_0 + \Delta P = P_0 + (\rho_0 + P_0)(p_0 + p_2 P_2), \tag{E.3}$$

$$\rho \equiv \rho_0 + \Delta \rho = \rho_0 + (\rho_0 + P_0) \frac{\partial \rho_0}{\partial P_0} (p_0 + p_2 P_2), \qquad (E.4)$$

where P_0 and ρ_0 denote the corresponding quantities in the nonrotating case. Finally, the stress-energy tensor is the standard one,

$$T^{\mu\nu} = (P + \rho)u^{\mu}u^{\nu} + g^{\mu\nu}P,$$
 (E.5)

where u^{μ} is the fluid four-velocity. By plugging the decompositions above into the gravitational equations $G_{\mu\nu} = 8\pi T_{\mu\nu}$, and by solving the equations order by order in the spin, we obtain a system of ODEs for the rotating background, which can be solved by standard methods [16, 23, 24].

E.2 Perturbations of a Slowly-Rotating Object

Perturbations of slowly rotating and oscillating compact objects can be studied by perturbing the solution discussed above. Scalar, vector and tensor field equations in the background metric (E.2) can be linearized in the field perturbations. Any perturbation function δX can be expanded in a complete basis of spherical harmonics, similarly to the static case. Schematically, in the frequency domain we have

$$\delta X_{\mu_1\dots}(t,r,\vartheta,\varphi) = \delta X_{lm}^{(i)} \mathcal{Y}_{\mu_1\dots}^{lm\,(i)} e^{-i\omega t} \,, \tag{E.6}$$

where $\mathcal{Y}_{\mu_1...}^{lm\,(i)}$ is a basis of scalar, vector or tensor harmonics, depending on the tensorial nature of the perturbation δX . As in the spherically symmetric case, the perturbation variables $\delta X_{lm}^{(i)}$ can be classified as "polar" or "axial" depending on their behavior under parity transformations.

The linear response of the system is fully characterized by a coupled system of ODEs in the perturbation functions $\delta X_{lm}^{(i)}$. In the case of a spherically symmetric background, perturbations with different values of (l, m), as well as perturbations with opposite parity, are decoupled. In a rotating, axially symmetric background, perturbations with different values of m are still decoupled but perturbations with different values of l are not.

(E.8)

To second order, the perturbation equations read schematically as (cf. [21] for details)

$$0 = \mathcal{A}_{l} + \tilde{a}m\bar{\mathcal{A}}_{l} + \tilde{a}^{2}\hat{\mathcal{A}}_{l} + \tilde{a}(\mathcal{Q}_{l}\tilde{\mathcal{P}}_{l-1} + \mathcal{Q}_{l+1}\tilde{\mathcal{P}}_{l+1})$$

$$+\tilde{a}^{2} \left[\mathcal{Q}_{l-1}\mathcal{Q}_{l}\check{\mathcal{A}}_{l-2} + \mathcal{Q}_{l+2}\mathcal{Q}_{l+1}\check{\mathcal{A}}_{l+2} \right] + \mathcal{O}(\tilde{a}^{3}), \qquad (E.7)$$

$$0 = \mathcal{P}_{l} + \tilde{a}m\bar{\mathcal{P}}_{l} + \tilde{a}^{2}\hat{\mathcal{P}}_{l} + \tilde{a}(\mathcal{Q}_{l}\tilde{\mathcal{A}}_{l-1} + \mathcal{Q}_{l+1}\tilde{\mathcal{A}}_{l+1})$$

$$+\tilde{a}^{2} \left[\mathcal{Q}_{l-1}\mathcal{Q}_{l}\check{\mathcal{P}}_{l-2} + \mathcal{Q}_{l+2}\mathcal{Q}_{l+1}\check{\mathcal{P}}_{l+2} \right] + \mathcal{O}(\tilde{a}^{3}), \qquad (E.8)$$

where $\tilde{a}=a/M$, $\mathcal{Q}_l=\sqrt{\frac{l^2-m^2}{4l^2-1}}$ and the coefficients \mathcal{A}_l and \mathcal{P}_l (with various superscripts) are *linear* combinations of axial and polar perturbation variables, respectively.

The structure of Eqs. (E.7)–(E.8) is interesting. In the limit of slow rotation there is a Laporte-like "selection rule" [25]. Perturbations with a given parity and index l are coupled to: (i) perturbations with *opposite* parity and index $l \pm 1$ at order ϵ_a ; (ii) perturbations with *same* parity and *same* index l up to order ϵ_a^2 ; (iii) perturbations with *same* parity and index $l \pm 2$ at order ϵ_a^2 . Furthermore, from the definition of Q_l it follows that $Q_{\pm m} = 0$, and therefore if |m| = l the coupling of perturbations with index l to perturbations with indices l-1 and l-2 is suppressed. This general property is usually called [25] "propensity rule" in atomic theory, and states that transitions $l \to l+1$ are strongly favored over transitions $l \to l-1$. Indeed, the slow-rotation technique is well known in quantum mechanics and the coefficients Q_l are related to the usual Clebsch-Gordan coefficients.

Scalar Perturbations of a Slowly-Rotating Star E.2.1

The formalism above can be applied to any type of perturbations of a generic stationary and axisymmetric background. The simplest example is a probe scalar field governed by the Klein-Gordon equation (2.36) and propagating on the fixed geometry (E.2). The entire procedure is performed in a publicly available MATHEMATICA[®] notebook, cf. Appendix A.

We start by the standard decomposition of the scalar field in spherical harmonics in Fourier space,

$$\Phi = \sum_{lm} \int d\omega \, \Psi_l(r) Y^l(\vartheta, \varphi) e^{-i\omega t} \,. \tag{E.9}$$

By plugging this equation into (2.36) and using the line element (E.2), we obtain the following equation in schematic form:

$$A_l Y^l + \hat{A}_l \cos^2 \vartheta Y^l + \tilde{B}_l \cos \vartheta \sin \vartheta Y^l_{\vartheta} = 0, \qquad (E.10)$$

where a sum over (l, m) is implicit, and the explicit form of the radial coefficients A_l , \hat{A}_l and \tilde{B}_l is given in the notebook. The coefficients \hat{A}_l and \tilde{B}_l are proportional to terms quadratic in the spin, so they vanish to first order. Indeed, to first order the equation reduces to $A_l = 0$ which can be explicitly written as in Eq. (4.57).

The separation of Eq. (E.10) can be achieved by using the identities [17]

$$\begin{split} \cos\vartheta Y^{l} &= \mathcal{Q}_{l+1}Y^{l+1} + \mathcal{Q}_{l}Y^{l-1} \,, \\ &\sin\vartheta \, \vartheta_{\vartheta}Y^{l} = \mathcal{Q}_{l+1}lY^{l+1} - \mathcal{Q}_{l}(l+1)Y^{l-1} \,, \\ &\cos^{2}\vartheta Y^{l} = \left(\mathcal{Q}_{l+1}^{2} + \mathcal{Q}_{l}^{2}\right)Y^{l} + \mathcal{Q}_{l+1}\mathcal{Q}_{l+2}Y^{l+2} + \mathcal{Q}_{l}\mathcal{Q}_{l-1}Y^{l-2} \,, \\ &\cos\vartheta \sin\vartheta \, \vartheta_{\vartheta}Y^{l} = \left(l\mathcal{Q}_{l+1}^{2} - (l+1)\mathcal{Q}_{l}^{2}\right)Y^{l} + \mathcal{Q}_{l+1}\mathcal{Q}_{l+2}lY^{l+2} - \mathcal{Q}_{l}\mathcal{Q}_{l-1}(l+1)Y^{l-2} \,, \end{split}$$

and so on, as well as the orthogonality property of scalar spherical harmonics. The result reads

$$A_{l} + \mathcal{Q}_{l+1}^{2}[\hat{A}_{l} + l\tilde{B}_{l}] + \mathcal{Q}_{l}^{2}[\hat{A}_{l} - (l+1)\tilde{B}_{l}]$$

+ $\mathcal{Q}_{l-1}\mathcal{Q}_{l}[\hat{A}_{l-2} + (l-2)\tilde{B}_{l-2}] + \mathcal{Q}_{l+2}\mathcal{Q}_{l+1}[\hat{A}_{l+2} - (l+3)\tilde{B}_{l+2}] = 0$. (E.11)

Therefore, at second order, perturbations with harmonic index l are coupled to perturbations with $l \pm 2$. Crucially, this coupling does not contribute to the eigenfrequencies to second order [19, 21]. Therefore, for given values of l and m, the eigenspectrum of the scalar perturbations is governed by a single ODE:

$$A_l + Q_{l+1}^2 [\hat{A}_l + l\tilde{B}_l] + Q_l^2 [\hat{A}_l - (l+1)\tilde{B}_l] = 0.$$
 (E.12)

In the online notebook HartleThorne.nb we show that the equation above reduces to (4.58) and we give the explicit form of V_2 , which is too involved to be reproduced here.

Appendix F

WKB Analysis of Long-Lived and Unstable Modes of Ultracompact Objects

As discussed in Sect. 4.11.2, ultracompact objects have two light rings [26]. From a point of view of massless fields, which propagate as null particles in the eikonal regime, the light rings effectively confine the field and give rise to long-lived modes, which may become unstable if they form within the ergoregion. Here we perform a WKB analysis of these trapped modes.

Let us first discuss static, spherically symmetric spacetimes described by a line element given in Eq. (4.60) with $\varpi=0$. Various classes of perturbations of this geometry are described by a master equation of the form (3.50) where $V_{\rm eff}=\omega^2-V_{sl}(r)$, and the effective potential for wave propagation reads [26]

$$V_{sl}(r) = f \left[\frac{l(l+1)}{r^2} + \frac{1 - s^2}{2rB} \left(\frac{f'}{f} - \frac{B'}{B} \right) + 8\pi (p_{\text{rad}} - \rho) \delta_{s2} \right], \quad (\text{F.1})$$

and the prime denotes derivative with respect to the coordinate r, which is related to the tortoise coordinate r_* through $dr/dr_* = \sqrt{f/B}$. In the potential (F.1) $l \ge s$, s = 0, 1 for test Klein-Gordon and Maxwell fields, respectively, whereas s = 2 for axial perturbations of a (generically anisotropic) fluid in GR (where $p_{\rm rad} = T_r^r$ and $\rho = -T_t^t$ are the radial pressure and the energy density of the fluid, respectively).

Figure 4.20 shows an example of $V_{sl}(r)$ for two representative ultracompact objects: the so-called gravastar model discussed in Sect. 5.8.2 and a constant density star which, in the static case, is described by the line element (4.60) with $\varpi = 0$ and

$$F(r) = \frac{1}{4R^3} \left(\sqrt{R^3 - 2Mr^2} - 3R\sqrt{R - 2M} \right)^2 , \tag{F.2}$$

$$B(r) = \left(1 - \frac{2Mr^2}{R^3}\right)^{-1} \,, \tag{F.3}$$

where R is the radius of the star. The pressure is given by

$$P(r) = \rho_c \frac{\sqrt{3 - 8\pi R^2 \rho_c} - \sqrt{3 - 8\pi r^2 \rho_c}}{\sqrt{3 - 8\pi r^2 \rho_c} - 3\sqrt{3 - 8\pi R^2 \rho_c}},$$
 (F.4)

where $\rho_c = 3M/(4\pi R^3)$ is the density of the uniform star.

This potential $V_{sl}(r)$ shares many similarities with the geodesic potential to which it reduces in the eikonal limit [27]: it has a local maximum, diverges at the origin and is constant at infinity. Because the potential necessarily develops a local minimum, it is possible to show that in the eikonal limit $(l \gg 1)$ the spectrum contains long-lived modes whose damping time grows exponentially with l [27–29]. To first order in the eikonal limit, the potential can be approximated as $V_{sl}(r) \sim l^2 f/r^2$. Let us define r_a , r_b and r_c to be the three real turning points of $\omega_R^2 - V_{sl}(r) = 0$ as shown in Fig. 4.20 for the black solid curve. When such turning points exist, the real part of the frequency of a class of long-lived modes is given by the WKB condition:

$$\int_{r_a}^{r_b} \frac{dr}{\sqrt{f/B}} \sqrt{\omega_R^2 - V_{sl}(r)} = \pi (n + 1/2),$$
 (F.5)

where *n* is a positive integer. The imaginary part of the frequency ω_I of these modes is

$$\omega_I = -\frac{1}{8\omega_R \gamma} \exp\left[-2 \int_{r_b}^{r_c} \frac{dr}{\sqrt{f/B}} \sqrt{V_{sl}(r) - \omega_R^2}\right], \tag{F.6}$$

where

$$\gamma = \int_{r_a}^{r_b} \frac{dr}{\sqrt{f/B}} \frac{\cos^2 \chi(r)}{\sqrt{\omega_R^2 - V_{sl}(r)}}, \qquad \chi(r) = -\frac{\pi}{4} + \int_{r_a}^{r} \frac{dr}{\sqrt{f/B}} \sqrt{\omega_R^2 - V_{sl}(r)}.$$
(F.7)

By expanding Eqs. (F.5) and (F.6), one can show that, to leading order in the eikonal limit, the mode frequency reads

$$\omega \sim a \, l - i \, b \, e^{-cl} \qquad l \gg 1 \,, \tag{F.8}$$

where a, b and c are positive constants. By expanding Eq. (F.5) near the minimum of the potential displayed in Fig. 4.20, it is possible to show that [26]

$$a \sim \Omega_{\rm LR2} \equiv \frac{\sqrt{f(r_{\rm LR2})}}{r_{\rm LR2}},$$
 (F.9)

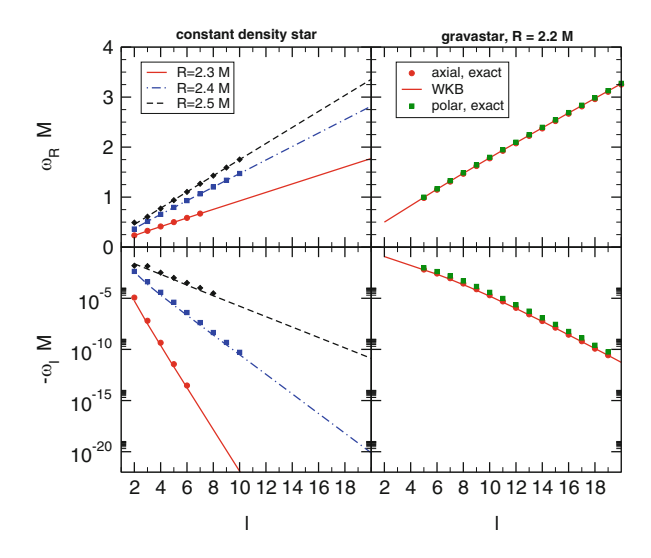


Fig. F.1 Real and imaginary parts of the long-lived modes of a uniform star for different compactness (*left panels*) and for a gravastar with $R = 2.2 \,\mathrm{M}$ (*right panels*). The *lines* are the WKB results, whereas markers show the numerical results obtained in [26] by using direct integration or continued fractions. For uniform stars we show gravitational axial modes, whereas for gravastar we show both axial modes (*red circles*) and gravitational polar modes with $v_s = 0.1$ (*green squares*), where v_s is related to the speed of sound on the shell [30]. See [26] for details

where Ω_{LR2} is the angular velocity of the *stable* null geodesic at the light-ring location $r = r_{LR2}$. Note that the damping time of these modes is exponentially large, so that they are arbitrarily long-lived in the large-l limit. In Fig. F.1, we compare the long-lived modes computed through the above WKB formula with the exact numerical result [26] for two representative ultracompact objects, showing a quite good agreement in the large-l limit.

Practically, the long-lived modes of a static ultracompact object are metastable and it is reasonable to expect that they can turn unstable when rotation is included. In the slow-rotation limit one may consider a probe scalar field propagating on the approximate spinning geometry (4.60); the Klein-Gordon equation in the eikonal limit reduces to Eq. (4.62), which is suitable for a WKB analysis similarly to the nonrotating case [31, 32]. By defining $W = \frac{B(r)}{f(r)}(\bar{\omega} - V_+)(\bar{\omega} - V_-)$, the quasi-bound unstable modes are determined by

$$m\int_{r_a}^{r_b} \sqrt{W(r)} dr = \frac{\pi}{2} + n\pi, \quad n = 0, 1, 2, \dots$$
 (F.10)

and their characteristic time scale can be computed through

$$\tau = 4 \exp\left[2m \int_{r_b}^{r_c} \sqrt{|W|} dr\right] \int_{r_a}^{r_b} \frac{d}{d\bar{\omega}} \sqrt{W} dr, \qquad (F.11)$$

where r_a , r_b are solutions of $V_+ = \bar{\omega}$ and r_c is determined by the condition $V_- = \bar{\omega}$. This result agrees with Eq. (4.64) quoted in the main text. As discussed in Sect. 4.11, the long-lived modes become unstable (i.e. their imaginary part changes sign) above a critical spin and precisely when an ergoregion forms in the geometry [26, 31, 32].

References

- 1. http://blackholes.ist.utl.pt/?page=Files
- A. Starobinski, Amplification of waves during reflection from a rotating black hole. Zh. Eksp. Teor. Fiz. 64, 48 (1973) [Sov. Phys. JETP 37, 28 (1973)]
- A.A. Starobinski, S.M. Churilov, Amplification of electromagnetic and gravitational waves scattered by a rotating black hole. Zh. Eksp. Teor. Fiz. 65, 3 (1973) [Sov. Phys. JETP 38, 1 (1973)]
- D.N. Page, Particle emission rates from a black hole: massless particles from an uncharged, nonrotating hole. Phys. Rev. D13, 198–206 (1976)
- 5. C.W. Misner, K. Thorne, J. Wheeler, *Gravitation* (Freeman, San Francisco, 1974)
- J. Bekenstein, Extraction of energy and charge from a black hole. Phys. Rev. D7, 949–953 (1973)
- R. Ruffini, Black Holes: les Astres Occlus (Gordon and Breach Science Publishers, New York, 1973)
- 8. J.D. Jackson, Classical Electrodynamics, 3rd edn. (Wiley, New York, 1999)
- P. Chrzanowski, Vector potential and metric perturbations of a rotating black hole. Phys. Rev. D11, 2042–2062 (1975)
- A. Ori, Reconstruction of inhomogeneous metric perturbations and electromagnetic four potential in Kerr space-time. Phys. Rev. D67, 124010 (2003). arXiv:gr-qc/0207045 [gr-qc]
- S.A. Hughes, Computing radiation from Kerr black holes: generalization of the Sasaki-Nakamura equation. Phys. Rev. D62, 044029 (2000). arXiv:gr-qc/0002043 [gr-qc]
- 12. A.R. King, Black-hole magnetostatics. Math. Proc. Camb. Philos. Soc. 81, 149 (1977)
- 13. S. Teukolsky, W. Press, Perturbations of a rotating black hole. III Interaction of the hole with gravitational and electromagnet ic radiation. Astrophys. J. 193, 443–461 (1974)
- A.A. Starobinskij, S.M. Churilov, Amplification of electromagnetic and gravitational waves scattered by a rotating black hole. Zh. Eksp. Teor. Fiz. 65, 3–11 (1973)
- A.A. Starobinskij, S.M. Churilov, Amplification of electromagnetic and gravitational waves scattered by a rotating black hole. Sov. Phys. JETP 38, 1–5 (1973)
- J.B. Hartle, Slowly rotating relativistic stars.
 Equations of structure. Astrophys. J. 150, 1005– 1029 (1967)
- Y. Kojima, Equations governing the nonradial oscillations of a slowly rotating relativistic star. Phys. Rev. D46, 4289–4303 (1992)
- Y. Kojima, Normal modes of relativistic stars in slow rotation limit. Astrophys. J. 414, 247–253 (1993)
- 19. P. Pani, V. Cardoso, L. Gualtieri, E. Berti, A. Ishibashi, Perturbations of slowly rotating black holes: massive vector fields in the Kerr metric. Phys. Rev. **D86**, 104017 (2012). arXiv:1209.0773 [gr-qc]
- R. Brito, V. Cardoso, P. Pani, Massive spin-2 fields on black hole spacetimes: instability of the Schwarzschild and Kerr solutions and bounds on the graviton mass. Phys. Rev. D88, 023514 (2013). arXiv:1304.6725 [gr-qc]
- 21. P. Pani, Advanced methods in black-hole perturbation theory. Int. J. Mod. Phys. A28, 1340018 (2013). arXiv:1305.6759 [gr-qc]

 S. Chandrasekhar, The Mathematical Theory of Black Holes (Oxford University Press, Oxford, 1983)

- J.B. Hartle, K.S. Thorne, Slowly rotating relativistic stars. II. Models for neutron stars and supermassive stars. Astrophys. J. 153, 807 (1968)
- 24. P. Pani, E. Berti, I-Love-Q, spontaneously: slowly rotating neutron stars in scalar-tensor theories. Phys. Rev. **D90**, 024025 (2014). arXiv:1405.4547 [gr-qc]
- S. Chandrasekhar, V. Ferrari, On the non-radial oscillations of slowly rotating stars induced by the lense-thirring effect. Proc. R. Soc. Lond. A433, 423–440 (1991)
- 26. V. Cardoso, L.C.B. Crispino, C.F.B. Macedo, H. Okawa, P. Pani, Light rings as observational evidence for event horizons: long-lived modes, ergoregions and nonlinear instabilities of ultracompact objects. Phys. Rev. **D90**, 044069 (2014). arXiv:1406.5510 [gr-gc]
- 27. V. Cardoso, A.S. Miranda, E. Berti, H. Witek, V.T. Zanchin, Geodesic stability, Lyapunov exponents and quasinormal modes. Phys. Rev. **D79**, 064016 (2009). arXiv:0812.1806 [hep-th]
- 28. G. Festuccia, H. Liu, A Bohr-Sommerfeld quantization formula for quasinormal frequencies of AdS black holes. Adv. Sci. Lett. 2, 221–235 (2009). arXiv:0811.1033 [gr-qc]
- 29. E. Berti, V. Cardoso, P. Pani, Breit-Wigner resonances and the quasinormal modes of anti-de Sitter black holes. Phys. Rev. **D79**, 101501 (2009). arXiv:0903.5311 [gr-qc]
- P. Pani, E. Berti, V. Cardoso, Y. Chen, R. Norte, Gravitational wave signatures of the absence of an event horizon. I. Nonradial oscillations of a thin-shell gravastar. Phys. Rev. D80, 124047 (2009). arXiv:0909.0287 [gr-qc]
- 31. N. Comins, B.F. Schutz, On the ergoregion instability. Proc. R. Soc. Lond. Ser. A Math. Phys. Sci. 364(1717), 211–226 (1978). http://www.jstor.org/stable/79759
- 32. V. Cardoso, P. Pani, M. Cadoni, M. Cavaglia, Ergoregion instability of ultracompact astrophysical objects. Phys. Rev. **D77**, 124044 (2008). arXiv:0709.0532 [gr-qc]